NANOPARTICLES FROM ALKYLGLYCERYL-MODIFIED POLYSACCHARIDES FOR DRUG DELIVERY TO THE BRAIN

PETR TOMAN

November 2012

The thesis is submitted in partial fulfilment of the requirements for the award of the degree of Doctor of Philosophy of the University of Portsmouth.

Biomaterials and Drug Delivery Research Group
School of Pharmacy and Biomedical Sciences
University of Portsmouth

I

ABSTRACT

The loading of therapeutic actives into polymeric nanoparticles represents one of the approaches towards drug transport through the blood-brain barrier – the main obstacle to drug delivery into the central nervous system. The non-toxic, biocompatible and biodegradable polysaccharides chitosan and dextran were modified with permeation-enhancing alkylglyceryl pendant chains through reaction with epoxide precursors. The modified polysaccharides were characterised by spectroscopic methods (^{1}H-, ^{13}C-NMR and FT-IR). These polysaccharides were further formulated into nanoparticles using three methods, namely: nanoprecipitation, solvent displacement *via* dialysis and electrospraying. The resultant colloidal systems formed were characterised using Dynamic Light Scattering, Nanoparticle Tracking Analysis and Electrophoretic Mobility Measurements. Dried nanoparticles were further characterised by Scanning Electron Microscopy and Atomic Force Microscopy. Formulations of alkylglyceryl-dextran derivatives were found to be stable at the physiologically relevant pH of 7.4. Over the same range of pH values, formulations of alkyglyceryl-chitosans formed aggregates. Respectively dependent upon the method of formulation and the pH, nanoparticles from poly(lactic acid)-*graft*-butylglyceryl-modified dextran exhibited diameters in the range 100-400 nm and zeta potentials of between -15 and -30 mV. The preparation of nanoparticulate congeners that incorporated a fluorescent marker molecule (Doxorubicin, Rhodamine B or Fluorescein) allowed the studies of the capabilities of nanoparticles to accommodate and release a model therapeutic load. Rhodamine B-loaded nanoparticles further allowed the study of the uptake of nanoformulations by mouse (bEnd3) brain endothelial cells. The interactions of nanoparticles with modelled blood-brain barriers (mouse bEnd3 and human hCMEC/D3) were studied by Electric Cell Substrate Impedance Sensing and also by means of the Transwell

model. Data from MTT and Presto Blue assays were consistent with the absence of nanoparticle-induced cytotoxic effects. An *in ovo* study that used 3-day chicken embryos indicated the absence of whole-organism acute toxicity effects but failed to unmask the biodistribution profile of nanoparticles. The results have shown that poly(lactic)-*graft*-alkylglyceryl-modified dextran nanoparticles possess some promising features (size, stability, loading capacity, and toxicity) that render them candidates for further evaluation as biocompatible nanocarriers for drug delivery to the brain.

II

DEDICATION

To my family

III

ACKNOWLEDGEMENT

I would like to express my gratitude to my supervisors Dr Eugen Barbu, Prof Darek Górecki and Dr John Tsibouklis for all their kind support, important advice and precious guidance through the duration of my PhD.

I would like to acknowledge Dr Éva Molnár for her introduction into the beauty of chemistry and Dr Chun-Fu Lien for his guidance through the adventurous field of *in vitro* experiments. I would also like to mention my colleagues for their kind help: Dr James Smith with AFM, Dr Gina Doddi with GPC analysis, Dr Simon Cragg and Mrs Christine Hughes with SEM, Dr Susanne Dietrich for providing the sources for the embryonic work, Dr Zeeshan Ahmad for the introduction into electrospraying, Prof Geoff Pilkington for providing the facilities for human tissue culturing and Dr Qin An for providing kind environment in the lab of Neuro-oncology group. I would also like to mention Mrs Val Ferrigan for logistical and technical support and to Mrs Nicola Noyce for her help with the academic registry matters.

Special thanks to my colleagues Miss Sarah Upson, Dr Hamde Nazar, Miss Ghezlane Id Doud and Mr Anthony Sinadinos for their company on the journey of the PhD.

I would like to acknowledge the Institute of Biomedical and Biomolecular Sciences for the financial support.

IV

DECLARATION

Whilst registered as a candidate for the degree of Doctor of Philosophy, I have not been registered for any other research award. This work was sponsored by Institute of Biomedical and Biomolecular Sciences, University of Portsmouth. The material contained within this thesis is all my own work and has not been submitted for any other academic award.

Petr Toman

2012

V

CONTENTS

VI

ABBREVIATIONS

AFM	Atomic force microscopy
AKG	Alkylglycerol
ATR	Attenuated total reflectance
BBB	Blood-brain barrier
bEnd3	Mouse brain endothelial cells
C-6	Rat glioma cells
cAMP	3',5'- cyclic adenosine monophosphate
CAM	Chorrio-allantoin membrane
CDI	1,1'-Carbonyldiimidazole
CS	Chitosan
CS-OXn	Alkylglyceryl modified chitosan
CS-OX4	Butylglyceryl-modified chitosan
CS-OX5	Pentylglyceryl-modified chitosan
CS-OX8	Octylglyceryl-modified chitosan
DCC	*N,N`*-dicyclocarbodiimide
dBcAMP	N(6),2'-O-dibutyryl 3',5'- cyclic adenosine monophosphate
DEX	Dextran
DEX-OXn	Alkylglyceryl-modified dextran
DEX-OX4	Butylglyceryl-modified dextran
DEX-OX8	Octylglyceryl-modified dextran
DEX-S	Dextran sulphate
DIGIT	Digitonin
DLS	Dynamic light scattering

DMAP	4-(dimethylamino)pyridine
DMF	Dimethylformamide
DMEM	Dublecco's modified Eagle medium
DMSO	Dimethyl sulfoxide
DOX	Doxorubicin
ECIS	Electric cell-substrate impedance sensing
EGM-2	Endothelial cell growth medium from Lonza
EPM	Electrophoretic mobility measurements
FBS	Foetal bovine serum
FITC	Fluorescein isothiocyanate
FITC-DEX	Fluorescein-labelled dextran
FT-IR	Fourier transform-infrared spectroscopy
HBSS	Hank's balanced salt solution
hCMEC/D3	Human endothelial cells
hFGF-B	Human fibroblast growth factor -B
HS	Human serum
NMR	Nuclear magnetic resonance
Nps	Nanoparticles
NTA	Nanoparticle tracking analysis
o-CS	Chitosan oligosaccharide
P 188	Poloxamer 188
P 407	Poloxamer 407
PCL	Poly(ε-caprolactone)
PDI	Polydispersity index
PBS	Phosphate buffered saline
PLA	Poly(lactic acid)
PLA-DEXn	Poly(lactic acid)-*graft*-dextran
PLA-DEX-OXn	Poly(lactic acid)-*graft*-alkylglyceryl-modified dextran

PLA-DEX-OX4	Poly(lactic acid)-*graft*-butylglyceryl-modified dextran
PLA-DEX-OX8	Poly(lactic acid)-*graft*-octylglyceryl-modified dextran
PLGA	Poly(lactic-*co*-glycolic acid)
PMMA	Poly(methyl methacrylate)
PVA	Polyvinyl alcohol
RES	Reticulo-endothelial system
R3-IGF-1	Insulin-like growth factor 1
RO-20-1724	Selective phosphodiesterase inhibitor
RPM	Revolutions per minute
SEM	Scanning electron microscopy
SIOS	Scanning ion occlusion spectroscopy
TEM	Transmission electron microscopy
TJ	Tight junction
TMC-CS	Trimethyl chitosan
TMC-CS-OX4	Butylglyceryl-modified trimethyl chitosan
TMC-CS-OX8	Octylglyceryl-modified trimethyl chitosan
TPP	Sodium tripolyphosphate
UV/VIS	Visible and ultraviolet spectroscopy
VEGF	Vascular endothelial growth factor
Z-av.	Z-average mean diameter
ZP	Zeta potential

VII

LIST OF FIGURES

VIII

LIST OF TABLES

1

INTRODUCTION AND AIMS

Brain disorders represent almost one third of the total burden of diseases in Europe [1]. In the future, the increase of average life expectancy is predicted to result in a growth of neurodegenerative diseases in the elderly population, while the current advances in diagnostic methods are expected to add to an already long list of known neurodegenerative, cerebrovascular, inflammatory and infectious brain ailments [2]. Consequently, the market for drugs for central nervous system disorders is estimated to grow by five times, reaching the same size to that of the cardiovascular disease market [3].

The intravascular route of drug delivery to the brain is preferred over that through other routes (*e.g.* intranasal or intraocular) due to the proximity of the brain parenchymal cells to brain capillaries (20 μm) and also due to the large surface area of the brain vessel network (20 m^2) [4]. Intravenous drug delivery to the brain is generally impeded by the blood brain barrier (BBB). The BBB has a role in maintaining the specific environment required for neuronal signalling. The presence of tight junctions and efflux proteins, together with processes such as selective abluminal transport and the flow of intracerebral fluid, result in a restricted entry into the brain of toxins, xenobiotics and endogenous molecules present in the circulatory system, which may otherwise compromise the delicate homeostasis of the neuronal environment.

Nanoparticulate drug delivery systems benefit from favourable pharmacokinetic characteristics. The therapeutic potential of nanoparticles formulated from biodegradable, nontoxic, and non-immunoactive polymers for drug delivery to the brain is currently a very active area of research [5-7]. The surface features of nanoparticles can be finely tuned so that they can influence the particle distribution into specific tissues and trigger the release of the

drug load in appropriate conditions. Nanoparticulate carriers can also prolong the lifetime of a drug in the bloodstream. Due to their accessibility, biocompatibility and biodegradability, polysaccharides have been extensively studied as promising materials for drug delivery systems as they have the added advantage of bearing functional moieties that easily allow their chemical modification. In parallel, intracarotidally administered short chain alkylglycerols are known to enhance the permeability of drugs through the BBB.

This project was aimed at the study of the potential of nanoparticulate carriers from alkylglyceryl-modified polysaccharides to transport therapeutic agents to the brain[8-10]. More specifically, the main objectives of this work were to:

- prepare and characterise alkylglyceryl-modified chitosan and alkylglyceryl-modified dextran;
- use these alkylglyceryl-modified polysaccharides as support matrixes for nano-sized drug carrier systems;
- explore the potential of colloidal suspensions of these systems as candidate systems for intravascular drug delivery, *via* an assessment of their stability in simulated physiological conditions;
- employ fluorescent marker molecules to assess the loading capacity and release profiles of nano-formulations;
- assess toxicity, cellular uptake and interaction with a modelled BBB of cell monolayers through *in vitro* studies of the effects of the nano-formulations on mouse or human brain endothelial cells;
- investigate the *in ovo* biodistribution and associated toxicity of fluorescently labelled nanoparticles using chicken embryos.

2

LITERATURE BACKGROUND

2.1. Delivering actives to the brain – why is it so important?

It is estimated that brain disorders such as anxiety, stroke, dementia, mood disorders or psychotic illnesses represent approximately 35 % of the total burden of diseases in Europe and affect about one third of the population [1]. For the European Union, the estimated total cost related to brain disorders in 2010 was ca. €798 billion. With high average cost per inhabitant of €5 550 (ranging from €285 for headache to €30 000 for neuromuscular disorders) [2] this is comparable to the cost of cardiovascular diseases, cancer, and diabetes together.

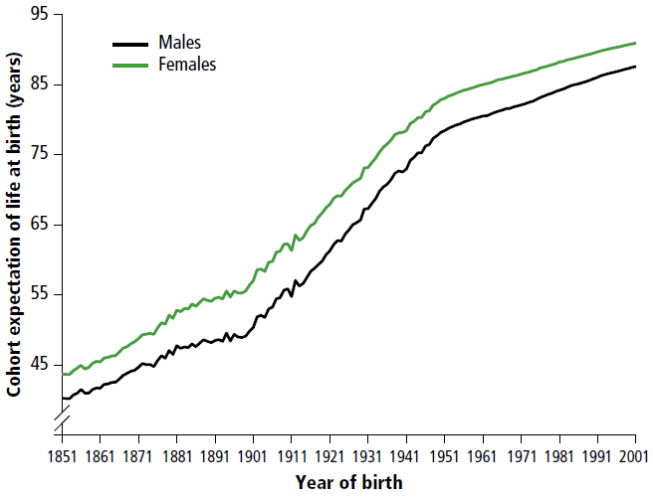

Figure 2.1. Life expectation at birth, UK population. Adopted from [11].

While more diseases and infections are now being cured successfully compared to the past due to advances in modern medicine, the average human lifespan has been growing continuously over the last 150 years *(Figure 2.1.)*, reaching *ca*. 78 years for males and 82 years for females in UK (2008 data; [12]). This means a higher chance of experiencing CNS disorders [13]. Despite all research efforts, patients suffering from serious neurodegenerative diseases

such as brain tumours, HIV encephalopathy, epilepsy, cerebrovascular diseases or neurodegenerative disorders outnumber those dying of all types of systemic cancers and heart diseases [14].

2.2. The anatomy and physiology of the blood-brain barrier

The brain is the emotional and rational control centre of the human body that helps us to survive. This organ provides us with the thinking capacity that makes humankind different from other organisms on this planet. The most complex structure of the body, the brain consists of 1×10^{11}neurons [15], impulse-conducting cells, and about 1×10^{12} astrocytes that act as supporting cells [16].

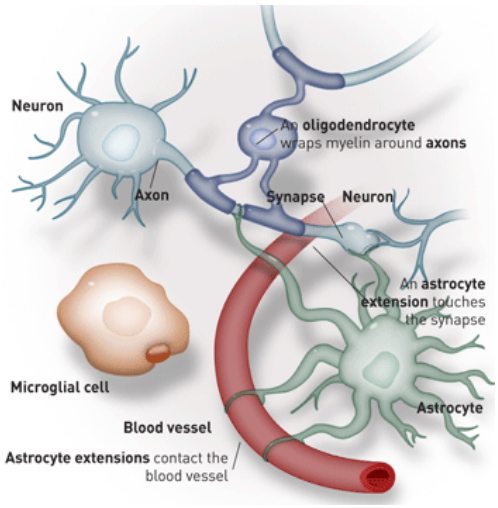

Figure 2.2. Schematic display of the cells in the CNS; adapted from [17].

A neuron can have 1 000 - 10 000 synapses, connections between individual neurons, where the electrical impulse changes to chemical, with the total number of synapses reaching 1×10^{14} to 5×10^{14} in an adult (or even 10^{15} in a new-born, *Figure 2.2.*). Morphologically, the brain is protected by the cranium against mechanical damage. Between the neuronal tissue of the brain and bone of the cranium, there are soft layers of *neurocranium*, so called meninges (*pia mater, arachnoid* and *dura mater; Figure2.3.*) that provide "buffering" to absorb mechanical stress and allow the branched microvasculature to supply the required bloodstream

components to the neuronal tissue [18]. At the same time, the circulation of cerebrospinal fluid (CSF) provides maintenance for CNS. The CSF is cleared into the blood through *arachnoid granulations* to remove the metabolites from the brain [19]. The brain is separated from the internal body environment by the presence of the blood-brain barrier.

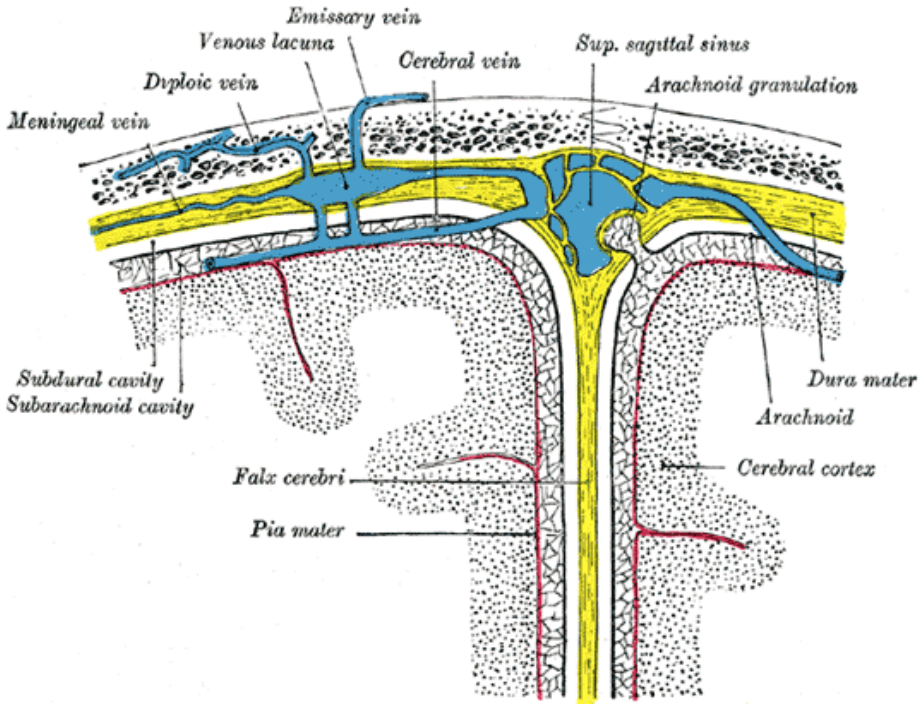

Figure. 2.3. Schematic representation of the meninges; adopted from [20].

The blood-brain barrier (BBB) provides a morphological structure which strictly divides the brain tissue from blood vasculature [21], in order to maintain the delicate homeostatic balance of nutrients, ions and signalling molecules required in the brain environment for proper neuronal communication [22]. The BBB limits the entry of plasmatic components, red blood cells, and leukocytes into the brain. If these cells cross the BBB following an ischemic injury, inflammation, Intracerebral haemorrhage or vascular disorder, neurotoxic products are generated that can compromise synaptic and neuronal functions [23]. The BBB serves as a defence line that protects the brain compartment from the entry of unwanted molecules such as blood-borne metabolites, toxins, virions, bacteria and xenobiotics[24]. However, in protecting the brain, the BBB does not allow the entry of a large list of CNS-active molecules, including

therapeutic peptides, protein based neuropharmaceuticals, and more than 98% of all small drug molecules [24, 25].

The existence of a barrier between brain and bloodstream was suggested by Ehrlich and confirmed by Lewandowski in 1900, when bile acids or ferrocyanide applied intravenously could not be found in the brain [26]. In 1909, Goldman showed that a dye, Trypan Blue, could cross between the brain and the cerebro-spinal fluid but was excluded from passing between these regions and the blood. From this observation Goldman concluded that there was no impermeable barrier between brain and spinal cord tissue [27]. Electron microscopy studies using horseradish peroxidase have subsequently shown that the BBB is localised at the level of tight junctions (TJ) present between adjacent endothelial cells [28, 25].

Morphologically, the BBB comprises of neurovascular groups of cooperating adjacent cells such as endothelial cells and glial cells [25] *(Figure 2.4.)*. The endothelial cells are anchored to the basal lamina [22] with the astrocyte end-feet tightly covering the vessel wall and appearing to be critical for the induction and maintenance of the barrier properties of the endothelial cells [29].

Glial cells comprise *microglia*, *macroglia*, and *oligodendrocytes*. *Microglia* including pericytes, which may regulate the BBB [30], and macrophage-like precursor cells [31]. *Macroglia* include astrocytes that support the neurons and enhance the TJ function by providing cellular links [22].

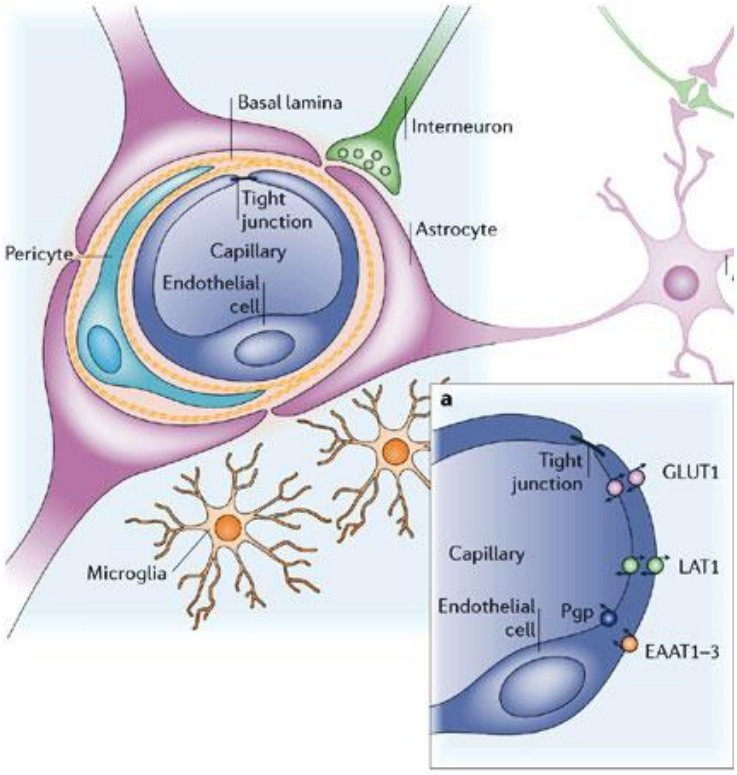

Figure 2.4. Blood-brain barrier neurovascular unit: capillary endothelial cells are surrounded by basal lamina and astrocyte perivascular end feet. ***a)*** *detail of an endothelial cell showing a tight junction (TJ) and endogenous transporters such as EAAT1–3 (excitatory amino acid transporters), GLUT1 (glucose transporter 1), LAT1 (L-system for large neutral amino acids), Pgp (P-glycoprotein); adapted from [22].*

The pericytes embrace the brain capillary endothelium intimately. They are a morphologically, physiologically, and biochemically heterogeneous class of cells which take part in transport processes across the BBB [32]. Pericytes are also thought to regulate the proliferation of endothelium *via* the transforming-growth factor-β (TGF-β) [33]. Moreover, it seems that the number of pericytes present at the vasculature corresponds with the level of endothelial junction "tightness" [32, 34].

Astrocytes are adjacent to the endothelial cells and pericytes and are important for TJ formation [35, 36]. They enhance the membrane barrier properties as over 99 % of the external wall of brain blood vessels is enveloped by astrocyte end-feet. However, individual feet are not sealed and astrocytes can communicate *via* protein exchange through small gaps [37].

Astrocytes support neurons by maintaining homeostasis in the brain *via* potassium uptake, gliotransmitter synthesis and phagocytosis [38]. The neurovascular unit is also comprised of the basal lamina, an extracellular matrix that provides a membranous connection between endothelial cells, astrocytes and pericytes *(Figure 2.4.)* [39]. The basal lamina is a 30-40 nm thick structure containing collagen type IV, fibronectin, laminin and other extracellular matrix proteins, which are likely to be involved in TJ maintenance [40].

The main features that contribute to the protective role of a normal BBB are [41]:

- Tight junctions sealing the intercellular gaps;
- A reduced rate of pinocytosis from the luminal side;
- No fenestration of the endothelium;
- An enzymatic barrier controlling uptake of nutrients;
- An efflux transporter system such as P-glycoproteins which remove molecules from the endothelial cells.

In some situations the BBB can become compromised, for instance in the case of brain tumours [42-44].During inflammation, tumour necrosis factor α (TNF α) can influence BBB permeability [45, 46]. Inflammation can also increase the adhesion of lymphocytes to endothelium and their penetration through the BBB. The endothelial cells express cell adhesion molecules VCAM-1, PECAM-1, and ICAM-1 which attract the cells [47]. Also, in chronic conditions the barrier may be further compromised during continuous transendothelial migration of inflammatory cells [48]. Cells that have left the bloodstream and are entering the brain may be considered in relation to three compartments: the vessel wall, the perivascular (Virchow–Robin) space, and the *neuropil* (last two are separated by the *glia limitans*). As capillaries which do not possess perivascular space, the basement membrane of the vessel wall and the basement membrane of the *glia limitans* could merge into a ‘fused gliovascular membrane’ that allows intimate contact of astrocytes with pericytes and endothelial cells [26].

2.2.1. Tight junctions

The microvascular brain endothelial cells differ from endothelial cells found in other tissues because of their increased mitochondrial content, lack of fenestrations, low pinocytic activity and presence of tight junctions (TJ) (*Figure 2.5.*) [49-51]. The tight junction network in the BBB is a complex structure of transmembrane proteins that includes junctional adhesion proteins and cytoplasmatic proteins [52, 53], *Figure 2.5.*

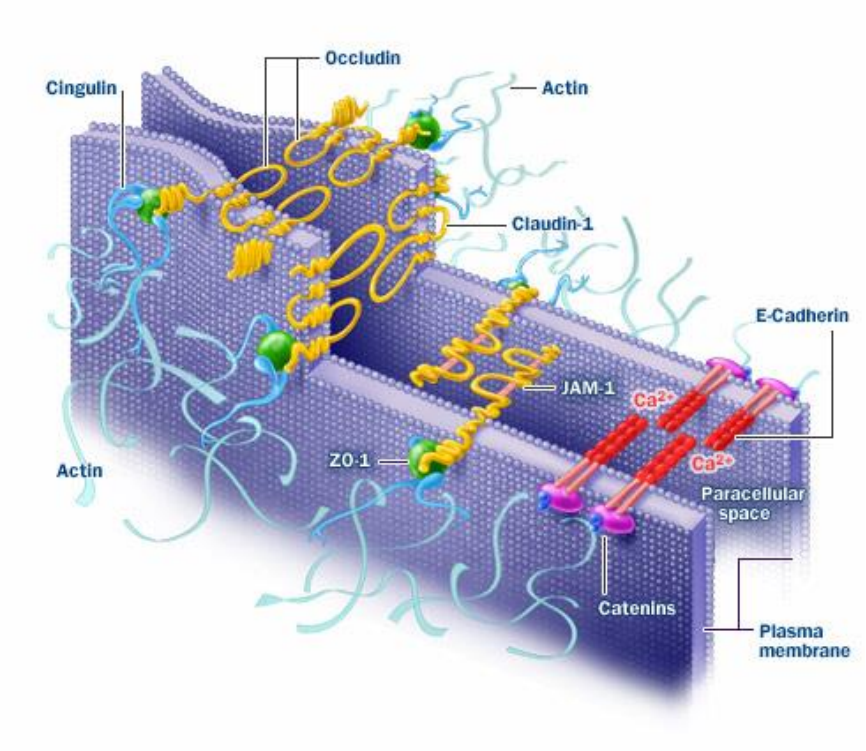

Figure 2.5. Schematic representation of a BBB tight junction. Junctional proteins such as occludins, claudins, ZO-1, JAMs, catenins and E-cadherin (all linked to actin, part of the cell cytoskeleton) are involved in the formation of the tight junction; adapted from [54].

The transmembrane proteins are linked to the cytoskeletal proteins present in cytoplasma (spektrin, actin) *via* zonulaoccludens proteins (ZO-1, ZO-2, ZO- 3 [18]); catenins and E-adherin are also involved in the formation of the TJ [49], though it appears that occludin plays a critical role in establishing the barrier properties of the BBB [18]. If occludin is down-regulated by various brain disorders, the BBB becomes more permeable [55]. Gap junctions that

provide cell-to-cell signalling connections [56] have also been discovered, but their role in BBB function is not yet known [57].

2.2.2. Blood-brain barrier transport activity

The blood-brain barrier does not serve as a passive and rigid defence facility but acts as a dynamic interface that has a high metabolic activity. Active transport processes requires energy that is supplied by the high number of mitochondria present in the endothelial cells [58]. Drug efflux transporters such as P-glycoprotein, Multidrug Resistance Proteins or Organic Anion Transporting Polypeptides are expressed at the endothelial cell or astrocyte end-feet levels. These transporters are key elements in a molecular machinery that confers special permeability properties to the BBB, and their combined actions can result in a rapid efflux of xenobiotics from the brain [29]. Multidrug Resistance Proteins (MRP) belong to the family of ATP-binding Cassette (ABC) transporters, which are multidomain integral membrane proteins present in all mammalian species and that utilise the energy of ATP hydrolysis to translocate solutes across cellular membranes [29, 51, 59].

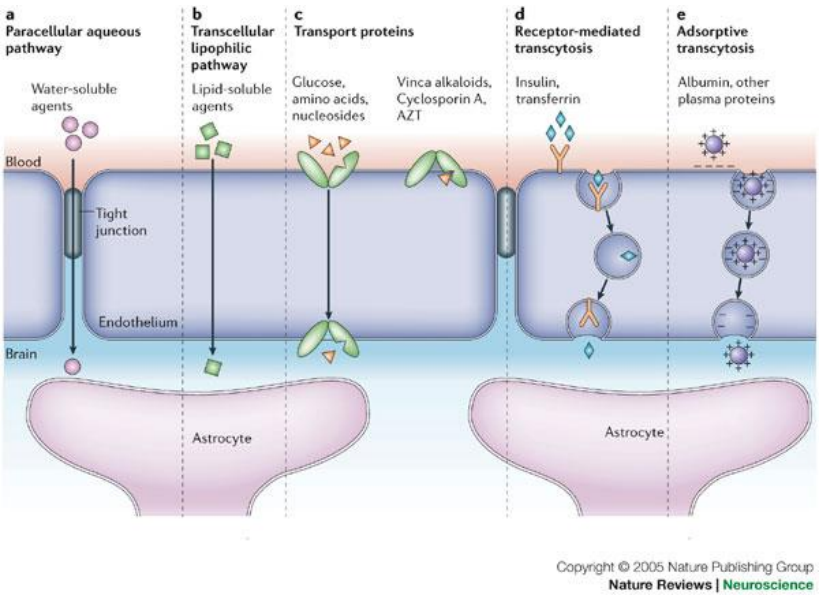

Figure 2.6. Schematic representation of transport mechanisms across the BBB; adapted from [22].

Potential transport mechanisms of various molecules across the blood-brain barrier are represented in *Figure 2.6.* Tight junctions restrict water-soluble molecules (a), while small lipid-soluble substances can diffuse through the membranes of the endothelial cells (b). Various transporters present at the BBB level are subject to competition from endogenous substrates like glucose, amino acids, purine bases, nucleosides, choline and other substances as xenobiotics (c); P-glycoprotein is an example of an efflux protein that removes molecules from the cytoplasm of the endothelial cells and returns them into the lumen of the blood vessels. Specific proteins, such as insulin or transferrin, can be taken up by receptor specific endocytosis followed by transcytosis across the endothelial cells (d), while cationic particles can interact with the negative charges present on the membranes of endothelial cells *via* adsorptive-mediated endocytosis and transcytosis (e) [22].

2.3. Drug delivery to the brain

The majority of the CNS-related research efforts at the beginning of this millennium were devoted to CNS drug discovery. Only a small portion or research was directed to CNS drug delivery. This imbalance led to the current situation where huge resources have been used for the development of numerous CNS actives that, despite perfect hits with intracellular targets, were in most cases not able to cross the BBB [60].

The methods devised to overcome the BBB can be divided into invasive and non-invasive. The invasive methods include intra-cerebroventricular injection, convection-enhanced diffusion [61], the use of intra-cerebral implants [62], high frequency focused ultrasound [61, 63] and vasoactive agents [64]. Hyperosmotic tight junction opening caused by mannitol or arabinose [63] can also be used to increase permeability through the BBB, as can bradykinin analogues, such as RMP-7 (also known as lobradamil) [65, 66] and short-chain alkylglycerols [9, 67]. Less invasive approaches include chemical modification (lipidisation) of molecules (*e.g.* morphine-heroin [68]), targeting natural receptors with antibodies (OX26 monoclonal antibody

against transferrin receptor [69]), or employing colloidal nano-sized carriers that can also enhance the favourable pharmacokinetic characteristics of actives [70].

2.3.1. Invasive routes

Methods that result in a non-selective opening of the BBB or that lead to the direct application of drugs, colloidal systems or implants into the brain are normally classified as invasive. These methodologies involve direct intracranial surgery followed by convection enhanced delivery [71] or by placement of implants [72], application of focused ultrasound [73] *(Figure 2.7.)* or use of microwaves [74, 75]. Other methods include hyperosmotic disruption by polyol solutions [65], application of bradykinin-anologue RMP-7 [66], application of alkylglycerols [10] or sodium caprate [76] and some other experimental approaches [77, 78]. Also, it was shown that a GSM phone signal influenced the permeability of the BBB in rats [79].

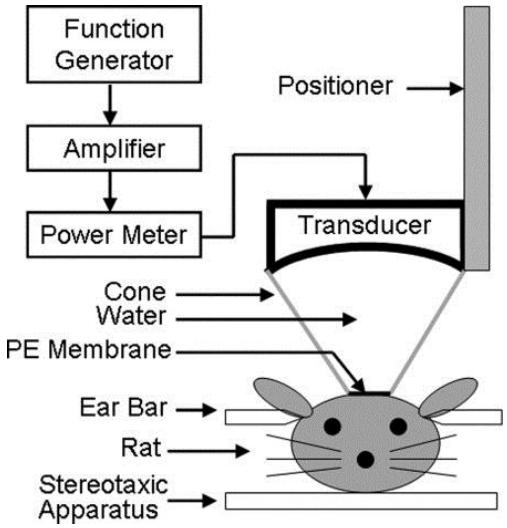

Figure 2.7. Experimental setup for the application of 1 MHz ultrasound in 30 s cycles; adopted from [73].

2.3.1.1. Intracerebral injections, infusions and implants

Active pharmaceutical ingredients can be delivered into the brain by intra-cerebro-ventricular infusion or intra-cerebral implants [80]. A drug can be directly injected into the brain in the form of solution (Convection Enhanced Brain Drug Delivery) [81], in the form of a colloidal system such as a liposomal formulation [71, 82], or in the form of an implant containing a slow releasing drug [64] such as PLGA microparticles loaded with Paclitaxel [72]. These methods are highly invasive procedures that require neurosurgery and special equipment, and carry a high risk. If for instance an injected volume or a solid implant is rapidly introduced into brain tissue, it may damage that area of the brain [64]. In addition, once actives are introduced using such a method, the diffusion rate in brain parenchyma has been found to be very poor [83].

2.3.1.2. Hyperosmotic disruption

BBB permeability can also be manipulated by intracarotidal arterial infusion of hyperosmotic solutions such as those of some polyols (mannitol and arabinose) [64, 65, 84]; oral administration of sugar was also claimed to increase the delivery to the brain of co-administered drug molecules [64]. This effect has been explained by the osmotic stress that induces a variety of cyto-skeletal changes that ultimately contribute to the opening of the barrier [85]; the mechanism of action is a reversible “shrinkage“ of endothelial cells by draining water from the cells thus lowering the transepithelial electric resistance of the endothelium. This has been shown to lead to an increased permeability of paracellular markers, such as sucrose and inulin, through both a brain endothelial cell layer model and in animal studies [86]. However, this effect appears to be non-selective for tumour tissues (e.g. mannitol was found to provide a relative high accumulation of cytotoxic drugs in a tumour-free brain tissue [87]).

Recent clinical studies suggested that BBB disruption by intra-arterial hyperosmotic mannitol can enhance the penetration of anticancer drugs and prolong survival in patients with malignant brain tumours [88]. However, despite successful application in some clinical centres,

the method has not been widely spread because the procedure is difficult, invasive, and there is a risk of post-treatment neurotoxicity developing [63].

2.3.1.3. Blood-brain barrier modulating agents

Molecules such as bradykinin or its analogue (RMP-7) [66, 89], sodium caprate [76] or alkylglycerols [10]were found to exhibit modulation of the blood-brain barrier.

Alkylglycerols were shown to increase the amount of co-distributed drugs in the brain following intra-carotidal administration [9, 10, 67, 90-95].

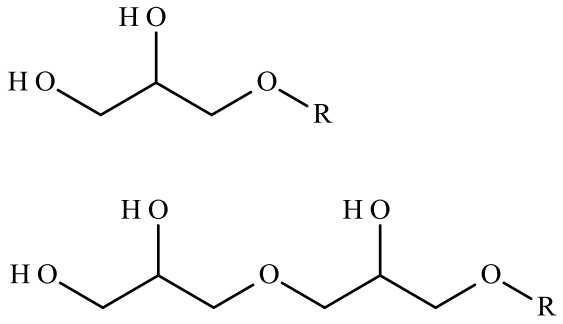

Figure 2.8. Chemical structures of the alkylglycerols studied by Erdlenbruch et al. [95].

1-O-Alkylglycerols (mostly with 16 and 18 carbon atom chains) are naturally found in human haematopoietic organs (bone marrow), in human milk and (in abundance) in shark liver oil [96, 97]. In terms of biological activity, 1-O-alkylglycerols were found to exhibit antitumour effects – interestingly, sharks have a very low incidence of cancer [96, 98, 99]. Also, supplementation with 1-O-alkylglycerols in tumour-bearing rats promoted gain in body weight, a reduction of tumour weight, and maintained glycemia and liver glycogen content to values similar to control healthy rats [97]. Alkylglycerols can also influence the basic fibroblast Growth Factor-stimulated endothelial cell proliferation [100], and amplify biosynthesis of platelet-activating factor in monocyte cell lines produced by mammalian sperm (which makes alkylglycerols important activators of sperm motility) [101]. Other biological actions of

alkylglycerols include antibacterial [102], and antifungal [103]; they were also used in the prophylaxis of radiation side effects associated to cancer treatment [104]. Submicron vesicules for drug delivery (300-800 nm; algosomes) were formulated by hydrating a film consisting of a mixture 1-O-alkylglycerols, cholesterol and dicetyl phosphate [105].

As mentioned previously, mono- and di-alkylglycerols have been reported to temporary open the BBB when administered intracarotidally [9, 91, 106]. The delivery of methotrexate to brain was increased 2 to 230 fold into ipsilateral hemisphere compared to the control, however, only intracarotidal administration of alkylglycerols seems to be efficient, while the intravenous application did not show any positive results [10]. The alkylglycerols, given to the carotid artery were shown to increase brain uptake of antineoplastic agents as cisplatin and methotrexate and the antibiotics vancomycin and gentamycin in rats drugs by C6 glioma bearing [92] and RG2 implanted tumours [90] rats when co-administered into the right internal carotid. The effect was pronounced in the ipsilateral hemisphere, as expected, and in the same range for tumorous and tumour-free tissue [92].

1-O-pentylglycerol induced the extravasation of fluorescein, albumin and methotrexate in the ipsilateral brain and to the tumour by enhancing paracellular permeability of tight junctions. The effect of 1-O-pentylglycerol was lower than that of hyperosmotic mannitol, and much higher than the effect of bradykinin but, in contrast to mannitol, it did not enhance BBB permeability in the contralateral brain hemisphere or the *cerebellum* and brain stem [8]. *In vivo* Near Infrared Time-Domain Optical Imaging showed that delivery of fluorescent molecules after application of hexyldiglycerol was still detectable after 24 hours after application *(Figure 2.9.)* [91]. The effect and duration of alkylglycerol-induced BBB-opening was more rapid and localized to the site of injection, with less *in vivo* toxicity [8], offering a safer alternative of BBB disruption to using hyperosmotic mannitol [63].

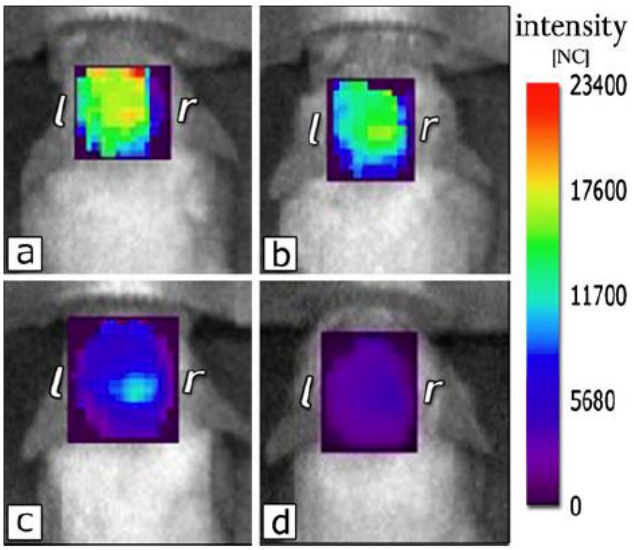

Figure 2.9. In vivo Near Infrared Time-Domain Optical Imaging. Normalised fluorescence intensity of fluorescent tracer in mouse brain after application of helxyldiglycerol: 6 (a), 9 (b), 24 (c) and 72 (d) hours after alkylglycerol mediated BBB opening followed by intracarodial injection of marker. Adapted from [91].

The effect of alkylglycerols on the BBB was described as the result of their interaction with the endothelial cell membranes, when the lipid bilayer was disorganised and fluidified in a manner that facilitated trans-endothelial incorporation and diffusion of the drug molecules [67]. Marigny *et al.* explained this effect of endothelial modulation through the alteration of lipid signalling of phospholipase C conducted *via* diacylglycerol signalling pathway [94].

Sodium caprate was found to open the BBB in a reversible manner; experiments using it showed a greater flux of tracer compared to hyperosmotic opening by mannitol, and had twice the effect of the intracarotidal infusion of bradykinin and a comparable effect to alkylglycerols. However, its toxicity and the risk of possible brain oedemas were raised as important disadvantages [76].

Natural peptides such as *bradykinin* or its analogue RMP-7 [66, 89] were shown to increase the delivery of chemotherapeutic agents to tumour tissue in the brain, however the increase was limited to two-fold when compared to the control [65].

2.3.1.4. Rare experimental methods

Some CNS-active drugs can also modify the permeability of the BBB for other substances; cholinomimetic arecolines have been reported to induce changes in penetration of drugs through the BBB [78]. A rather invasive method to disrupt the BBB involves the parenteral administration of purified cell wall fragments of eubacteria such as *Streptococcus pneumoniae* [77]. A major limitation is however related to the non-specificity of the approach, which leads to the entry of non-invited molecules into the brain [64] (this applies to all non-specific methods of BBB opening when, even with a minimal disruption of the BBB, the circulating neurotoxins, hormones and ions can enter into the neural tissues and unbalance the internal brain homeostasis or induce cell damage [107]).

2.3.2. Non-invasive routes

These methods do not access the brain parenchyma directly nor disrupt the BBB in a non-selective way. They include chemical drug delivery systems (prodrugs) [68] and targeted drug delivery platforms [69] and colloidal drug delivery systems [6, 108-111].

2.3.2.1. Prodrugs

Lipid solubility of a drug is one of the key factors in regulating its passive diffusion into the brain [64], so a facile transport of a passive molecule has been associated with an increase in its lipophilicity. Most drugs used to treat CNS diseases are small molecules ranging between 150 and 500 Da and express the log octanol/water partition coefficient between 0.5 and 6.0 [112]. In contrast, molecules that have permanent charges or are polar or highly branched and contain rotating bonds have been found to exhibit a lower BBB penetration [68].

The prodrug approach for brain delivery involves the administration of a drug that has had its lipophilicity increased through a chemical modification, so it becomes more able to penetrate the BBB. The prodrug is then converted within the brain into its active form [113].

This ‘lipid penetration’ approach can be classically illustrated with a series of related compounds such as morphine, codeine and heroin [64] Morphine shows a relatively low brain uptake, but by replacing one of hydroxyl groups with methoxy (to obtain codeine) the lipid solubility is increased, and significantly increases in turn the brain uptake *(Figure 2.10)*. Further lipidisation by adding two acetyl groups to the molecule of morphine to form heroin increases the brain uptake significantly. Inside the brain, heroin is rapidly metabolised to 6-acetyl-morphine and then to morphine. Morphine, being a more polar molecule than heroin, becomes locked inside the brain as it cannot diffuse back into the blood through the BBB [114].

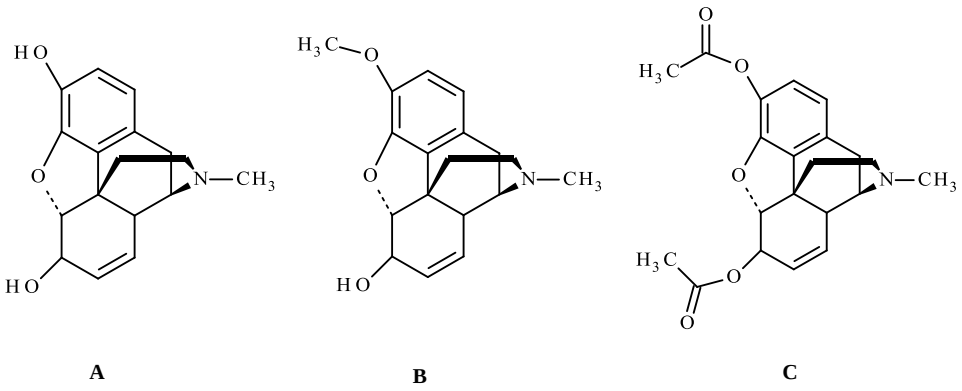

*Figure. 2.10. Structures of **A** - morphine, **B** - codeine, and **C** - heroin*

The advantage of the lock-in mechanism is that an active metabolite can retain significant concentrations of parent compound in blood stream. A drug can be simply attached to a vector, which may simply increase the lipid solubility of the drug or may render the drug acceptable for BBB transport system. The linkage between drug and vector should be labile once the drug has penetrated into the brain, such as an ester bond [112]. This extension of the prodrug principle has been termed as chemical delivery [68]. However, despite advantages this approach has also several limitations; lipidisation of molecules generally increases the distribution volume, especially plasma protein binding, which affects all pharmacokinetic parameters. While increased lipophilicity can improve diffusion transport across the BBB, it also may affect the uptake in other tissues [64].

2.3.2.2. Colloidal drug delivery systems

More recent approaches that have been considered for drug delivery to the brain employ colloidal systems such as nanoparticles and liposomes [6, 109-111]. Nanoparticles are colloidal particles consisting of macromolecular substances that vary in size from 10 nm to 1000 nm [41, 115]. Other drug delivery devices in the submicron range are liposomes [116], exosomes [117], solid lipid nanoparticles [118], polymeric micelles [119] and dendrimers [120].

Colloidal drug delivery systems can potentially possess outstanding advantages [121]: 1) the passage through the smallest capillary vessels due to their small size 2) the penetration of the cells and tissues and targeted delivery to organs such as liver, spleen or lung; 3) controlled-release properties due to the biodegradability, pH, ion and/or temperature sensibility 4) improved stability of drugs and reduced toxic side effects. An ideal colloidal drug delivery system is expected to possess specific features such as being non-toxic, non-immunogenic, biodegradable and biocompatible, and also being stable in the blood thus ensuring a prolonged circulation time. In case of brain drug delivery the colloidal drug delivery system is expected to express BBB targeting or BBB penetrating moieties and to carry therapeutic molecules [36, 108].

2.3.2.3.Nanoparticles

There are several approaches considered in order to enhance nanoparticle crossing the BBB. One of the well-studied methods involves coating nanoparticles with Polysorbate 80. It was shown that nanoparticles from poly(butylcyanoacrylate) (PBCA), coated with Polysorbate 80 delivered drugs into the brain [5, 109, 110, 122, 123]. Several interpretations of the mechanism of nanoparticle translocation across the BBB were suggested [122], such as: an increased flux of nanoparticles due to the concentration gradient; inhibition of P-glycoprotein by Polysorbate 80; a general toxic effect of nanoparticles on the endothelial cells [6]; endocytosis of nanoparticles; or, most probable, the apolipoproteins present in the blood were adsorbed onto these nanoparticles due to their coating with surfactant [124, 125]. Since the

Polysorbate 80 coated nanoparticles were shown to adsorb apolipoproteins A-I, E and B from blood, the following scenario was suggested [110]: after injection, the coated nanoparticles adsorb apolipoproteins A-I, E and B from the blood; in case of apolipoproteins E and B, the particles could mimic lipoprotein particles and would be taken up by the brain endothelial cells that express numerous endothelial receptors for apolipoprotein endocytosis, so in this case nanoparticles behave as 'Trojan Horses' [126]. This whole hypothesis is supported by finding that a covalent attachment of apolipoproteins A-I, E and B to drug loperamide makes the drug active in the brain while the free drug was found to exhibit no effect [64, 110, 127]. Polysorbate 80 was applied on other kind of nanoparticles; poly(lactic-*co*-glycolic acid) PLGA nanoparticles coated with Polysorbate 80 were found to perform best during *in vivo* studies that compared various nanoparticles coatings for brain drug delivery applications (*Figure 2.11.)*[128].

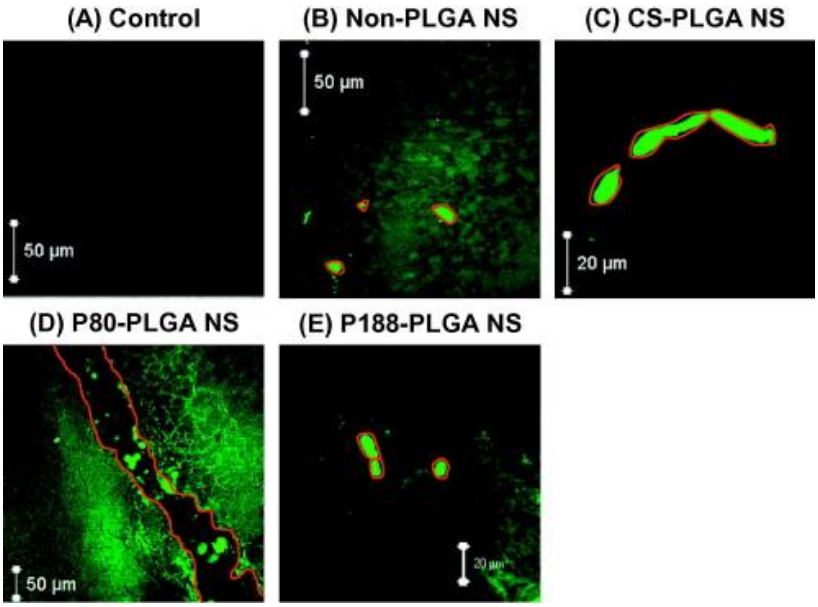

Figure 2.11. Nanoparticles from PLGA loaded with Fluorescein and taken up into the brain in vivo. The influence of surfactant coating: a) no nanoparticles; b) no coating; c) chitosan; d) Polysorbate 80; e) Poloxamer 188. Adapted from [128].

Other attempts to employ colloidal drug delivery systems for drug delivery to the brain include alkylglyceryl-chitosan based nanoparticles [129], poly(ε-caprolactone)-poly(ethylene glycol) nanoparticles [130], poly(acrylamide)-poly(ethylene glycol) nanoparticles [131] or liposomal formulations [132, 133] and those modified with cell permeating protein TAT [134].

2.3.2.4. Liposomes and solid lipid nanoparticles

Bilayer phospholipid systems, called liposomes, were first described in 1965 [135]. They are small artificial vesicles of usually spherical shape that can be produced from non-toxic natural phospholipids and cholesterols [116]. Drug molecules can be either entrapped in the aqueous space or intercalated within the lipid bilayer of liposomes, depending on the physiochemical characteristic of the drug *(Figure 2.12.).*

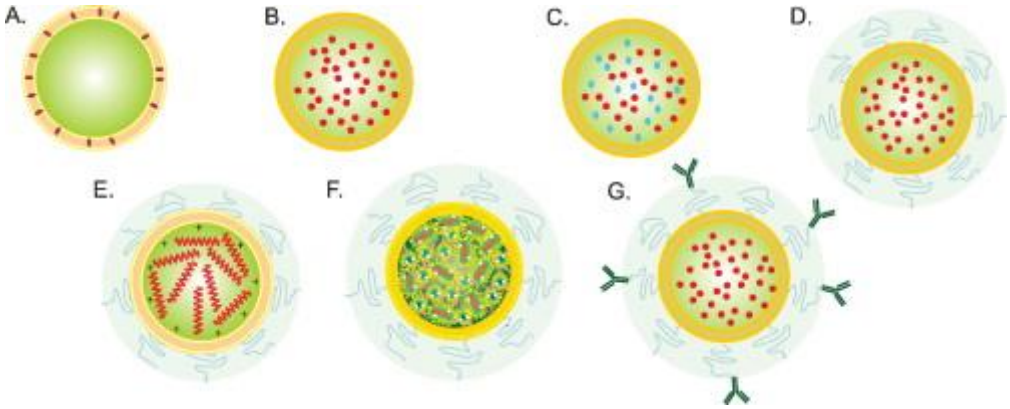

Figure 2.12. Liposomal drug delivery systems: a) drug entrapped into the phospholipid bilayer; b) drug entrapped into the core; c) combination of drugs; d) long circulating liposomes, e) liposomes containing nucleic acid, f) triggered release liposomes, g) ligand-targeted liposomes; adopted from [136].

The properties of liposomes vary with lipid composition, size, surface charge and method of preparation. Liposomes are classified by the number of layers into unilamellar or multilamellar systems [136]. Early liposomes were designed as carriers that hold the drug inside their hydrophilic core or within the hydrophobic phospholipid bilayer coat. Using monosialoganglioside in the structure of the liposomal bilayer (”Stealth” liposomes; Trademark of Sequss Pharmaceuticals Inc, Menlo Park, CA [137]) has been shown to contribute to the avoidance of the Reticulo-endothelial system (RES). A similar effect of extending the circulation time of liposomes was also obtained by incorporating distearoylphosphatidylcholine in the liposomal bilayer for the delivery of Daunorubicine (DaunoXome by NexStar Inc, San Dimas, CA) or by employing hydrophilic poly(ethylene glycol) (PEG) chains [138, 139].

Liposomes have been employed in brain drug delivery in various applications, such as for targeting neutrophils and monocytes to facilitate the transport of serotonin over the BBB [140], by conjugation with antibodies [133], or using convection-enhanced delivery to transport contrast agents for magnetic resonance imaging in the brain of primates [83, 141]. The liposomes were found as a potentially promising tool for brain drug delivery [36, 140, 142, 143].

Solid lipid nanoparticles are colloidal drug delivery systems with a mean size between 100 and 400 nm, with a matrix composed of lipids being solid at room and body temperatures, dispersed in an aqueous surfactant solution [144]. The solid lipid nanoparticles consist of triglycerides (*e.g.* trimyristin, tripalmitin), hard fat molecules (*e.g.* glyceryl stearate, cetyl palmitate, decanoic acid) and emulsifiers (*e.g.* soy or egg lecithin, phosphatidylcholine or Poloxamers) [145, 146]. Solid lipid nanoparticles recently gained attention for brain drug delivery purposes [118]. Some of the long circulating formulations are established on the marked as PEG modified solid lipid nanoparticles containing Doxorubicin (Doxil brand name, Trademark of Sequss Pharmaceuticals Inc, Menlo Park, CA [137]).

2.4. Challenges faced by colloidal systems aimed at drug delivery to the brain

When administered intravenously, colloidal systems face several challenges in the body; being removed by the Reticulo Endothelial System (RES, based in lungs, spleen, liver and lymphatic nodes), being filtered in the kidneys, or reacting with the immune system are among the most important [147]. Even after managing to overcome the general difficulties faced in the bloodstream, a drug delivery system can still be stopped by the Blood Brain Barrier from entering the internal brain compartment [122]. The RES which is responsible for the “first pass effect” [148], is a part of the immune system occurring in blood providing natural defence for organism, consists of phagocytotic cells (monocytes and macrophages, Kupfer cells and histiocytes) in various tissues (in lymph nodes, in liver, spleen and lungs). RES can remove

malfunctioning or damaged circulating cells as erythrocytes and lymphocytes, but also invading bacteria, toxins, xenobiotics and nanoparticles [41]. The phagocytotic process is modulated by opsonisation – a process, which is described as adsorption of proteins (immunoglobulins and antibodies, namely C3 and C5 components of complement, fibronectin, C-reactive protein and tuftsin) on the surface of cells or nanoparticles, making these objects more recognisable for the RES [149].

The strategy of avoiding RES consists mainly of surface modifications of nanoparticles [150], however in the 1980's and 1990's placebo pre-dosing of empty nanocarriers was employed to saturate the RES phagocyting capacity [151]. Moreover, attempts at RES moderation were performed by transient destruction of macrophages in the liver by administration of gadolinium chloride [152] or clodronate entrapped inside liposomes [153]. Such approaches, despite success in experimental models, found no justification in clinical practise due to impairing the natural defensive system of the body [150]. The PEG corona at the surface of PLA nanoparticles was shown to reduce non-specific interaction with blood elements [154]. Similar results were obtained with poly(acryl amide), polyvinylpyrrolidone, poly(acryloyl morpholine) [155]. Also, employment of polysaccharides as dextran [156, 157] or hyaluronic acid [158] was investigated as a protection against protein adsorption and possible avoidance of RES uptake. Furthermore, surface modification with PEG chains can be combined with targeting moieties, *e.g.* nanoparticles from hydrophobic poly(lactic acid) (PLA) crosslinked with PEG attached to monoclonal antibody against transferrin receptor MAb OX26 [159].

Once the Drug Delivery System is designed to overcome the RES, the challenge of reaching the brain parenchyma remains the primary task [41]. After the nanoparticles overcome last 20-30 nm of BBB, they became diluted in Cerebrospinal fluid (CSF, 5 litres of blood to 150 mL of CSF) which is the maintenance liquid for the brain. It keeps the homeostasis, ions and nutrients in balance necessary for precise function of neurons [3]. The pressure of CSF can drift nanoparticles back to blood as CSF flows from ventricles, where it is produced, across *cisterna* and through *arachnoidal villi* to blood microvasculature due to higher pressure than blood [19].

The turnover of total volume of CSF is 3–4 times per day and it can be considered as one mechanism of NPs clearance from the brain [41].

2.5. Polymeric materials for nanoparticle preparation

Polymers employed in the preparation of nanoparticles have to be non-toxic, non-immunogenic, biodegradable and biocompatible [108]. Such features can be exhibited by both natural and synthetic polymers [160, 110]. Materials such as dextran, chitosan and poly(lactic acid) - which have been selected for this study due to their adequate properties for the application considered - will be described below in more detail.

2.5.1. Chitosan

Polysaccharides, a heterogeneous group of polymers with a wide range of molecular weights and varying reactive groups and chemical composition [161], can be sourced from various origins e.g., algal, such as alginate [162]; microbial, such as dextran [163]; from plants, such as pectin or guar gum or pullulan [164]; or from animals chitosan [165], hyaluronan [166] and chondroitin [167].

Chitosan (CS) can be obtained from the deacetylation of chitin, a naturally occurring (mainly in marine crustaceans) and biocompatible polysaccharide [165]. Chemically, chitosan comprises of a 2-acetamido-2-deoxy-β-D-glucan (1→4) linked to 2-amino-2-deoxy-β-D-glucan *(Figure 2.13.).*

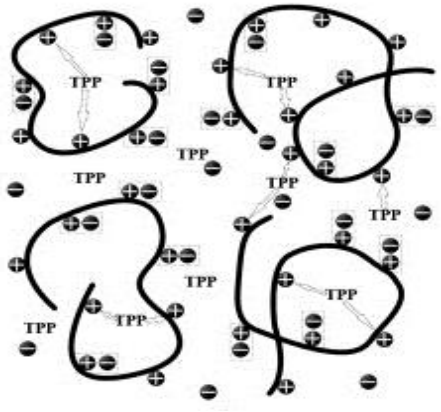

Figure 2.13. Schematic presentation of chitosan nanoparticles cross-linked with TPP. Adopted from [436].

Chitosan has been investigated as a biopolymer suitable for drug delivery and biomedical applications [165, 168], as well as for cosmetics, food industry and agriculture [169]. Nanoparticles from chitosan can be prepared by covalent crosslinking with glutyraldehyde however this approach is associated with increased toxicity [161, 170]. Chitosan bears positive charges in acidic environments due to the amino groups, which can be protonated and generate electrostatic complexes with polyanions to create nanoparticles (*Figure 2.13*). The counter ions employed for ionotropic crosslinking can be Sodium Tripolyphosphate (TPP) [171-175], Dextran Sulphate (DEX-S) [176-181] or BSA-conjugated Dextran [182]. Moreover, chitosan can be conjugated or modified chemically with other polymers to produce nanoparticles (*e.g* nanoparticles prepared by linking CS with PLGA [183] or with PLA [184-187] or with PEG [188]). In some cases, chitosan was used to coat nanoparticles from various materials such as PLGA [128, 189].

Chitosan is considered a good candidate for brain drug delivery systems as it has been suggested it can open tight junctions [190]. Also, nanoparticles from modified chitosan have been studied for drug delivery to the brain (such as alkylglyceryl chitosan croslinked with TPP [129, 173], trimethylchitosan-PLGA conjugate for Coenzyme Q_{10} delivery [191]; chitosan-based nanoparticles were also studied for intranasal delivery of dopamine [192], venlafaxine [193], rivastigmine [194] or estradiol [195].

In many cases, nanoparticles prepared from chitosan were found to exhibit suitable features for drug delivery under preparation conditions (i.e. acidic pH), however the transfer of nanoparticles to physiological pH has been shown to be accompanied by increase in nanoparticle size and agglomeration [173, 196, 197]. Perhaps it is for this reason that many reports do not state the dimensions of nanoparticles at neutral pH. Also there exists controversy about the non-toxicity of chitosan on one hand [129, 196, 198] versus reports about the toxicity of nanoparticles from chitosan on the other [199, 200]. Due to the toxicity some authors suggest, chitosan should not be used in *parenteral* applications but only in *per oral* formulations [201].

2.5.2. Dextran

Dextran is an extracellular polysaccharide produced by bacteria of *Leuconostoc, Streptoccocus Lactobacillus, Rhizopus* species [202, 203] *(Figure 2.14.)*. The polymer consists of main α (1->6) glucan polysaccharide backbone with side branching chains α (1->3). Approximate degree of branching was estimated about 5 % [203].

In 1861 Pasteur observed the formation of dextran in wine; its name was given by Scheibler, in 1874, who demonstrated that dextran is a carbohydrate with a positive optical rotation [204]. It was found latter, in 1941, that the *Leuconostoc* extracts had the ability to synthesise dextran [203], and the enzyme responsible for the biosynthesis of dextran was identified as Dextransucrase (1,6-α-D-glucan-6-α-glucosyl transferase, EC. 2.4.1.5). Dextran can be easily degraded by the enzyme Dextranase (o-1,6-D-glucan-6-glucanohydrolase, E.C.3.2.1.11.) [205].

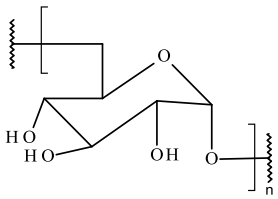

Figure 2.14. Chemical structure of dextran.

Dextran was recognised as a useful polymer in medicinal applications when Gronwall and Ingelman used dextran in 1947 to cure shock in their patients [206, 207]. Since then, it has been employed as a plasma-expander in emergency cases when there was not enough quantity of blood available [208, 209]; more recently, dextran was approved by FDA as a plasma volume substitute [210]. The molecular weight of natural dextran ranges from 12 kDa to 600 000 kDa [211], however for medicinal purposes lower molecular weight fragments are used [212]. The first production was established with *Leuconostoc mesenteroides* strand 7E, however in 1951 the production was switched to strand B-512F (isolated from a bottle of infected root beer),

[213]. Interestingly, Dextran caused reversible red blood cells aggregation in concentrations above 2g/100 mL of blood and in range of high molecular weights (70 kDa - 28 000 kDa) [214]. Although the optimal properties were found in Dextran Mw < 25 kDa, Dextran 40 was selected with respect to renal excretion of small molecules [215]. Dextran was linked to haemoglobin to serve as plasma expander and oxygen transporter as well. This construct was causing hyperaggregation however such phenomenon was not found harmful and the aggregation was a reversible process [216].

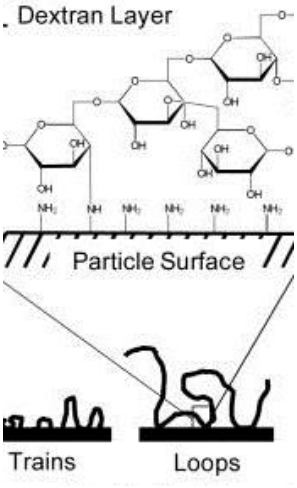

Figure 2.15. Organisation of modified dextran chains on the surface of silica particles. Adapted from [217].

Dextran was also investigated for use in various drug delivery systems: Dextran based polymethacrylate derivatives were found as biocompatible *in vivo* [218]. Polyvinyl co-polymers of Dextran were formulated by nanoprecipitation into nanoparticles in range of diameters 100-200 nm [219]. Dextran, as a polysaccharide coating, provided prolonged circulation times to nanoparticles from PBCA when compared to uncoated nanoparticles [220]. Moreover, nanoparticles with corona from Dextran of various molecular weights attached to the core of PBCA polymer were investigated for interaction with plasma proteins. The study revealed that certain composition of dextran chains (associated to high molecular weight) on the surface of nanoparticles was activating complement component C3 to C3b more than low molecular weight Dextran *(Figure 2.15.)* [221]. Apparently, long chains were bound to the surface of PBCA nanoparticles in form of “loops” and “trains” whereas short chains appeared to be in

"brush-like" formation, leaving poor accessibility of OH groups. Moreover, a similar study compared dextran and PEO in activity towards restricting opsonisation of particles by blood proteins [222]. It was found that a specifically side-on grafted dextran onto the nanoparticle surface was as active as PEO in preventing fibrinogen adsorption.

In vivo experiments showed the capability of dextran and heparin surface coverage to prolong the circulation of poly(methylmethacrylate) (PMMA) nanoparticles: both polysaccharides on the surface of nanoparticles provided long circulation times (still detectable after 48 hours) however bare PMMA nanoparticles were found to have a half-life of only 3 min. Indeed, the dextran or heparin modifications of PMMA nanoparticles appeared as weak complement activators when compared to crosslinked dextran (Sephadex) or bare PMMA nanoparticles [223]. Also, dextran was investigated as protection against protein adsorption and possible avoidance of RES uptake [156, 157]. Controversially, several studies showed no capability to reduce protein adsorption (BSA and fibrinogen) by dextran or PEO when grafted onto polydimethylsiloxane surfaces [224]. Furthermore, in a different study the dextran was found less active than PEO in repelling BSA when grafted onto a silica surface [217]. BSA was selected as a model protein in studies mentioned above, because it can take part in classical C3 complement activation pathway by binding in complex BSA/anti BSA to erythrocytes [225].

2.5.3. Poly(lactic acid)

Poly(lactic acid) acid (PLA) is known as a material with good biocompatibility and biodegradability [226, 227], though a drawback of this polymer could be the lack of moieties that would allow easy functionalisation. A modification of PLA can take part at the carboxylic end [228], or another promising approach could be radical grafting. Grafted PLA could be then substituted with an active [229-231] or cross-linked with another polymer [232].

Poly(lactic acid) can be prepared by ring opening polymerisation of lactide [233] *(Figure 2.16.)*. Since the monomer is a chiral molecule, the product may be obtained as L, D or in a meso form [234]. Degradation of PLA occurs by autocatalytic cleavage of the ester bonds

and can further continue to Krebs´ cycle, where it can be finally degraded to water and CO_2 [235]. When used for nanoparticle preparation, the PLA-based products are reported to be stable both in fridge (4°C) and at room temperature (20°C) for weeks. However, at body temperature their decomposition occurs in days [236]; the process is size dependent as structures larger than 10 μm took longer time to decompose in human body as particles of this size cannot be phagocytosed [237].

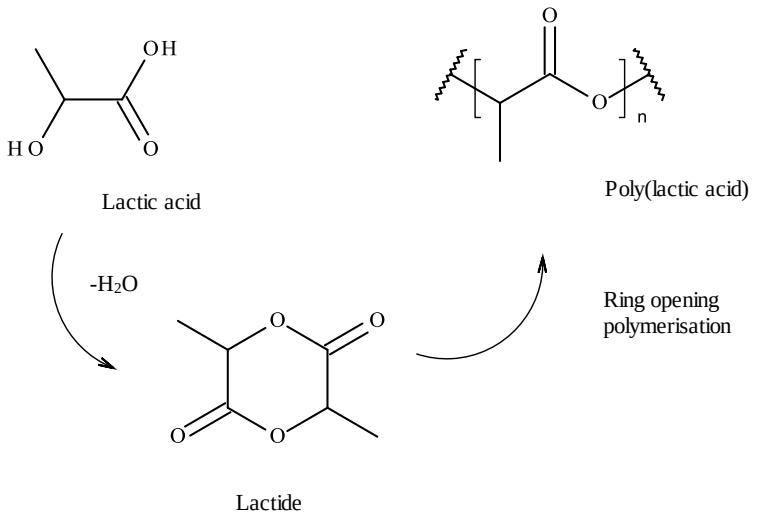

Figure 2.16. Preparation of poly(lactic acid) by ring opening polymerisation [233].

PLA has been known to form small size nanoparticles with a low polydispersity index [238], with many applications in drug delivery being investigated [239-244]. Methods for preparing PLA-based nanoparticles include nanoprecipitation (a key technique described by Fessi [245]), emulsification-evaporation process [246] and solvent displacement process *via* dialysis (discussed in Chapter 2.6. [247]).

Following intravenous application, nanoparticles of bare PLA have been found to be rapidly removed from the blood stream by macrophages by phagocytosis; the blood half-lives were between 2 and 3 min [248]. To avoid this, hydrophilic coatings by covalent binding of poly(ethylene glycol) (PEG) have been used, and were found to reduce opsonisation and phagocytosis [64, 249, 250]. PLA-PEG copolymers were used in combination with chitosan films for buccal delivery of insulin [246]. Connecting PLA to dextran yielded copolymers that

could be formulated into nanoparticles exhibiting core-shell properties [220, 251-254]. As a biocompatible polymer, PLA has been also investigated for use in implants [255] or as tissue scaffolds [256].

2.6. Methods for preparation of nanoparticles

Nanoparticles can be prepared from various types of polymers. The main methods to prepared nanoparticles from prefabricated biodegradable polymers include: nanoprecipitation; solvent displacement *via* dialysis; emulsification; electrospraying; and electrostatic complexation. Other methods include salting [257, 258], supercritical fluid technology [259, 260] and desolvation method [261, 262]. Nanoparticles can be prepared also by polymerisation of monomers, e.g. emulsion polymerisation in water, a method that requires a poorly water-soluble monomer, water soluble initiator and a surfactant [263-265].The removal of the surfactant is sometimes a difficult step in the preparation process, therefore surfactant-free polymerisation is receiving more attention [266, 267]. Other polymerisation methods include mini-emulsion polymerisation [268], interfacial polymerisation [269] and controlled/living polymerisation [270]. When required, drug loading into/onto nanoparticles can be accomplished by absorption, adsorption, or encapsulation [271].

2.6.1. Nanoprecipitation

An easy and rapid way to obtain small nanoparticles is the interfacial solvent displacement, also known as nanoprecipitation and described by Fessi [245]. A polymer (plus a drug or other molecule to be loaded) dissolved in a low boiling point solvent (usually acetone, though other organic solvents can be used as well) is added dropwise to a non-solvent which is miscible with the solvent. This operation usually takes place at room temperature under moderate stirring. The mechanism of nanoparticle formation *via* nanoprecipitation can be imagined as the nucleation of small aggregates of macromolecules followed by aggregation of

these nuclei. The process stops at the moment of reaching the colloidal stability [310]. Solvent diffuses deep into the non-solvent, leaving the polymer and drug in form of a nanoparticle *(Figure 2.17.)*. The rest of solvent is evaporated under reduced pressure, and the nanoparticles can be separated by centrifugation [272]. The size of the resulting nanoparticles can be influenced by the choice of solvent/non-solvent system, namely by the miscibility of the two phases and the interaction parameter χ expressing the affinity of solvent and non-solvent [276], the concentration, the viscosity and the dielectric constant), by the dropping rate of the solvent, the speed of stirring, or the presence and concentration of a surfactant in the non-solvent phase (polyvinyl alcohol, Poloxamer 188, Polysorbate 80) [273].

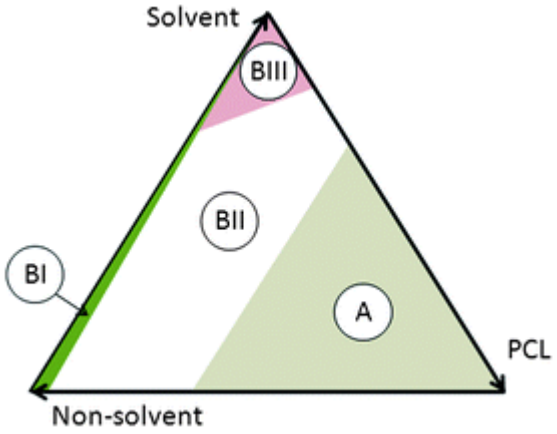

Figure 2.17. Ternary phase diagram of PCL in solvent/non-solvent system: the region of insolubility A, the area of flocculation BII, the area of nanoprecipitation BI and they are of dissolution of PCL BIII. Adopted from [310]

Nanoprecipitation is used widely to produce nanoparticles from polyesters (poly(lactic acid) [245], dextran-polylactide copolymers [163, 251], poly(lactic-co-glycolic acid)), cellulose derivatives [274], cyanoacrylates [275] or poly (ε-caprolactone) [276]. Due to the nature of solvent/non solvent system, the method is suitable for entrapment of hydrophobic drugs, however it can be been modified to entrap hydrophilic molecules as well [276].

2.6.2. Solvent displacement *via* dialysis

In the dialysis method, the polymer is dissolved in an organic solvent and placed inside a dialysing tube. Dialysis is performed against environment, which is miscible with the solvent but it acts as a non-solvent for the polymer. The displacement of the solvent inside the membrane is followed by progressive rearrangement of the polymer chains as a result of an increasingly limited solubility and ultimately by the formation of nanoparticles *(Figure 2.18.)*. Though the mechanism has not been fully elucidated yet, it may be similar to nanoprecipitation [263]. Detailed investigations suggested that the formation of nanoparticles could be divided into three steps: (1) aggregation – individual polymeric chains start binding to each other in solution; (2) formation of polymeric particles; (3) solidification of nanoparticles [277].

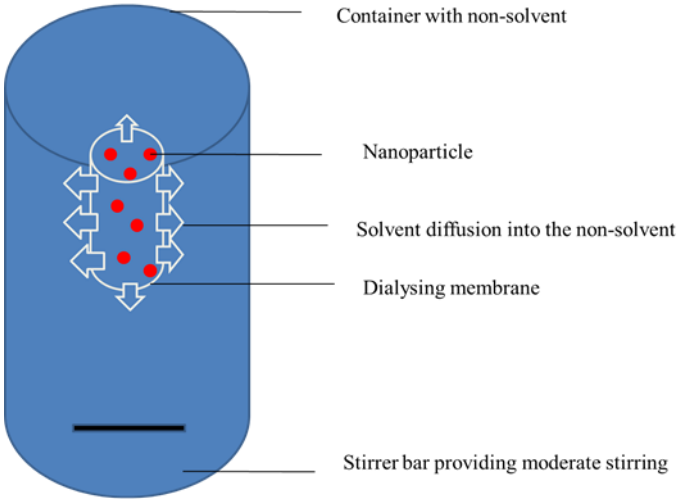

Figure 2.18. Schematic representation of the solvent displacement (dialysis) method

The dialysis is a suitable method for preparation of nanoparticles from various polymers including PLA or PLGA and is very useful for copolymers that are soluble only in solvents with high boiling point (*e.g.* dimethyl sulfoxide, dimethylformamide or dimethylacetamide). Nanoparticles from PLA [277], PLGA-PEG [278], PLA-DEX [252], PCL[279], poly(*N*-isopropylacrylamide)-*graft*-poly(ethylene oxide) [280] were prepared *via* dialysing method.

2.6.3. Emulsification-evaporation and double emulsification

Emulsification allows encapsulation of lipophilic substances [281, 282] and involves two phases: organic and aqueous. For the nanoencapsulation of a lipophilic active, the organic phase contains the polymer, the active and an organic solvent (which is partially miscible with water). This organic medium acts as a solvent for the different components of the organic phase. The aqueous phase comprises of the aqueous dispersion with a stabilizing agent while the dilution phase is usually water [282]. Ethyl acetate is the organic solvent of choice, though propylene carbonate, benzyl alcohol and dichloromethane can also be used. Suitable polymers are polyesters (especially PLA and PLGA) or their copolymers (such as PLA-PEG) [283]. Polyvinyl alcohol (PVA) is usually employed as a surfactant in the water phase [242]. The mechanism of formation comprises of two steps: emulsification and evaporation. The size of the particles is determined by the first step [284]. The theory indicates that each emulsion droplet produces several nanocapsules and that these are formed by the combination of polymer precipitation and interfacial phenomena during solvent diffusion [285]. The solvent is evaporated after this step.

Double emulsions are “emulsions of emulsions”, and allow encapsulation of both hydrophilic and lipophilic substances [282]. These systems can be either water-oil-water emulsion (w/o/w) or oil-water-oil emulsion (o/w/o) [281]. Double emulsions are usually prepared in a two-step emulsification process using two surfactants: a hydrophobic one designed to stabilize the interface of the w/o internal emulsion and a hydrophilic one to stabilize the external interface of the oil globules for w/o/w emulsions. The mechanisms of formation of nanoparticles are associated with both nanoprecipitation and emulsification-diffusion principles [286]. During a typical procedure of double emulsification, the primary emulsion is formed by ultrasound and the w/o surfactant stabilizes the interface of the w/o internal emulsion. The second emulsion is also formed by ultrasound and nanocapsule dispersion is stabilized by the addition of the stabilizing agent. Finally, the solvents are removed by evaporation or extraction by vacuum, leaving hardened nanocapsules in an aqueous medium *(Figure 2.19.)* [282].

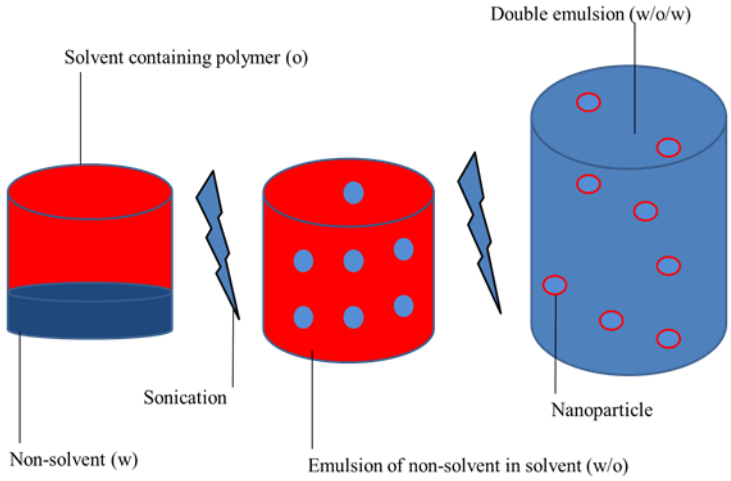

Figure 2.19 . Schematic representation of the double emulsion/evaporation method.

A study using poly(caprolactone) as a model polymer investigated the influence of the preparation method (nanoprecipitation and emulsion evaporation) in terms of characteristics of the resulting colloidal system. It was discovered that the nanoprecipitation produced smaller nanoparticles than emulsification. Moreover, zeta potential and drug release from nanoparticles was influenced by the method [273].

2.6.4. Electrospraying

Electrohydrodynamic atomisation (or electrospraying) is a method, which uses electric forces for producing nanoparticles *via* fluid atomisation [287, 288]. Compared with traditional emulsion fabrication techniques, electrospraying has the potential to reduce denaturation of proteins, and it can afford tight regulation over particle size distribution and morphology [289]. In the process of electrospraying, the liquid at the outlet of a nozzle is subjected to an electrical shear stress by the high electric potential of the nozzle *(Figure 2.20.)*. A cone shape of the spray is preferred, when the droplets can be extremely small, down to the nanometre range.

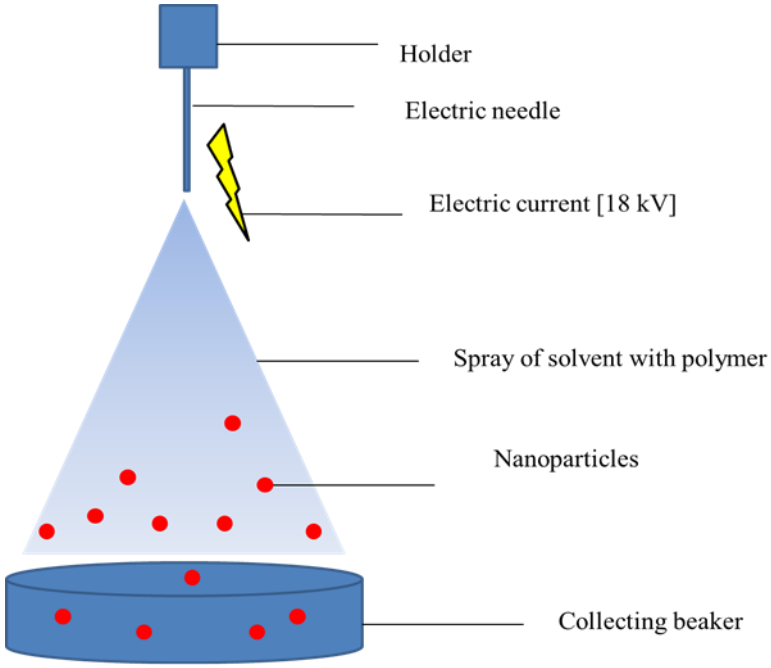

Figure 2.20. Schematic representation of the electrospraying method

The charge and size of the droplets can be controlled by adjusting the flow rate and voltage applied to the nozzle [287]. Electrospraying in the cone-jet mode can be described in three stages: the acceleration of the liquid in the liquid cone; the breakup of the jet into droplets; and the development of the spray after droplet formation [290]. The resulting size distribution of the droplets can be nearly monodisperse. The fact that the droplets are electrically charged facilitates control of their motion in the electric field. Charged droplets are self-dispersing in space incurring no droplet coagulation.

The smallest nanoparticles so far obtained by electrospraying method (the setup was equipped with neutralisation chamber with a radioactive source) were from sucrose (4 nm diameter [291]). There were prepared several formulations for drug delivery purposes *via* the electrospraying method: PCL microparticles loaded with Paclitaxel [292], PLGA nanoparticles (250 nm) loaded with Paclitaxel [293], PLA microparticles containing Paclitaxel [294]

2.6.5. Electrostatic complexation

The method of electrostatic complexation (also known as ionotropic gelation) employs attractive forces of counter ions to crosslink molecules – pectin with magnesium chloride [295] or chitosan with counter-ions as TPP *(Figure 2.13)* [296, 297, 173], dextran sulphate [178, 298] or hyaluronan [299]. The chitosan derivatives are dissolved in a weak acid and added to the counter-ion which is dissolved in aqueous phase where the crosslinking takes part. The molecule to be entrapped should bear a charge to take part directly in the structure of nanoparticles. The release of such molecule from nanoparticles is usually low due to the electrostatic forces, as in case of release of Evans Blue dye from chitosan nanoparticles crosslinked by sodium tripolyphosphate [173].

2.7. Methods for nanoparticle characterisation

The most important physical characteristics of nanoparticles are size, shape and zeta potential. The size and shape of nanoparticles can be visualised directly using scanning electron microscopy (SEM), transmission electron microscopy (TEM) and atomic force microscopy (AFM) [300]. Dynamic light scattering (DLS) and nanoparticle tracking analysis (NTA) can be used to determine the particle diameter by analysing particle Brownian motion in a controlled environment [301, 302]; these methods measure the hydrodynamic diameter in solution. Other methods employed to determine the size of nanoparticles include Analytic centrifugation [303-305] and Scanning ion occlusion spectroscopy (SIOS) [306, 307]. The zeta potential of nanoparticles gives an indication of the stability of a particular colloidal system. Zeta potential is usually calculated from electrophoretic mobility (EPM), which is behaviour of nanoparticles under electric field [308-310]. The current chapter briefly reviews the relevant techniques for characterising nanoparticles employed in this experimental study.

2.7.1. Dynamic light scattering

Particles, emulsions and molecules in suspension move in solution due to the bombardment of the solvent molecules – thermodynamic phenomenon called Brownian motion. When a laser illuminates the particles, the intensity of the scattered light fluctuates in a mode that is dependent on the size of the particle. The smaller particles are moving faster than the large ones. Analysis of the fluctuations of intensity delivers the velocity of the Brownian motion; the size of the particle can be calculated using Einstein-Stokes equation [301]:

$$d = \frac{kT}{3\pi\eta D}$$

where d is the hydrodynamic diameter (in m), k is the Boltzmann constant(J K^{-1}), η is the solvent viscosity(kg s^{-1} m^{-1}) and T is the absolute temperature (K). The Brownian motion is followed as a function of time by irradiating the particles with a laser beam and collecting the scattered light. At certain angle the diffusion of nanoparticles causes rapid changes in intensity signal *(Figure 2.21. A).*

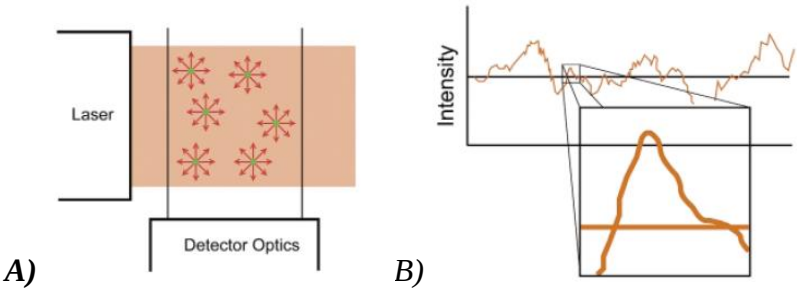

Figure 2.21. Schematic representation of: A) the DLS method (scattering angle 90°); B) non-random intensity signal in a "random" set of data (from [311]).

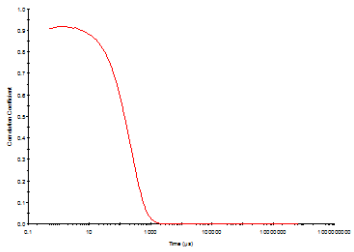

Figure 2.22. Typical correlation function obtained by DLS, represented as correlation coefficient over time.

The correlation of the signal to the time is a statistical technique employed to measure the degree of non-randomness in a "random" set of data *(Figure 2.21. B)*. The correlation coefficient is typically normalised to 1 and develops as a function of time [311]. The endpoint time of the plateau and the decay curve gradient can give an indication of parameters such as particle size and polydispersity *(Figure 2.22.)*. The cumulant fit of the correlation curve is the analysis method recommended by the International Standards Organisation [311]. The hydrodynamic size is calculated by this method as an average value (Z-average), which is weighted by the scattering intensity of the signal of the particle. While the cumulant algorithm and the Z-average are useful for describing general solution characteristics, for multimodal solutions consisting of multiple particle size groups the Z-average value can be misleading (*Figure 2.23.)* [312]. For multimodal solutions, it is more appropriate to fit the correlation curve to a multiple exponential form, using common algorithms such as CONTIN or non-negative least squares [311].

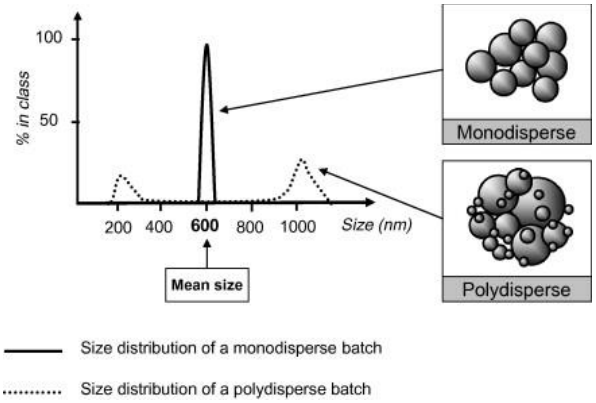

Figure 2.23. Example of DLS results for a polydisperse sample; adapted from [312].

Dynamic Light Scattering is a well-established, rapid and reproducible method that can be successfully employed to determine the size of nanoparticles in uniform samples (when polydispersity index is low). However, in many cases samples exhibit greater polydispersity indexes so the size distribution of such samples determined by DLS is likely to be not entirely accurate (*Figure 2.24.*) and in all cases, the results should be confirmed by another analytical method such as nanoparticle tracking analysis, Atomic force microscopy or Scanning electron microscopy. However, it may be possible that results will be different as each method is based

on a different principle, but by combining several methods a more accurate representation of the true nature of the sample can be obtained [301, 313].

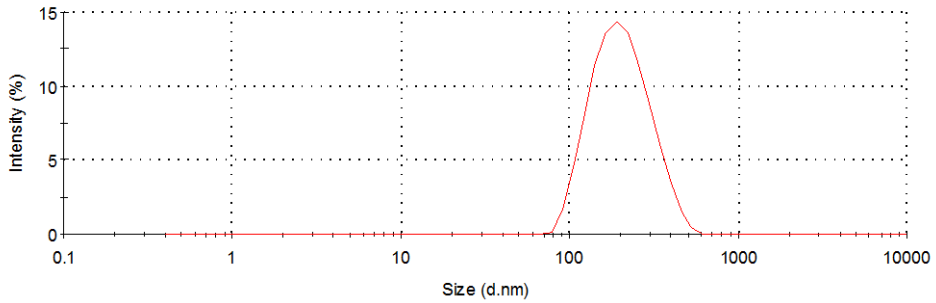

Figure 2.24. Intensity distribution of poly(lactic acid) nanoparticles as measured by a Malvern Nano Zetasizer instrument. The z-average diameter [nm] is displayed on a logarithmic scale.

2.7.2. Nanoparticle tracking analysis

Nanoparticle tracking analysis was developed by Carr et al. who commercialised the method under the Nanosight brand in 2003 [314]. The method allows real time visualization and analysis of nanosized structures in liquids, where the Brownian motion of individual nanoparticles is visualized by laser and tracked/captured (30 fps) by a CCD camera mounted on a microscope *(Figure 2.25.)*.

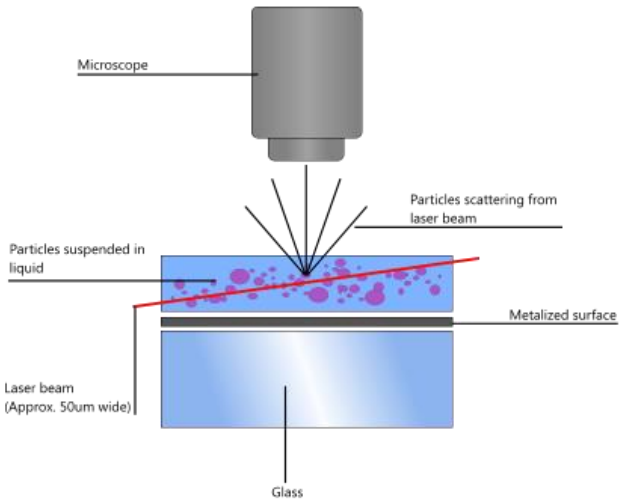

Figure 2.25. Schematic representation of the Nanoparticle Tracking Analysis method [315].

The software analyses the trajectory of each single particle in time and the diameter is calculated from the Einstein-Stokes equation [302]:

$$d = \frac{kT}{3\pi\eta D}$$

where d is the hydrodynamic diameter (in m), k is the Boltzmann constant(J K^{-1}), η is the solvent viscosity(kg s^{-1} m^{-1}) and T is the absolute temperature (K). This formula can be adjusted to obtain the coordinates of a particle in 2D system, as follows:

$$\overline{(x,y)^2} = \frac{2kTt}{3r\eta}$$

where T is the temperature, t is the time (s), k is Boltzmann constant, η is the viscosity of the medium and r is the hydrodynamic radius (m) [301].

As the particle size distribution of a sample presented by NTA is based on measurements of individual particles, the result describes the sample from a different perspective compared to DLS (where the result is expressed as intensity weighted Z-average distribution). Moreover, the different intensities of particles can be seen and total number of particles in sample can be estimated as well *(Figure 2.26.)*. The instrument (Nanosight LM 14) usually uses a single mode diode laser (usually 635 nm or 638 nm, less than 35 mW); the sample cell volume is ca. 250 μL; the magnification of the microscope is 100 *x* [302].

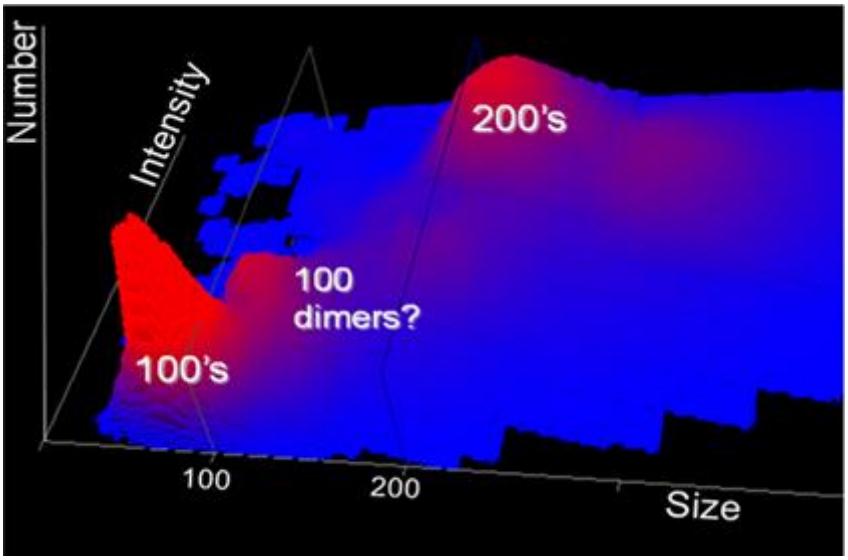

Figure 2.26. 3D projection of nanoparticle distribution. Colour coding is a representation of the ability to distinguish different nanoparticle populations based on size and intensity [315].

NTA seems more suitable for polydisperse samples (usually organic samples, *Figure 2.26.*) than DLS. The NTA method relies on calculations based on movements of individual particles unlike DLS method which fits the data of correlation function to theoretical curves. It is beneficial to employ both methods in parallel to obtain a more realistic picture about a biological sample [301, 302, 316, 317].

2.7.3. Microscopic methods

Nanoparticles are too small to be visualised using normal optical techniques, however this becomes possible by using a beam of electrons (SEM, TEM) or by indirectly imaging by Atomic force microscopy (AFM). These methods allow visualisation of samples *in vacuo* (SEM, TEM) however modifications of traditional SEM (Environmental SEM) and AFM instruments can operate in liquids under certain conditions.

Scanning electron microscopy. The SEM technique was developed in early 1948 by Oatley [318]. A Scanning electron microscope employs a beam of electrons to visualise the surface of a solid sample; the electrons are emitted from a Tungsten cathode (2700 K) and accelerated by an electric field (1-50 kV). The electron beam is scanning the surface line by line

by adjustment of the deflection coils *(Figure 2.27).* Detectors collect X-rays, backscattered electrons, and secondary electrons which are emitted by the sample and convert them into a signal that is sent to a CRT collector, which produces the final image. Data is collected over an area of the surface of the sample, and a two-dimensional image is generated. Magnification ranges from 20X to approximately 30,000X.

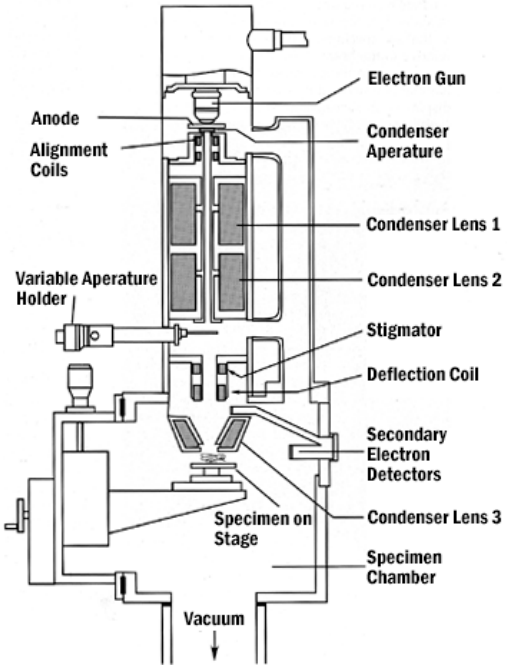

Figure 2.27. Schematic representation of a Scanning Electron Microscope; adopted from [318].

The sample for traditional SEM should exhibit conductive features in order to interfere with the electron beam. All metals are conductive and require no preparation before being used however non-metal samples need to bear a conductive layer. The coating is provided by gold in a sputter coater. The sample is placed in a vacuum under argon atmosphere. An electric field causes an electron to be removed from the argon, making the atoms positively charged. The argon ions then become attracted to a negatively charged gold foil. The argon ions knock gold atoms from the surface of the gold foil. These gold atoms fall and settle onto the surface of the sample producing a thin gold coating [319].

Environmental SEM. The environmental SEM (ESEM) technique allows visualisation of samples without coating, or in a wet state [320]. The water molecules in vapour take part in

secondary electron detection [321]. Recent developments have led to an imaging mode known as "wet-STEM", which allows observations directly in liquid phase. The idea behind was to perform SEM in transmission mode in an environmental SEM [318].

Transmission electron microscopy. Transmission Electron Microscopy (TEM) was developed in 1930's by Ruska, who received a Nobel Prize for his efforts in 1986 [322]. TEM operates on the same principle as a light microscope. Instead of light the TEM employs a beam of electrons which is transmitted through the sample. The electrons interact with the sample as they pass through the sample (not more than 100 nm thick) and the non-scattered electrons hit a fluorescent screen. The final image, after a magnification, can be directly visualised, or captured on a camera.

Atomic force microscopy. Atomic force microscopy (AFM), described for the first time in 1986 by Binning and his group [324], belongs to a group of scanning probing microscopy techniques. AFM can measure local properties of a sample such as height, friction, or magnetism. The method employs a probe, a very thin needle at the end of a cantilever which can monitor the surface of a sample. The changes in position of the cantilever are magnified by a laser beam *(Figure 2.28.)* [325].

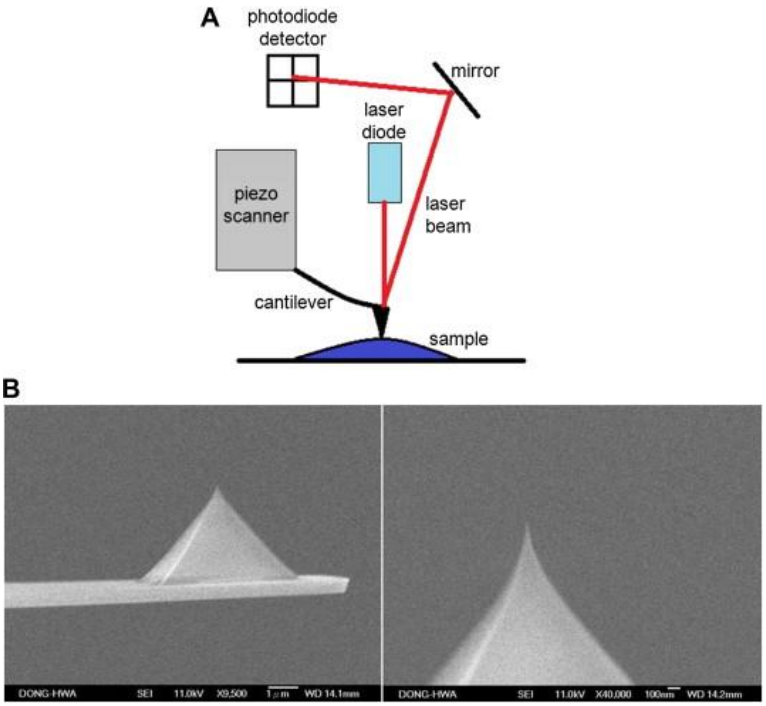

Figure 2.28. ***A:*** *Schematic representation of the AFM technique.* ***B:*** *Detail images of an AFM tip; Adopted from[323].*

AFM operates by measuring force between a probe and the sample. The probe is a sharp tip, which can be 3-6 μm tall pyramid with 15-40 nm radius. The lateral resolution of AFM is low (~30 nm) due to the convolution, the vertical resolution can be up to 0.1 nm [324]. The cantilever reflects off a laser beam which creates an optical lever. The reflected laser beam hits a four segment photo-detector. The differences between the segments of photo-detector indicate the position of the laser spot on the detector and thus the angular deflections of the cantilever [326].

AFM can operate in contact (the cantilever touching the surface) or in non-contact (cantilever oscillates 5-15 nm over the surface) modes. AFM is very sensitive to the intermolecular forces present between the tip and the studied surface; in contact mode the interactions between the probe and sample is repulsive. The drift of the tip across the sample (caused by normal force) creates a substantial friction force, which can damage the sample if the force is not controlled properly. In the non-contact mode the forces between the tip and the sample are repulsive or attractive and depend on the distance [327]. The forces taking part are

weak van der Waals forces or Coulomb and dipole interactions. The changes of forces induce changes in the oscillation pattern of the cantilever. In order to achieve a precise image, the probe needs to be brought in small proximity of the surface of the sample, the tip can slightly touch the surface to become semi-contact (tapping mode) AFM which is a beneficial method for biological samples [323, 327] or rather in combination with other analytic size determining techniques [328].

2.7.4. Scanning ion occlusion spectroscopy

Scanning Ion Occlusion Spectroscopy (SIOS) is technique that employs a permeable elastic membrane that has an adjustable pore [306, 307, 329]. As the sample passes through the pore, there is a linear relationship between the particle volume and electric resistance across the pore [330] *(Figure 2.29.)*. The diameter of nanoparticles is defined according the linear calibration with particles of known sizes. The device demonstrated reliability in comparison with other methods in range 200 -1000 nm [331].

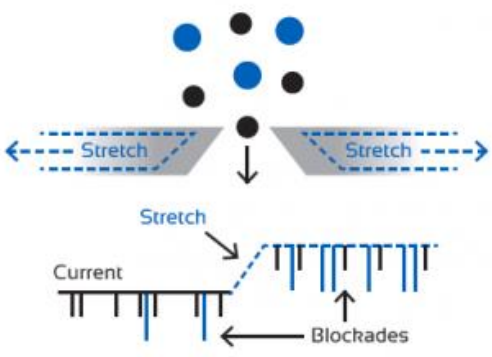

Figure 2.29. Schematic representation of the Scanning Ion Occlusion Spectroscopy, technique; adopted from [330]

.

The pore is precision manufactured into polyurethane membrane. This produces an approximately conically shaped pore with a size that is dependent on the puncturing process. The membrane containing this pore is then sandwiched in a fluid cell in the SIOS device and stretched onto four jaws, which provide stretch in two dimensions in the horizontal plane.

Macroscopic stretching of these jaws produces nanoscopic changes in the pore size (*Figure 2.30.)*. The fluid cell incorporates electrodes, which are used to apply an electric field and to monitor the current produced in the electrolyte solution contained in the fluid cell. A change in the pore size is then detected as a change in the base current level, while the passage of suspended particles through the pore is detected as a momentary drop in the measured current (a 'blockade'). A count of these blockades in a measured time gives the particle count rate [331].

Scanning Ion Occlusion Spectroscopy instruments - commercialised under the Izon brand) is able to measure the diameter and zeta potential of individual particles [332, 333] *(Figure 2.30.).* The flow of nanoparticles through the pores is influenced by various forces: hydrodynamic, electro-osmotic and electrophoretic. Individual forces can be distinguished and thus the electrophoretic mobility can be derived through single particle movement as well.

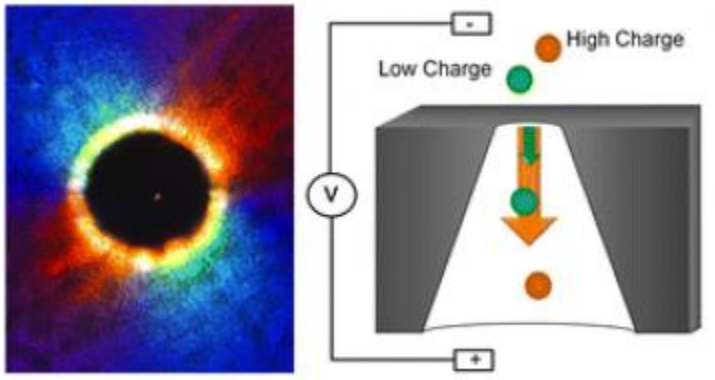

Figure 2.30. Scanning Ion Occlusion Spectroscopy combined with zeta potential measurements: ***A)*** *particle in transit through the pore* ***B)*** *individual particle measurement` adapted from [332].*

2.7.5. Zeta potential measurements

Zeta potential is a measure of the electrokinetic potential in a colloidal system. As an application of the DVLO theory the Zeta potential is an indicator of the stability of a dispersed system against aggregation [334]. The environment surrounding the particle exists as two layers; an inner region (Stern layer, *Figure 2.31.)* where the ions are strongly bound and an outer (diffuse) region where the ions are looser. When a particle moves in a liquid environment, ions within the Stern layer are associated and move as well; however ions in diffuse layer do not

travel with the particle. The electric potential at this boundary, also called the surface of hydrodynamic shear, is defined as the zeta potential. Particles with a high zeta potential of the same charge, will repel each other. Conventionally a high zeta potential is considered in absolute sense (-30mV and +30mV). The high value indicates stability of the dispersive system against aggregation. Additionally, in some cases the system can be stable not because of charge related repulsion forces but because of steric conformation on the surface of the particles, *e.g.* PEG chains [246, 335, 336] or polysaccharides [309].

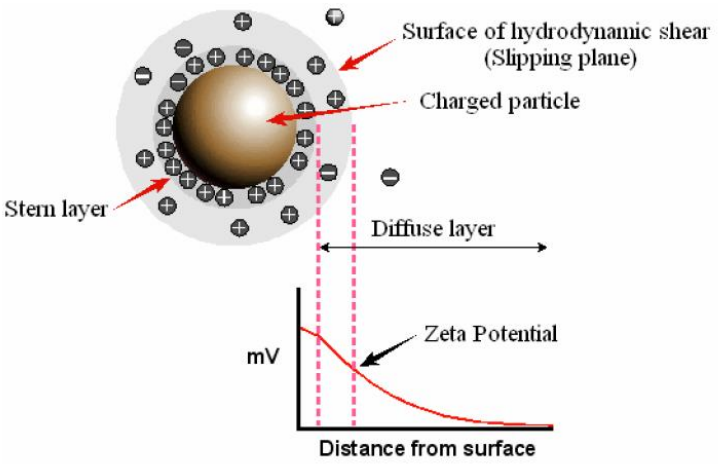

Figure 2.31. Schematic representation of the diffuse layer and the charge variability in the space around individual nanoparticles. Adapted from [337].

Laser Doppler electrophoresis is also known as laser Doppler velocimetry. An electric field is applied across a sample in solution, causing charged particles to migrate toward the poles of opposite charge. Light scattered from these particles will be Doppler or frequency shifted, with the magnitude of the Doppler shift being dependent upon the particle surface charge. A laser beam is passed through the sample in the capillary cell undergoing electrophoresis and the scattered light from the moving particles is frequency shifted:

$$\Delta f = 2v \sin\left(\frac{\theta}{2}\right)\lambda^{-1}$$

Δf	*frequency shift (Hz)*
V	*the particle velocity (cm.s^{-1})*
λ	*laser wavelength (nm)*
θ	*scattering angle (^{o})*

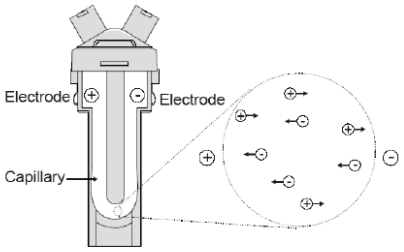

Figure 2.32. Longitudinal section in a Malvern folded-capillary cuvette [337].

Henry's function for aqueous media with moderate electrolyte concentration has a value of 1.5 (Smoluchowski approximation) when the particles are larger than 0.2 μm and the electrolyte concentration is higher than 10^{-3} M. For small particles with low dielectric constant and in non-aqueous solutions, F(*ka*) is 1 (Huckel approximation) [334]. Zeta potential is related to the electrophoretic mobility, according to Henry's equation:

$$U_e \frac{2\,\varepsilon z F(ka)}{3\,\eta}$$

U_e electrophoretic mobility (cm. s^{-1})
Z zeta potential (mV)
E dielectric constant
η viscosity (Pa.s)
F(*ka*) Henry's function

2.8. *In vitro* models of the blood-brain barrier

Blood-brain barrier models can be based on primary brain cells, such as the model designed by Nakagawa *et al.* which consisted of rat endothelial cells, pericytes and astrocytes [338], or with porcine primary cells [339]. As the acquisition of primary cells can be sometimes difficult, using manipulated cell lines is in many cases considered an acceptable alternative. Monocultures of immortalised endothelial cells of different origin, such as porcine [340], human (hCMEC/D3 [341, 342]), or murine (bEnd3 [129, 343]) were previously shown to be sufficient to mimic the barrier function of the BBB. However, to make the model more robust, some researchers recommend the combination of endothelial cells with astrocytes [344]

(employed in Transwell setup *Figure 2.33.*) and also the addition of pericytes to strengthen the tight junctions [49, 345].

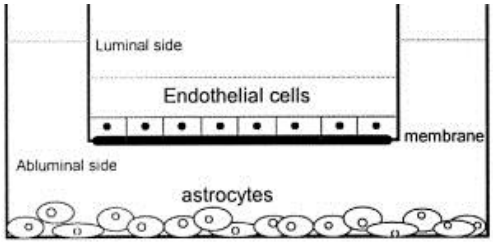

Figure 2.33. Schematic representation of a blood-brain barrier model; adopted from[344].

Advanced BBB models can simulate the flow of cell media to mimic blood circulation and also simulate the change in the concentration of the applied active as well as induce a shear stress into the model, as in case of models based on porcine [346] or human models [347, 348]. An indicator of the BBB properties can be measurement of transendothelial electrical resistance (TEER). The high values indicate better barrier properties (mouse endothelial cells approx. 800 Ω [129], human endothelial cells approx. 1800 Ω in mono-culture [49]); the co-cultures of endothelia cells with astrocytes usually perform better than mono-cultures [345].

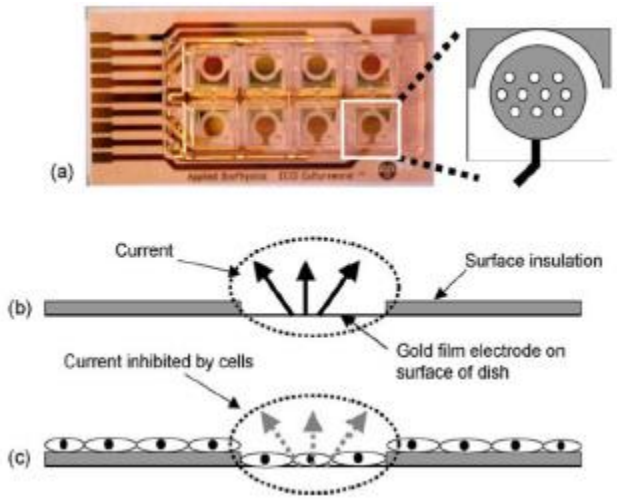

Figure 2.34. Scheme of electric cell to substrate impedance sensing (ECIS): (a) 8 well plate with electrodes, (b) empty electrode, (c) electrode with cells; adopted from [349].

TEER can be measured either within the Transwell setup [49, 350, 351] or in independent experiments with cells planted on electrodes [129]. The latter, known as electric cell to substrate impedance sensing (ECIS), can signalise changes in the cell populations as attachment, movement or change of shape [349, 352]. The principle can be found in relation between the electrical current and resistance, in Ohm's law *(Figure 2.34)*.

2.9. *In ovo* model for toxicity and biostribution studies

Mammalian models are frequently used for preclinical *in vivo* evaluation of new drug delivery systems (rat [128, 353]; mouse [354-356]; rabbit [357, 358] macaque [357, 359], cat [360], dog [361, 362], calf [363], pig [364, 365]), however such models tend to be costly and add an administrative burden in terms of legal and ethical implications. The alternatives to mammalian models can be provided by zebrafish *Danio rerio* [366, 367] or even simpler organisms such as *Drosophila* [368]. These models cannot substitute mammal models however such simple options bridge the gap between *in vitro* and *in vivo* testing. One of the approaches includes employment of chicken embryos [369-371].

The low cost and the simplicity and rapidity of setting up an *in ovo* model make chick embryos *(Figure 2.35.)* interesting candidates that could be used to establish an intermediate step between *in vitro* cellular tests and preclinical mammalian *in vivo* models, especially for studies related organism toxicity [371]. The transparency of embryos allows easy monitoring of the fate of the administered fluorescently labelled nanoparticles and can provide an early indication of the effect of nanoparticles at the organism level. Although chick embryos are not yet widely used for the evaluation of new drug carriers, the US Food and Drug Administration (FDA) has already approved products pre-clinically evaluated with chick embryos [371]. Indeed, FDA guidance for industry from 2006 regarding the development of products for the treatment of chronic cutaneous ulcer and burn wounds, considered the chicken chorio-allantoin membrane (CAM) model as an alternative for preclinical testing [371]. CAM of chicken embryo was used as *in vivo* models for photodynamic therapy. This method has been successfully used

for the treatment of choroidal neovascularization in age-related macular degeneration [372] or to test compound toxicity [373], or for material construct biocompatibility [374], wound healing [375] or anticancer agents [371] were also tested using this model. Nanoparticulate behaviour in embryotic blood vessels of CAM was investigated for the first time by Clancy, who employed a perfusion method combined with fluorescence correlation microscopy [376].

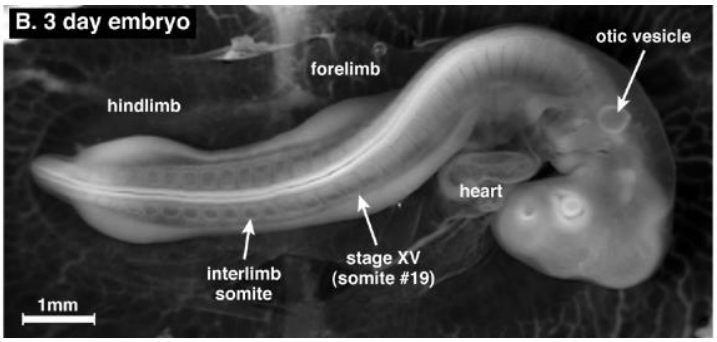

Figure 2.35 Image of chicken embryo (Adopted from [377]).

Depending on the stage of development the chicken embryo has functioning cardio-circulation system and an immunity system with B and T lymphocytes, toxicity of drugs could be easily evaluated in terms of embryo death or adverse effects on the CAM. Two approaches for such embryo studies have been thus far developed: an *"in ovo"* method, where the embryos are left inside the eggshell during their development and also for the duration of the assay, and an *"ex ovo"* method, where the embryos are actually cultivated in recipients simulating the eggshell. The approach ultimately depends on the age of the embryo at the beginning of the experiment and on the nature of the intervention [371].

Table 2.1. Classification of embryo damage caused by photodynamic therapy, (Adopted from Lange [372]).

Damage scale	Criterion
0	No damage
1	Partial closure of capillaries < 10 μm
2	Closure of capillary system, partial closure of blood vessels of diameter < 30 μm
3	Closure of vessels < 30 μm and partial closure of higher order vessels
4	Total closure of capillaries < 70 μm and partial closure of large vessels
5	Total occlusion of vessels in the irradiated area

A special scale that can be used for toxicity studies employing embryonal model was developed by Lange *et al* [372] (*Table 2.1.).* The scale helps with the assessment of various stages of damage to the embryo (Lange was interested in particular in the anti-neoangiogenesis induced by photo-dynamic therapy). Chicken embryos were also used in toxicity studies of porphyrin loaded PLGA nanoparticles [370].

3

CHEMICAL MODIFICATIONS OF POLYSACCHARIDES

Selected polysaccharides were modified by covalent attachment of alkylglyceryl pendant chains to the available hydroxyl groups. This was achieved by treatment of polysaccharides (chitosan and dextran) with a range of alkyloxiranes (*n*-pentyloxymethyl oxirane, OX5, and *n*-octyloxymetyloxirane, OX8, were synthesised in house, while *n*-butoxymethyloxirane, OX4, was sourced commercially). A series of alkylglyceryl modified polysaccharides: butylglyceryl chitosan (CS-OX4), pentylglyceryl chitosan (CS-OX5), octylglyceryl chitosan (CS-OX8), butylglyceryl dextran (DEX-OX4) and octylglyceryl dextran (DEX-OX8), were prepared following the above method. Further covalent binding of alkylglyceryl-modified dextran to poly(lactic acid) was achieved using carbodiimide chemistry to yield poly(lactic acid)-*graft*-butylglyceryl dextran (PLA-DEX-OX4) and poly(lactic acid)-*graft*-octylglyceryl dextran (PLA-DEX-OX8). The possibility of increasing number of reactive groups in the molecule of poly(lactic acid) (to attach more alkylglyceryl dextran molecules) was attempted *via* free radical grafting.

3.1. Materials and instrumentation

Epibromohydrin, 1-octanol, sodium hydride (60 % w/w suspension in mineral oil), chitosan (low MW, degree of deacetylation 75-85 %), dextran from *Leuconostoc* (MW 6 kDa), dimethyl sulfoxide (DMSO, anhydrous, ≥ 99.9 %), butyloxymethyloxirane (OX4, 95 %), 4-(dimethylamino)pyridine (DMAP, puriss. > 99 %), $Zn(BF_4)_2$, potassium *tert*-butoxide (*t*-BuOK; reagent grade > 97 %), carbonyldiimidazole (CDI, reagent grade), benzoyl peroxide (BPO),

toluene (anhydrous, 99.8 %), and maleic anhydride (MA, *puriss.*, ≥ 99 %) were obtained from Sigma Aldrich UK. Dicyclohexylcarbodiimide (DCC, ≥ 99 %,) was obtained from Fluka. Tetrahydrofuran (THF anhydrous, ≥ 99.9 % stabilised by 250 ppm BHT), hydrazine monohydrate, 4-(4-nitrobenzyl)pyridine, tetraethylenepentamine, and non-anhydrous solvents were obtained from Fisher Scientific, UK. Poly(lactic acid) with free carboxyl group (PLA, MW 15 kDa) was obtained from Purac, Netherlands. *n*-Pentyloxymethyloxirane (OX5) was a gift from Dr. Molnár. All reagents were used as obtained.

Solvent removal under reduced pressure was performed using a Büchi Rotovapor R-200 powered with a Sogevac Saskia PIZ 100 vacuum pump equipped with a liquid nitrogen trap. When required, solvents were degassed using three freeze-thawing cycles. Sonication was performed using a Grant ultrasonic bath XB3 (Farnell, UK). Thin Layer Chromatography silica gel plates F254 were obtained from Merck, UK. Dialysis was performed using Visking membrane tubing (Medicell International Ltd, UK) with cut-off either 12-14 kDa or 3 kDa in a discontinuous system (10.0 L deionised water. exchanged 3 times/day). Low speed centrifugation was performed using a Jouan B4i centrifuge equipped with a S40 rotor (4 000 rpm; 15 minutes, unless otherwise specified).

The products were characterised by ^{1}H- and ^{13}C-NMR spectroscopy using a JEOL Eclipse 400+ instrument (Jeol, UK; 400 MHz for ^{1}H- and 100 MHz for ^{13}C-NMR); samples were dissolved in either $CDCl_3$, D_2O or DMSO-d_6 employing 0.2 % TMS as a reference The spectra were processed using the JEOL Delta v 5.0.2 software. FT-IR spectra were recorded using a Nicolet 6700 instrument (Thermo Scientific, UK) equipped with an ATR Smart Orbitt accessory with diamond crystal, at 128 scans and 4 cm^{-1} data spacing. The analysis of spectra was performed using the Omnic Specta 8.0 software. The molecular weight of alkylglyceryl-dextran derivatives was estimated using a GPC Shimadzu (PL-GPC 120) system equipped with 3 serial PL-aquagel-OH columns (8 μm particle size; 20, 40 and 60 Å pore type, respectively) and a refractive index detector, under thermostatted conditions (30 °C). A phosphate buffer (pH=7; prepared from 0.2M $NaNO_3$ and 0.01M NaH_2PO_4) was run as eluent at a flow rate of 1.0

mL/min. The calibration was performed with pullulan standards (Shodex Denko) of MW 0.6×10^4, 1×10^4, 2.17×10^4, 4.88×10^4 and 11.3×10^4, 21×10^4, 36.6×10^4, 80.5×10^4 g/mol. Static light scattering (SLS) measurements were performed to estimate the molecular weight of alkylglyceryl-dextran derivatives. A Malvern Zetasizer Nano instrument with scattering angle 173° (backscatter) or 90° powered by Malvern software was employed to perform the SLS analysis; toluene was used as an internal scattering standard. Samples were dissolved in ultrapure water and double filtered *via* 200 nm filter polyethersulfone membranes (GD/X) from Whatman, UK.

3.2. Methods

3.2.1. Synthesis of *n*-alkyloxymethyloxiranes

The synthesis of *n*-alkyloxymethyloxiranes was carried out according to a literature procedure [378] that was further optimized in-house [111]; the preparation of *n*-octyloxymethyloxirane (OX8) is exemplified below *(Figure 3.1.)*. Briefly, epibromohydrin (11.0 mL; d = 1.601 g/mL, 129 mmol; working extremely carefully due to its toxicity) was added to anhydrous THF, (80.0 mL) containing sodium hydride (60 % w/v dispersion in mineral oil; 6.0 g, 150 mmol) under continuous magnetic stirring in a round bottom flask placed in an ice bath. *n*-Octanol (19.5 mL, 0.827 g/mL, 150 mmol) was added dropwise. The reaction was performed under nitrogen atmosphere and was monitored by TLC (silica as stationary phase and DCM as mobile phase). The compounds were visualised by spraying with a solution of 4-(4-nitrobenzyl) pyridine (2% w/v in acetone) and subsequent heating the plate to 100 °C following by immersion into a solution of Tetraethylpentylamine (10% w/v in acetone) to observe the development of purple spots (epoxide containing compounds). After approx. 3 hours the reaction mixture was poured into iced water and extracted with diethyl ether (3 x 70.0 mL) to afford a crude liquid product (yields 65 – 83 %), which were purified by vacuum distillation (0.177 kPa; bp 120-121°C). The pure *n*-octyloxymethyloxirane was a colourless liquid (total

yield 23 – 49 %). The structural confirmation analysis was carried out using FT-IR and ^{1}H-NMR.

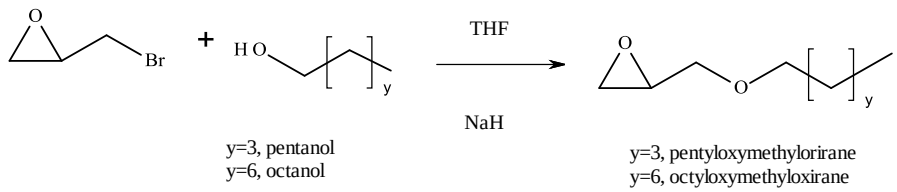

Figure. 3.1. Preparation of n-alkyloxymethyloxirane derivatives.

3.2.2. Synthesis of alkylglyceryl-modified chitosan derivatives

The modifications of chitosan were performed according to a three-step protocol established in-house [111], the free amino groups were protected by phthaloylation (which also yielded solubility in polar organic solvents such as DMSO and DMF) prior to selectively reacting the saccharidic hydroxyl functionalities with *n*-alkyloxymethyloxiranes (OX4, OX5, and OX8) in alkaline conditions followed then by deprotection of the amino groups using hydrazine. The experimental details are presented below.

Synthesis of phthaloyl-chitosan (CS-PH). A solution of chitosan (2.0 g, 2.92 mmol) dissolved in anhydrous DMF (100 mL) was added dropwise to solution of phthalic anhydride (5.4 g, 35.00 mmol) in DMF (50 mL), and the reaction mixture was refluxed (152 °C) for 18 hours under nitrogen atmosphere with continuous magnetic stirring *(Figure 3.2.)*. The reaction mixture was then poured into ice-water (ca. 1.0 L). The precipitate obtained was collected by filtration and washed with ethanol and diethylether, and further purified overnight by Soxhlet extraction with ethanol. Drying in a desiccator over P_2O_5 afforded phthaloyl-chitosan (CS-PH) as a beige compound (yields 43 - 85 %) and characterised by FT-IR and^{1}H-NMR spectroscopy.

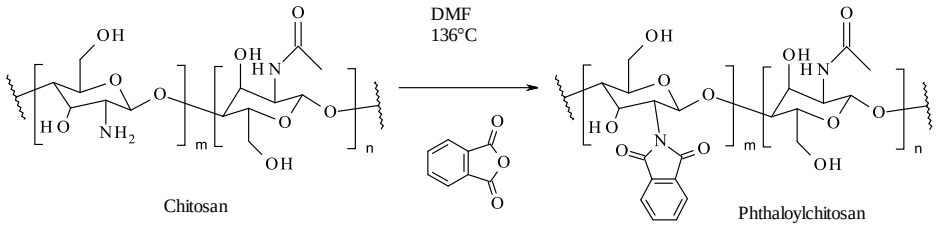

Figure 3.2. Preparation of alkylglyceryl-modified chitosans - the phthaloylation step.

General method for the preparation of alkylglyceryl-modified phthaloyl-chitosans (CS-PH-OX4; CS-PH-OX5; CS-PH-OX8). Phthaloyl-chitosan (1.0 g; 3.66 mmol) was dissolved in anhydrous DMF (100 mL) under a nitrogen atmosphere and the mixture was being added dropwise to a solution of potassium *tert*-butoxide (1.6 g; 14.64 mmol) dissolved in anhydrous THF (10 % w/v). After stirring the mixture for 30 min at room temperature, a solution of an alkyloxirane (*n*-butyloxymethyloxirane OX4, *n*-pentyloxymethyloxirane OX5, *n*-octyloxymethyloxirane OX8), dissolved in anhydrous DMF (50 % v/v, 14.64 mmol) was added dropwise (ca. 30 min, *Figure 3.3.*). The reaction mixture was stirred overnight at room temperature, then the solution was poured into ice-water (500 mL) and the solvents were removed at low pressure using a rotary evaporator. The brown solid residue was resuspended in water and dialyzed against deionised water for 4 days. Freeze drying of the dialyzed solution afforded the final products (CS-PH-OX4; CS-PH-OX5; CS-PH-OX8) as light brown powder (yields 55 – 71 %), which were characterised by FTIR and ^{1}H-NMR spectroscopy.

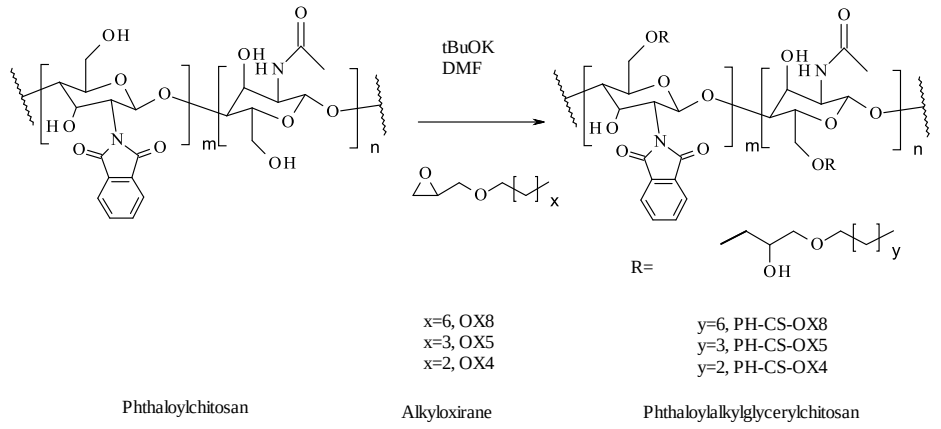

Figure 3.3. Preparation of alkylglycery-modified chitosans–the reaction between protected chitosan and oxiranes.

General procedure for the removal of phthaloyl groups leading to the preparation of alkylglyceryl-modified chitosans (CS-OX4, CS-OX5, CS-OX8). Alkylglyceryl-modified phthaloyl-chitosan (eitherCS-PH-OX4, CS-PH-OX5 or CS-PH-OX8 (0.25 mmol)) was suspended in a solution of hydrazine monohydrate (0.7 mL; d= 1.032; 14.00 mmol) and water (3.0 mL), which was refluxed for 15 hours *(Figure 3.4.)*. After cooling, the reaction mixture was diluted with water (10.0 mL) and the solvents were removed under reduced pressure. The solid residue was dialysed in water for 4 days and finally freeze dried to afford alkylglyceryl-modified phthaloyl-chitosans (CS-OX4; CS-OX5; CS-OX8) as beige powder (yields 44 - 64 %), further characterised by FT-IR, ^{1}H-NMR spectroscopy analysis.

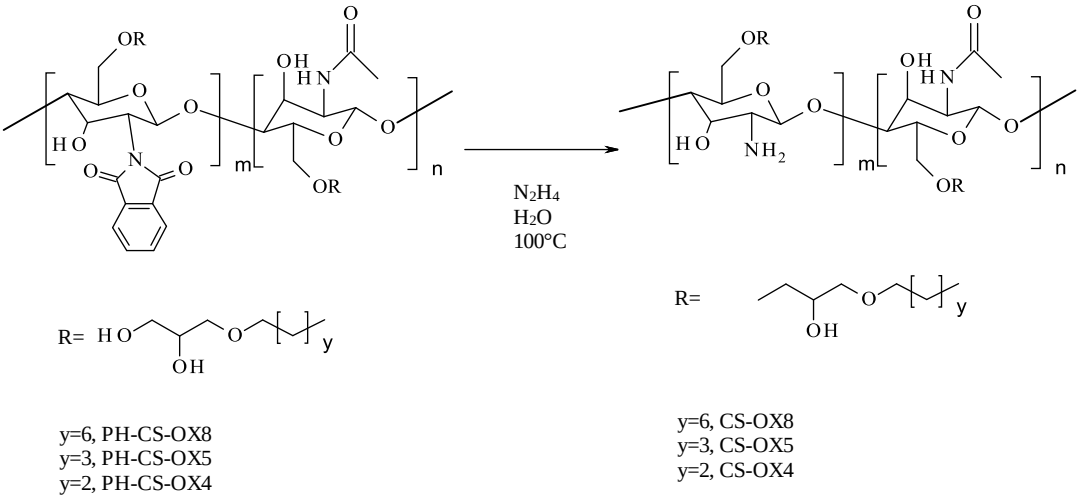

Figure 3.4. Preparation of alkylglyceryl-modified chitosans – the deprotection step.

3.2.3. Synthesis of alkylglyceryl-modified dextran derivatives

Dextran was modified by attaching alkylglyceryl side chains to the hydroxyl groups *via* a two-step reaction that involved the transformation of saccharidic hydroxyl groups into more reactive alcoholates using a strong base (either potassium *tert*-butoxide, pyridine or DMAP) followed by reaction with *n*-alkyloxymethyloxirane (*n*-butyloxymethyloxirane OX4 or *n*-octyoxymethyloxirane OX8), as described below *(Figure 3.5.).* An alternative route investigating zinc tetrafluoroborate hydrate as a catalyst in aqueous environment was tested as well.

Method A) in organic environment. Dextran (1.00 g; 6.10 mmol) was dissolved in anhydrous DMSO (200 mL). The base (potassium *tert*-butoxide; 1.36 g; 12.20 mmol and 2.72 g; 22.40 mmol; pyridine 0.96 g; 12.20 mmol; and DMAP 1.49 g; 12.20 mmol) dissolved in anhydrous THF (50 mL) was then added dropwise into the DMSO solution of Dextran, and the mixture was allowed to react for 2 hours under continuous stirring, followed by the dropwise addition of a solution of oxirane (OX4 - 63 mmol; 9.0 mL; d=0.91, or OX8 - 63 mmol; 12.6 mL) in DMSO (20.0 mL; *Figure 3.5.*). The reaction mixture was stirred for 48 hours at room temperature (25 °C) then poured into a dialyzing membrane (MWCO 3 kDa) and dialysed extensively against deionised water (10.0 L; exchanged 3x per day) for three days. The content of the dialysing membrane (approx. 400 mL) was then washed three times with diethylether (3 × 150 mL) in a separation funnel to remove water-insoluble impurities. After removing the traces of volatile solvents in a rotoevaporator under reduced pressure (25°C) the aqueous layer was lyophilised affording alkylglyceryl-modified dextrans (butylglyceryldextran DEX-OX4 and octylglyceryldextran DEX-OX8) as a slightly brown powder. The yields were in range 52-73 %. The final products were characterised with FTIR, ^{1}H - and ^{13}C – NMR spectroscopy. (The spectra and characterisation are in APPENDIX I and II.)

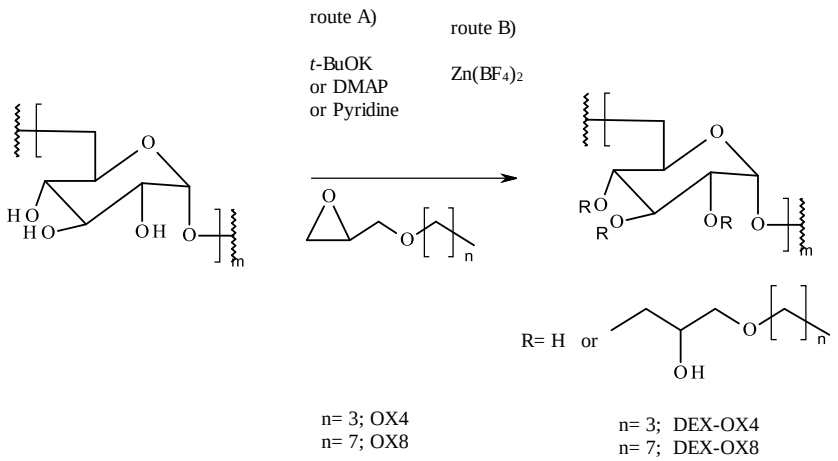

Figure 3.5.Synthesis of alkylglyceryl-modified dextrans.

Method B) in aqueous environment. In this method the aqueous system was employed: Dextran (1.0 g, 6.10 mmol) was dissolved in water (50 mL) with pH 1 adjusted by concentrated hydrochloric acid. Zinc tetrafluoroborate hydrate $Zn(BF_4)_2$ (2.92 g, 12.20 mmol) was added and stirred for 2 hours. Subsequently butyloxirane (OX4 63 mmol, 9.0 mL, d=0.91) was dropwise added to the aqueous solution and stirred overnight. After 14 hours the reaction was stopped and the reaction mixture was submerged for dialysis for 72 hours and lyophilised. The yields were in range 55-81 %. The structural confirmation analysis was carried out by FT-IR (ATR), ^{1}H- and ^{13}C-NMR spectroscopy; the molecular weight of products was estimated by GPC against pullulan standards (range of MW: 0.6×10^4, 1×10^4, 2.17×10^4, 4.88×10^4 and 11.3×10^4, 21×10^4, 36.6×10^4, 80.5×10^4 g/mol) in a phosphate buffer in pH 7 (APPENDIX V).

The absolute molecular weight of alkylglyceryl-modified dextrans was also measured by Static Light Scattering using a Malvern Zetasizer Nano instrument, with toluene as an internal scattering standard. The aqueous polymer solutions (concentration range 1.0 - 0.0001 mg/mL) were used to construct a Debye plot of concentrations. These attempts were not successful due to the polydisperisty of the samples.

3.2.4. Synthesis of poly(lactic acid)-*graft*-alkylglyceryl modified dextran

Alkylglyceryl modified dextran derivatives were attached to poly(lactic acid) using carbodiimide zero length cross-linkers. Such modifications were conducted in ratio to react one molecule of poly(lactic acid) to one molecule of alkylglyceryl-dextran. Furthermore, attempts were carried out to attach more molecules of alkylglyceryl-modified dextran to one molecule of poly(lactic acid). For that reason it was necessary to introduce more reactive groups into the polymeric backbone of poly(lactic acid). The groups were provided by maleic anhydride which was grafted *via* free radical mechanism to the poly(lactic acid). As these attempts exhibited low

degrees of grafting and the steps of further binding the alkylglyceryl-dextran were not continued.

3.2.4.1. Synthesis using zero length cross-linkers

The covalent attachment between poly(lactic acid) (PLA) and alkylglyceryl-dextrans (DEX-OX4 and DEX-OX8) was achieved using zero length cross-linkers such as N,N'-dicyclohexylcarbodiimide (DCC) [278, 379] or N,N'-carbodiimidazole (CDI) [252, 380].

Method A) using DCC

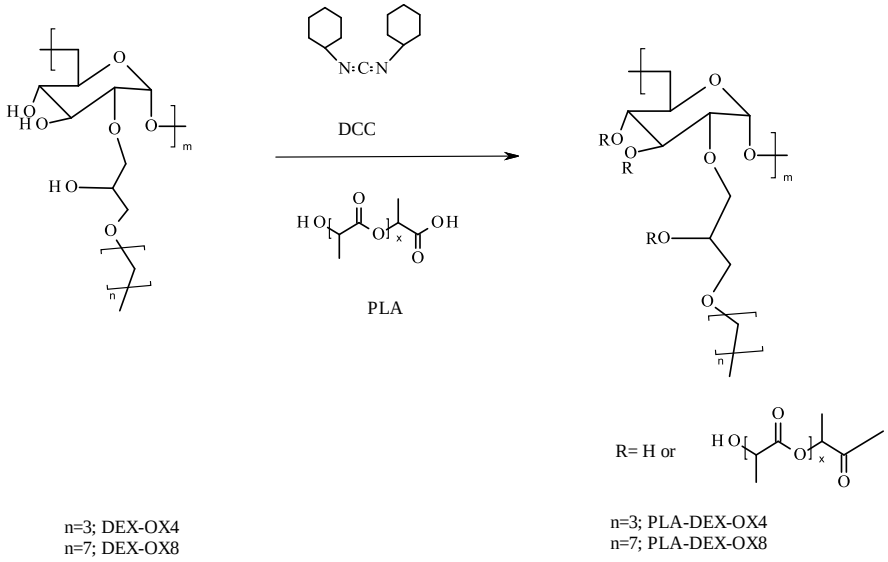

Figure 3.6. Attachment of poly(lactic acid) to alkylglyceryldextran via DCC.

The reaction was carried out following Choi's procedure [379]. Briefly, DCC (0.045 g, 0.20 mmol) dissolved in DMSO (10 mL) was added to a PLA solution (1.750 g, 0.11 mmol) in 100 mL DMSO under stirring in a round bottom flask that was previously degassed and purged with nitrogen and equipped by a magnetic stirrer bar. After stirring for 30 min, this solution was added to an alkylglyceryl-dextran solution (DEX-OX4, 0.700 g, 2.20 mmol, DEX-OX8, 0.850 g, 2.20 mmol) in DMSO (100 mL) to which 4-(dimethylamino)pyridine (DMAP, 0.026 g, 0.22 mmol) was previously added. The reaction was continued with stirring and under nitrogen at room temperature (25 °C) for 24 hr. The reaction mixture was then filtered to remove any by-

product (dicyclohexylurea) and dialyzed (MWCO 12 kDa) against deionised water for 48 h followed by freeze drying. The resulting off-white powder was washed with acetone to remove any un-reacted PLA, dried under vacuum at room temperature and then washed with water to remove un-reacted alkylglyceryl-dextran and finally freeze-dried again. The structures of copolymers (PLA-DEX-OX4 and PLA-DEX-OX8) were confirmed by ^{1}H- and ^{13}C- NMR and FT-IR analysis. (The spectra and characterisation are in APPENDIX III and IV.) The yields were in range 33-56%.

Method B) using CDI

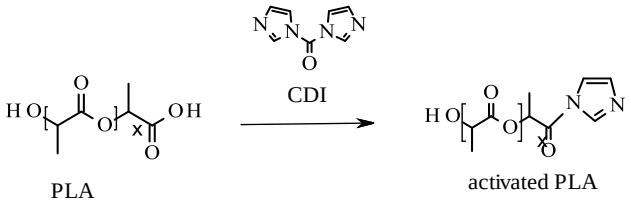

Figure 3.7. Activation of poly(lactic acid) with CDI in chloroform.

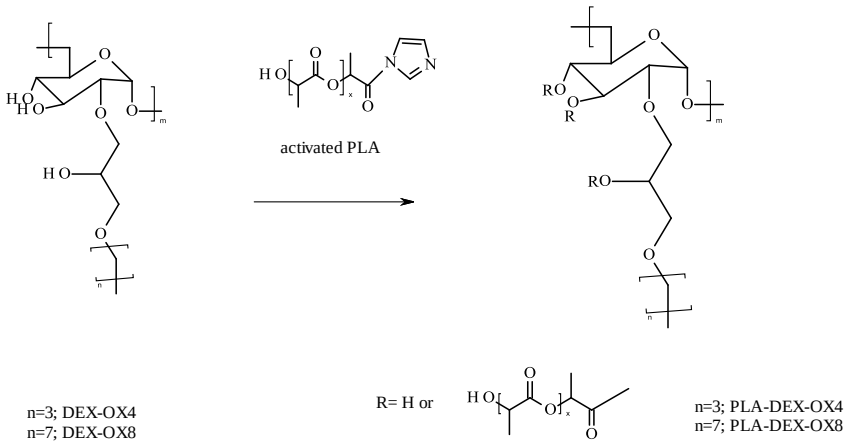

Figure 3.8. Attachment of activated poly(lactic acid) to alkylglyceryldextran in DMSO.

This preparation was carried out by a modification of Nagahama's procedure [252], as follows. The reaction apparatus was degassed and purged with nitrogen, then poly(lactic acid) (PLA, 0.50 g, 0.033 mmol) dissolved in anhydrous chloroform (7.0 mL) was added dropwise to the carbodiimidazole solution (CDI, 0.11 g, 0.66 mmol) in anhydrous chloroform (5.0 mL). The

reaction mixture was stirred for 6 h at room temperature under nitrogen, and then washed with a large amount of ethanol (10 mL) to remove the excess CDI and imidazole. The resultant precipitate was collected by centrifugation and dried overnight *in vacuo* (25 °C). The presence of the imidazoyl group in the CDI-activated PLA (yield 82-90%), obtained as white crystalline powder, was confirmed by ^{1}H-NMR spectroscopy. In the second step alkylglyceryl-dextran (DEX-OX4 0.20 g, 0.66 mmol, DEX-OX8, 0.24 g, 0.66 mmol) and 4-(dimethylamino)pyridine (DMAP, 0.08 g, 0.60 mmol) were dissolved in anhydrous DMSO (50 mL) separately, CDI-activated PLA (0.40 g, 0.027 mmol) was dissolved in anhydrous DMSO (50 mL) and dropwise added to the DEX-OX & DMAP solution. The reaction mixture was stirred at room temperature for 24 h under nitrogen, then the reaction was stopped by adding conc. HCl (150 μL) to neutralize any DMAP and imidazole. The reaction mixture was dialysed against deionised water for 48 h then freeze-dried. The solid residue was washed with acetone to remove un-reacted PLA and with water to remove un-reacted alkylglyceryl-dextran. The purified products (yields 68-81%) were freeze-dried and analysed by FT-IR, ^{1}H- and ^{13}C-NMR spectroscopy.

3.2.4.2. Modification of poly(lactic acid) using maleic anhydride

Poly(lactic acid) (PLA) was modified with maleic anhydride *via* free radical grafting in order to gain more reactive groups in the molecule for further modification with alkylglyceryl-dextran. Poly(lactic acid) (PLA, 0.10 g, 0.008 mmol) and maleic anhydride (MA, 0.10 g, 1.020 mmol) were dissolved in degassed anhydrous toluene (10 mL), followed by the addition of benzoyl peroxide (BPO) in various ratios (2.5 to 20 % w/w, relative to PLA). The reaction mixture was kept stirring at 100 °C for 12 h, under nitrogen flow. The product was separated and purified by precipitation in ethanol, then dried under vacuum at room temperature (yields 52-74%). The characterisation was performed by FT-IR, ^{1}H-NMR spectroscopy. The degree of grafting of maleic anhydride units to poly(lactic acid) backbone was low therefore the subsequent step of synthetizing alkylglyceryl-dextran derivatives was discontinued.

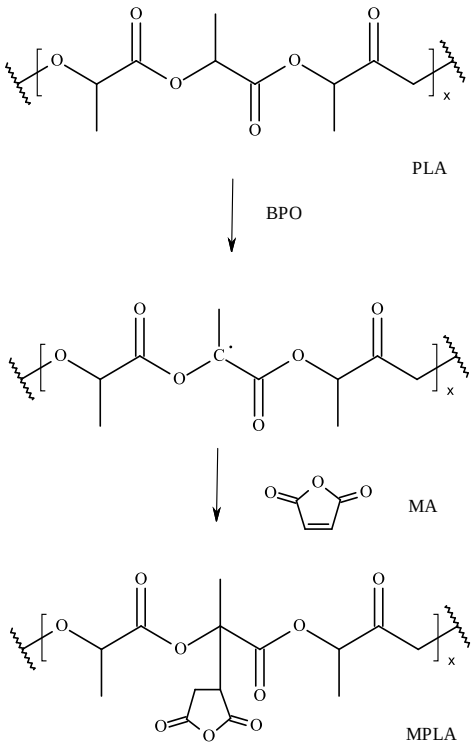

Figure 3.9.Reaction scheme of grafting maleic anhydride onto the backbone of poly(lactic acid) in the presence of radical initiators (Adopted from [229]).

3.3. Results and discussion

3.3.1. Synthesis of *n*-alkyloxymethyloxiranes

n-Octyloxymethyloxirane (OX8) was prepared by a nucleophilic substitution reaction between epibromohydrin and primary alcohol following a method described in the literature [381, 382] and optimised in-house [111]. The purification of the crude product was achieved by vacuum distillation (yields 23 – 49 %). The final products appeared as colourless liquids with specific odour (b.p. 128 °C; 105 kPa)

The product structure was confirmed by FT-IR (ATR mode) and ^{1}H-NMR spectroscopy and was found in agreement with previously published data [111]. The broad band corresponding to the O-H stretching vibration present in the FTIR spectra of the alcohol (3400 cm^{-1}) disappeared completely in the spectra of the final product, indicating that the hydroxyl group was transformed into an ether group which was confirmed by vibration C-O-C (1107cm^{1}). The ^{1}H-NMR showed characteristic alkyl peaks at 0.90, 1.24 and 1.55 ppm (in ratio

approx. 3:10:2) for the octyl group of the OX8 *(Figure 3.10.)*. The results matched earlier obtained characterisation data [111].

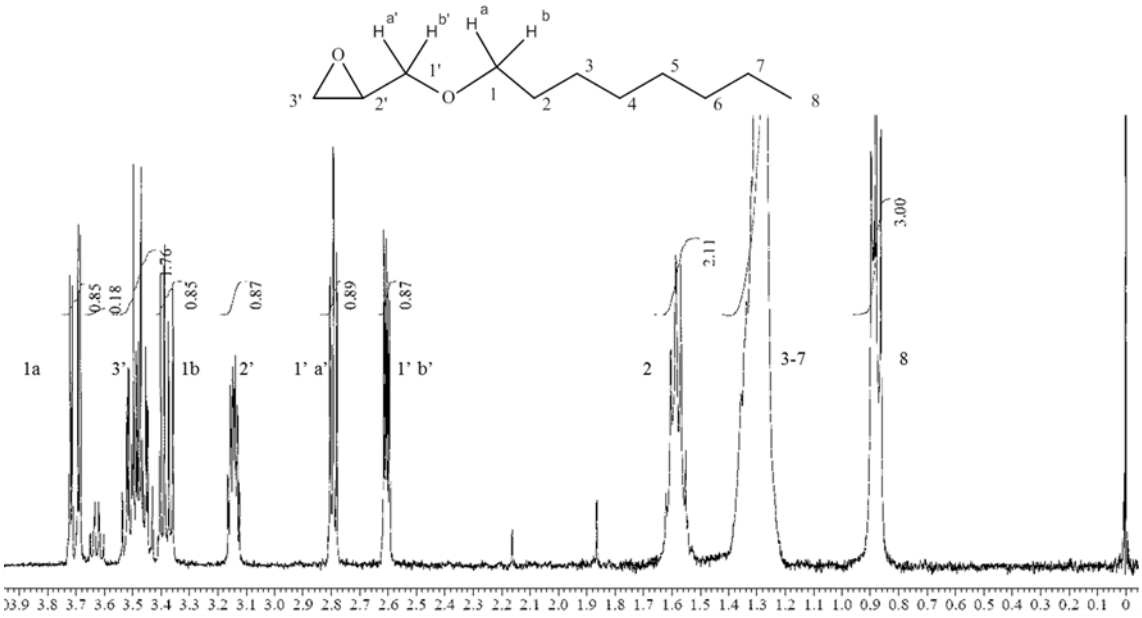

Figure 3.10. [1]H-NMR of n-octyloxymethyloxirane (OX8) with structure (numbers indicate groups of protons, letters individual protons).

3.3.2. Synthesis of alkylglyceryl modified chitosan derivatives

Preparation of phthaloyl-chitosan. Phthaloyl chitosan (CS-PH) was prepared from commercially available low molecular weight chitosan (Sigma; DDA 75-85 %) by treatment with phthalic anhydride in DMF. The product (phthaloylated chitosan) was soluble in polar organic solvents such as DMSO and DMF due to changes in inter- and intra-molecular hydrogen bonding [111, 383]. The infrared spectra of CS-PH displayed a broad band at 3460 cm^{-1}, indicative of OH stretching vibrations, and a C=O band at 1711 cm^{-1} typical of anhydrides and signal for aromatic ring (721 cm^{-1}). ^{1}H-NMR spectra consisted of pyranose signal (3.0-5.1 ppm) and aromatic ring signal (7.4-7.9 ppm, *Figure 3.11.*). The product was obtained as a beige compound (yields 43 - 85 %). The characterisation data were identical with previous description in original source [111].

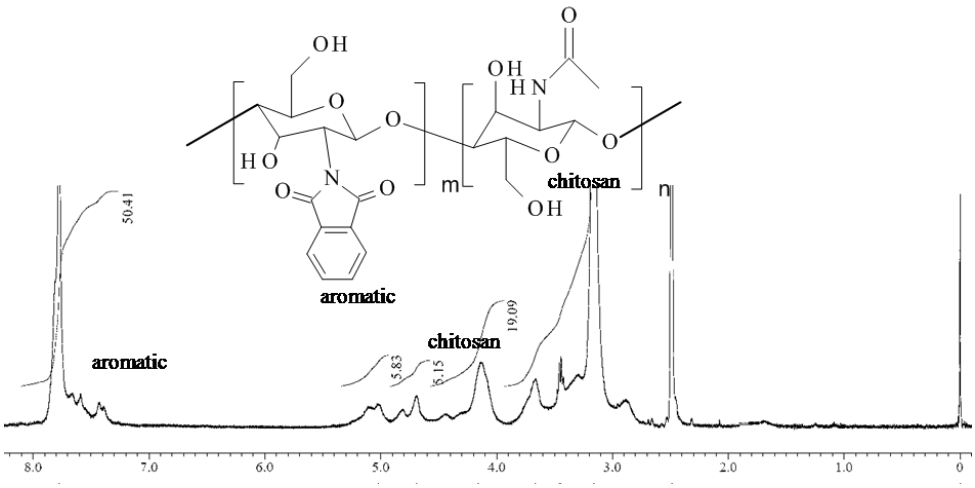

Figure 3.11.[1]H-NMR spectrum of phthaloyl-chitosan (CS-PH).

Synthesis of alkylglyceryl-modified phthaloyl-chitosan derivatives. The phthaloylated alkylglyceryl-modified chitosan derivatives were prepared by treatment of phthaloyl chitosan with alkyloxiranes *via* a nucleophilic substitution reaction *(Figure 3.3.)*. The products were obtained as light brown powders (yields 55-71%).

The FTIR spectrum of all the phthaloylated alkylglyceryl-modified chitosan derivatives contained absorption bands characteristic for both CS-PH and alkylglycerols. Absorption bands at approx. 3070, 2950, 2900 cm^{-1}, the C-H stretching vibrations, belong to the alkylglycerols, signals at approx. 1770, 1710 cm^{-1} were characteristic C=O adsorption bands for the carbonyl groups of the *N*-phthalimido group and approx. 1660, 1560 cm^{-1} vibrations were the amido groups of chitosan. In ^{1}H-NMR spectra, signals appearing at approx.0.8 and 1.7 ppm (characteristic chemical shifts for alkyl hydrogen atoms), were indicative of the presence of alkylglyceryl chains. NMR signals due to the hydrogens of the polysaccharidic units of chitosan appeared between 2.8 - 4.3 ppm, and were partially overlapped by the broad D_2O signal. The presence of the phthaloyl group was confirmed by the signals appearing at 7.1 - 7.9 ppm *(Figure 3.12.)*. The characterisation data were found in agreement with original source [111].

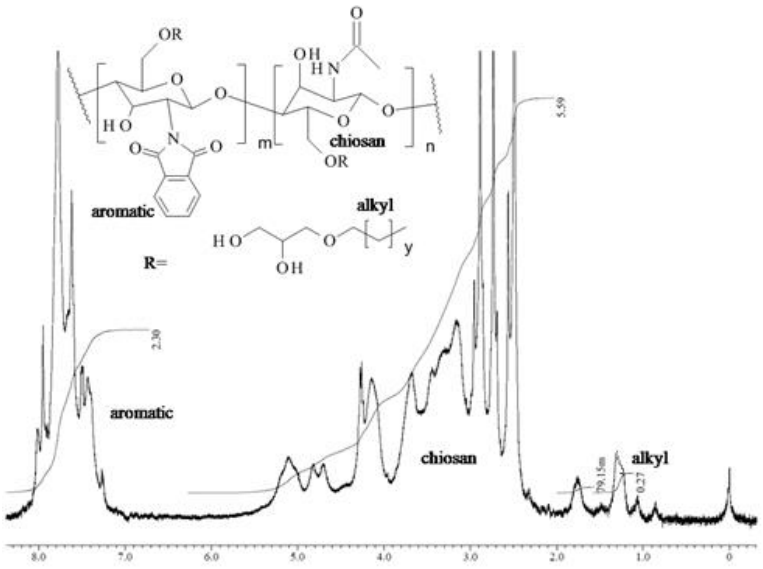

Figure 3.12. [1]H-NMR spectrum of phthaloyl-alkylglyceryl modified chitosan (CS-PH-OX4).

Preparation of alkylglyceryl modified chitosan CS-OX4, CS-OX5, CS-OX8. Removal of the phthaloyl groups from CS-PH-OX4, CS-PH-OX5 and CS-PH-OX8 was carried out with hydrazine monohydrate in water at 100°C for 15 hours [111]. The products were purified by dialysis and after freeze-drying were recovered as white-off powders.

The FT-IR spectra of the resulting alkylglyceryl-modified chitosan derivatives exhibited the expected amino group band around 1630 cm^{-1}, while the bands corresponding to the phthalimido groups (approx 1700 cm^{-1}) disappeared. The removal of the phthaloyl groups was also confirmed by ^{1}H-NMR, as the signals for phthalimido groups (7.1 - 7.9 ppm) disappeared whereas the signals attributed to alkyl chains (0.8, 1.2 and 1.4 ppm) and to the aminoglycosidic ring (2.8-4.3 ppm) were confirmed. The characterisation data are in agreement with previously published source [111].

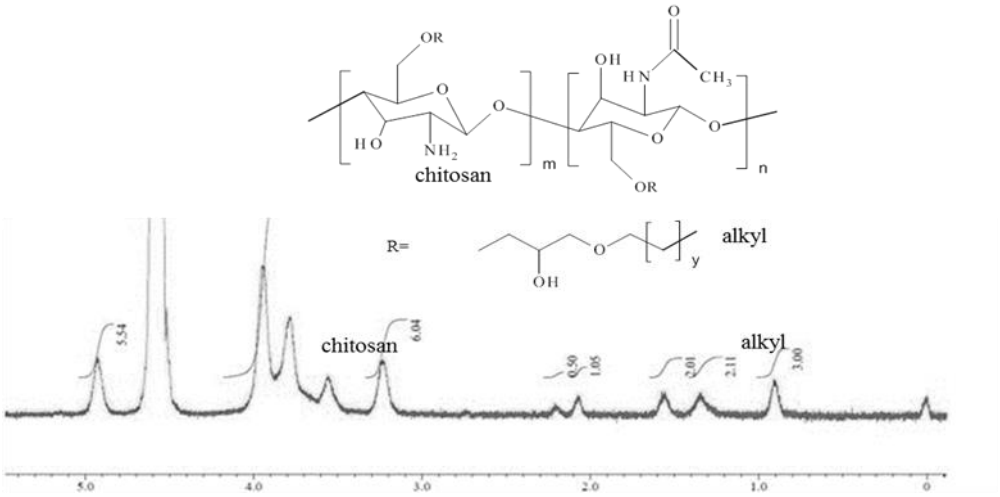

Figure 3.13. [1]H-NMR spectrum of alkyl-modified chitosan (CS-OX4).

The degree of substitution of the primary hydroxyl group *(Table 3.1.)* was calculated from the relative intensities of the signals assigned to the long alkyl CH_3 group (H_y; 0.8 ppm) and to the CH_3 group of the acetylated chitosan (H_{CH3}), as illustrated in *Equation 3.2*. The degree of deacetylation (DDA, *Equation 3.1*) was also determined from the ^{1}H-NMR spectra, by calculating the ratio of the integral of peak at 4.9 ppm (attributed to the C_1 protons) and integral of peak at 2.1 ppm (terminate CH_3 group of deacetylated chitosan unit). The degree of substitution obtained for derivatives CS-OX4, CS-OX5 and CS-OX8 are shown in *Table 3.1.* The characterisation data are in agreement with previously published source [111].

$$DDA(\%) = \left(\frac{H_b}{H_b + CH_3/3}\right) \times 100$$

DDA (%)	degree of deacetylation
H_b	integral of the 4.9 ppm signal assigned to the CH_1 proton of chitosan
CH_3	integral of the 2.1 ppm signal assigned to the CH_3 proton of chitosan

$$DS(\%) = \frac{H_{CH_3} \times DDA}{3H_y}$$

DS (%)	degree of substitution
H_{CH3}	integral of the 2.1 ppm signal assigned to the CH_3 proton of chitosan
H_y	integral of the 0.8 ppm signal assigned to the terminal methyl of alkylglyceryl group

Table 3.1. Degree of substitution of alkylglyceryl-chitosan derivatives.

	Degree of substitution [%]
Butylglyceryl-chitosan (CS-OX4)	88
Pentylglyceryl-chitosan (CS-OX5)	32
Octylglyceryl-chitosan (CS-OX8)	14

3.3.3. Synthesis of alkylglyceryl-modified dextran derivatives

The modification of dextran with alkylglyceryl chains was carried out *via* a nucleophilic substitution reaction involving the attack of the hydroxyl groups (transformed into alcoholates) to the oxirane ring, following a similar procedure published on chitosan [173, 381]. A number of different bases have been employed for this purpose *(Table 3.2.).*

Table 3.2. List of bases employed for the attachment of alkylglyceryl moieties.

	pKa [water]
potassium tert-butoxide	17.0
Dimethylaminopyridine	9.2
Pyridine	5.2

Using the potassium *tert*-butoxide (*t*BuOK) afforded higher degree of substitution compared to other basic catalysts such as DMAP; pyridine as base was unsuccessful (*Table3.*). The degree of substitution was found to increase as the excess ratio of both base and oxirane increased. Moreover, four times an excess ratio of (DEX: *t*BuOK: OX4 - 1:4:4) resulted in higher than if the amounts were only doubled (1:2:2). The amount of oxirane employed was the same as the base (or catalyst).

Attempts to modify dextran with butylglyceryl chains by employing $Zn(BF_4)_2$ as a catalyst in aqueous media (pH 1) - as suggested by [180, 384] – resulted in a low degree of substitution (Table 3.4). The OX4 exhibited a limited solubility in water (2 % v/v) [385]) so it is likely that the solubility of the oxiranes influences the reaction. The literature also mentioned using aqueous systems employing NaOH as a base however such approach can be limited by solubility of the epoxy compounds [156, 386].

Table 3.3. Optimisation of base/catalyst for synthesis of DEX-OX4.

DEX->DEX-OX4 reaction		Mw [g/mol]	Ratio to Dextran	Duration [hours]	Solvent	Degree of Substitution [%]
Base	DMAP	122	2	24	DMSO	2.1-6.6
	Pyridine	79	2	24	DMSO	0
	t-buOK	112	2	24	DMSO	0 - 12.0
			4	48	DMSO	19.1 – 75.3
Catalyst	$Zn(BF_4)_2$	161	3	24	H_20/ HCl pH1	0 - 1.8

The modification of dextran was confirmed by FT-IR spectroscopy *(Figure 3.14.)* mainly by changes in the fingerprint area. Introduction of alkylglyceryl chains resulted in the formation of a new secondary alcohol in the glyceryl pendant, however the increase of hydroxyl groups in whole macromolecule did not happen as a hydroxyl group on C2 was transformed to new ether bond. The main bands in the IR spectra of dextran can be assigned as follows [387]: bands present in the range 400–700 cm^{-1} are due to skeletal vibrations, (C–C–C), (C–C–O), (C–O) and (C–C), with a relative intensity as a function of water content. The bands present at 537 and 550 cm^{-1} were assigned to the (C–C–O) bending vibration. The spectral range 1000–1200 cm^{-1} has been suggested to be dominated by contributions from, (C– C) and (C–O) stretching vibration. The band centred at 1127 cm^{-1} could be assigned to (C–O–C). The vibrational band at 1012 cm^{-1} in the spectrum was assigned to the (C–O) vibration. It has been suggested that the absorption bands in spectral range between 1200 cm^{-1} and 1500 cm^{-1} may be caused mainly by (CH) deformation vibrations and (COH) bending vibrations. The spectrum shows one mode around 1273 cm^{-1} assigned to the (C–O) stretching mode in the ring. The band at 1343 $cm^{-1}$is supposed to be the (O–C–H) vibration and 1539 cm^{-1} can be assigned as (CH_2) group vibration.

The bands present at 2913 cm^{-1} and 3215 cm^{-1} were assigned as (C–H) and (O–H) stretching vibrations, respectively.

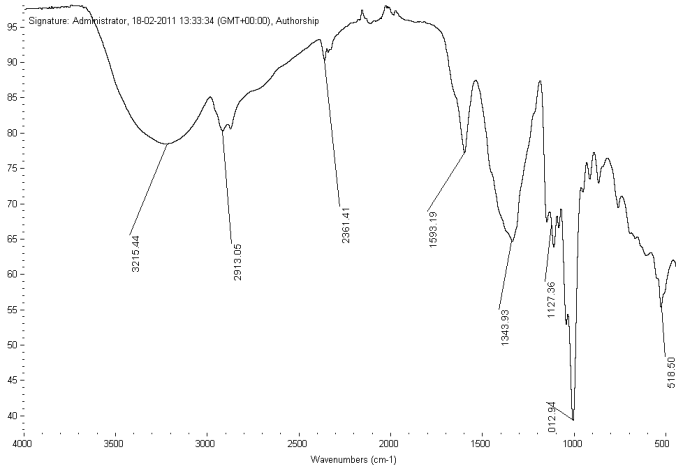

Figure 3.14: FT-IR spectra of butylglyceryl dextran DEX-OX4.

In the ^{1}H-NMR spectrum of butylglyceryl-modified dextran, the signal of the anomeric (C^{1}) proton (4.67 ppm) was well separated from the signals of the other protons on glucopyranosyl ring (3.2–3.7 ppm), in agreement with values reported in the literature [387-389]. The multiplet at 4.96 ppm represents the protons from hydroxyl groups of dextran [388]. The NMR spectroscopy of the novel products revealed peaks at 0.86 ppm, 1.29 ppm and 1.45 ppm which were indicative of the presence of the alkyl group (*Figure 3.15;* The spectra and characterisation are in APPENDIX I and II.)

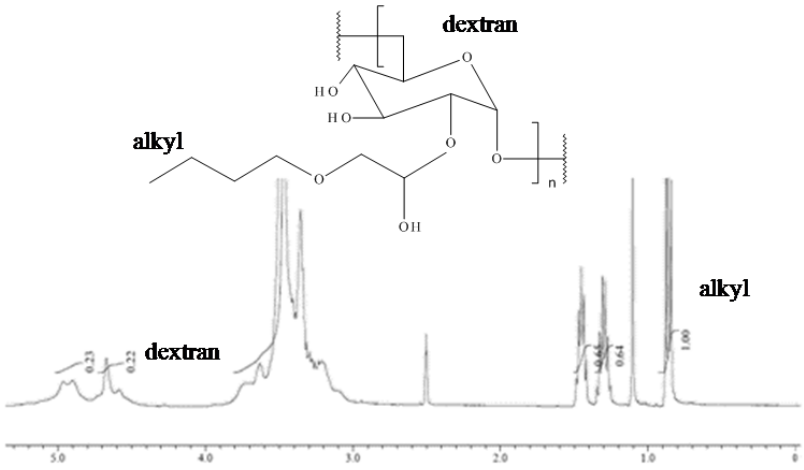

Figure 3.15. ^{1}H-NMR spectrum of DEX-OX4.

The degree of substitution with alkylglyceryl chains (expressed as percentage of substituted saccharide units bearing alkylglyceryl group -e.g. 100 % means each glucopyranose unit is substituted with one alkylglycerol) ranged from 0.7 to 75.1 % for DEX-OX4, and between 16.5 and 38.2 for DEX-OX8 depending on amount of base employed in the reaction. The degree of substitution found in DEX-OX4 and DEX-OX8 was calculated *(Equation 3.3.)* from the ratio of peak integrals corresponding to the alkyl chain end CH_3 group (C4' group in case of DEX-OX4 at 0.86 ppm) and to the anomeric C1group proton of the glucopyranose ring (4.67 ppm).

$$DS[\%] = \frac{\frac{1}{3} \times \int \mathrm{C4'}}{\int C1} \times 100$$

The degree of substitution was found to be dependent on the type of catalyst, the solvent used and the excess of reactants It can be assumed that only the hydroxyl group at C2participated in the reaction, as the reactivity of the hydroxyl groups in dextran towards alkylation agents was determined as decreasing in the order C2>C4>C3[380, 390-392] (likely due to the proximity to the anomeric C1 carbon [203]) and the calculated degree of substitution (using *Equation 3.3*.) never exceeded 100 %.

The molecular weight of modified dextrans (DEX-OX4 and DEX-OX8) were analysed by GPC *(Figure 3.16.)* and compared to the molecular weight of the starting material, following a conventional calibration performed using pullulan standards (APPENDIX V). It appeared that the molecular weight of the modified dextrans decreased compared to the starting material which may indicate the cleavage of glycosidic bonds between individual glucopyranose units in strong alkaline conditions. This is in contrast with literature data regarding the stability of dextran in alkaline conditions [393]. The decrease of molecular weight can be associated to impurities presented in starting material however those could be removed during reaction process (dextran was not purified prior to reactions). Another reason may be the change of conformation of the product after attaching the alkylglyceryl moieties which could depend on

the degree of substitution *(Table 3.4.)*. The different shape of molecule possibly could change the interaction with the stationary phase of the GPC column [394].

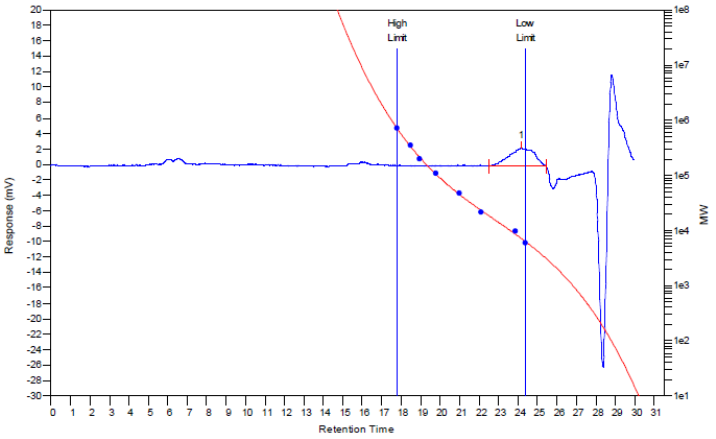

Figure 3.16. GPC chromatogram of butylglyceryl-modified dextran (DEX-OX4).

While molecular weights (MW) of natural dextrans are in the range of 9 - 500 million Dalton [395], the values from producers may differ significantly [396]. Indeed, the starting material employed in this study (Dextran from *Leuconostoc spp*. obtained from Sigma) was reported by the manufacturer as having a nominal M_w 6000 whereas the molecular weight determined by GPC was 10 477 *(Table 3.4).*

Table 3.4. Molecular weight of alkylglyceryl-modified dextran derivatives , as determined by GPC.

Compound	Mn	MW	PDI	DS [%]
DEX (Sigma, MW ~6000)	9363	10477	1.12	0
DEX-OX4	6863	7743	1.13	36.12
DEX-OX8	9092	10157	1.12	16.58

Another possibility of determining the molecular weight of polysaccharides is by using static light scattering [397], however this method is normally limited to low dispersity samples as it is based on scattering intensity of a molecule in various concentrations. Our attempts to analyse the synthesized alkylglyceryl-dextrans using this method were not successful (measurements of samples in different concentrations indicated various dimensions of the molecule), likely due to the rather high polydispersity of the samples (0.854; obtained by

Dynamic Light Scattering measurements of size of the molecule), such a value is normally unsuitable for cumulant analysis.

3.3.4. Synthesis of poly(lactic acid) -*graft*- alkylglyceryl-modified dextran

This section discusses the attachment of alkylglyceryl-modified dextran derivatives (DEX-OXn) to poly(lactic acid) (PLA) in order to gain a copolymer which can be formulated into nanoparticles. Two approaches were investigated. One approach employed the terminal carboxyl group of PLA to bind to a hydroxyl group of one molecule of DEX-OXn. Another approach explored binding more DEX-OXn molecules to one molecule of PLA. For that purpose it was attempted to increase the number of reactive groups in the PLA molecule. Despite partial success in grafting of PLA the attempts were discontinued due to low grafting degrees of the products.

3.3.4.1. Synthesis using zero lenght crosslinkers

The poly(lactic acid) was attached to alkylglyceryl-dextran *via* carbodiimide chemistry. A number of alternatives involving the use of anhydrous organic solvents and zero-length cross-linkers such as carboiimides [252, 278, 379, 398] were considered. Two candidates were examined: dicyclohexyl carbodiimide (DCC) and carbodiimidazole (CDI). The use of DCC was reported by Bhat [399] for attaching 4-azidobenzoic acid to dextran; however, one drawback in using any carbodiimide in a one-step reaction is that it may introduce intramolecular crosslinking between the hydroxyl groups in the modified dextran, especially if the carbodimide and base are in excess and the carboxyl groups were already consumed [400]. A solution for this problem could be to isolate and purify the intermediate (namely the activated PLA by CDI), before reacting it subsequently with alkylglyceryl dextran; this would avoid intramolecular crosslinking and would result in more defined modified products. Moreover, using DCC results in the formation of toxic dicyclohexylurea as a byproduct that needs to be removed from the

solution containing the final product; a better alternative would involve the use of CDI, which generates nontoxic CO_2 and imidazole byproducts [395]. On the other hand, if CDI activated PLA was not isolated in the first step, the intramolecular crosslinking of hydroxyl groups of dextran would occur in presence of DMAP as well.

The reactions were carried out in anhydrous conditions. Purification of products included washing of products with water (removed water soluble un-reacted DEX-OX) and acetone (removed un-reacted PLA). After drying in a desiccator the final products were obtained as off-white powders (DCC route yielded 33-56 % and CDI route yielded 68-81 % respectively). The products were characterised by FT-IR and NMR spectroscopies which confirmed identical results from both synthetic routes. The FT-IR spectra of the products showed a significant band at 1751 cm^{-1} , which can be attributed to C=O stretching vibration of PLA, while the broad band at 3352 cm^{-1} represents OH stretching vibrations of DEX-OX derivatives *(Figure 3.17).*

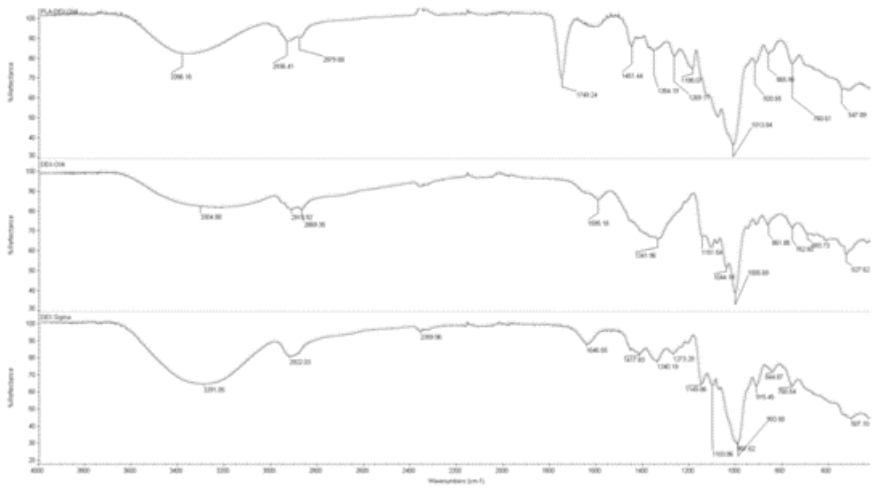

Figure 3.17. Comparison of dextran derivatives FT-IR spectra; dextran (DEX - bottom), butylglyceryl dextran (DEX-OX4 - middle) and poly(lactic acid)-graft-butylglyceryldextran copolymer (PLA-DEX-OX4-top).

^{1}H-NMR spectra of PLA-DEX-OX4 exhibited peaks for both the butylglyceryl-modified dextran DEX-OX4 (0.87 ppm terminal CH_3 of pendent alkylglyceryl; 3.22-5.14 ppm glucopyranose ring) in addition to the peaks for poly(lactic acid) (1.44 ppm for CH_3 of PLA, 5.19 ppm CH of PLA). The PLA-DEX-OX8 exhibited similar spectra; DEX-OX8 part of the

molecule (0.87 ppm for end CH_3 of pendent alkylglyceryl; 3.00-4.92 ppm glucopyranose ring) in addition to poly(lactic acid) (1.35 ppm for CH_3 of PLA, 5.20 ppm CH of PLA, *Figure 3.19*). (The spectra and characterisation are in APPENDIX III and IV.) The products from CDI route only were employed in further formulations.

A conjugate of poly(lactic acid) and commercial dextran (PLA-DEX) was prepared *via* the CDI route, ^{1}H-NMR confirmed peaks for both dextran (3.2 ppm – 5.2 ppm) and poly(lactic acid) (1.3ppm and 5.3 ppm). This polymer was used for formulation of nanoparticles which served as a control to alkylglyceryl-modification containing nanoparticles. The degree of grafting (DG) was expressed as a ratio of PLA and DEX-OXn (defining number of PLA units per 100 glucopyranose units of DEX-OXn, according de Jong *et al.*, who used the formula for PLA-DEX conjugate [401], *Table 3.5*). The DG for was calculated using ^{1}H-NMR spectra.

$$DG = \frac{\frac{1}{3}\int \mathrm{a}}{\int C1} \times 100$$

a integration of protons of CH_3 group of PLA (at 1.31 ppm)

C^1 integration of the anomeric proton of DEX-OXn (at 5.17 – 4.39 ppm)

Table 3.5. Degree of grafting of products. Expressed as number of units of PLA per 100 units of dextran derivative.

Derivative	Degree of grafting [range]
PLA-DEX	130-142
PLA-DEX-OX4	108-120
PLA-DEX-OX8	88-112

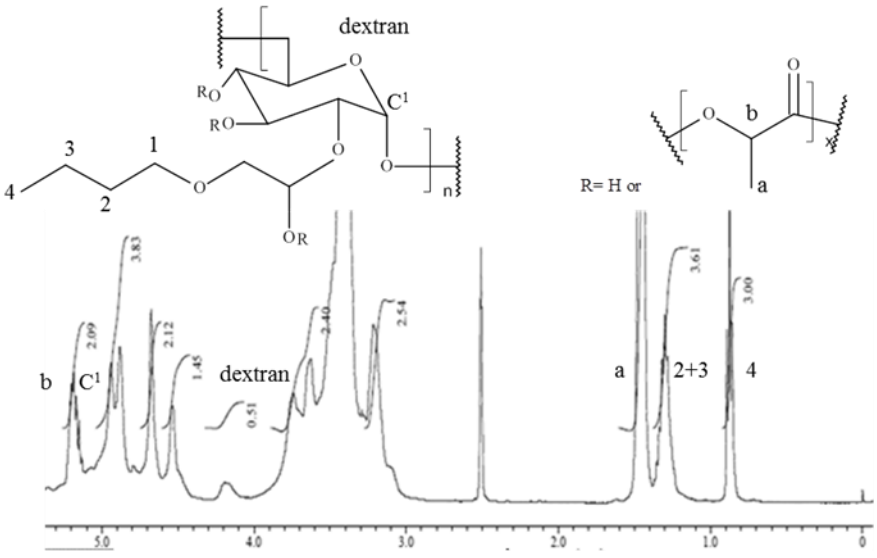

Figure 3.18: ^{1}H NMR spectra of PLA-DEX-OX4, groups of protons are assigned by numbers (dextran part of the molecule) or by letters (PLA).

3.3.4.2. Modification of poly(lactic acid) with maleic anhydride

A second approach to link alkylglyceryldextran to poly(lactic acid) (PLA) considered the possibility of increasing the degree of grafting by modifying PLA with maleic anhydride (MA) 'anchors' [402] (instead of employing the only one carboxyl group of PLA) followed by a carbodiimide-type reaction of the potential carboxylic moieties with alkylglyceryldextran. Free radical initiator benzoylperoxide (BPO) was employed to generate ternary radicals at the C^2carbon atom of PLA. Such a radical attacked a double bond of maleic anhydride *(Figure 3.20.)*. The reaction took place in anhydrous conditions and the product was purified by precipitation from ethanol (yields 52-74%).

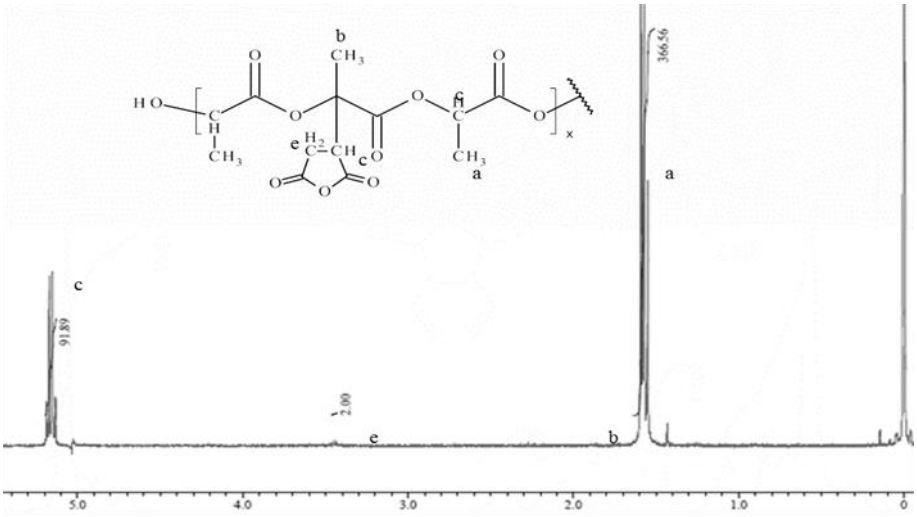

Figure 3.19. Peak assignment of poly(lactic acid) grafted with maleic anhydride

The degree of grafting with maleic anhydride (DG) was calculated from the ^{1}H- NMR spectra as a ratio of peak integrals using the signals at 5.1 ppm (assigned to the CH proton in poly(lactic acid)) and at 3.8 ppm (assigned to the CH_2 protons in maleic anhydride), as described in the literature [403]. The degree of grafting was in the range 0.81-2.21 % (expressed as percentage of lactic acid units modified with maleic anhydride) – which is in accordance with literature (ca. 1-3 % [402], [229]) and this was found to be dependent on the amount of initiator *(Table 3.6.)*. However, even when relatively high amounts of initiator were used (up to 20 % w/w relative to PLA), the degree of grafting was not increased to a level comparable to natural polysaccharides (to serve as a structure to attach multiple molecules of alkylglyceryl dextran derivatives to one molecule of poly(lactic acid) *via* the carbodiimide approach described in chapter 3.3.4).

Table 3.6. Degree of grafting of maleic anhydride onto poly(lactic acid)

BPO content relative to PLA [% w/w]	Degree of grafting [%]
5	0.81
10	2.10
20	2.21

Among the researchers attempting the radical grafting of PLA with MA, the Xufeng group reported 1.61-3.16 % [402] and Jun Pan acquired 1.86-2.68 % [229]. A decrease of the

MW of poly(lactic acid) caused by scission from high contents of acidic maleic anhydride was also reported in the literature [229, 230, 402], while the low degree of grafting obtained was explained by the low activity of BPO [229]. However, employing a different initiator, dicumyl peroxide, led to an even lower degree of grafting, 0.5 % [404]).

The low degree of grafting led to discontinuation of subsequent attaching of alkylglyceryldextran derivatives to carboxyl groups of modified poly(lactic acid).

3.4. Conclusions

Chitosan and dextran were selected as polysaccharides of choice due to their biocompatibility, lack of toxicity, biodegradability and presence of easily modifiable functional groups such as amino and hydroxyl. The functionalisation of these polysaccharides with alkylglyceryl moieties was aimed at providing blood-brain barrier permeating features (as expected from the alkylglycerol behaviour reported in the literature) to the modified polymers.

The *n*-alkylmethyloxiranes employed for the modification of chitosan and dextran were prepared (where not available commercially) in moderate yield (*n*-octylmethyloxirane ca. 23 – 49 %) by the nucleophilic substitution of epibromohydrin with the corresponding alcohol.

Alkylglyceryl-modified chitosan derivatives were synthesised in three successive steps: the treatment of commercial chitosan with phthalic anhydride yielding phthaloylchitosan (which protects the amino groups while increasing the solubility in organic solvents) was followed by treatment with either *n*-butyloxymethyloxirane, *n*-pentyloxymethyloxirane or *n*-octyloxymethyloxirane to afford the corresponding alkylglyceryl-phtaloyl chitosans, which were finally deprotected by removing the phthaloyl groups by treatment with hydrazine (12-39 %, overall yield). The products (butylglycerylchitosan CS-OX4, pentylglycerylchitosan CS-OX5 and octylglycerylchitosan CS-OX8, respectively) were analysed by spectroscopic methods

(FT-IR, ^{1}H-NMR), when the degree of substitution with alkylglyceryl chains was determined as being in the range 14 - 88 % (as determined from proton spectra).

Alkylglyceryl-modified dextran derivatives were prepared by reacting commercially available dextran with *n*-alkyloxymethyloxiranes in the presence of a strong base (such as potassium *tert*-butoxide) in anhydrous DMSO. The products were purified by dialysis and freeze-drying, affording butyglyceryl-dextran and octylglyceryl-dextran (yields 35-80 %), which were identified by NMR and FT-IR. The degree of substitution was in the range of 1.2-84 %, as determined by ^{1}H-NMR spectroscopy. Using a different base in environment of DMSO (such as 4-(dimethylamino)pyridine or pyridine) or employing $Zn(BF_4)_2$ as a catalyst in an aqueous system did not afford higher degrees of substitution compared to using potassium *tert*-butoxide. The synthesised alkylglyceryl-dextran derivatives were analysed by Gel Permeation Chromatography against pullulan standards, and the results indicated a decrease in the molecular weight of the products (average MW 6.07 kDa for butylglyceryl-dextran DEX-OX4 and MW 9.73 kDa for octylglyceryl-dextran DEX-OX8) compared to the starting material (MW 10.7 kDa, dextran from Sigma, nominative MW 6 kDa). However the reaction conditions were not expected to break the bonds between the polysaccharide units therefore the results could represent different interaction of materials with the separation column (related to the degree of substitution), rather than expressing any change of molecular weight.

The alkylglyceryl-dextran derivatives further reacted with poly(lactic acid) in the presence of carbodiimide zero-length crosslinkers (such as dicyclohexylcarbodiimide (DCC) and carbonyldiimidazole (CDI)) to afford a graft co-polymer that can be formulated into nanoparticles (normal dextran is water soluble and does not self-aggregate into nanoparticles, nor possesses any hydrophobic moieties or permanent charges that could be used for ionic crosslinking). Both CDI and DCC afforded successful binding of both polymers as confirmed by spectroscopic methods. However, using CDI in Nagahama's two step procedure, that involves isolating the activated poly(lactic acid), appears to exclude the possibility of internal cross-linking between the hydroxyl groups of the alkylglyceryl-modified dextran potentially

caused by an excess of carbodiimide to yield alkylglyceryl-dextran-*graft*-poly(lactic acid) derivatives. The degree of grafting was calculated using ^{1}H-NMR spectroscopy (degree of grafting of butylglyceryl-dextran-*graft*-poly(lactic acid) was in range 88-102 and octylglyceryl-dextran-*graft*-poly(lactic acid) was in range 109-120 units of poly(lactic acid) per 100 units of modified dextran).

A possibility of attaching multiple alkylglyceyl-dextran molecules to one molecule of poly(lactic acid) was exploited by increasing number of reactive groups in poly(lactic acid) molecule by free radical grafting. Poly(lactic acid) was grafted with maleic anhydride *via* a free-radical reaction in the presence of benzoyl peroxide as an initiator; the degree of grafting was low (0.8-2.2 %). Due to limited success in the grafting step the subsequent modification with alkylglyceryl-dextran was not continued.

4

PREPARATION AND CHARACTERISATION OF POLYSACCHARIDE NANOPARTICLES

4.1. Materials and instrumentation

Trehalose, sodium tripolyphosphate (TPP), chitosan, dextran, Evans Blue, Rhodamine B, dextran sulphate, fluorescein, polyvinylalcohol (PVA) were purchased from Sigma Aldrich. Poloxamer 188 (P188) and Poloxamer 407 (P407) were obtained from BASF. Poly(lactic acid) (PLA) was received from Purac and doxorubicin hydrochloride was obtained from LGM Pharma, USA. Chitosan oligomer (o-CS, Mw 700 Da) was sourced from the stock previously synthesised in-house. Solvents such as DMSO, acetone, acetic acid were obtained from Fisher Scientific. Cellulose nitrate membrane filters (0.2 μm) were obtained from Whatman, UK.

Dialysis was performed employing dialyzing Visking tubing MWCO 12-14 kDa or 3 kDa, Medicell International Ltd, UK; the container with deionised water (10.0 L) was exchanged 3 times a day. The purified water was obtained from PURELAB Optima lab system. Ultracentrifugation was performed using a X3 Ultracentrifuge (Beckman Coulter Ltd. UK) with Ti 70.1 rotor at 20 °C *in vacuo* (40 000 rpm, 30 min). Pre-centrifugation was performed with an Eppendorf MiniSpin centrifuge equipped with a F-45-12-11 rotor (Eppendorph UK). Freeze drying of aqueous samples was performed using a Modulyod Freeze Dryer equipment attached to an EDWARDS RV3 vacuum pump. Organic solvents were removed under reduced pressure using a Büchi Rotovapor R-200 and a Sogevac Saskia PIZ 100 vacuum pump equipped with a liquid nitrogen trap. Sonication was performed using a Grant ultrasonic bath XB3 from Farnell, UK. The high voltage power supply PSIFC30R04.0-22; Glassman High Voltage Inc, USA was used for electrospraying experiments fed by a syringe pump Alladin 300; World Precision

instruments, USA. A combined linear shaking thermostatted bath Grant OLS 200, Farnell, UK, was used for dye release studies. An Lambda 650 Ultra Violet/Visible Spectrometer from Perkin Elmer was used for UV/VIS spectroscopy measurements (Perkin Elmer UV Lab software).

Dynamic Light Scattering (DLS) was used to determine the hydrodynamic diameter of nanoparticles - a Malvern Zetasizer Nano ZS instrument from Malvern, UK, equipped with a 633 nm He-Ne laser (173° back scattering angle detection) was used for this purpose. Samples were analysed in triplicates in polycarbonate disposable clear cuvettes at 25 °C following an equilibration time of 2 min; the equipment was powered by Zetasizer software v. 6.01 software. Results of cumulative analysis were expressed as Z-average mean (Z-av.), the polydispersity index (PDI) was also determined. Zeta potential (ZP) was determined from electrophoretic mobility (EPM) measurements, which were performed with the same instrument. Samples were measured in polycarbonate disposable clear zetasizing cuvettes (software analysis employed Smoluchowski model, Henry's function $f(ka)$ = 1.5). The titrations of colloidal systems were carried out to assess the Z-av, and ZP in conditions of various pH; the experiments employed MTP-2 (Multi Purpose Titrator-2, Malvern, UK) equipped with a solvent degasser. The sample (10 mL) was titrated automatically with aqueous NaOH solutions (5 mM and 50 mM) from pH 3 to pH 8, and with aqueous HCl solutions (5 and 50 mM) from pH 8 to pH 2. All solutions were filtered via 0.2 μm PES filters (Whatman) prior to use. Nanoparticle Tracking Analysis (NTA) was performed using a Nanosight instrument equipped with a thermostatted LM-14 unit with 532 nm green laser at 25 °C. The image capture (length 60 s) was achieved using a CCD Marlin camera; the instrument was powered by NTA 2.2 analytical software.

The morphology of nanoparticles was investigated by Scanning Electron Microscopy. Nanoparticles recovered from freeze drying were redispersed in ultrapure water, then a droplet was placed onto a metallic stub and dried in a nitrogen flow. As organic samples need to be covered by a thin conductive alloy layer, the nanoparticles were coated with golden alloy in argon atmosphere (current 20 mA, pressure 10^{-3} Pa, 5 min) using a Quorum coater Q150RES

sputtering equipment from Quorum Technologies Ltd., UK. The samples were investigated using a JEOL-JSM-6060LV SEM Microscope (high vacuum, voltage 15 kV, working distance 11 mm, spot size 40) from Jeol, Japan. The shape of dried nanoparticles was also investigated using AFM: nanoparticles were dispersed in ultrapure water, and one drop of the suspension was placed on a mica surface and dried in a nitrogen flow. The deposits were then investigated with a MultiMode/NanoScope IV Scanning Probe Microscope (Digital Instruments, USA) and in tapping mode in air under ambient conditions (T = 23 °C, RH = 21%) using the J-scanner (max. xy = 200 mm) using Si cantilevers with integrated tips (t = 3.5–4.5 mm, l = 115–135 mm, w = 30–40 mm, f = 200–400 kHz, k = 20–80 N m^{-1}, R o 10 nm; Model: RTESP, Veeco Instruments, France) and an RMS amplitude of 0.8 V was used. The results were analysed using a Nanoscope Veeco v 710 software from Digital Instruments, USA.

The statistical analysis was performed using OriginPro 7 software from OriginLab, USA by one-way analysis of variance (ANOVA) followed by post hoc Tukey test (p values were set at level 0.05 unless stated otherwise). Measurements are presented as mean ± standard deviation unless stated otherwise.

4.2. Methods

4.2.1. Nanoparticles formulated from alkylglyceryl-modified chitosan derivatives

Nanoparticles from chitosan (CS) and alkylglyceryl-modified chitosan (CS-OXn) derivatives were prepared by ionotropic gelation using counterions such as sodium tripolyphosphate (TPP) or dextran sulphate (DEX-S). Alkylglyceryl-modified chitosan derivatives were also employed for coating PLA core nanoparticles in the presence of various surfactants. As previous studies [129, 173] indicated nanoparticles formulated with TPP could have low stability at physiological pH, the possibility of using DEX-S as a different cross-linking agent to provide more stable structures was investigated here.

4.2.1.1. Nanoparticles formulated from alkylglyceryl-modified chitosan crosslinked with sodium tripolyphosphate

Solutions of either CS or CS-OXn (n = 4, 5, 8; 0.28% w/v) were prepared by dissolving the corresponding polysaccharide in acetic acid (AcOH, 0.35 % v/v) overnight under stirring. All solutions were filtered (0.2 μm PES) prior to use. Typically, 14 mL of TPP solution (0.063 % w/v) was added dropwise by means of a peristaltic pump over 30 minutes into 35 mL of polysaccharide solution, under moderate stirring, in a 55 mL plastic container. The solutions were then mixed for an additional 30 minutes.

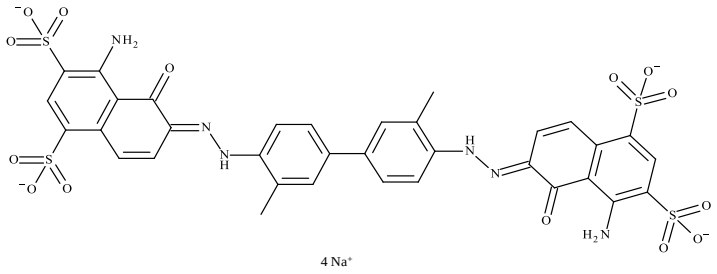

Figure 4.1. The chemical structure of Evans Blue.

For the preparation of fluorescently-labelled nanoparticles, an Evans Blue *(Figure 4.1.)* solution (0.01 % w/v) in HPLC water was added to the polysaccharide solution (0.28 % w/v, prepared as described above) and stirred for 30 minutes before the dropwise addition of TPP. The formulations were then centrifuged (4 000 RPM; 15 min) using a Jouan B4 centrifuge to remove the large aggregates; the supernatant was separated and the hydrodynamic diameter (DLS, NTA), zeta potential (ZP) and polydisperisty (DLS) of nanoparticles were measured in the preparation media (pH 3-4).

The nanoparticles were then isolated by ultracentrifugation (rotor 70.1 Ti, 40 000 RPM for 30 min, at 20 °C) washed with water and lyophylised. Dialysis was also investigated as an alternative purification method (3 days; 10.0 L of deionised water exchanged 3 times per day), followed by lyophilisation. Nanoparticles were characterised again after redispersion in PBS (pH 7.4, saline 0.9%).

The loading of Evans Blue into the nanoparticles was determined by UV/Vis spectrophotometry (λ=640 nm, APPENDIX VI). The lyophilised pellets of nanoparticles were dissolved in acetic acid (55 %) in concentration 1 mg/ mL. The obtained absorbance was used to acquire the concentration of Evans Blue in the sample according the calibration curve in 55 % acetic acid. The loading is expressed as ratio of mass of the dye in respect to mass of the whole pellet (% w/w).

4.2.1.2. Nanoparticles formulated from alkylglyceryl-modified chitosan by ionic crosslinking with dextran sulphate

Butylglycerol-modified chitosan (CS-OX4) was dissolved (0.15 % w/v) overnight in acetic acid (0.32 %, v/v, 25 mL) in a conical flask under vigorous stirring. Dextran sulphate (DEX-S) was dissolved in A) water (25 mL) or B) in acetic acid (0.32 %, 25 mL) in various concentration ratios (CS-OX4 : DEX-S = 1:5; 1:10; 1:20). The solution of CS-OX4 was added dropwise using a peristaltic pump to the DEX-S solution, under vigorous stirring. After completing the addition, the mixture was allowed to stir for an additional 30 minutes.

For labelling the nanoparticles with Evans Blue, the dye was dissolved in the DEX-S phase (25 mL) in 0.1 % (w/v) concentration prior to the dropwise addition to the CS-OX4 solution. The dispersion was centrifuged (3 000 RPM; 3 min, Eppendorph MiniSpin) prior to characterization by DLS to determine the hydrodynamic diameter and polydispersity and by EPM to determine zeta potential in the preparation medias well. Further isolation and purification of nanoparticles were performed by ultracentrifugation followed by freeze-drying the pellet. The redispersion of the pellet in PBS (pH 7.4, saline 0.9 %) was carried out in the sonic bath for 15 min.

The loading of Evans Blue into the nanoparticles was determined by UV/Vis spectrophotometry (λ=640 nm). The lyophilised pellets of nanoparticles were dissolved in acetic acid (55 %) in concentration 1 mg/ mL. The obtained absorbance was used to determine the

concentration of Evans Blue in the sample according the calibration curve. The loading is expressed as ratio of mass of the dye in respect to mass of the whole pellet (% w/w).

Nanoparticles from CS-OX crosslinked with both TPP and DEX-S were investigated for their stability to various pH conditions by titration with NaOH solution. An automatic MTP-2 titrator equipped with a degasser and a flow-cell were employed for measuring the hydrodynamic diameter and zeta potential as a function of pH using a Malvern Zetasizer nano ZS instrument. The pH was varied from pH 3.0 to 8.0 by using NaOH solutions (0.05 M and 0.005 M).

4.2.1.3. Nanoparticles from poly(lactic acid) coated with akylglyceryl-modified chitosan

Nanoparticles from poly(lactic acid) (PLA) were prepared by nanoprecipitation [245]. Briefly, PLA was dissolved in acetone (5 mL, 10.0 mg/mL) and the solution was added dropwise into deionised water (25 mL) under stirring (all solutions were filtered using 0.2 μm cellulose nitrate membrane filters prior to use). The mixture was stirred for an additional 30 min, and the residual acetone was removed under reduced pressure. The final concentration of nanoparticles was adjusted (25 mL, 2.0 mg/mL) with ultrapure water. The formulations were freeze-dried after characterisation by DLS and EPM.

Nanoparticles prepared from PLA were dispersed in water (2.0 mg/mL) with surfactants (Poloxamer 407 (P407); Poloxamer 188 (P188); polyvinyl alcohol (PVA); 0.1 mL; 1.0 mg/mL or 10.0 mg/mL). The mixture was incubated with 100 μL butylglyceryl chitosan (CS-OX4; DS 85.0 %; dissolved in 0.35 % w/v acetic acid) solution (15.0 mg/mL) for 5 minutes under stirring. The samples (1.5 mL) were centrifuged (3 000 RPM; 3 min, Eppendorph MiniSpin) to remove possible aggregates and the supernatant was characterised by DLS and EPM for hydrodynamic diameter and zeta potential, respectively.

Redispersion of PLA nanoparticles coated with butylglyceryl-modified chitosan in the presence of surfactants. A crude suspension of butylglyceryl chitosan (CS-OX4) coated PLA nanoparticles was centrifuged (1.4 mL, 7 500 RPM; 10 min) on a trehalose bed (0.1 mL; 0.7 g/mL) and the pellet was transferred into an Eppendorf tube. After the addition of 1.5 mL of water, the tube was vortexed for 30 sec and sonicated for 5 minutes to redisperse the nanoparticles. The sample was centrifuged at low speed (3 000 RPM, 3 min, Eppendorph MiniSpin) to remove potential non-dispersed aggregates and the supernatant containing the CS-OX4-coated PLA nanoparticles, redispersed in water, was analysed to measure the size and zeta potential with Malvern Zetasizer Nano ZS.

pH titrations of PLA nanoparticles coated with butylglycerylchitosan.10 mg of PLA nanoparticles coated with CS-OX4 was redispersed in water (10 mL, 1.0 mg/mL). The suspension was employed in a closed circuit of Zeta sizing cuvette which was connected to Malvern Zetasizer ZS attached to a titrator (MTP-2 from Malvern Instruments). The titration started acidic (adjusted by 0.05 M HCl), from pH approx. 4.0 was increased to pH 8.5 using 0.05 M and 0.005 M NaOH as a titrant. Zeta potential and size of nanoparticles were measured after pH increment of about 0.3.

4.2.2. Nanoparticles formulated alkylglyceryl-modified dextran derivatives

Alkylglyceryl-modified dextran derivatives were formulated into nanoparticles by complexation with chitosan (chapter 4.2.2.1.) and by nanoprecipitation with poly(lactic acid) (chapter 4.2.2.2.). The nanoparticles from copolymers of alkylglyceryl-modified dextran and poly(lactic acid) were formulated *via* dialysis method, nanoprecipitation and electrospraying (chapter 4.2.2.3.).

4.2.2.1. Nanoparticles formulated from alkylglyceryl-modified dextran and chitosan oligomer

Nanoparticles were prepared from a combination of alkylglyceryl-modified dextran (butylglyceryl dextran DEX-OX4 was chosen as a model candidate) and chitosan oligomer (o-CS, MW ca. 700) in the presence of Poloxamer 407 (P 407). To a solution of DEX-OX4 (0.1 % w/v, 15 mL) and P 407 (varying concentrations 0.1 - 0.6 % w/v) in HPLC water, a solution of chitosan (0.02 % w/v, 5 mL) in acetic acid (0.063 % v/v) was added dropwise with stirring. The mixture was stirred for further 30 minutes at room temperature, the nanoparticles were isolated by ultracentrifugation (40 000 RPM; rotor 70.1 Ti, 10 min) into a trehalose bed; after discarding the supernatant the pellet was redispersed in water within an ultrasonic bath (Gant XB2).

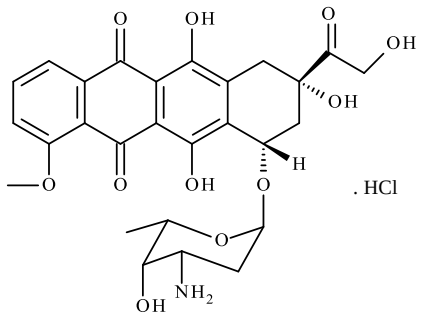

Figure 4.2. The structure of Doxorubicin hydrochloride.

Doxorubicin-loaded nanoparticles from butylglyceryl-modified dextran and chitosan. Doxorubicin is an anthracycline antibiotic used as an anticancer agent [405] and was supplied as a hydrochloride salt. To remove the hydrochloride the drug was dissolved in water (50 mg/ 1.0 mL) and triethylamine was added (0.1 mL); Doxorubicin free base was extracted (3 x) with chloroform using a separating funnel, the combined organic layers were dried over magnesium sulphate and the organic solvent was removed in a roto-evaporator to afford the free base (yield 68%). Doxorubicin free base (1.0 mg), butylglyceryl-modified dextran (DEX-OX4, 15 mg) and Poloxamer 407 (15.0 mg) were dispersed in water (15.0 mL) by sonication (30 min). The nanoparticles were formed after the dropwise addition of chitosan (3.0 mg) dissolved in acetic acid (0.03 %, 3.0 ml). Drug loading was determined (as %, w/w) by measuring the

non-entrapped drug in the supernatant after *via* fluorescent method (excitation 480 nm, emission 590 nm, Optima Fluorimeter) after removing the nanoparticles by ultra-centrifugation (40 000 RPM, 30 min, rotor 70,1 Ti). A calibration curve (APPENDIX VII) was constructed and employed for this purpose.

4.2.2.2. Nanoparticles formulated from poly(lactic acid) and akylglyceryl-modified dextran

Nanoparticles were obtained by nanoprecipitation of PLA into a DEX-OX4 solution, as follows: a PLA solution of acetone (5.0 mg/mL) was added dropwise to a solution of DEX-OX4 (varying concentrations: 0.07, 0.47, 1.00; 1.40, and 5.00 mg/mL) in water (15 mL) under stirring, which was then continued for an additional one hour; the remaining organic solvent was removed *in vacuo* in a rotary evaporator. The nanoparticles were isolated by centrifugation (10 000 RPM; 15 min) using an Eppendorph MiniSpin centrifuge and then were resuspended in HPLC water prior to the further analysis. The entrapment of (normally water-soluble) butylglyceryl dextran (DEX-OX4) in the nanoparticles was verified by FT-IR analysis (ATR mode) of the centrifuged (10 000 rpm; 10 min; Eppendorph MiniSpin) and then freeze-dried nanoparticles. The pellet of nanoparticles was analysed after first and after additional three redispersion-centrifugation-lyophilisation cycles and in the presence of both polymers (PLA and DEX-OX4).

4.2.2.3. Nanoparticles formulated from poly(lactic acid)-*graft*-alkylglyceryl-modified dextrans

Three methods were employed to formulate nanoparticles from poly(lactic acid)-*graft*-alkylglyceryl-modified dextran (PLA-DEX-OX4): the solvent displacement (*via* dialysis), the nanoprecipitation and the electrospraying.

A. Solvent displacement method (*via* dialysis).PLA-DEX-OX4 (either 0.5; 1.0; 3.0; or 5.0 mg/mL) was dissolved in DMSO (10.0 mL), the solution was filtered through a 0.2 μm filter (PP membrane) and then dialysed (MWCO 12 000 Da) against deionised water for 72 h (10.0 L; exchanged 3 times per day) to remove the DMSO (nanoparticles from PLA-DEX and PLA-DEX-OX8 were prepared from concentration 1.0 mg/mL). After 48 h, the content of the dialyzing tubing was freeze-dried and the solid material was redispersed as nanoparticles in PBS (0.9 % NaCl; pH 7.4) or in ultrapure water (conductivity 18 MΩ; pH 7.0). The suspension was centrifuged at low speed (3 000 RPM; 5 min, Eppendorph MiniSpin) to remove any potential large aggregates formed, then the nanoparticles were analysed by DLS, NTA and EPM.

B. Nanoprecipitation method. PLA-DEX-OX4 was dissolved in DMSO (3.0 mL, concentration 5, 10, 20 mg/ mL), the solution was filtered *via* a 0.2 μm filter (PP membrane, Whatman) and added dropwise into ultrapure water (30.0 mL) under vigorous stirring, which was continued for an additional 30 min after addition. The dispersion was then centrifuged (3 000 RPM; 5 min; Eppendorph MiniSpin) and the supernatant containing nanoparticles was either dialysed (Medicell, MWCO 12 kDa) for 72 h against deionised water (10.0 L; exchanged 3 times per day), or ultracentrifuged (40 000 RPM, 30 min, rotor 70,1 Ti). Finally, the products of purification were freeze-dried to obtain a white-off powder, which was redispersed in PBS (pH 7.4; 0.9 % saline) or in ultrapure water (conductivity 18 MΩ, pH 7.0). The suspension was centrifuged at low speed (3 000 RPM; 5 min, Eppendorph MiniSpin) to remove any aggregates, then the supernatants containing nanoparticles were analysed by DLS, NTA and EPM.

C. Electrospraying method. Nanoparticles from PLA-DEX-OX4 were prepared using the setup presented in *Table 4.1*. A solution (1.0 mL) of PLA-DEX-OX4 in DMSO (5 % w/v) was injected with a syringe pump (Alladin 300; World Precision instruments, USA) into a needle which was connected to the high voltage generator (PSIFC30R04.0-22; Glassman High Voltage Inc) and the sprayed material was collected onto water surface (a circular dish containing water, 143.1 cm^2; 50 mL). The purification of the resulting dispersion was performed either *via* ultracentrifugation (Beckman, Rotor 70.1 Ti; 40 000 RPM; 30 min; 20 °C) or *via* dialysis (for 3

days, 10.0 L of deionised water exchanged 3 x per day) and freeze-drying. The nanoparticles were then redispersed in ultrapure water or PBS (pH 7.4; 0.9 % saline) and the suspension was centrifuged at low speed (3 000 RPM, 3 min) to remove any potential aggregates prior to being analysed by DLS, EPM and NTA.

Table 4.1. Electrospraying method - experimental conditions.

Electrospraying of polymeric solutions took place under specific conditions	
Mixture	5 % w/v PLA-DEX-OX4 in DMSO 1 % w/v dye (Rhodamine B Base or Doxorubicin Base)
Flow rate	15 µL/min
Needle inner diameter	380 µm
Air gap distance	20 cm
Electric field	18 kV
Volume of ultrapure water for nanoparticle collection	50 mL
Surface area of ultrapure water collecting the nanoparticles	143.14 cm^2
Injecting time (to allow passage of 1 mL of solution)	67 minutes

pH stability. Zeta potential was acquired from electrophoretic mobility measurements using a Malvern Zetasizer Nano ZS instrument. The zeta potential was assessed in range of pH by the Zetasizer instrument equipped with a flow cell and an MTP-2 automatic titrator. The suspensions of PLA-DEX-OX4 nanoparticles redispersed in ultrapure water (10.0 mg; 10.0 mL; pH 8, as adjusted with 0.005 M NaOH) were titrated with HCl 0.05 M from. pH 8 to pH 2, while measuring the diameter and zeta potential of nanoparticles (at 0.3 pH increment).

Purification and redispersion. For each of the three methods, yields after purification processes (as mentioned above) were determined. One route was performed *via* ultra-centrifugation (40 000 RPM, 30 min, 20°C, Beckman 70.1 Ti rotor). Alternatively, the dialysis (10.0 L, exchanged 3 x daily for 3 days) was employed as a purification method. The yields were determined as ratio of starting material to final product in per cent.

Loading and release of fluorescent molecules. Fluorescent dyes such as Fluorescein, Rhodamine B or Doxorubicin have been employed as markers and model actives to

study drug loading and nanoparticle-cell interactions. All three model molecules were used for loading by solvent displacement *via* dialysis and nanoprecipitation; Rhodamine B and Doxorubicin were used for electrospraying experiments. In the encapsulation experiments the dyes were added (10 % w/w in respect to the polymer) to the organic phase (DMSO). Doxorubicin was supplied as a hydrochloride salt therefore the hydrochloride group was removed by treatment with triethylamine [253] as described in section 4.2.2.1.Drug loading was determined spectrophotometrically (Rhodamine B 318 nm; FITC 493 nm; Doxorubicin 478 nm, APPENDIX VIII) as follows: the nanoparticles were separated by ultracentrifugation (40 000 RPM, 30 min, 20°C, Beckman, rotor 70.1 Ti) and the pellets freeze-dried. The pellets were weighted and dissolved in DMSO to determine the amount of the dye in the pellet by UV/Vis spectroscopy. The obtained results are plotted against the calibration curves of the fluorescent molecules in DMSO. The corresponding calibration curves are presented in APPENDIX IX.

For the release studies the freeze-dried nanoparticles from PLA-DEX-OX4 were redispersed (1.0 mg/mL) in PBS (15 mL, pH 7.4, saline 0.9 %) and distributed in 1.0 mL aliquots into 15 Eppendorph tubes, which were placed in a thermostatted shaking water (37 °C). Tubes were individually removed at pre-determined time points and centrifuged (13 000 RPM; 15 min; Eppendorph MiniSpin). Three aliquots (0.1 mL each) were removed from the supernatant and placed into a 96 well-plate which was kept in the freezer (-20 °C) until all samples were collected; the plate was then equilibrated at room temperature (25 °C) and subsequently analysed using an Optima fluorimeter. The release profiles of dyes in PBS were based on calibration curves of the fluorescent molecules in PBS (APPENDIX IX).

4.3. Results and discussion

A series of nanoparticulate formulations were prepared from the materials considered in this study *(Table 4.2.)*, either on their own or in combination with poly(lactic acid): (alkylglyceryl chitosan derivatives CS-OX4, CS-OX5, CS-OX8; alkylglyceryl dextran derive DEX-OX4 and poly(lactic acid)-*graft*-alkylglyceryl dextran PLA-DEX-OX4 and PLA-DEX-OX8) using various methods (ionotropic crosslinking, nanoprecipitation, solvent displacement, and electrospraying). Nanoparticles were characterised in terms of hydrodynamic diameter and zeta potential in simulated physiologically-relevant conditions; promising nanoformulations were studied for their loading and release properties using fluorescent actives and markers.

Table 4.2. Alkylglyceryl-modified materials and methods for nanoparticle formulation.

Material	**Method to form nanoparticles**
Alkylglycerylchitosan **(CS-OXn)**	Ionotropic crosslinking with TPP Ionotropic crosslinking with DEX-S Coating of nanoparticles from PLA
Alkylglyceryldextran **(DEX-OXn)**	Mixing with CS Coating of nanoparticles from PLA
Poly(lactic acid)-*graft*-alkylglyceryl dextran **(PLA-DEX-OXn)**	Solvent displacement *via* dialysis Nanoprecipitation Electrospraying

4.3.1. Nanoparticles formulated from alkylglyceryl-modified chitosan derivatives

Nanoparticles were formulated from alkylglyceryl-modified chitosans (CS-OX4, CS-OX5 and CS-OX8) by crosslinking with either sodium tripolyphosphate (TPP) or dextran sulphate (DEX-S). These nanoparticles were studied for size, zeta potential, loading with dye Evans Blue and stability in various pH conditions. Furthermore, nanoparticles of poly(lactic acid) (PLA) were coated with CS-OX4 and the influence of surfactants upon the pH stability of the colloidal system was studied.

4.3.1.1. Nanoparticles formulated from alkylglyceryl modified chitosan by crosslinking with sodium tripolyphosphate

Nanoparticles from alkylglyceryl-modified chitosans (CS-OX4, CS-OX5 and CS-OX8) were prepared by crosslinking with TPP following a method reported in the literature [111]. As prepared (pH 4; in 0.035 % acetic acid v/v), nanoparticles formulated from these chitosan derivatives exhibited submicron diameter and positive zeta potential (Table 4.3.), however noticeable aggregation was observed (sometimes into the micron range) when the pH was changed to neutral by redispersion in PBS (pH 7.4) (Table 4.3.).

Table 4.3. Characteristics of nanoparticles formulated from chitosan and alkylglyceryl chitosans with different degree of substitution by crosslinking with TPP (n=3). using different techniques (DLS – Dynamic Light Scattering; NTA – Nanoparticle Tracking Analysis, EPM - Electrophoretic Mobility Measurements, PDI – polydispersity, ZP – Zeta Potential).

	pH 4.0				**pH 7.4**
	DLS		**NTA**	**EPM**	**DLS**
	Z-av. ± SD [nm]	PDI	Diam. ± SD [nm]	ZP ±SD [mV]	Z-av. ±SD [nm]
CS	143± 2	0.308	153 ± 75	40.1 ± 1	963 ± 145
CS-OX4 (15%)	133 ± 3	0.284	128 ± 54	36.0 ± 0	1555 ± 396
CS-OX4 (95%)	151 ± 2	0.200	124 ± 55	36.9 ± 1	1101 ± 367
CS-OX5 (67%)	100 ± 10	0.227	100 ± 20	39.0 ± 6	871 ± 325
CS-OX8 (127%)	188 ± 50	0.367	125 ± 54	42.7 ± 3	1273 ± 290

The macroscopic aggregation of the nanoparticles was observed during the purification of the nanoparticles by dialysis. The centrifugation, employed as second purification method, yielded pellets for further freeze-drying (Table 4.3.). The yields were calculated as a ratio of mass of material used in formulation and mass of the pellet after freeze drying (expressed in per cent). It was apparent that the alkylglyceryl substitution of chitosan had influenced the yields of nanoparticles as the highest yields were obtained from unmodified chitosan derivatives and the lowest from the CS-OX8. In some cases there was no pellet at all *(Table 4.4.)*.

Table 4.4. Percentage recovery of polymeric materials used for crosslinking with TPP; pellet after centrifugation (n=3).

Material	Yield of nanoparticles w/w [%]
CS	6-30
CS-OX4	0-14
CS-OX5	0-19
CS-OX8	0-8

The morphology of alkylglyceryl-chitosan nanoparticles. Scanning Electron Microscopy investigation of butylglycerolchitosan (CS-OX4) nanoparticles after lyophilisation revealed spherically shaped particles with a diameter in the micron range (an example of CS-OX4 is given in *Figure 4.3.*). Such findings can confirm the studies using Dynamic Light Scattering on nanoparticles redispersed in neutral media conditions *(Table 4.3.)*.

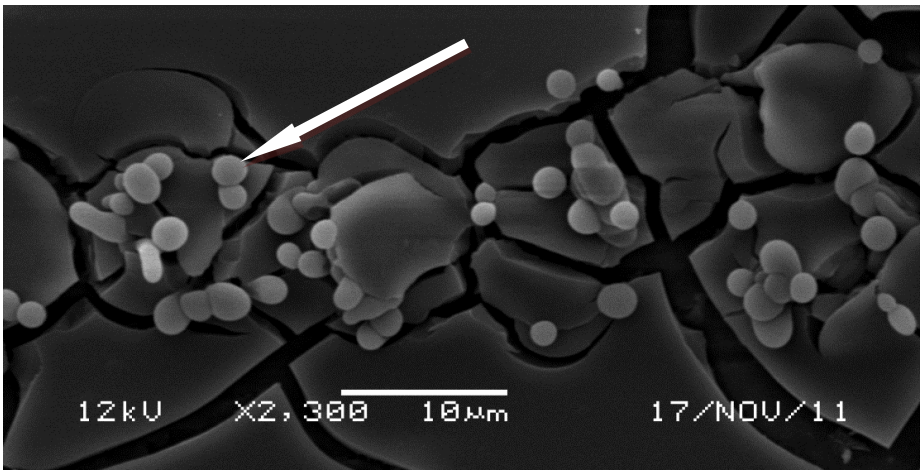

Figure 4.3. SEM photograph of nanoparticles (ARROW) prepared from CS-OX4 crosslinked with TPP.

4.3.1.2. Nanoparticles formulated from alkylglyceryl modified chitosan by crosslinking with dextran sulphate

Nanoparticles from butylglyceryl modified chitosan (CS-OX4) and dextran sulphate (DEX-S) were prepared by ionic crosslinking in two modifications: the DEX-S was dissolved either in water or in a diluted acetic acid (0.035 % v/v) while CS was dissolved in diluted acetic acid in all the cases. Nanoparticles were characterised by DLS and it was found that, when

acetic acid was used a solvent for both CS-OX4 and DEX-S, particle size was generally smaller and it was dependent on the ratio of CS-OX4 and DEX-S *(Table 4.5.)*; no such a trend was observed when DEX-S was dissolved in water. The influence of the solvent on the diameter of nanoparticles was significant when the same concentrations were compared (ANOVA, $p<0.05$). Electrophoretic mobility measurements in acidic conditions (pH 3-4) revealed in all cases a negative zeta potential of about – 40 mV.

Table 4.5. Nanoparticles of CS-OX4 crosslinked with DEX-S, influence of ratio (n=3; ±SD).

DEX-S solvent	**CS-OX4:DEX-S Ratio**	**Average PDI**	**Average Zeta Potential [mV]**	**Average diameter DLS [nm]**
HPLC water	1:5	0.54±0.22	- 47.0 ±3.0	505 ±12
	1:10	0.56 ±0.12	- 47.6 ±4.6	471 ±22
	1:20	0.60±0.15	- 35.1 ±3.1	547 ±17
Acetic Acid	1:5	0.41±0.18	- 40.3 ±1.1	224 ±16
	1:10	0.34±0.24	- 43.6 ±4.1	315 ±90
	1:20	0.53±0.20	- 47.2 ±4.4	434 ±33

These results appear similar to those obtained by Chen *et al.* [177] for particles prepared from normal chitosan (CS) and dextran sulphate (DEX-S), when it was observed that an excess of CS led to larger particles. His research focused on investigation of ratios DEX-S to CS. In an excess of chitosan (the ratio CS: DEX-S was 5:3) the size of particles was found in micrometre range (2100 nm ± 400, PDI 0.86) and Zeta potential was positive (50 mV). On the other hand, the excess of DEX-S produced nanoparticles 250-350 nm with negative Zeta potential (-25 to -47 mV). The influence of the ratio of the polysaccharides on the diameter was also found *(Table 4.5.).* The ratio 1:20 exhibited the largest diameters in each environment group (ANOVA, $p<0.05$). This would also support the previous findings that the size of nanoparticles was dependent on the total concentration of polymers in solution. That could be explained by

the fact that diluted solutions tend to create small coacervation nuclei, while highly concentrated solutions support complexation and coacervation of large nanoparticles [177].

Morphology of nanoparticles of alkylglyceryl-chitosan crosslinked by dextran sulphate. SEM analysis of nanoparticles prepared from CS-OX4 crosslinked with DEX-S (prepared in acetic acid, ratio 1:5) and isolated by centrifugation revealed that these nanoparticles were compacted together during separation; it appears that the subsequent drying of the pellet collapsed the material and destroyed the structure of individual particles *(Figure 4.4.)*.

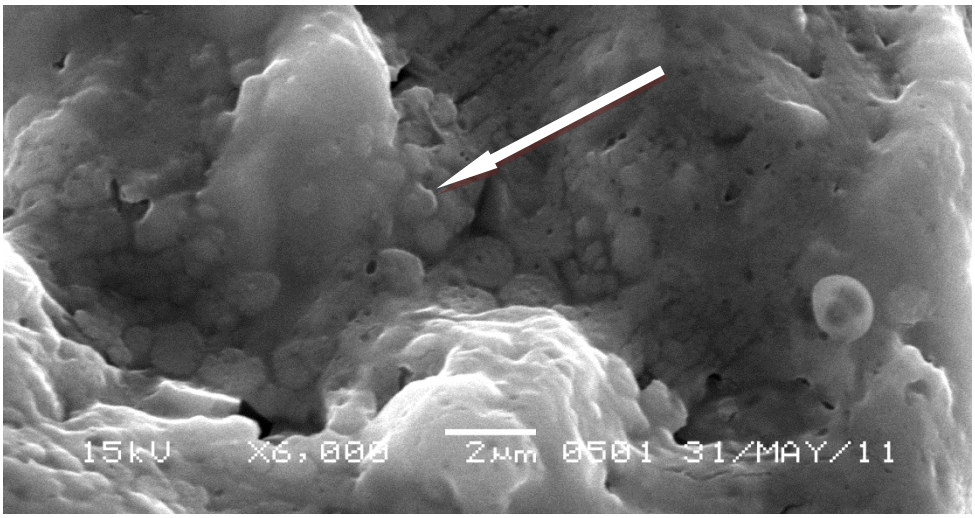

Figure 4.4. SEM micrograph representing the collapsed nanoparticles (ARROW) prepared from CS-OX4 crosslinked with DEX-S.

Stability of nanoparticles of alkylglyceryl-chitosan crosslinked by dextran sulphate. Nanoformulations prepared from butylglyceryl-modified chitosan (CS-OX4) crosslinked with either sodium tripolyphosphate (TPP) or dextran sulphate (DEX-S) were investigated for their stability in different pH conditions. Nanoparticle diameter and zeta potential were measured while varying the pH in the range of approx. pH 4 - 9 using a titration with NaOH solutions. The comparison of these results indicated an improved stability of CS-

OX4 nanoparticles across a wide pH range when DEX-S was employed as a crosslinker compared to TPP *(Figure 4. 5.)*.

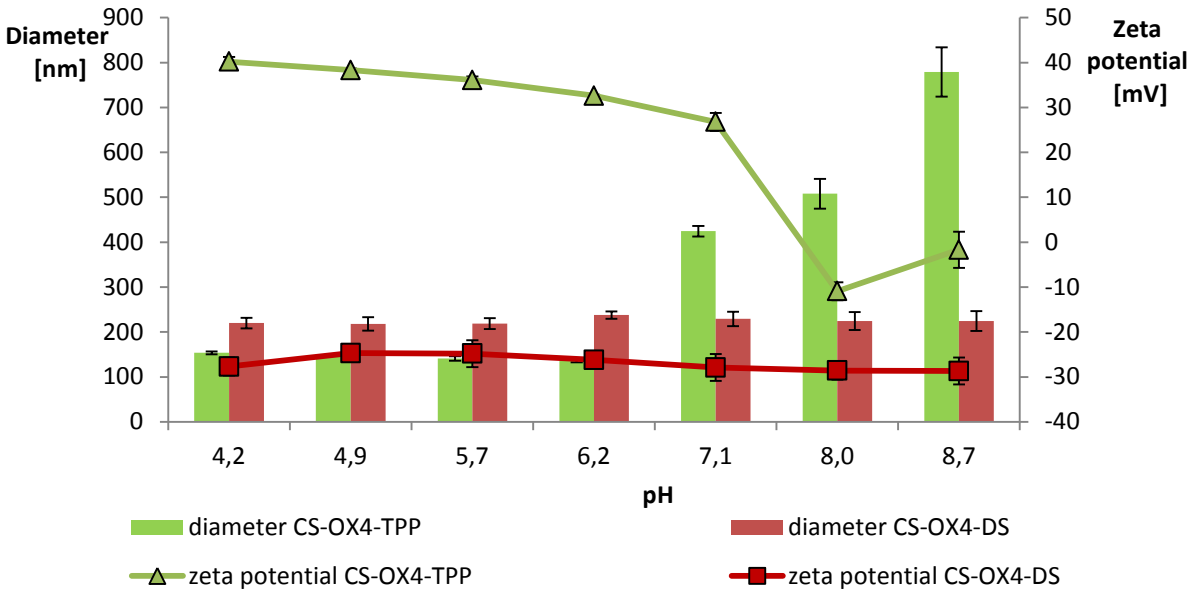

Figure 4.5. Variation of hydrodynamic diameter (column bars) and zeta potential (triangle) of nanoparticles prepared from CS-OX4 crosslinked with either TPP (green) or DEX-S (red) with increasing pH. (n=3, error bars represent standard deviation).

Nanoparticles from CS-OX4 crosslinked with DEX-S exhibited an almost constant diameter of ca. 200 nm over the whole range of pH, and a negative zeta potential (-30 mV), while nanoparticles obtained from CS-OX4 crosslinked with TPP also exhibited a low diameter (ca. 140 nm) and a stable and positive zeta potential (ca. 40 mV) but only in acidic conditions. However, when TPP was employed as a crosslinker, and in stark contrast to the behaviour of the formulations obtained using DEX-S, a noticeable increase in diameter accompanied by a decrease of the zeta potential occurred above the pK_a value of chitosan (ca. 6.5 [406]). As a result of the chitosan interactions with TPP being affected by the deprotonation of the amino groups, hydrodynamic diameter increased to 500 nm and zeta potential dropped to negative values, leading to gradual sample agglomeration. Interestingly, this behaviour was not observed when CS-OX4 was ionotropicaly crosslinked with DEX-S. The explanation may lie in a

different interaction of amino groups from chitosan with either sulphate groups of DEX-S or with phosphate groups of TPP [407].

Nanoparticles prepared from CS-OX4 crosslinked with either TPP or DEX-S were loaded with Evans Blue as a model fluorescent marker; although different properties as diameter and zeta potential, both types of systems showed similar loading capacity (3.67 ± 0.21 % and 3.01± 0.13 % respectively, *Table 4.6*, determined from a calibration curve.. The loaded nanoparticles from CS-OX4 with TPP had slightly smaller diameter (and positive zeta potential)compared to those obtained from CS-OX4 crosslinked with DEX-S, that were negatively charged (*Table 4.6.)*.

Table 4.6. Characteristics of Evans Blue-loaded nanoparticles obtained from CS-OX4 crosslinked with either TPP or DEX-S (pH 3.5; n=3; ±SD).

CS-OX4 crosslinked with	Z-ave diameter (DLS) [nm]	Zeta potential [mV]	Evans Blue loading capacity [% w/w]
TPP	183 ± 12	43.6 ± 1.2	3.67 ± 0.21
DEX-S	243 ± 22	-23 ± 3.3	3.01 ± 0.13

4.3.1.3. Nanoparticles from poly(lactic acid) coated with akylglyceryl-modified chitosan

In an attempt to improve the stability of nanoformulations based on alkylglyceryl chitosan at physiologically relevant pH values, butylglyceryl chitosan (CS-OX4) was coated on core nanoparticles of poly(lactic acid) (PLA), in the presence of various surfactants.

Poly(lactic acid) nanoparticles were prepared by nanoprecipitation and were coated by butylglyceryl modified chitosan (CS-OX4), as in chapter 4.2.1.3. The hydrodynamic diameter, polydispersity index and zeta potential of poly(lactic acid) core nanoparticles are presented in *Table 4.7*. The PLA nanoparticles coated with CS-OX4 are similar to those PLA nanoparticles coated with chitosan reported in the literature [128, 243, 408]. *Table 4.7.* also presents the same characteristics of butylglyceryl chitosan-coated nanoparticles in the presence of various

surfactants such as Poloxamer 407 (P407), Poloxamer 188 (P188) and polyvinylalcohol (PVA). Coating with CS-OX4 did not induce changes in the hydrodynamic diameter of PLA nanoparticles and led to a change of their global charge (zeta potential shifted from ca. -30 mV for uncoated nanoparticles to ca. +30 mV for coated ones), when measured in an acidic environment. However after purification (10 000 RPM, 10 min, Eppendorph MiniSpin centrifuge), when the nanoparticles were redispersed at neutral pH, CS-OX4 coating appeared to induce a significant increase in size in comparison to uncoated nanoparticles (ANOVA, $p < 0.05$), while zeta potential changed back to negative. At neutral pH, PVA seemed to slightly increase the size and lower the zeta potential of coated nanoparticles compared to the other surfactants considered in this study, but no general trends could be observed.

Table 4.7. Characteristics of CS-OX4-coated PLA core nanoparticles prepared in the presence of different surfactants,(P407 – Poloxamer 407; P188 – Poloxamer 188; PVA – polyvinylalcohol; n=3; ±SD).

Surfactant	Surfactant conc. [mg/mL]	Z-ave diameter, mean [nm ± sd]		Zeta potential, mean [mV ± sd]	
		pH 4	pH 7	pH 4	pH 7
-	0	173.2 ± 3.1	197.2 ± 3.7	-29.3 ± 3.4	-27.6 ± 3.3
P407	1	176.4 ± 2.2	392.2 ± 2.5	26.2 ± 2.1	-30.9 ± 2.2
	10	171.7 ± 2.6	306.0 ± 2.9	46.7 ± 2.2	-38.5 ± 3.0
P188	1	171.9 ± 2.7	366.3 ± 3.0	46.6 ± 4.1	-33.9 ± 2.1
	10	174.6 ± 2.6	303.2 ± 2.1	44.5 ± 2.1	-26.3 ± 3.2
PVA	1	183.9 ± 2.8	1269.7 ± 65.1	22.5 ± 2.7	-17.3 ± 2.9
	10	163.6 ± 3.3	489.3 ± 13.4	49.9 ± 2.7	-25.2 ± 3.3

4.3.2. Nanoparticles prepared from alkylglyceryl-modified dextran derivatives

Two techniques (complexation with chitosan oligomers and coating of nanoparticles from poly(lactic acid)) were employed to formulate butylglyceryl dextran (DEX-OX4) (prepared as described in chapter 4.2.2.) into nanoparticles. These were further characterised under simulated, physiologically relevant conditions in terms of, hydrodynamic diameter, zeta

potential and morphology. Nanoparticles prepared from poly(lactic acid)-*graft*-alkylglycerol-modified dextran are described in 4.3.2.3.

4.3.2.1. Nanoparticles formulated from alkylglyceryl-modified dextran and chitosan oligomers

Nanonoparticles based on DEX-OX4 and chitosan oligosaccharide (o-CS, MW approx. 700 Da) were prepared in the presence of Poloxamer 407 (P407) following the method described in chapter 4.2.2.1. The formulation of nanoparticles was optimised by varying the amount of P 407. The nanoparticles were characterised for size and zeta potential in conditions of preparation and after redispersion in conditions of physiological pH.

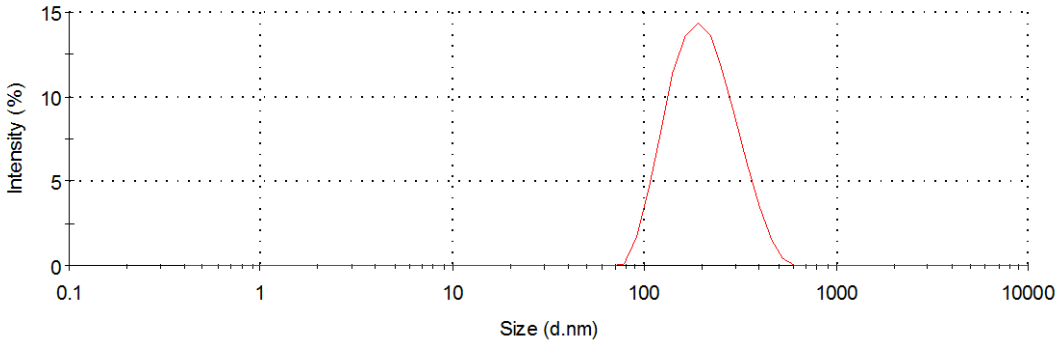

Figure 4.6. Size distribution of nanoparticles prepared from DEX-OX4 (1 mg/mL) and CS oligomer (0.02 mg/mL) in the presence of surfactant (P407, 1 mg/mL), represented as percentage intensity (Malvern Zetasizer Nano ZS).

The formulation required only a small amount of surfactant (i.e. 1 mg/mL, for Z-av. diameter approx. 150 nm, *Figure 4.6.*) as nanoparticles were not forming in its absence; at the same time, an increased amount of P407 was found to lead to an increase in both size and polydispersity index (*Figure 4.7.).*

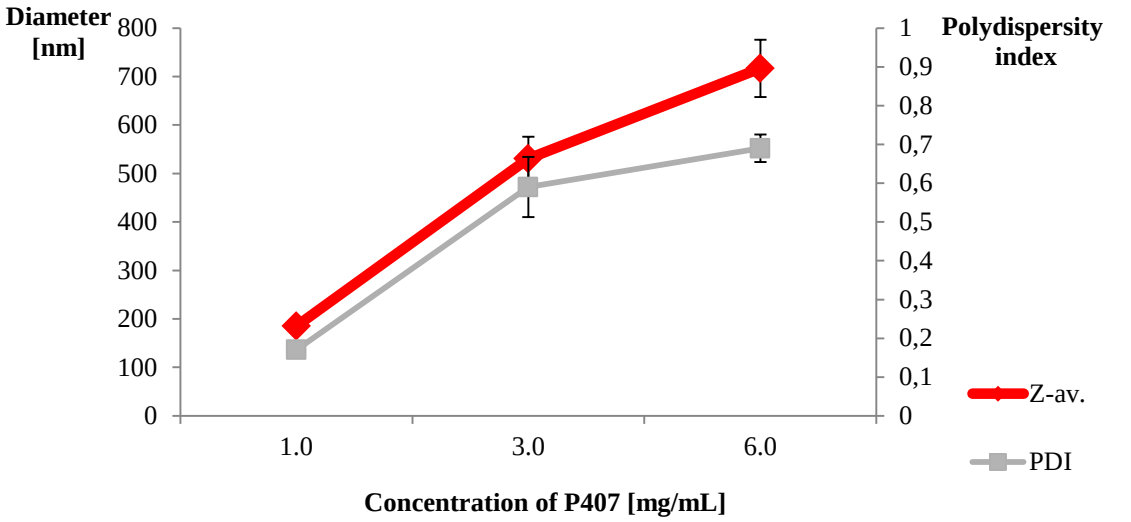

Figure 4.7. Variation of hydrodynamic diameter and polidispersity index with the concentration of surfactant for nanoparticles prepared from butylglyceryldextran and chitosan oligomer in the presence of Poloxamer P407 (n=3, ±SD).

The mechanism of nanoparticle formation could possibly lie in hydrogen bonding; a similar effect was observed in concentrated dextran solutions [389] or van der Waals forces, observed in [181, 409]. When CS was replaced with polyethyleneimine there was no formation of nanoparticles observed (excluding possible electrostatic forces), however exclusion of CS from the formulation whilst keeping P407 did not result into formation of nanoparticles either.

Nanoparticles were further separated by ultracentrifugation (40 000 RPM, 30 min, 20 °C, Rotor 70.1 Ti) and redispersed in PBS (pH 7.4, saline 0.9 %). The characteristics of nanoparticles after redispersion are presented in *Table 4.8.*

Table 4.8. Characteristics of nanoparticles prepared from DEX-OX4 and CS oligomer in the presence of surfactant (P407), following separation and redispersion in PSB (pH 7.4;.n=3; ±SD).

Nanoparticle formulation	Characteristics		
	Diameter [nm]	PDI	Zeta pot. [mV]
As prepared (pH 4)	123.4 ± 35.5	0.22 ± 0.07	17.20 ± 2.65
Redispersed in PBS (pH 7.4)	222.3 ± 29.43	0.28 ± 0.12	0.68 ± 4.74

Results indicated that the redispersion of nanoparticles influenced both the diameter (size increased from ca. 120 nm to ca. 220 nm) and the zeta potential (decreased from 17.20 to 0.68 mV) of these nanoparticles. However, the low zeta potential measured after redispersion did not induce and immediate agglomeration of the sample as it was noticed in the case of nanoparticles prepared from CS-OX4 (chapter 4.2.1.); the presence of P407 might provide a possible explanation for the stability observed in this case.

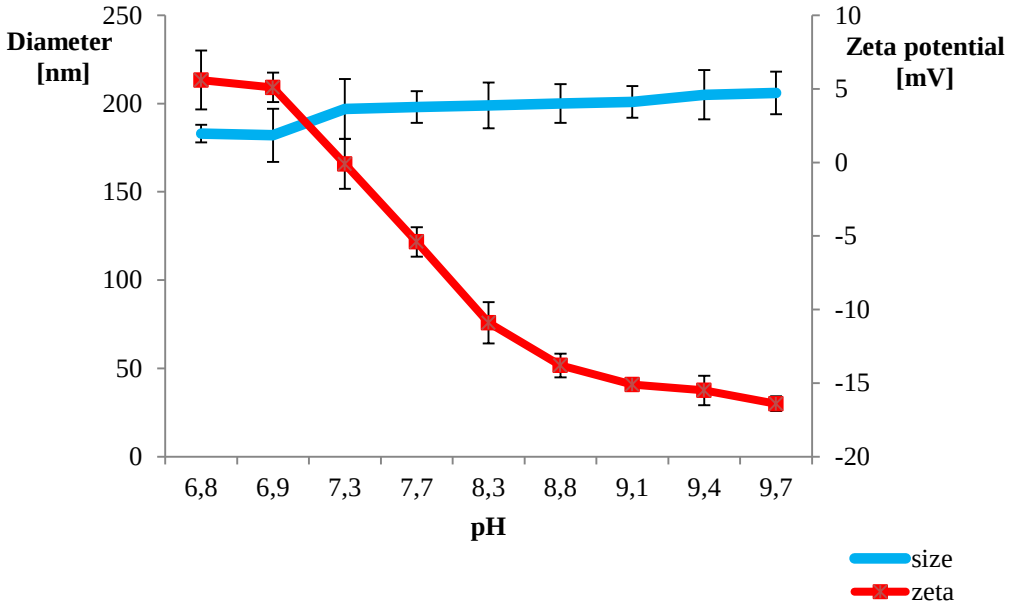

Figure 4.8. The influence of pH on the characteristics of DEX-OX4 (5.0 mg/mL) complexes stabilised by CS (0.5 mg/mL) and P407 (1.0 mg/mL) (n = 3, ±SD).

Automatic pH titrations (using 0.05 M NaOH, *Figure 4.8.*) of the formulations prepared from DEX-OX4 and CS and P407 (DEX-OX4 5.0 mg/mL, CS 0.5mg/mL, P407 1.0 mg/mL) also indicated these nanoparticles maintained (or had only a minimal increase in) their size (ca. 200 ± 20 nm) when the environment turned neutral/alkaline despite the zeta potential turning negative, possibly an effect of the stabilisation likely induced by P407 providing steric repulsion [410].

Nanoparticles prepared from DEX-OX4 and CS and P407 (DEX-OX4 5 mg/mL, CS 0.5mg/mL, P 407 1 mg/mL) were loaded with doxorubicin-the drug was incorporated into the nanoparticles at acidic pH (approx. 4). The amount of doxorubicin loaded was determined

indirectly by UV-Vis by measuring the drug content in supernatant after removing the nanoparticles by centrifugation (chapter 4.2.2.1.). The nanoparticles exhibited similar features to the unloaded ones (approx. 130 nm, zeta potential 15 mV). The content of doxorubicin loaded in the nanoparticles was found to be in the range 0.9 - 4.1 % w/w (compared to 12.7-55.8 % w/w) for other polysaccharide-based nanoparticles (CS and DEX) reported in the literature [182].

The morphology of nanoparticles prepared from DEX-OX4 and CS and P407 (DEX-OX4 5.0 mg/mL, CS 0.5mg/mL, P407 1.0 mg/mL) was studied by Scanning Electron Microscopy (SEM) following their separation by centrifugation, freeze-drying and coating with golden alloy. An example of a SEM image of freeze-dried nanoparticles is presented in *Figure 4.9.*

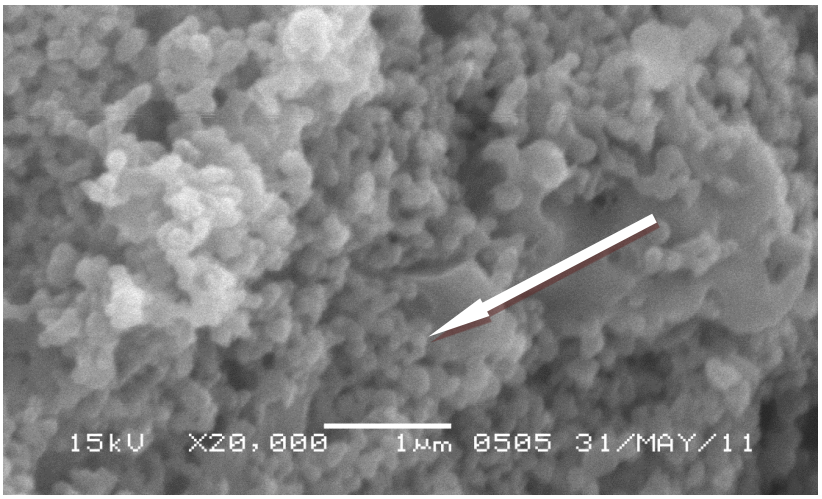

Figure 4.9. SEM micrograph of nanoparticles (ARROW) prepared from DEX-OX4 and CS and P407 (DEX-OX4-5.0 mg/mL, CS-0.5mg/mL, P407 1.0 mg/mL).

4.3.2.2. Nanoparticles from poly(lactic acid) coated with akylglyceryl-modified dextran

Nanoparticles were prepared by a dropwise addition of poly(lactic acid) (PLA) solution in acetone (5 mg/mL) to an aqueous solution of butylglyceryl dextran (DEX-OX4) (conc. range 0.66 – 5.00 mg/mL) under magnetic stirring (chapter 4.2.2.2.). The diameter of nanoparticles, measured by DLS after purification by centrifugation, was in the range 100 - 150 nm; though no

trend associated with an increase in the DEX-OX4 amount could be observed *(Figure 4.10.)*. These results would suggest that the ratio of DEX-OX4 / PLA does not influence much the size of nanoparticles (in accordance to previous literature report about modified dextran as a surfactant in PLA nanoparticles preparation [150]) and that DEX-OX4 was possibly adsorbed to a certain limit onto a poly(lactic acid) core, as Rouzes *et al.* found following studies on the influence of hydrophobic modified dextrans acting as surfactants during preparation of PLA nanoparticles [411]. Zeta potential was determined by electrophoretic mobility measurements in range -15 mV to -23 mV.

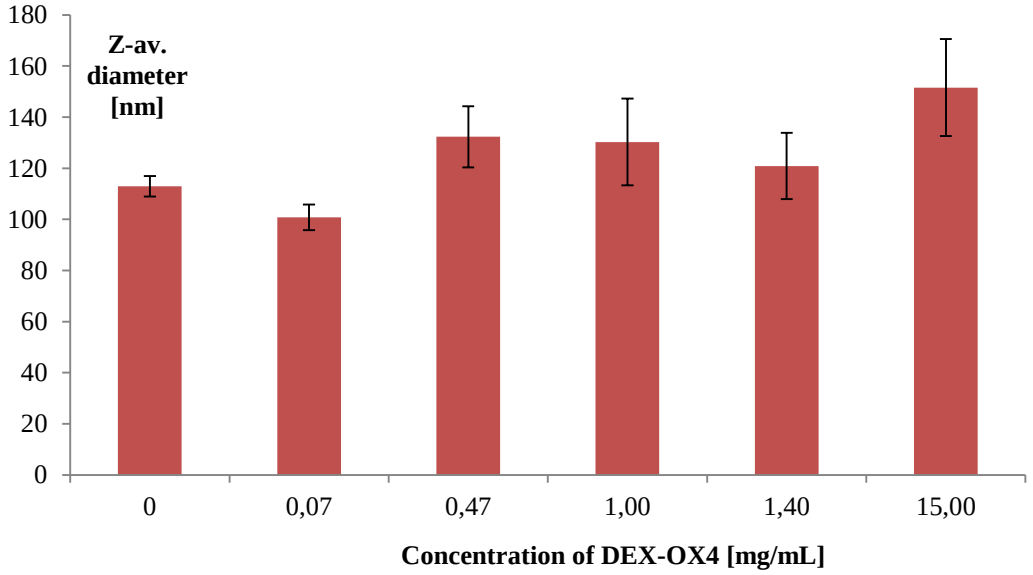

Figure 4.10. The hydrodynamic diameter (Z-av.) of nanoparticles from PLA and DEX-OX4 obtained using different DEX-OX4 concentrations (volume 15 ml, n=3; ± SD).

The presence of both dextran and PLA nanoparticles core was confirmed by FT-IR spectroscopy. The nanoparticles were centrifuged and the pellets were freeze-dried and analysed in ATR mode. Both molecules were confirmed in the structure after preparation. The band at 3500 cm^{-1} is indication for OH groups of modified dextran and band at the 1750 cm^{-1} indicates C=O group for poly(lactic acid). However the amount of DEX-OX decreased after further purification (*via* centrifugation 10 000 rpm, 15 min, Eppendorph Mini Spin) followed by redispersion in water by sonication, and appeared to be removed completely after three purification cycles *(Figure 4.11.)*. This would point towards adsorption of DEX-OX4 on the

surface of the nanoparticles rather than its incorporation into the hydrophobic core of poly(lactic acid) nanoparticles during the nanoprecipitation process.

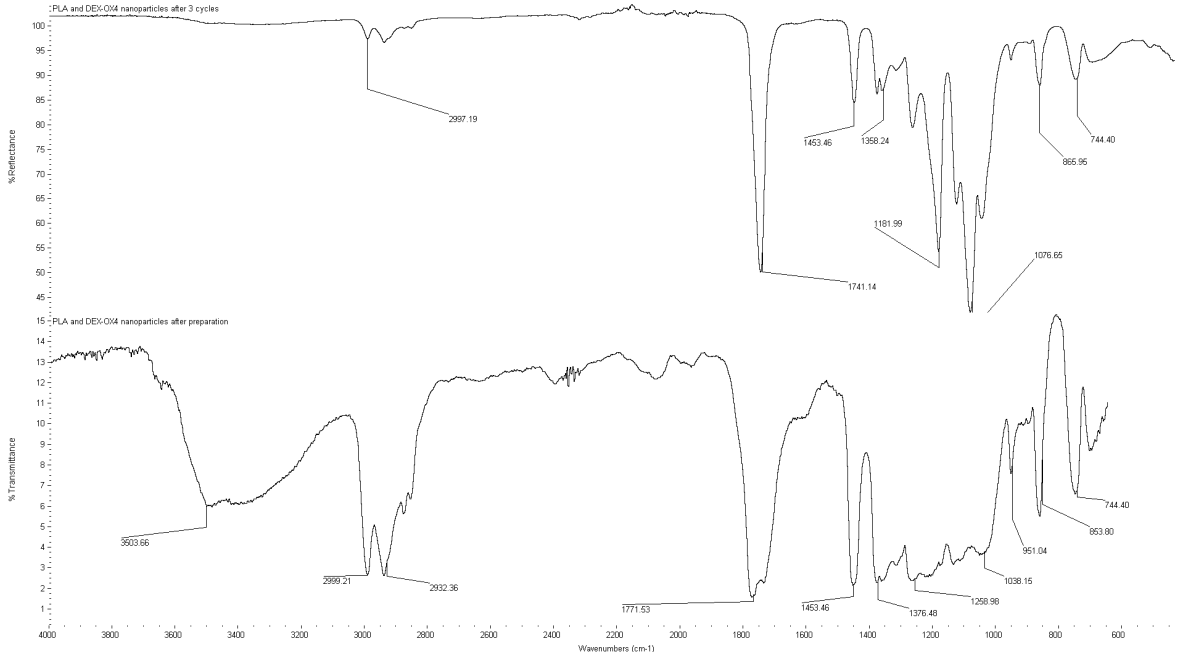

Figure 4.11. FT-IR spectra (ATR) of nanoparticles prepared by nanoprecipitation of PLA into water containing DEX-OX4, bottom-one cycle of purification, top-three cycles of purification

4.3.2.3. Nanoparticles formulated from poly(lactic acid)-graft-alkylglyceryl-modified dextran

Nanoparticles were formulated from poly(lactic acid)-*graft*-butylglyceryl-modified dextran (PLA-DEX-OX4) using three techniques: solvent displacement, nanoprecipitation and electrospraying. Nanoparticles were characterised in terms of dimension, stability, morphology, and loading/release of fluorescent markers such as Fluorescein, Rhodamine B or Doxorubicin.

A) Solvent displacement. Nanoparticles were prepared by dialysing a DMSO solution of PLA-DEX-OX4 of different concentrations in deionised water for 2 days, freeze-dried and redispersed in HPLC water, affording 100 - 400 nm size nanoparticles (depending on concentration of polymer in DMSO) with PDI values in the range 0.20 - 0.45. The results presented in *Figure 4.12.* would suggest the nanoparticle diameter increased with an increase of the concentration of polymer in DMSO, however statistical treatment of data, apart from the

highest one, could not evidence a significant difference between other values (ANOVA, $p>0.05$). Furthermore there was no statistical difference between various polymers (PLA-DEX, PLA-DEX-OX4, PLA-DEX-OX8) at conc. 1.0 mg/mL in DMSO.

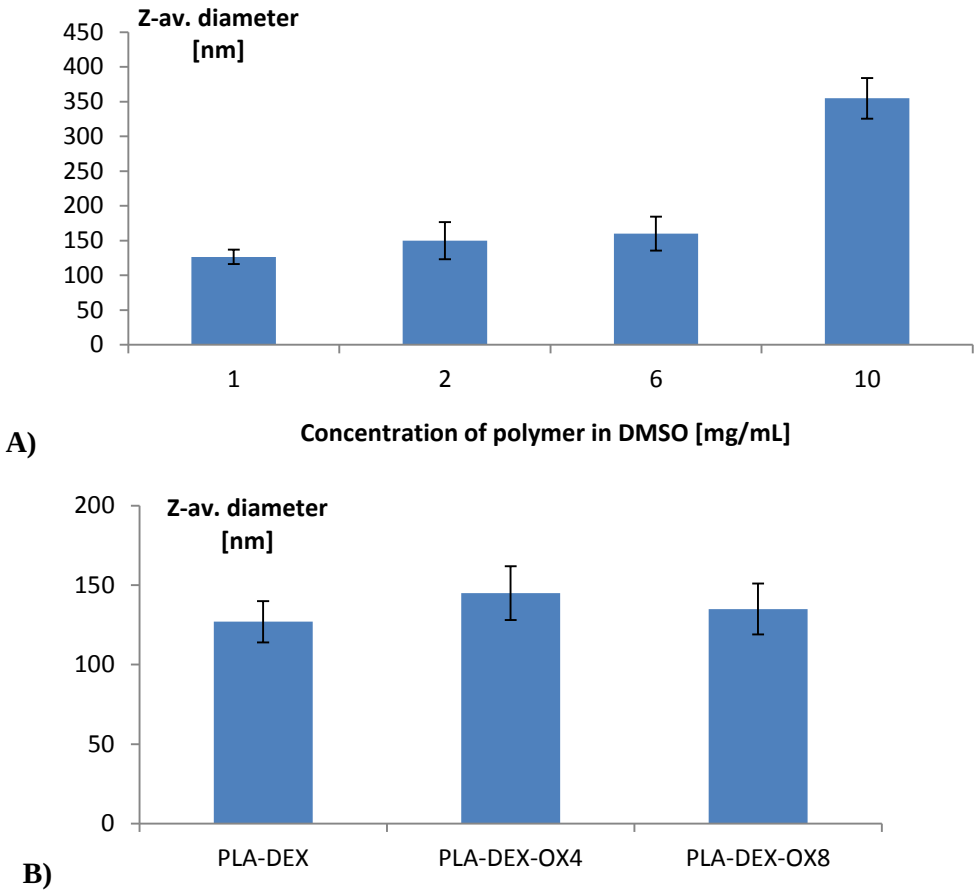

Figure 4.12. A) The influence of polymer concentration in DMSO on the hydrodynamic diameter of nanoparticles formulated from PLA-DEX-OX4 via solvent displacement, B) Comparison of PLA-DEX, PLA-DEX-OX4, PLA-DEX-OX8 at 1.0 mg/mL (n=3; ±SD).

B) Nanoprecipitation. A dropwise addition of a PLA-DEX-OX4 in DMSO solution into water (as described in chapter 4.2.2.3.) produced nanoparticles in the range 100 - 300 nm (*Figure 4.13.* concentration dependent), similar to nanoparticles from poly(lactic acid) dextran copolymer (PLA-DEX) prepared *via* similar method (80 - 125 nm [252]; 50-200 nm [253]). As DMSO (a solvent for PLA-DEX-OX4) has a higher boiling point (189 °C at 1010 mbar) than the non-solvent (water) it needs to be removed from the preparation mixture by dialysis or alternatively, nanoparticles have to be separated by centrifugation.

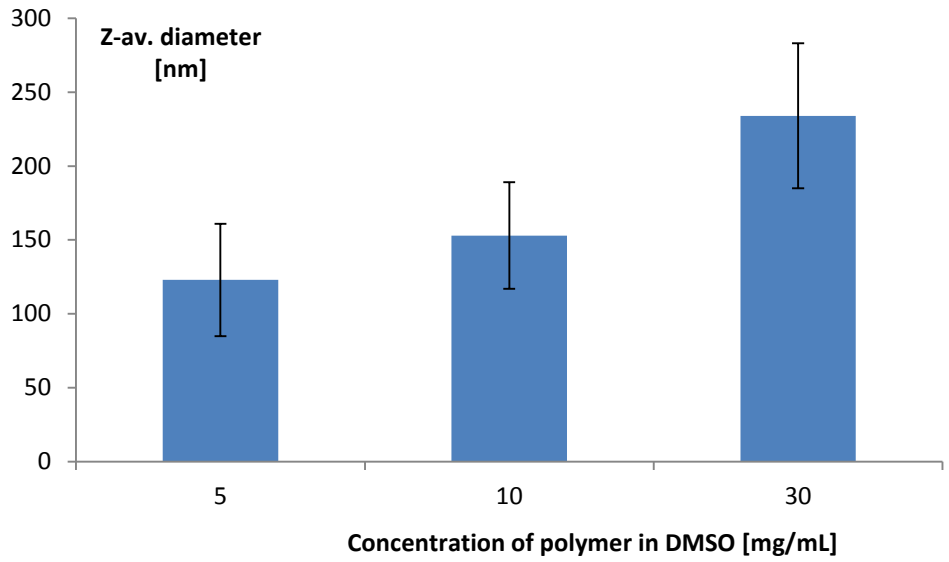

Figure 4.13. The influence of concentration of polymer on the diameter of nanoparticles prepared from PLA-DEX-OX4 by nanoprecipitation (n=3, ±SD).

C) Electrospraying. Poly(lactic acid)-*graft*-butylglyceryl dextran (PLA-DEX-OX4) nanoparticles were also prepared by electrostatic atomisation (electrospraying) of a solution of polymer dissolved in DMSO (as described in chapter 4.2.2.3.), which resulted in the formation of particles 100 - 200 nm in diameter having a negative zeta potential (-15 to -30 mV), *Table 4.9*. The spray was collected into a circular dish containing water (as DMSO has low volatility during electrospraying) and nanoparticles were further purified by dialysis (10.0 L exchanged 3 times a day for 48 hours) or by ultra-centrifugation (40 000 RPM, 30 min, 20 °C).

The comparison of nanoparticles from PLA-DEX-OX4 prepared by all three methods (*Table 4.9.*) showed that products of each method exhibited hydrodynamic dimensions suitable for drug delivery at physiological pH, measured in PBS (pH 7.4; saline 0.9 %). In optimal preparation conditions for solvent displacement *via* dialysis (concentration 1.0 mg/mL of polymer in DMSO), nanoprecipitation (concentration 5.0 mg/mL of polymer in DMSO) or electrospraying (concentration 50 mg/mL of polymer in DMSO) the nanoparticles were in 100 - 200 nm range bearing negative zeta potential -15 to -30 mV. Such a diameter is considered to be ideal for intravascular drug delivery system [412].

Table 4.9. Characteristics of nanoparticles prepared from PLA-DEX-OX4 by various methods acquired by optimal conditions.

PLA-DEX-OX4 nanoparticles	Diameter NTA nm [±SD]	Diameter DLS nm [±SD]	Zeta Potential mV [±SD]	Yields (after purification) % [±SD]	
				Dialysis	Centrifugation
Solvent displacement*	123[±85]	161 [±61]	-22 [±7]	71[±19]	N/A
Nanoprecipitation**	142[±53]	152 [±48]	-23 [±7]	44 [±23]	15[±7]
Electrospraying***	155 [±63]	143 [±69]	-25 [±8]	61[±16]	20 [±13]

* concentration of PLA-DEX-OX4 in DMSO was 1 mg/mL
** concentration of PLA-DEX-OX4 in DMSO was 5 mg/mL
*** concentration of PLA-DEX-OX4 in DMSO was 50 mg/mL

Zeta potential of nanoparticles prepared from PLA-DEX-OX4. The stability of PLA-DEX-OX4 nanoparticles in different pH conditions was investigated by titration in ultrapure water while measuring their diameter and zeta potential. *Figure 4.14.* shows that both parameters were stable over a wide range of pH values, however an increase could be noticed (in particular for the zeta potential) around the isoelectric point (pK_a 3.1 [413]); as expected, the acidic solution led, in time, to nanoparticles starting to agglomerate.

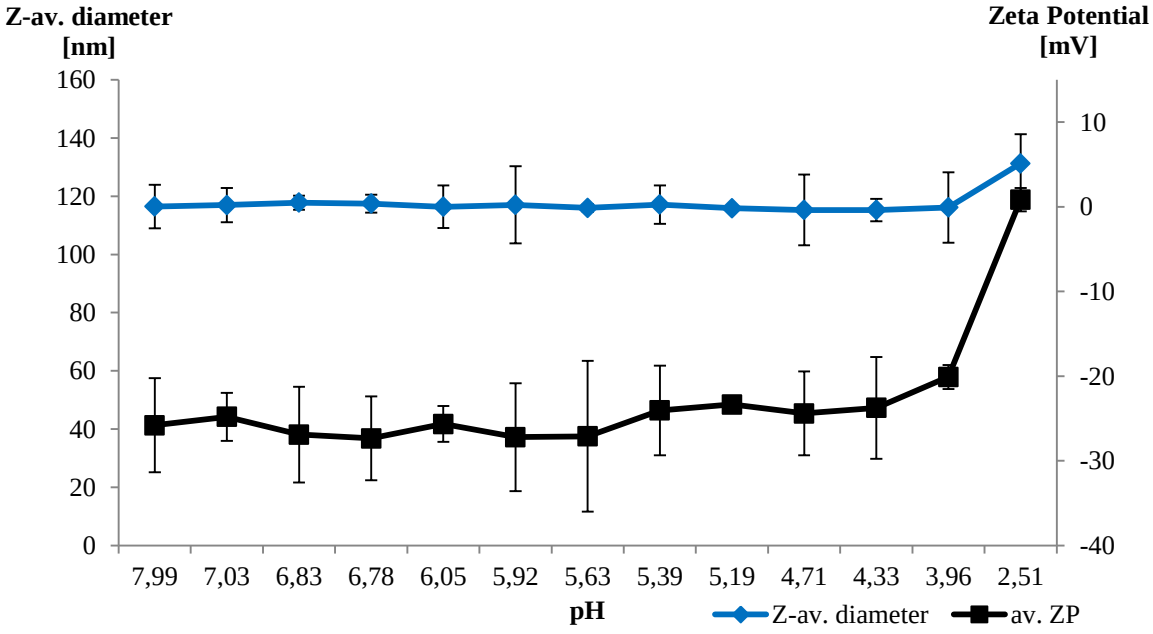

Figure 4.14. Variation of PLA-DEX-OX4 nanoparticle characteristics (size and zeta potential) with pH,(1 mg/mL suspension; prepared by solvent displacement, automatic titration with NaOH 0.05 M, Malvern instrument).

Purification of PLA-DEX-OX4 nanopaticles. Generally, higher yields were obtained when nanoparticles were purified by dialysis followed by freeze drying rather than by redispersion followed by centrifugation (when there might be redispersion-related loss of material and when not all fine particles can be recovered, *Table 4.10.* Using a glycerol or trehalose bed (which can also act as a cryoprotectants during the freeze-drying step [414, 415]) at the bottom of the centrifugation tube can help with redispersion by lessening the degree to which the centrifugation pellet is being compacted, however neither of these two additives did influence positively the redispersion of samples of PLA-DEX-OX4 nanoparticles (produced by nanoprecipitation). In some cases authors recommend combination of purification methods as centrifugation and dialysis to ensure the high level of purity of the products [416].

Table 4.10. The purification methods of PLA-DEX-OX4 nanoparticles.

PLA-DEX-OX4 nanoparticles	*Yields (after purification) % [±SD]*	
	Dialysis	*Centrifugation*
*Solvent displacement**	*71[±19]*	*N/A*
*Nanoprecipitation***	*44 [±23]*	*15[±7]*
*Electrospraying****	*61[±16]*	*20 [±13]*

* concentration of PLA-DEX-OX4 in DMSO was 1 mg/mL
** concentration of PLA-DEX-OX4 in DMSO was 5 mg/mL
*** concentration of PLA-DEX-OX4 in DMSO was 50 mg/mL

Morphology of dry PLA-DEX-OX4 nanoparticles. Scanning Electron Microscopy has been employed to investigate the morphology of freeze-dried nanoparticles of poly(lactic acid)-*graft*-alkylglyceryl dextran (PLA-DEX-OX4) prepared by dialysis as described in chapter 4.1. The nanoparticles exhibited micron/submicron diameter and spherical shape *(Figure 4.15.)*. It was also shown that not all the polymer was converted into the nanoparticles.

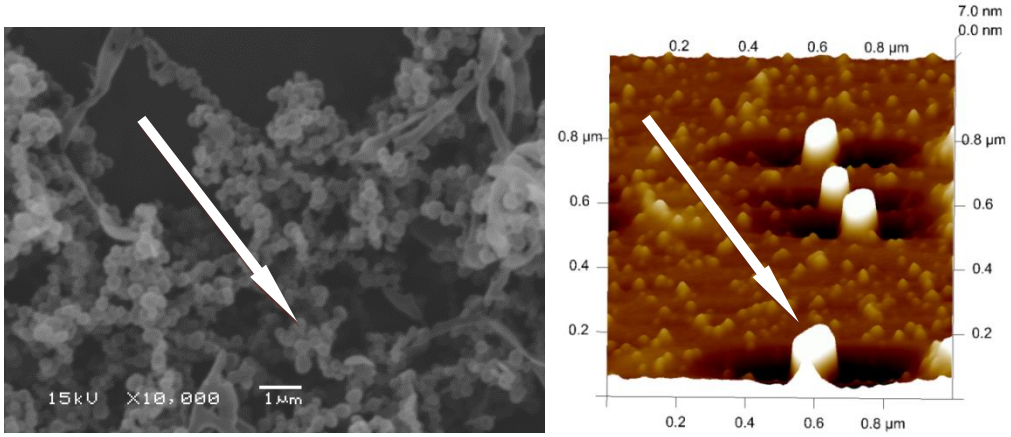

Figure 4.15. SEM micrograph (LEFT) and AFM image (RIGHT) of freeze-dried PLA-DEX-OX4 nanoparticles (prepared via solvent displacement by dialysis).

AFM was also employed to investigate the shape of *PLA-DEX-OX4* nanoparticles, which appear – when scanned in dried state, *Figure 4.15.* - as oval having a vertical diameter of ca. 15 nm and ca. 60 nm horizontal *(see also Table 4.11.)*. The difference between vertical and horizontal dimensions may be explained by the deformation induced by the pressure exerted by the cantilever on the top of the nanoparticle. The difference observed when comparing these results to those presented in *Table 4.9.* for the same type of nanoparticles but measured in aqueous environment can be explained by the hydration of the outer layer of the nanoparticle and possibly by the different conformation of the polymeric chains present on the surface of the particles [182].

Table 4.11. AFM dimension of nanoparticles

Nanoparticles	Horizontal diameter/ SD [nm]	Vertical diameter/ Standard deviation [nm]
PLA-DEX-OX4	64.4 ± 11.7	15.4 ± 2.2
PLA-DEX	52.5 ± 15.4	14.4 ± 4.5

Loading and release of fluorescent molecules from PLA-DEX-OX4 nanoparticles. Fluorescein isothiocyanate (FITC), Rhodamine B base and Doxorubicin base, selected for their fluorescence characteristics such as good detection limits and limited photobleaching, were loaded into PLA-DEX-OX4 nanoparticles that were prepared by either solvent displacement or

by electrospraying. Typically, the dye was dissolved in the DMSO and added during the formulation as described in chapter 4.2.2.3. The amount of each type of dye loaded into PLA-DEX-OX4 nanoparticles was determined using calibration curves in DMSO; the results are presented in *Table 4.12.* The results suggest that electrospraying provides a more efficient loading method compared to solvent displacement.

Table 4.12. Loading fluorescent molecules into PLA-DEX-OX4 nanoparticles using various methods

	Percentage of drug loaded (w/w) using different techniques	
	Solvent displacement *via* Dialysis	**Electrospraying**
Fluorescein	0.02 ± 0.01 %	N/A
Rhodamine B	0.32 ± 0.11 %	4.93 ± 0.76 %
Doxorubicin	0.50 ± 0.23 %	12.57 ± 3.17 %

Fluorescein isothiocyanate (FITC) was loaded into PLA-DEX-OX4 nanoparticles by solvent displacement method only, as the amount loaded was found to be minimal *(Table 4.12.)* and the release showed an instant burst effect that was complete within 30 min (which would indicate surface interaction of the dye with the nanoparticles). Rhodamine B base and especially Doxorubicin base showed better loading while their release also had an initial burst phase followed by a plateau *(Figure 4.16.)*, which is in agreement with literature for fluorescent marker-loaded PLA and PLGA nanoparticles [250, 379] and can be explained by the (more leaky) porous structure resulting from freeze-drying [417]. The release of drug from Doxorubicin-loaded (3 – 6 % w/w) PLGA-DEX nanoparticles (size 90-200 nm) was also described by Choi as burst for the first day, and followed then by a plateau for another 5 days [379].

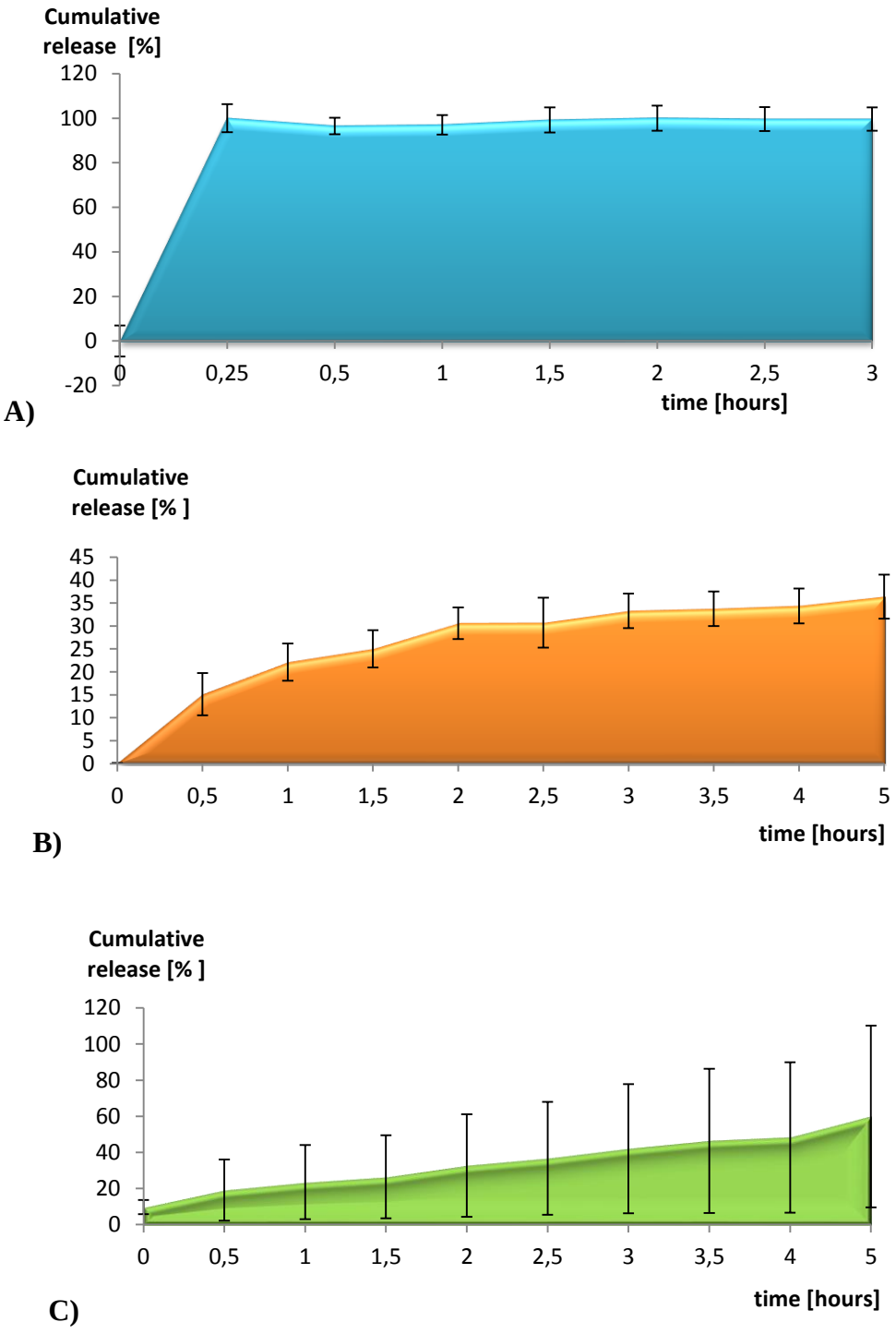

Figure 4.16. Release of A) FITC, B) Rhodamine B, C) Doxorubicin from loaded PLA-DEX-OX4 nanoparticles (1 mg/ml) in PBS (pH 7.4; saline 0.9 %) at 37 °C (n=3, ±SD).

4.3. Conclusions

Amongst other criteria, nanoparticulate systems employed for intravascular drug delivery purposes are expected to have submicron size (ideally between 100 and 200 nm) and to

show stability in physiological conditions furthermore, ease of purification and reconstitution of a colloidal system are important indicators of their practical potential.

Nanoparticles formulated from alkylglyceryl-modified chitosan (CS-OXn, where n = 4, 5, 8) were prepared by ionotropic gelation with sodium tripolyphosphate (TPP) in acidic environment, when their hydrodynamic diameter was found to be in the range of 100-200 nm (DLS). An increase in size (up to 800-1500 nm) was noticed when acidity decreased to pH 7 (using an automatic titrator) or after purification by dialysis (against deionised water) followed by re-suspension in a physiologically relevant simulated medium such as PBS saline (pH 7.4; 0.9 % salinity). Purification of nanoparticles by ultracentrifugation (144 000 g; 30 min) exhibited low yields (0 - 30 %); moreover, high speed centrifugation used for the separation of nanoparticles appeared to have a negative effect upon their subsequent redispersion in similar media, with sonication being of only marginal help.

Employing larger counterions compared to TPP (such as dextran sulphate) was expected to influence the stability of the synthesised chitosan-based colloidal systems in neutral conditions, for sterical reasons. Indeed, nanoparticles prepared from butylglycerylchitosan (CS-OX4) by ionotropic crosslinking with dextran sulphate (DEX-S) were in the range of 200-300 nm in an acidic environment (pH 4), and the diameter remained unchanged during titration up to pH 7.4; moreover, the zeta potential of the nanoparticles remained constant (-30 mV) across the whole pH range studied (pH 4 to 7.4). However, partial agglomeration has been noticed following purification by dialysis (possibly due to partial removal of DEX-S in the process), and their resuspension following ultracentrifugation was still not complete.

Butylglyceryl chitosan (CS-OX4) was also employed for coating nanoparticles prepared from poly(lactic acid) in the presence of different concentrations of surfactants (such as Poloxamer 407, Poloxamer 188 or Poly(vinyl alcohol)); employed as 1 mg/mL and 10 mg/mL conc.). The hydrodynamic diameter of normal PLA nanoparticles prepared by nanoprecipitation did not change after coating with CS-OX4 when measured in the preparation conditions (pH 4),

but the adsorption of CS-OX4 was evidenced by a major change of zeta potential (from ca. -29 mV of uncoated PLA nanoparticles, to ca. 40 mV when coated with CS-OX4). However, the size of coated nanoparticles increased significantly when the pH was changed to neutral (from ca. 170 nm to 300-1300 nm). Using Poloxamer 407 in the coating process allowed for the preparation of smallest size particles compared to those obtained using other surfactants (ca. 300 nm, at a Poloxamer 407 conc. of 10 mg/mL) while using Poly(vinyl alcohol) resulted in a significant increase in particle size (ca. 1270 nm. at a Poly(vinyl alcohol) conc. of 1 mg/mL). Generally, an increase in surfactant concentration resulted in smaller nanoparticles.

Nanoparticles prepared from butylglyceryl-modified dextran (DEX-OX4) and chitosan oligosaccharide in the presence of Poloxamer 407 exhibited size and zeta potential which were also found to vary with an increase in pH (size increased from 170 to 220 nm, while zeta potential decreased from +17 to -0.7 mV when pH was varied from 4 to 7.4). However the stabilising effect of P407 was not further reflected in the purification process (separation by centrifugation followed by redispersion led to significant agglomeration). Maximum loading of Doxorubicin was assessed by UV/VIS as 4.1 % w/w.

An attempt to prepare nanoparticles from poly(lactic acid) and DEX-OX4 by nanoprecipitation led to submicron size nanoparticles (100-140 nm) with negative zeta potentials (-18 mV to -25 mV), however DEX-OX4 appeared to be easily washed away in the centrifugation / redispersion process (as evidenced by FT-IR analysis; likely due to weak interaction between hydrophobic poly(lactic acid) and DEX-OX4).

In an attempt to study the influence of the preparation method on the characteristics of nanoformulations, solvent displacement, nanoprecipitation and electrospraying methods have been comparatively employed for obtaining nanoparticles based on polylactic acid-*graft*-dextran copolymer (PLA-DEX-OX4). It has been found that the size of the nanoparticles prepared using the three optimised methods were similar (in the range of 120-155 nm) and had a negative zeta potential (-20 mV to -25 mV). The stability of electrosprayed nanoparticles was observed across

a wide range of pH values (2.5 - 8.0); while the hydrodynamic diameter remained of ca. 120 nm, the zeta potential dropped from -20 mV (pH 7.4) to 0 mV (pH 2.5). SEM and AFM analysis of freeze-dried nanoparticles from PLA-DEX-OX4 confirmed the spherical shape and low uniformity of nanoparticles. Though time consuming, dialysis seemed to afford better yields and a more facile redispersion when employed as a purification technique compared to centrifugation. When fluorescent molecules were employed as model actives, electrospraying provided also better loading capacity for Doxorubicin and Rhodamine B when compared to solvent displacement (4.9 % *vs.* 0.3 % w/w for Rhodamine B; 12.57 % *vs.* 0.5 % w/w for Doxorubicin). The loading of FITC in PLA-DEX-OX4 nanoparticles was extremely low; a burst release was observed in all cases, independent of the method of preparation (this was complete within 30 min for FITC while for Doxorubicin and Rhodamine B it seemed to be sustained for at least several hours).

5

STUDIES *IN VITRO*

Cell cultures of mouse and human origin were employed to study the interactions between brain endothelial cells and the modified biopolymers and their corresponding nanoformulations described earlier. Aspects such as cytotoxicity, cell uptake, influence on the cell layer permeability and transendothelial electric resistance were investigated with a view to establish the influence of the alkylglyceryl modifications on the cell-nanoparticle interactions.

5.1. Materials and instrumentation

DMEM media, TrypLE Express, Hoechst Blue 33342, PBS, PrestoBlue assay were purchased from Invitrogen, Life technologies. Matrigel was sourced from BD Biosciences and EGM-2 media was purchased from Lonza as an EGM-2 Bullet Kit. Recovery Medium, HBSS, and distilled water (cell culture quality) were purchased from Gibco. Trypan blue, FITC dextran, and L-cysteine were purchased from Sigma Aldrich. Cryo-vials Greiner bio-one, Nunc 96 well-plates were purchased from Fisher Scientific. The Transwell system (24 well-plates) was sourced from Millipore (Millicell-24 Cell Culture Plate; polyethylene terephthalate membrane; 1.0 μm; filtration surface 0.33 cm^2; pore density $2x10^6$ per cm^2), 8WE10 array for ECIS was sourced from Applied Biophysics, USA. The trimethyl-chitosan derivatives (TMC, TMC-OX4 and TMC-OX8) were gift from Dr. Molnár.

The cells were cultured under humidified atmosphere (human cells hCMEC/D3 in a standard Mini Galaxy E incubator, mouse cells bEnd3 in a Nuaire DH AUTOFLOW Air-Jacketed incubator) at 37 °C and 5 % CO_2 in small T25 culturing flasks (Fisher). Nunclon F 96-well plates were sourced from Thermo Scientific. The analysis of the well-plates was performed

using a PolarStar Optima (BMG Labtech) fluorimeter. Cells were observed with an Olympus IX71 inverted phase microscope and images were taken using Olympus Soft Imaging System, UK. Images of cells were also obtained using an LSM 710 confocal microscope (ZEISS, fluorescence excitation at 405 nm, 488 nm and 633 nm; facilitated by a Twin Gate main beam splitter). Cells were counted using either a Vi-CELL XR Cell Viability Analyser (Beckman Coulter, UK) or a haemocytometer. Cell cultures were spun using a Beoco C28A centrifuge (Wolf Laboratories, UK). Electric Cell-substrate Impedance Sensing (ECIS) measurements were conducted using an ECIS Zθ instrument (Applied Biophysics) operating at a frequency range of 2 000-32 000 Hz and employing 8 well-arrays type 8W10E.

Butylglyceryl-modified dextran (DEX-OX4 DS 42 %), octylglyceryl-modified dextran (DEX-OX8 DS 17 %) were prepared as described earlier, dextran (MW 6 kDa) and chitosan (low MW) were sourced from Sigma Aldrich. Nanoparticles from poly(lactic acid)–*graft*-butylglycerol dextran (PLA-DEX-OX4, DS 42-55%), poly(lactic acid)–*graft*-octylglycerol dextran (PLA-DEX-OX8, DS 31%) and poly(lactic acid)–*graft*-dextran (PLA-DEX) were obtained by solvent displacement method (*via* dialysis). Nanoparticles from chitosan (CS) and alkylglycerolchitosan derivatives (CS-OX4 DS 88 % and CS-OX8 18 %), and trimethylchitosan (TMC, TMC-OX4 DS 23 %, TMC-OX8 DS 43 %) were prepared by ionic gelation.

5.2. Methods

Mouse (bEnd3) and human (hCMEC/D3) endothelial cells have been cultured as described in section 5.2.1. The following sub-chapters present the setups and methods employed for toxicity assays, cell-uptake experiments, live cell monitoring of endothelial electrical resistance (TEER) studies and trans-epithelial transport investigations.

5.2.1. Cell cultures

Mouse brain endothelial cells (bEnd3, *Figure 5.4-A.*) were sourced in-house (Molecular Medicine Laboratory; Prof. Górecki). The cells were kept in supplement-enriched DMEM media *(Table 5.1.)*. For optimal growth, bEnd3 cells were seeded onto surfaces that have been previously coated with 1.5 mg/mL Matrigel by incubating at 37 °C for 30 min.

Table 5.1. The composition of media and conditions employed for cell culturing.

	bEnd3	**hCMEC/D3**
Cell type	Mouse Endothelial cells	Human endothelial cells
Origin	Health Protection Agency Culture Collections, UK	Institut Cochin, INSERM, Paris, France
Passage no	31-35	30-37
Medium	DMEM (Invitrogen)	EGM-2 (Lonza)
Culturing flask	CORNING T25	
Medium volume	3-5 ml	
Serum	10 % (v/v) FBS	2 % (v/v) HS or 2 % (v/v) FBS
Supplements	1 % (v/v) non-essential amino acids 2 mM L-glutamine 1 mM sodium pyruvate 5 μM β-mercapthoethanol 100 U/mL penicillin 0.1 mg/mL streptomycin	Single Quots (one dose per 500 mL medium), consisting of: Hydrocortisone VEGF hFGF-B Gentamicin Amphotecerin-B R3-IGF-1 hEGF Ascorbic Acid Heparin
Coating of flasks	1.5 mg/mL Matrigel	1.5 mg/mL Matrigel/no coating

Human cerebral microvascular endothelial cells (hCMEC/D3) that were immortalised with hTERT/SV40 Lagre T antigen were also sourced in-house (Cellular and Molecular Neuro-Oncology group Laboratory; Prof. Pilkington). The human brain endothelial hCMEC/D3 cells *(Figure 5.4-B.)* were kept in EGM-2 media that was enriched in supplements as presented in *Table 5.1.* For optimal growth, the cells were seeded onto surfaces that have been previously coated with 1.5 mg/mL Matrigel by incubation at 37 °C for 30 min; unless specified that no coating was applied.

The endothelial cells were grown in a incubator (standard Mini Galaxy E incubator for hCMEC/D3 and Nuaire DH AUTOFLOW for bEnd3) in the corresponding media *(Table 5.1.)* under a humidified atmosphere at 37 °C and 5 % CO_2 in small T25 culturing flasks. After first day the medium was removed and the cells were washed twice with PBS, which was then replaced with fresh medium. This process was repeated every 3 - 4 days until the cells became confluent (80 - 90 %; as verified by optical microscope Olympus IX71 inverted phase microscope), at which point the cells required sub-culturing.

5.2.2. Cell passaging

Cells that reached the confluent state and were surplus for immediate experiments were passaged as follows: cells were washed twice with PBS, trypsinised with TrypLE Express (1 mL per T25 flask, equilibrated at 37 °C for 5 minutes to detach the cells from the flask; the TrypLE Express was deactivated by serum containing media, in a ratio of 1:1); cell dissociation was monitored using a microscope. The cell suspension was then centrifuged at 1 000 RPM for 5 min using a Boeco C28A centrifuge and the supernatant was discarded. The pellet was resuspended in fresh media and split into fresh culture flasks, and the cultures to be used for immediate experiments were counted by methods relying on Trypan Blue.

The classical haemocytometer method was employed for counting bEnd3 cells, as follows: 10.0 μL of cell suspension (normally, the pellet from one flask resuspended in 1.0 mL of fresh medium) was mixed with 90.0 μL of Trypan Blue solution. An aliquot of 10.0 μL (covered with a slide) was analysed by counting the living cells in the 5 visible squares (4 corners and middle) under a microscope (*Figure 5.3.)*; this was done in duplicate. The average count from one square was multiplied by 10^4 (the volume of the counting device) and by 10 (the dilution factor) to express the number of the living cells in 1.0 mL.

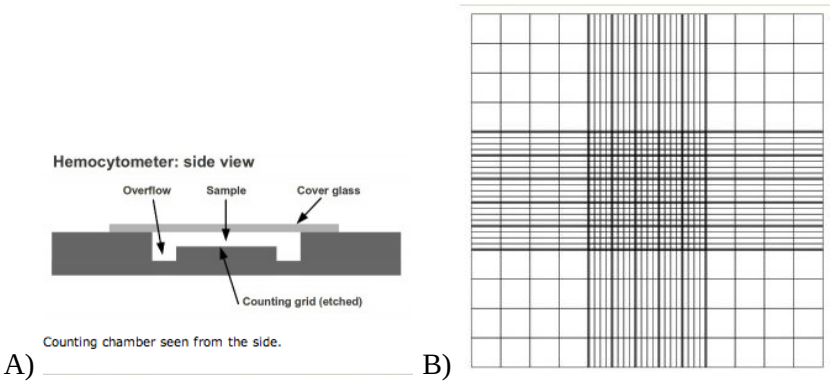

Figure 5.1. A) Structure of a haemocytometer B) counting area; image adopted from [418]

hCMEC/D3 cells were counted using an automatic Cell Viability Analyser Vi-CELL™ XR after mixing a 100 µL aliquot of cell suspension with 500 µL of medium in the sample cup (giving a dilution factor of 6).

Cryopreservation and resurrection of cell cultures. Cells were sub-cultured as described in the previous paragraph, and the pellet from one T25 culture flask was reconstituted in 1.0 mL of the Recovery Medium formulated with 10% DMSO (cold 2-8°C) inside the cryotube, which was then frozen at the rate of 1 °C / min, and stored overnight in a freezer at – 80 °C and second day finally immersed in the liquid nitrogen tank for storage.

To resurrect the cells, the cryotubes were removed from the nitrogen storing tank, placed into a plastic box for ca. 1 min and then transferred into a water bath (37 °C) to thaw the cell suspension. The content of each cryotube was then transferred into a T25 culture flask previously equilibrated with appropriate media (3.5 mL) at 37 °C. The flask was maintained in the incubator overnight and the medium was replaced the next day in order to remove the DMSO containing freezing medium.

5.2.3. Cytotoxicity assays of nanoparticles from alkylglyceryl-modified polysaccharieds

Nanoparticles were tested in various concentrations for toxicity against both mouse and human endothelial cells, at different time points (3 h and 24 h). A MTT assay [419] was employed for bEnd3 cells and a PrestoBlue assay [420] was used for hCMEC/D3 cells.

Toxicity against mouse bEnd3 cells. Materials (such as chitosan, dextran and modified dextrans DEX-OX4 and DEX-OX8) and nanoparticles (PLA-DEX, PLA-DEX-OX4 and PLA-DEX-OX8) were tested for toxicity against bEnd3 cells (seeding 10^4 cells, APPENDIX X) using an MTT assay. The compounds were dissolved in modified DMEM (1 mg/mL) except for chitosan which was dispersed due to its insolubility at in the media at pH 7.4. The compounds were incubated for 24 hours with confluent bEnd3 cells. PBS (no nanoparticles) and Digitonin (dispersion in PBS, 10 mg/mL) were used as negative and positive control, respectively. (MTT method in APPENDIX XI)

Toxicity against human hCMEC/D3 cells. Nanoparticles from dextran- based compounds (PLA-DEX-OX4 and PLA-DEX-OX8 and PLA-DEX) and chitosan-based compounds (CS, CS-OX4, CS-OX8, TMC, TMC-OX4 and TMC-OX8) were tested with hCMEC/D3 cells (seeding 10^4) by PrestoBlue assay (APPENDIX XI).

The nanoparticles (PLA-DEX-OX4 and PLA-DEX) were tested for toxicity in short time (3 hours, doses 1 mg/mL, 2 mg/mL and 4 mg/mL). The dose dependent toxicity (0.2 – 4.0 mg/mL) of PLA-DEX-OX4 nanoparticles was studied for 24 hours. Nanoparticles from chitosan derivatives were tested in concentration 1 mg/mL in 24 hours incubation. PBS and dispersion of Digitonin served as a negative and a positive control, respectively (PrestoBlue method in APPENDIX X).

5.2.4. The uptake of nanoparticles from poly(lactic acid)-*graft*-butylglyceryldextran by mouse endothelial cells

bEnd3 cells were employed for studying the nanoparticle-cell interactions. Cells (5.0 *x* 10^4) were seeded onto glass cover slips previously coated with Matrigel 1.5 mg/mL and incubated for 24 h in 2.0 mL of modified DMEM (composition given in *Table 5.1.*) in a 6 well plate. Media was then replaced with 2.0 mL of a nanoformulation (2 mg of PLA-DEX-OX4 nanoparticles loaded with Rhodamine B (0.5 % w/w) dispersed in modified DMEM) and the slips were incubated with nanoparticles for further 3 h. As a control, cells were treated with Rhodamine B solution of the same concentration as that of the nanoformulation (2.0 mL of cell media containing 0.001 mg of Rhodamine B base prepared from stock solution 1 mg/mL), another control was provided by cells in media without addition of nanoparticles or dye. After incubation the cells were washed twice with PBS, fixed for 10 min in paraformaldehyde (4.0 % w/v) at 4 °C, permeabilised for 20min with Triton X-100 (0.1 % v/v), and incubated for 40 min with nuclear counter-stain Hoechst 33342 (5.0 μg/mL) at room temperature. The cells were then visualised using a confocal microscope (LSM 710, ZEISS, 405 nm for Hoechst, 543 nm for Rhodamine B).

5.2.5. The effect of nanoparticles from poly(lactic acid)-*graft*-butylglyceryldextran on electrical resistance of endothelial cells

Nanoparticles prepared from PLA-DEX and PLA-DEX-OX4 were studied for their effect on the transendothelial resistance (TEER) of confluent (either mouse bEnd3 or human hCMEC/D3) brain endothelial cells with Electric Cell Impedance Sensing (ECIS). A polycarbonate 8 well array (Applied Biophysics, USA; 8W10E) was employed for these experiments (*Figure 5.2.)*. Each well has a surface area of 0.9 cm^2 and a maximum capacity of 600 μL (with a 400 μL recommended volume), and has 10 gold electrodes of 250 μm diameter that are capable of measuring altogether the signal arising from ca. 500 - 1000 cells.

Figure 5.2. ECIS array well plate (model 8W10E; Applied Biophysics).

The wells were washed twice with HBSS prior to use and equilibrated with cell culture grade water. The electrodes were stabilised by incubation for 15 min with L-cysteine (10 mM), at room temperature. The wells were washed again with HBSS and coated with Matrigel 1.5 mg/mL (incubation at 37 °C for 15 minutes). The wells were washed briefly with HBSS prior to seeding cells (hCMEC/D3; 2.5 x 10^5 cells per well bEnd3; 3.0 x 10^5 cells per well, one well was left empty serving as a no cell control), and the plate was incubated at 37 °C. After reaching confluency (indicated, after 40-50 h, by a plateau in resistance over time: ca. 1 500 Ω for hCMEC/D3 and ca. 800 Ω for bEnd3 cells) the media was replaced with a mix of fresh media (350 µl) and PBS-based nanoformulation (50 µl of PBS containing dispersed nanoparticles in various concentrations, final concentrations in range 1 – 4 mg/mL of PLA-DEX-OX4 and 4 mg/mL of PLA-DEX).After incubation with nanoparticles (24 h), the nanoformulation was removed and replaced with fresh media and monitored for further 24 hours. ECIS readings were taken continuously for the whole duration of the experiment using an ECIS Zθ instrument at 2 000 – 32 000 Hz frequency.

5.2.6. The effect of nanoparticles from poly(lactic acid)-*graft*-butylglyceryldextran on translocation of a fluorescent marker through barriers of endothelial cells

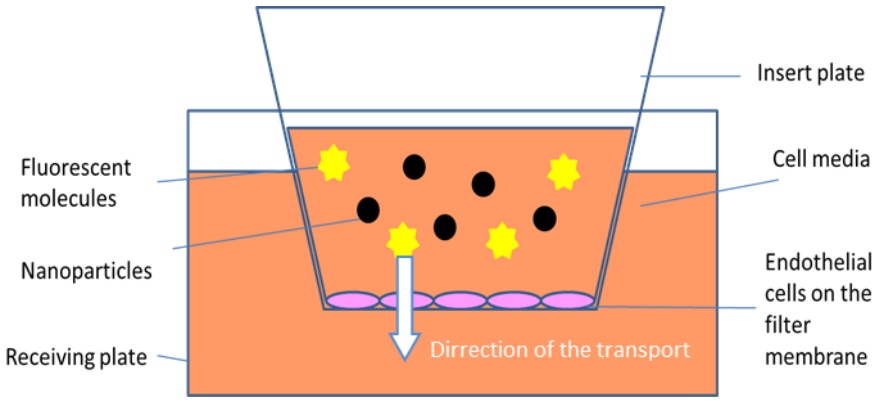

Figure. 5.3. Transwell setup used for translocation experiments.

Nanoparticles prepared from PLA-DEX-OX4 were investigated for their effect on the paracellular transport of FITC-labelled detran (FITC-DEX, MW 150 kDa; employed as a fluorescent marker) using a Transwell-type BBB model based on confluent brain endothelial cells *(Figure. 5.3.)*; both mouse and human endothelial cells were employed.. 24 well plates Millipore Millicell (PET membrane; 1 µm pore diameter; 600 µL max volume) were washed twice with HBBS (500 µL) and equilibrated with water for 15 min at 37 °C. After equilibration in water, filter membranes were coated with ice-cold 150 µL of Matrigel (1.5 mg/mL) and incubated for 15-30 min at 37 °C to promote better adhesion of the cells. After coating, filters were washed twice with HBBS, and cells were seeded (bEnd3, 3×10^5 cells per well; hCMEC/D, 2×10^5 cells per well) and maintained at 37 °C in incubator in appropriate media *(Table 5.1.)*. Media were replaced every 2 days in both (apical and receiving) compartments. Meanwhile, cells were also seeded alongside in a standard 24 well plate to monitor the health and confluency of the cells (the filter in Transwell was opaque hindering cell inspection). The experiments were carried out after reaching confluency, usually 3-4 days from seeding. In case of bEnd3 cells, a specific cocktail of barrier enhancers (consisting of 250 µM cAMP, 20 µM RO-20-1724, and 550 µM hydrocortisone) was applied after 24 h of cells reaching confluency.

The nanoparticles (PLA-DEX-OX in range 1-4 mg/mL and PLA-DEX at concentration 4 mg/mL, used as a control) were applied in media together with fluorescently-labelled dextran (FITC-DEX, 100 μg/mL) and the concentration of FITC-DEX in receiving compartment was investigated. The sampling was performed every 30 minutes, as follows: a sample (100 μL) was collected from the receiving compartment and the volume removed was replaced with fresh media. Samples (in triplicate) were collected into 96-well plates and analysed using a fluorescence plate reader Optima BMG (excitation 485 nm; emission 520 nm). The amount of FITC-DEX was determined using a calibration curve of FITC-DEX in cell media (APPENDIX XII) .

The concentration of FITC-DEX in the receiving compartment was used to calculate the apparent permeability coefficient (P_{app}), as described by Arthursson [421]:

$$P_{app}(cm.s^{-1}) = \frac{dQ}{dt} \times \frac{V_R}{A \times C_0 \times 60}$$

d*Q*/*d*t	the flux of FITC-DEX transported across the membrane (μg/sec);
V_R	the basolateral volume (600 μL);
A	the surface area of the filter insert (0.33 cm^2);
C_0	the initial mass concentration of FITC-DEX at the apical side (100 μg/mL)
60	a conversion factor (from minutes to seconds)

Statistical analysis. The statistical analysis was performed using OriginPro 7 software from OriginLab, USA by one-way analysis of variance (ANOVA) followed by post hoc Tukey test (p values were set at level 0.05 unless stated otherwise). Measurements are presented as mean ± standard deviation unless stated otherwise.

5.3. Results and discussion

The brain endothelial cells were chosen as a suitable model tissue for the studies relevant to drug delivery across the blood-brain barrier (BBB). Mouse brain endothelial cells (bEnd3, *Figure 5.4-A.*) were first characterised in the literature by Omidi *et al.* [422]. The bEnd3 cell line exhibits some favourable features (as expression of junctional and transport proteins) and were used as a model of the BBB in several cases: [423, 424, 129].

The human endothelial hCMEC/D3 cell line *(Figure 5.4-B.)* was chosen as a suitable model for simulation of the BBB based on previous research: descriptive studies [425-427] or *in vitro* models development [49, 428].

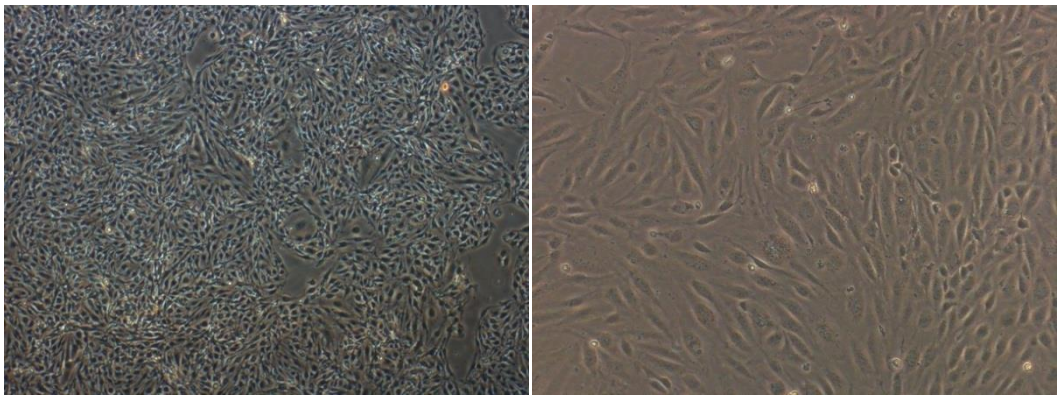

Figure 5.4. LEFT: Mouse brain endothelial cells (bEnd3) 4x magnification; RIGHT: human brain endothelial cells (hCMEC/D3) 10x magnification. Images taken by OLYMPUS IX71.

5.3.1. Cytotoxicity studies

Alkylglyceryl-modified dextran and chitosan derivatives (DEX-OX and PLA-DEX-OX derivatives and CS-OX derivatives) were investigated in terms of their toxicity towards either mouse or human endothelial cell cultures using MTT and PrestoBlue assays, at different exposure times and concentration. The MTT assay can determine toxicity by measuring the change of colour caused by the reduction of a yellow tetrazole (3-(4,5-dimethylthiazol-2-yl)-2,5-diphenyltetrazolium bromide) to purple formazan inside the living cells [419]. The Presto Blue assay is based on the reduction of a cell-permeable blue resazurin

compound (known also as Alamar Blue) inside the living cell to a fluorescent red [420]. This assay is supposed to be quicker and easier to run than MTT whilst providing accurate results [429].

5.3.1.1. Toxicity of materials

Materials (such as chitosan, dextran and modified dextrans DEX-OX4 and DEX-OX8) were tested initially for toxicity against bEnd3 cells as a 1.0 mg/mL solution in PBS, pH 7.4 (except chitosan derivatives, which did not dissolve and was used as dispersion) using an MTT assay *(Figure. 5.5.)*. Blank treatment with PBS and digitonin (10 mg/mL, known to act as cytotoxic agent [430]) were used as negative and positive controls respectively. The results express relative viability to no-nanoparticle (PBS treatment, 100 %). It appeared that modifying dextran with alkylglyceryl chains did not induce an increase in toxicity when compared to native dextran (both modifications exhibited viability above 80 %). Interestingly, the lowest viability (below 60 %) for the bEnd3 cells was observed following incubation with chitosan (ANOVA, $p < 0.05$), possibly explained by the microparticulate form due to the insolubility of normal chitosan in PBS at neutral pH and by positive charge of the polysaccharide [199]. On contrary, nanoparticles from chitosan derivatives were found to be non-toxic [196]. It should be noted that both assays were conducted with various kinds of cells.

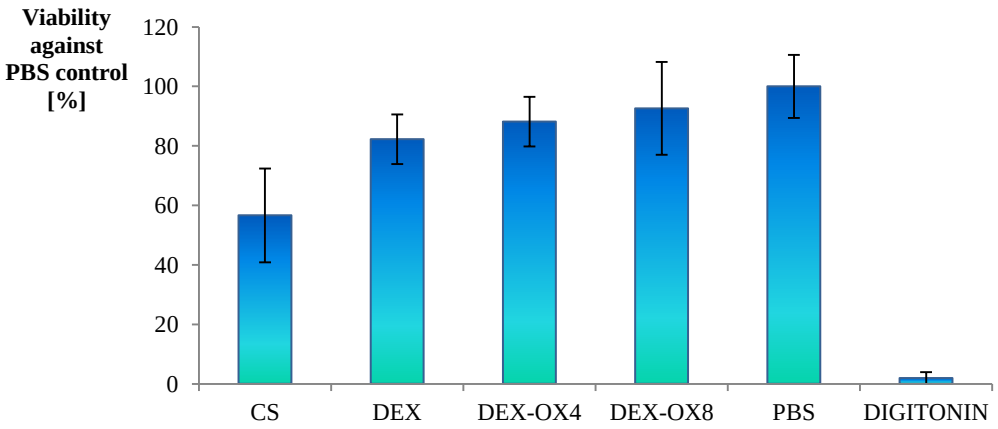

Figure 5.5. Relative toxicity of compounds employed further for various nanoformulations; bEnd3 cells incubated with 1 mg/mL material for 24 h; MTT assay; digitonin and PBS blank treatment as controls (n =12; ±SD; CS- chitosan; DEX-dextran, DEX-OX4 – butylglyceryl-modified dextran, DEX-OX8 – octylglyceryl-modified dextran, digitonin as a positive control).

5.3.1.2. Toxicity of poly(lactic acid)-*graft*-alkylglyceryl-modified dextran nanoparticles

A cytotoxicity assay following incubation of mouse brain bEnd3 endothelial cells for 24 h with poly(lactic acid)-*graft*-alkylglyceryldextran derivatives nanoparticles (1 mg/mL) revealed no significant toxicity induced by these nanoformulations compared to the PBS control *(Figure 5.6,* ANOVA $p < 0.05$). As previously reported earlier for chitosans [129, 173], modifying dextran with alkylglyceryl pendant chains did not appear therefore to lower significantly the mouse brain endothelial cell viability. It appeared that the viability of cells for treatment with nanoparticles from PLA-DEX, PLA-DEX-OX4 and PLA-DEX-OX8 was about 90 % (when compared to PBS control).

The non-toxicity finding was confirmed by experiments with human endothelial cells (hCMEC/D3) as no toxic effect of alkylglyceryl modification was observed in direct comparison of PLA-DEX with PLA-DEX-OX4 nanoparticles in concentrations 1 mg/mL, 2 mg/mL and 4 mg/mL after 3 hours of incubation (*Figure 5.7.),* even doses as high as of 4 mg/mL are well tolerated by human endothelial cells. It appeared that the alkylglyceryl modification exhibited even decreased toxicity when compared to PLA-DEX. This supports the original finding about non-toxic features of alkylglycerols [95].

A dose response experiment of PLA-DEX-OX4 nanoparticles (range 1 – 4 mg/mL) employing hCMEC/D3 human brain endothelial cells for 24 h exhibited reduced viability (74 %) at doses 2 mg/mL and higher (ANOVA, $p < 0.05$). The doses 0.2-1.0 mg/mL influenced the viability as well however not in a significant way *(Figure 5.8.)*.

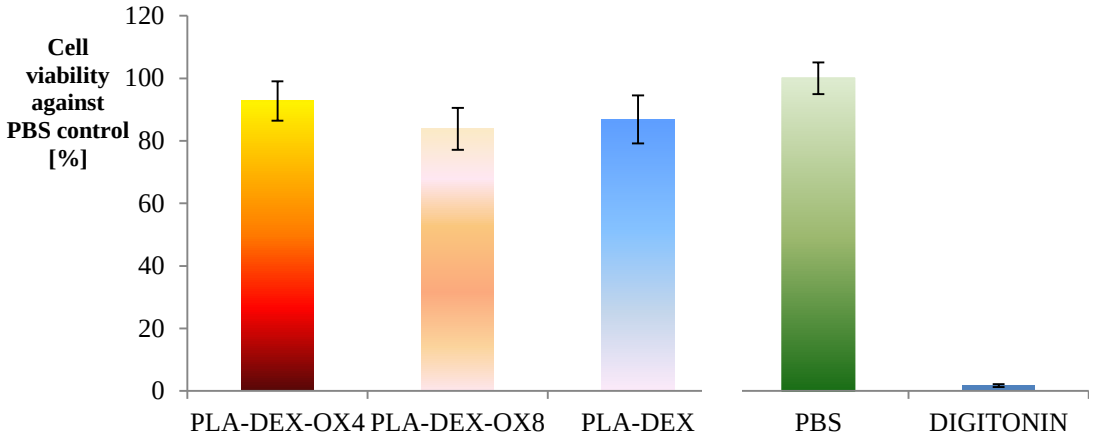

Figure 5.6. Relative toxicity of nanoparticles formulated from poly(lactic acid)-graft-alkylglyceryldextran derivatives; MTT assay; bEnd3 cells incubated with 1 mg/mL of nanoparticles for 24 h; PSB and, digitonin as controls (n=18, ±SD); (PLA-DEX-OX4 - poly(lactic acid)-graft-alkylglyceryldextran, PLA-DEX-OX8 - poly(lactic acid)-graft-butylglyceryldextran, PLA-DEX - poly(lactic acid)-graft-dextran, PBS and digitonin is as a negative and positive cytotoxic control respectively

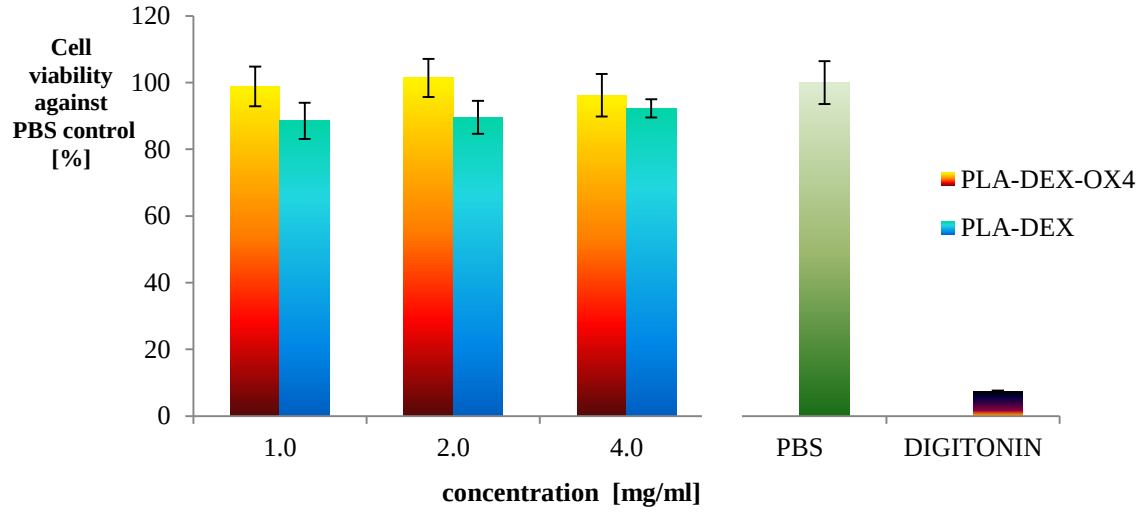

Figure 5.7. Relative toxicity of nanoparticles formulated from poly(lactic acid)-graft-alkylglyceryldextran derivatives; PrestoBlue assay; hCMEC/D3 cells incubated with nanoparticles for 3 h; PSB and, digitonin as controls (n=12, ±SD); (PLA-DEX-OX4 - poly(lactic acid)-graft-alkylglyceryldextran, PLA-DEX - poly(lactic acid)-graft-dextran, PBS as a control

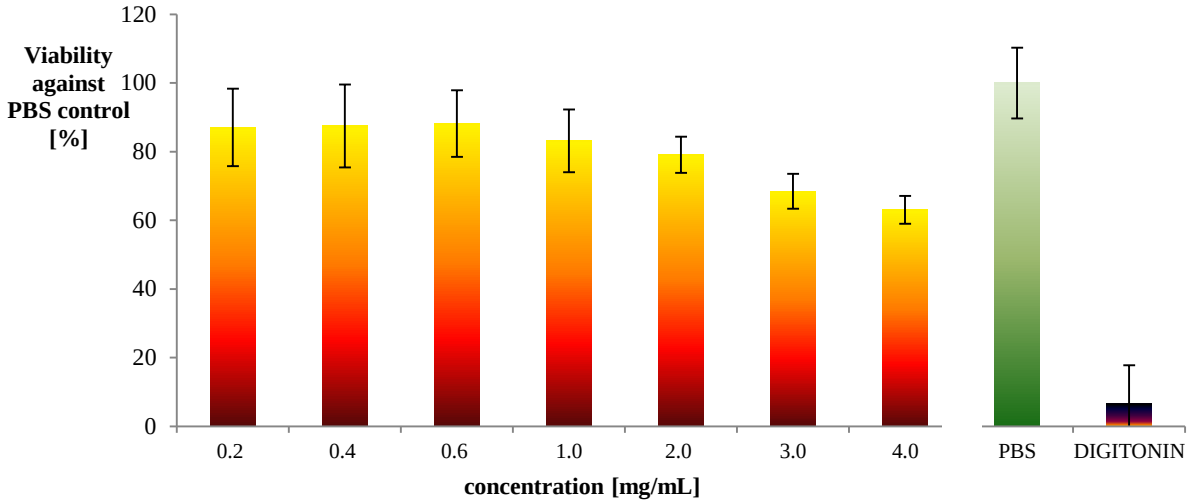

Figure 5.8. Relative toxicity of nanoparticles formulated from poly(lactic acid)-graft-alkylglyceryldextran derivatives (1 – 4 mg/mL); PrestoBlue assay; hCMEC/D3 cells incubated with nanoparticles for 24 h; PSB and, digitonin as controls (n=12, ±SD); (PLA-DEX-OX4 - poly(lactic acid)-graft-alkylglyceryldextran, PBS as a control).

5.3.1.3. Toxicity of alkylglyceryl-modified chitosan nanoparticles crosslinked with TPP

The cytotoxicity of nanoparticles prepared from alkylglyceryl-modified chitosan derivatives crosslinked with TPP was assessed on human endothelial cell cultures incubated for 24 h and using a Presto Blue assay. While chitosan (CS) and trimethylchitosan (TMC) appear non-toxic, their alkylglyceryl-modified counterparts seem to reduce cell viability *(Figure 5.9.).* However, this conclusion is questionable as (despite a large number of repeats) standard deviations were rather large and differences were not statistically significant. Occasional reproducibility issues due to the reduced stability at neutral pH of these chitosan-based nanoformulations (also mentioned in the literature [111, 173, 174]) represent a likely explanation for the large standard deviation observed.

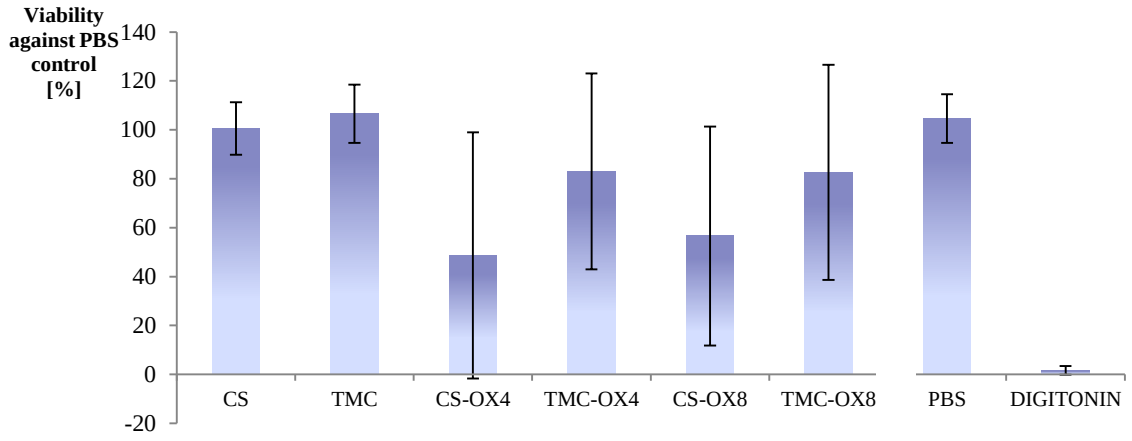

Figure 5.9. *Relative toxicity of nanoparticles formulated from chitosan-derivatives; hCMEC/D3 cells incubated with 1 mg/mL nanoparticles; PSB and digitonin as controls (n=36, ±SD); PrestoBlue assay; (CS - chitosan; TMC – trimethylchitosan; CS-OX4 - butylglycerylchitosan, TMC-OX4 trimethylbutylglycerylchitosan, CS-OX8 – butylglycerylchitosan, TMC-OX8 - trimethyloctylglycerylchitosan).*

5.3.2. The uptake of nanoparticles from poly(lactic acid)-*graft*-butylglyceryl-dextran by mouse endothelial cell

To investigate the uptake of the nanoparticles prepared from PLA-DEX-OX4 loaded with Rhodamine B (0.5 % w/w), bEnd3 mouse brain endothelial cells were incubated for 3 h with a 1 mg/mL of nanoformulation in modified DMEM (as described in chapter 5.2.4.); media was then removed and cells were washed with PBS twice (to remove nanoparticles and/or released Rhodamine that were not taken up) and observed using a confocal microscope. A Rhodamine B solution (5×10^{-4} mg/mL) was employed as a control. Images presented in *Figure 5.10.* are indicative of nanoparticle uptake as they show the presence of Rhodamine B-loaded carriers in the cell cytoplasm around the peri-nuclear space, while no evidence of Rhodamine B administered as a control solution could be found inside cells. While there is no evidence of particular targeting the nuclei, the nanoparticles appear to have been localised in vesicles (possibly Golgi apparatus, as previously demonstrated for CS-OX4 nanoparticles [129]) inside the bEnd3 cells as displayed on *Figure 5.11.* which is a 3 dimensional projection of z stack of a series of confocal sections.

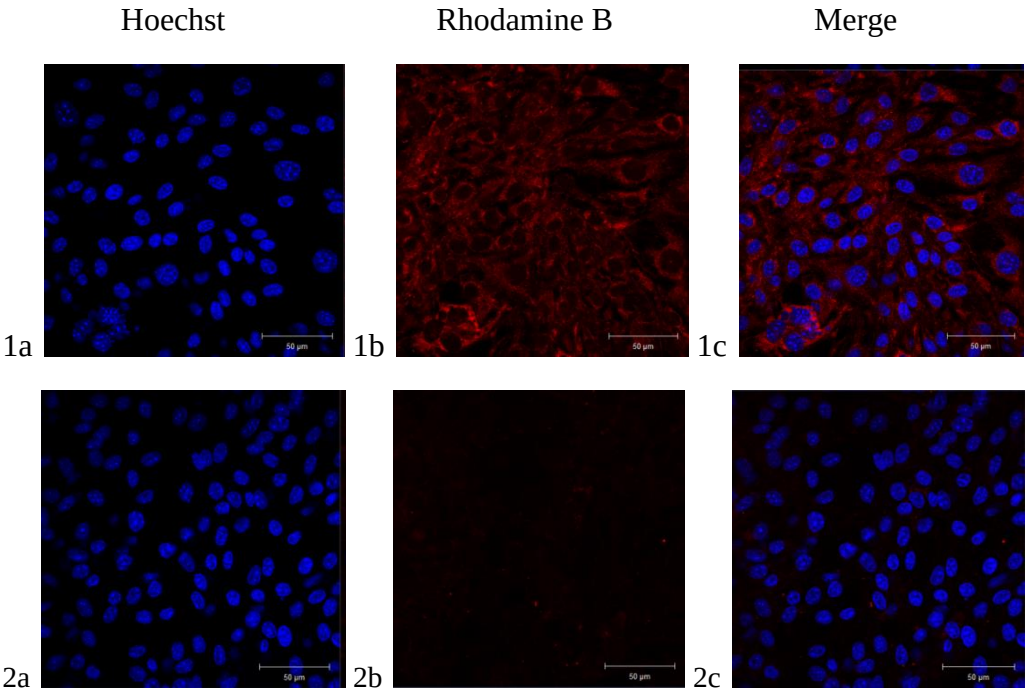

Figure 5.10. Confocal microscope images of bEnd3 cells following incubation with poly(lactic acid)-graft-butylglyceryldextran (PLA-DEX-OX4) nanoparticles for 3 h. Top (number 1)- nanoparticles, bottom (number 2)- dye control, a)-image of cell nuclei (laser 405 nm), b)-image of the Rhodamine B labelled structures (laser 543nm), c)-merge. Rhodamine B –loaded nanoparticles are visualised in red, while Hoechst-counterstained nuclei appear in blue.

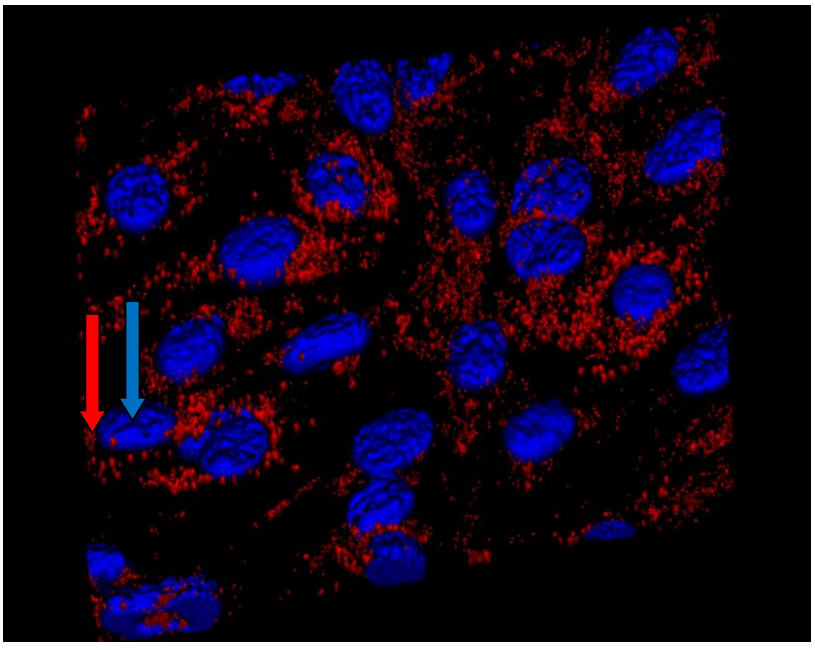

Figure 5.11. Three dimensional Z stack projection of optical sections of bEnd3 cells containing nanoparticles from PLA-DEX-OX4 loaded with Rhodamine B (red arrow). Nuclei stained with Hoechst (blue arrow).

5.3.3. The effect of nanoparticles from poly(lactic acid)-*graft*-butylglyceryl-dextran on electrical resistance of endothelial cells

The interactions of nanoparticles with brain endothelial cells were also studied by monitoring their Trans Endothelial Electrical Resistance (TEER) using Electrical Cell Impedance Sensing (ECIS). Both bEnd3 and hCMC/D3 cells were separately cultured on 8W10E, 8 well golden electrode arrays, previously coated with Matrigel 1.5 mg/mL to support the endothelial cell growth [129] (there can be used also other kinds of the extracellular matrix as rat tail collagen 1 [341] or fibronectin [49]), as described in section 5.2.5. The mouse model reached ca. 800 Ω resistance, while the human model exhibited a resistance of ca. 1200 Ω when the cell cultures achieved confluency (at 48 h, data not shown). The cells were then incubated with nanoparticles (PLA-DEX-OX4 1-4 mg/mL or PLA-DEX 4 mg/mL) for 24 h, after which nanoparticles were replaced with fresh media; cell behaviour was continuously monitored by TEER measurements.

The changes detected in the TEER of confluent cell layers both during incubation and following removal of nanoparticles are presented in *Figure 5.12.* (as relative value to PBS control with no nanoparticles). Mouse cells bEnd3 incubated with nanoparticles prepared from poly(lactic acid)-*graft*-butylglyceryldextran (PLA-DEX-OX4) showed a different behaviour compared to those incubated with poly(lactic acid)-*graft*-dextran (PLA-DEX) nanoparticles. A drop in TEER was observed during incubation with nanoparticles bearing the alkylglyceyl-modification in all concentrations. Furthermore, following nanoparticle removal, TEER recovered for all the formulations except in the case of the highest dose of PLA-DEX-OX4 (at point 72 h a statistical difference, ANOVA, $p<0.05$, *Figure 5.12.-A*). This can be attributed to long term toxicity of high doses of PLA-DEX-OX4 nanoparticles. No significant dose response effect could be observed for human brain endothelial cells when repeating the experiment using hCMEC/D3 cell cultures (*Figure 5.12.-B*).

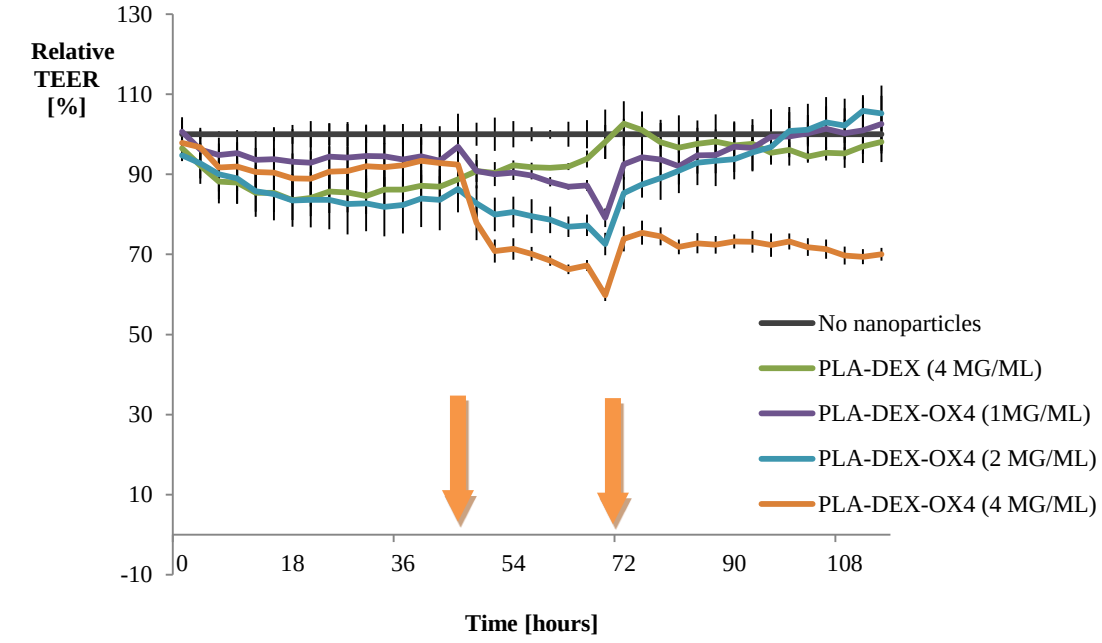

A)

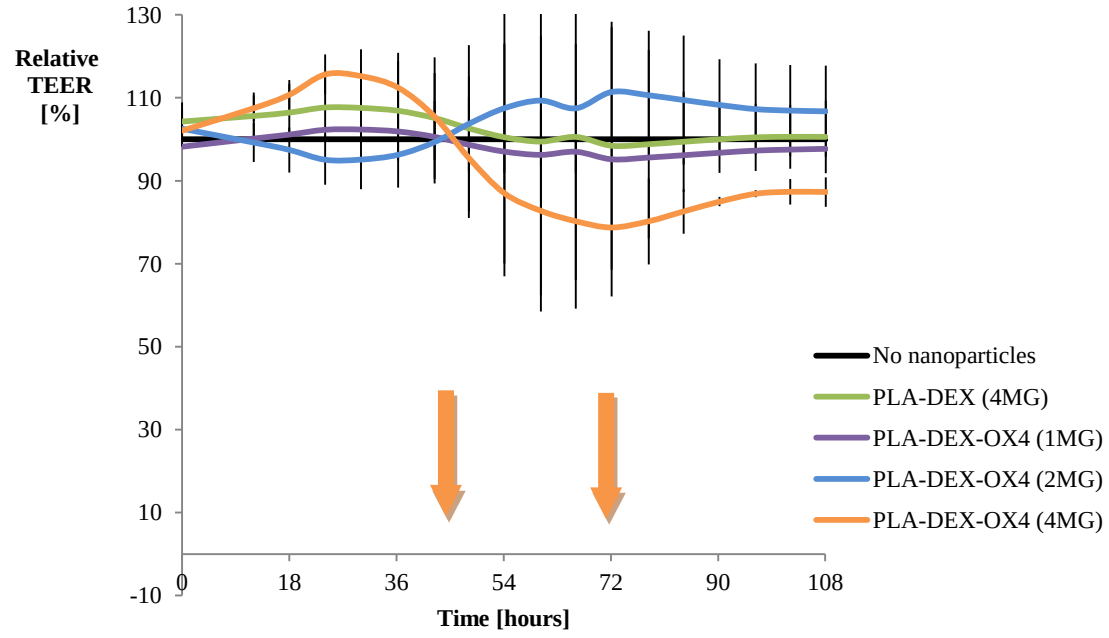

B)

Figure 5.12. ECIS plot (relative resistance of. PBS treated control) of TEER development (2000 Hz) on ***A)*** *bEnd3,* ***B)*** *hCMEC/D3 endothelial monolayers cultured on 8W10E test plates, following exposure to and then removal of nanoparticles(orange arrows). Treatment with nanoparticles prepared from PLA-DEX and PLA-DEX-OX4 (dose-response experiment). Nanoformulations were added to the cells at 48 h and removed at 72 h, after which the cells were allowed to recover for a further 48 h. Data are presented as means of at least three wells (n = 3) for each condition of a representative measurement (±SE). Untreated cells (PBS, no nanoparticles added) were employed as control.*

5.3.4. The effect of nanoparticles from poly(lactic acid)-*graft*-butylglyceryldextran on translocation of a fluorescent marker through barriers of endothelial cells

Permeation studies of PLA-DEX-OX4 nanoparticles through brain endothelial cell monolayers were performed using a translocation model system based on a Transwell setup, as described in chapter 5.2.6. Both mouse and human endothelial cells were employed in these studies; the permeability of each nanoformulation (PLA-DEX-OX4 1-4 mg/mL and PLA-DEX 4 mg/mL) was assessed using FITC-labelled dextran (MW 150 kDa), employed as a marker to verify the possibility of poly(lactic acid)-*graft*-butylglycerol-modified dextran nanoparticles (PLA-DEX-OX4) to influence permeability of the models of the blood-brain barrier.

It was found that the model based on human cells allowed less marker to pass through the barrier *(Figure 5.13.)*. The amount of transported FITC was used to calculate the apparent permeation coefficient. The apparent permeation coefficient (P_{app}) was determined by concentration of FITC-DEX in known volume transported across the barrier of known surface area (chapter 5.2.6.). The apparent permeability coefficient P_{app} was described by Arthursson [421] and has been used in numerous studies, e.g. by Gaillard [431], Ragnaill [432]. The formula can illustrate a translocating capacity of a cellular monolayer based on surface area of a population (given by the surface area of a filter membrane where the cells grow) of the cell culture and time.

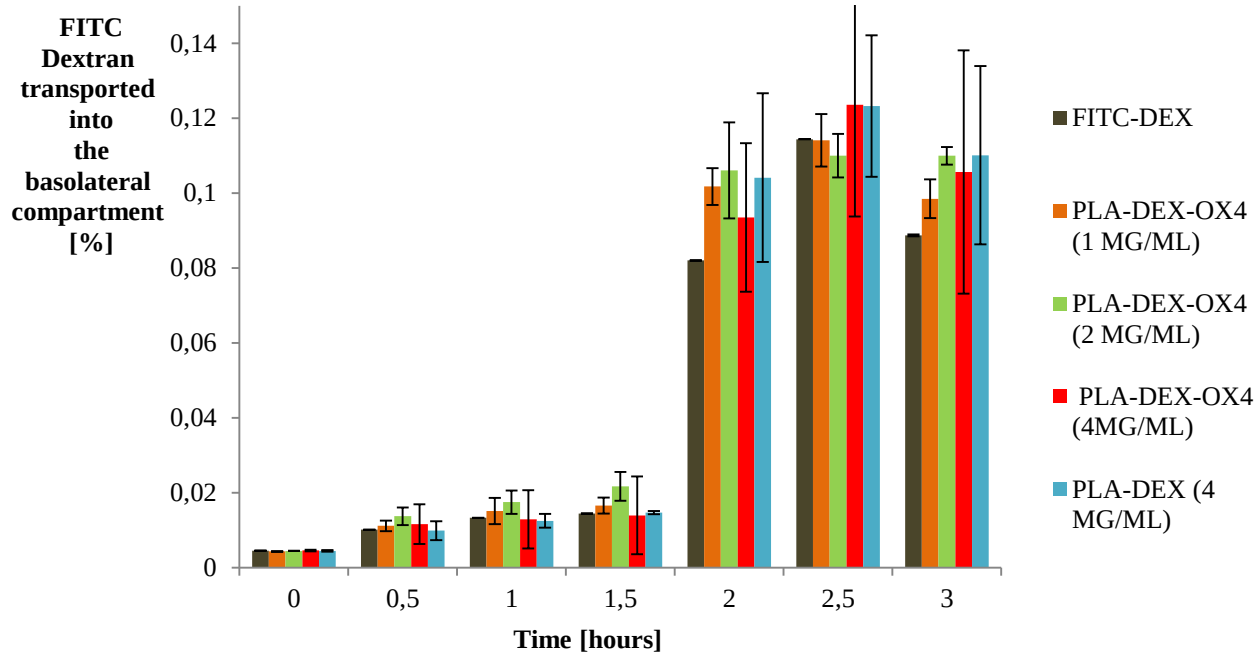

A)

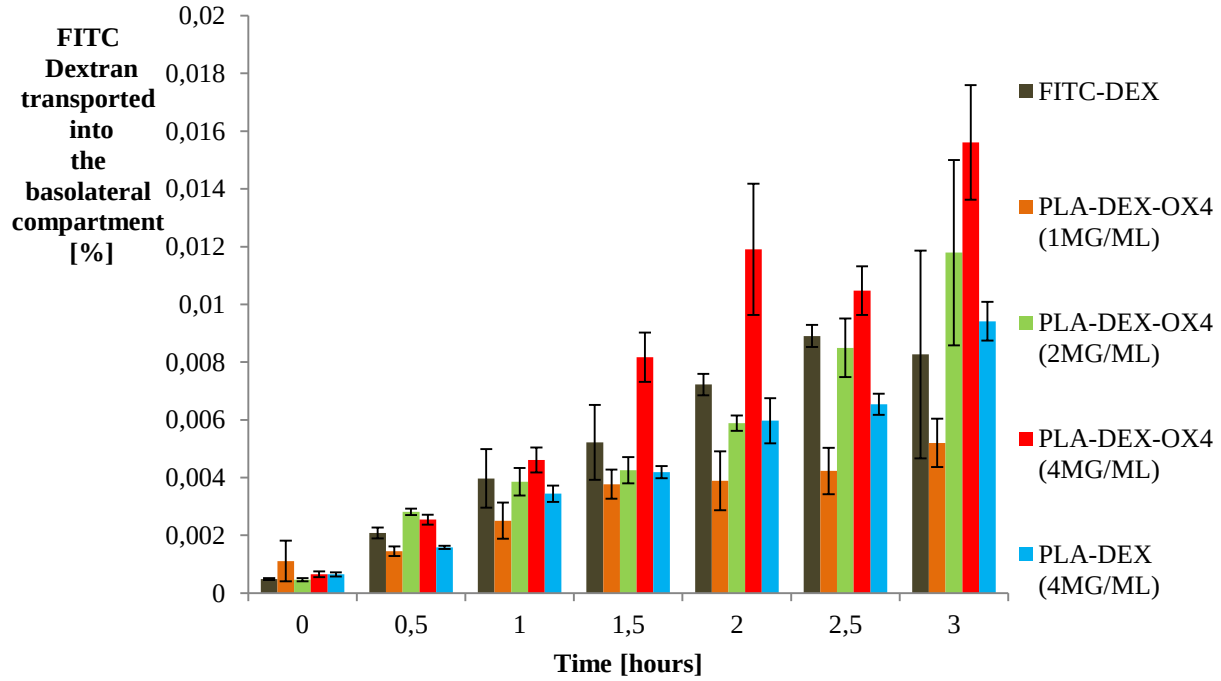

B)

Figure 5.13. FITC-dextran (150 KDa) translocation through an endothelial cell layer: ***A)*** *bEnd3 cells,* ***B)*** *hCMEC/D3 cells. Treatment with nanoparticles prepared from poly(lactic acid)-graft-dextran (PLA-DEX) or poly(lactic acid)-graft-butylglyceroldextran (PLA-DEX-OX4), at different doses. Variation in the percentage of FITC dextran transported across the barrier over time. FITC dextran only employed as a control (n = 5, ±SD).*

Table 5.2. P_{app} coefficients for PLA-DEX and PLA-DEX-OX4 nanoparticles using human and mouse endothelial cells at 3 h incubation time (FITC-DEX only as control, n=3, ±SD).

P_{app} [$cm.s^{-1}$] 3.0 hours	FITC-DEX 150 KDa	PLA-DEX-OX4 1 mg/mL	PLA-DEX-OX4 2 mg/mL	PLA-DEX-OX4 4 mg/mL	PLA-DEX 4 mg/mL
bEnd3	(1.36±0.24) x 10^{-7}	(1.52± 0.81) x 10^{-7}	(1.70± 0.51) x 10^{-7}	(1.70±0.39) x 10^{-7}	(1.63± 0.41) x 10^{-7}
hCMEC/D3	(1.38±0.22) x 10^{-8}	(1.22±0.09) x 10^{-8}	(1.95±0.03) x 10^{-8}	(2.41±0.13) x 10^{-8}	(1.41±0.06) x 10^{-8}

The results showed concentration dependent performance of PLA-DEX-OX4 nanoparticles (significant only in dose 4 mg/mL at 3 hours using human cells model, ANOVA $p<0.05$). Lower values of P_{app} were obtained for the hCMEC/D3 cell model compared to the bEnd3 one which points towards better barrier properties of human cell model *(Table 5.2.)* The values for human model were different to cases reported previously in the literature, which is not unexpected though, considering the different conditions employed in each reported study (as a different tracer molecule and different pore size of the filter), and the relative high concentration of nanoparticles used in these experiments [432, 433]. However values obtained with mouse model were consistent with previous findings of Lien *et al.* [129], who studied modified-chitosan nanoparticles (0.25 mg/mL) using bEnd3 cells and obtained P_{app} values of ca. 1 x 10^{-7} at 4 h of incubation of the cells with FITC-DEX, 150 kDa. As Lien discussed, a barrier enhancing formula was used to decrease the permeability of the Transwell cellular monolayer (though this has been previously debated in the literature as introducing a non-physiological feature into the system [86, 434]). Data presented in *Table 5.2.* suggest that PLA-DEX-OX4 nanoparticles were more effective in influencing the permeability for the FITC-DEX through both bEnd3 and hCMEC/D3 cell monolayers compared to PLA-DEX nanoparticles (3 hours of application, dose 4 mg/mL, ANOVA, $p<0.05$). Previous toxicity experiments revealed that the alkylglyceryl modification does not induce additional toxicity to cells for short time up to 3 h (section 5.3.1); therefore the increased transport of FITC-DEX should be not attributed to cell death and consequent development of "leaky holes" in the cell monolayers. While PLA-DEX nanoparticles were also seen to increase the transport of FITC-DEX to certain extent (possibly

via non-specific nanoparticle-cell interaction [154]), results appear to support therefore the hypothesis that the alkylglyceryl modification could possibly increase this permeability *via* mediated opening of the tight junctions [129].

5.4. Conclusions

The novel polymers (DEX-OX8 and DEX-OX4) and formulations of nanoparticles from chitosan based derivatives (CS-OX derivatives crosslinked with TPP), and novel dextran based derivatives (PLA-DEX-OX4 and PLA-DEX-OX8), were tested with both mouse (bEnd3) and human (hCMEC/D3) brain endothelial cells

The toxicity of alkylglyceryl-modified dextrans (DEX-OX) was tested on mouse brain endothelial cells (bEnd3) using an MTT assay. Both modifications were compared to native dextran and chitosan. DEX-OX4 and DEX-OX8 exhibited similar toxicity as native dextran however both DEX-OX derivatives were less toxic than chitosan in 24 hour incubation for concentration1mg/mL (ANOVA, $p<0.05$).

Toxicity of nanoformulations prepared from novel materials (poly(lactic acid)-*graft*-alkylglyceryl-modified dextran derivatives) was investigated using human brain endothelial cells (hCMEC/D3) by employing a Presto Blue assay. The nanoparticles from PLA-DEX-OX4 and PLA-DEX-OX8 were not found to be more toxic than nanoparticles without alkyglyceryl modification (PLA-DEX) in concentration 1 mg/mL after 24 h incubation. Furthermore, short time incubation (3 h) with a concentration range of 1 - 4 mg/mL revealed no significant differences in terms of toxicity between nanoparticles prepared from alkylglyceryl-modified polymer (PLA-DEX-OX4) and nanoparticles prepared from polymer without alkylglyceryl modification (PLA-DEX). When tested for long-term incubation (24 h), PLA-DEX-OX4 nanoparticles appeared non-toxic at low concentrations, though cell viability was found to decrease (down to ca. 70 %) at higher concentrations (differences become statistically significant above 2 mg/mL; ANOVA, $p=0.05$). For comparative purposes nanoparticles

prepared from alkylglyceryl-modified chitosans were also investigated for toxicity; however reproducibility issues due to low stability of chitosan-based nanoformulations at pH 7.4 did not allow a reliable interpretation of the results obtained.

Cell-nanoparticle interactions were studied on mouse brain endothelial cells (bEnd3) using PLA-DEX-OX4 nanoparticles loaded with Rhodamine B, employing confocal microscopy (cell nuclei were stained with Hoechst Blue while the dye was visualized in red). It was found that PLA-DEX-OX4 nanoparticles were rapidly taken up by the bEnd3 cells into vesicles that localized into the cytoplasm, around the nuclei. The Rhodmine B solution, employed as a control, was not detected inside the cells.

Electric Cell Impedance Sensing (ECIS) was employed to monitor changes in the transendothelial electrical resistance (TEER) of brain endothelial cell layers that were induced by the incubation with PLA-DEX-OX4 nanoparticles. Both mouse and human endothelial cells were tested (in monocultures), and PLA-DEX nanoparticles were used as controls. With bEnd3 cell cultures, PLA-DEX-OX4 nanoparticles were found to induce dose-dependent changes in TEER (concentration range 1 - 4 mg/mL, significant for highest concentration, ANOVA, $p<0.05$). TEER recovery was observed for all formulations except for the most concentrated one (4 mg/mL), that generated a significantly different behaviour compared to that observed for the other PLA-DEX-OX4 concentrations and also for the nanoparticles prepared from unmodified dextran-based material (PLA-DEX; 4 mg/ml). Interestingly, no significant differences could be observed in the cell behaviour induced by PLA-DEX or PLA-DEX-OX4 nanoformulations when they were tested in the same range of concentrations (1 - 4 mg/mL) using human brain endothelial cells (hCMEC/D3).

A blood brain barrier model based on a Transwell system was employed to assess the influence of PLA-DEX-OX4 nanoparticles on the transport of fluorescein labelled dextran (FITC-DEX) through a confluent layer of either mouse (bEnd3) or human (hCMEC/D3) brain endothelial cells. It was found that the translocation of FITC labelled dextran through the human

hCMEC/D3 cell layer was enhanced by PLA-DEX-OX4 nanoparticles in a concentration dependent manner (1 - 4 mg/mL), while the application of PLA-DEX nanoparticles, employed as control (4 mg/mL), did not appear to have a similar effect. Under the conditions studied, the mouse model was found to be leaky to allow reliable differentiation of the FITC tracer flux between treatments.

6

PRELIMINARY STUDIES *IN OVO*

This chapter investigates the interactions of nanoparticles from poly(lactic acid)-*graft*-alkylglyceryl-modified-dextran with chicken embryos *in ovo*. The purpose of this preliminary study also was to outline the possibilities and limitations of using chicken embryos as an alternative to the employment of mammalian models for the evaluation of drug delivery systems.

6.1. Materials and instrumentation

Embryos in their early stage of development (HH 19, day 2; eggs supplied from a local farm after fertilization) were employed for these studies. After delivery, eggs were stored prior use in a cold storing room (15 °C). Gentamycin and PBS were supplied from Gibco; fountain ink (India) was purchased from Pelikan. Fast green, Paraformaldehyde and Rhodamine B were obtained from Sigma, UK. A pumping device (Pneumatic PicoPump pv820, World Precise Instruments, USA) was used for intracardial administration *via* glass micro-needle (prepared in house). A vibratome Series 1000 (Section Vibratome System) was used for microscopy sample preparations, which were observed using a confocal microscope LSM 710, ZEISS, UK.. The nanoparticles from poly(lactic acid)-*graft*-alkylglyceryl-modified-dextran (PLA-DEX-OX4) were loaded with Rhodamine B (by electrospraying method, loading 0.5 % w/w).

6.2. Methods

Eggs (n = 6) were placed into an incubator (37 °C, 60-70 % humidity) 48 hours prior to nanoparticle injection. After 72 h in the incubator (Hamburger-Hamilton stage19-20), a needle

inserted through the eggshell at the narrow apex was used to remove the excess of egg white. The adhesive tape was used to cover the egg on the top and a small oval window was cut into the shell through the tape *(Figure 6.1.)*. The adhesive tape was able to keep the egg structure rigid without collapsing.

Figure 6.1. Egg with a window cut in the shell, the adhesive tape supports the opened shell

100 μL of gentamycin in PBS (10 % w/v) was instilled inside the egg as an antibiotic pre-treatment prior to any manipulation. Fountain pen ink was then injected under the embryo to provide a contrast background for easier orientation and manipulation. The vitelline membrane enveloping the embryo was then cut with a forceps to reach the heart area of the embryo. A thin glass micro-needle (diameter *ca*. 25 μm) connected to a pneumatic pumping device was used to inject the nanoformulation into the heart of the embryo, close to aorta. Rhodamine B-loaded PLA-DEX-OX4 nanoformulations (5 μL; 1 mg/mL; Rhodamine loading 1.5 % w/w) were employed for this study, with a Rhodamine B solution (5 μL; 0.015 mg/mL) used as a control. The examined solutions were stained by the Fast Green solution (1 % v/v) which was used to visualise the blood stream of the embryos. The egg cavity was instilled again with a dose of the antibiotic (as above), and the shell window was sealed with transparent adhesive tape. The eggs were then further incubated (37 °C, 60-70 % humidity) for 24 h before harvesting the embryos. The embryos were removed from the eggs and further purified by removing the rest of the vitelline membrane (by forceps), fixed for 15 minutes in paraformaldehyde solution in PBS (4 % w/v) and embedded in hot gelatine (60 °C). After 2 hours in fridge (4 °C) the embryos

were removed and cut using vibratome (50 μm thick slices). The analysis was performed by a confocal microscope (543 nm laser for Rhodamine B).

6.3. Results and discussion

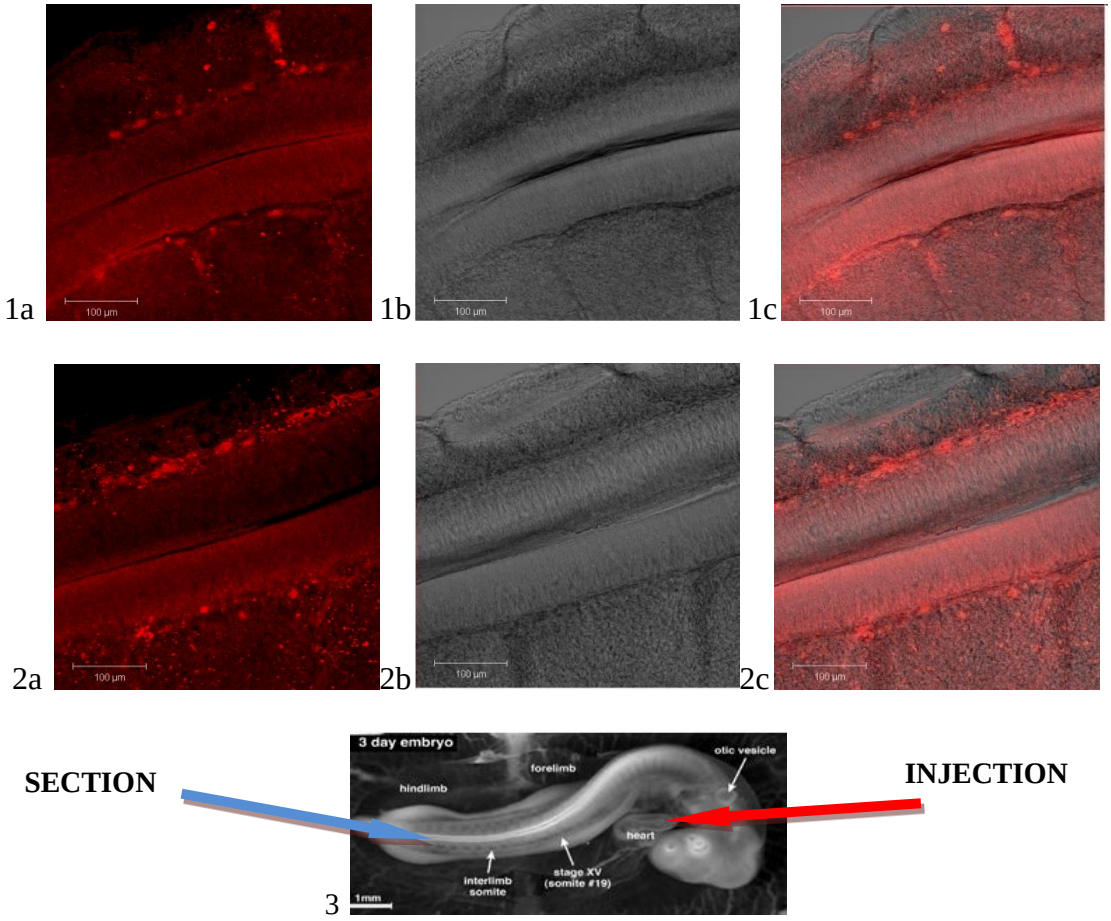

Figure 6.2. Confocal microscopy images of sections of somnites of chicken embryos: ***1) nanoparticles loaded with Rhodamine B****; **2)Rhodamine B solution** (a-fluorescence at 543 nm, b-Differential Interference Contrast (Nomarski) image, c-merge), 3) illustration of the site of injection and a sample of somnites.*

Nanoparticles prepared from PLA-DEX-OX4 and loaded with Rhodamine B (degree of loading 1.5 % w/w) were injected into the heart of chicken embryos as described in section 6.2. (Rhodamine B solution was used as control). Following injection, nanoparticles did not appear to aggregate in the circulation or to affect the viability of the embryos (100 % viability for both control and nanoparticles was recognised by the heart function of the embryos) for the duration of the experiment (min. 24 h following injections). No specific patterns could be observed in the

biodistribution of Rhodamine B, which appeared to be circulated freely in the embryo as the blood-brain barrier is still leaky at this stage [376, 435]. The dye was taken up by the tissues, most of the fluorescence appeared around blood vessels. Also, no differences could be observed in the distribution of Rhodamine B between the two administration methods employed (i.e. as solution, or loaded into nanoparticles and later released during incubation), *Figure 6.2;* (APPENDIX XIII).

6.4. Conclusions

Results of *in vitro* studies (reported in Chapter 5) have indicated the potential of nanoparticles prepared from poly(lactic acid)-*graft*-butylglyceryldextran (PLA-DEX-OX4) as permeating vectors in brain drug delivery applications therefore justifying their further investigation. However *in vivo* studies based on mammalian models require a rather complex setup so a rapid, simple and inexpensive method employing chicken embryos was used to preliminarily check for biodistribution and simple organism toxicity. While an important disadvantage of using chicken embryos is the absence of fully developed barriers (including the blood-brain barrier) prior to the early postnatal period, and while such methods cannot replace rigorous studies based on adult animal models, living embryos are complex enough to provide useful information between *in vitro* experiments using cell cultures and full scale *in vivo* studies on adult animals.

Nanoparticles prepared from PLA-DEX-OX4 loaded with Rhodamine B were applied *via* intracardiac microinjection (5 µl; 1 mg/mL), with free Rhodamine B solution injected in a control embryo. Transparency of embryos allowed direct observation of the distribution of the fluorescent hydrophilic dye (Rhodamine B) that has been loaded into the nanoparticles. The biodistribution was also studied by confocal microscope, and the vasculature appeared to be 'leaky', indicating no barriers in tissues that could resist permeation of the dye. The dye was taken up by the tissues and there was no different pattern of distribution of Rhodamine B observed between the control and loaded nanoparticles.

Furthermore, it was possible to assess the toxicity of nanoparticles during the investigated period (24 h): no aggregation of nanoparticles was observed in the cardiovascular system, indicating no visible interaction with the blood components. All embryos were alive after 24 h of incubation, indicating no acute toxicity at the administered dose (5 μL; 1 mg/mL), and no damage to organs could be detected under the microscope

.

7

GENERAL CONCLUSIONS

Being able to direct actives into the brain *via* non-invasive routes may be compared to seeking for the holy grail of drug delivery, and continues to pose challenges for current pharmaceutical research. The brain is well protected by the blood-brain barrier, which maintains specific conditions for neuronal signalling by regulating the traffic of metabolites and restricting non-invited compounds from entering the brain. Among a number of recent experimental approaches, the employment of short chain alkylglycerols was shown to improve permeation of co-administered drugs into the brain, as was the use of nanoparticulate drug delivery systems. This project was aimed at combining these two approaches by developing alkylglyceryl-modified nanoparticles and testing the ability of such delivery systems to cross the BBB.

Polysaccharides such as chitosan and dextran were selected for modification with alkylglyceryl pendent chains due to their biocompatibility, biodegradability and non-toxicity combined with good drug carrier properties. Following in-house preparation of the required oxiranes, alkylglyceryl-modified chitosan derivatives (CS-OXn; where n = butyl-, pentyl-, octyl-) were prepared with degrees of substitution varying from 14 to 88 % (calculated from ^{1}H-NMR spectra). Novel alkylglyceryl-modified dextran derivatives (DEX-OXn; where n = butyl, octyl) were prepared with degrees of substitution varying from 0.7 to 75.1 %.

Butylglyceryl-dextran (DEX-OX4) and octylglyceryl-dextran (DEX-OX8) were grafted onto poly(lactic acid) using zero-length crosslinkers (CDI and DCC) to yield PLA-DEX-OX4 and PLA-DEX-OX8 (degree of grafting 88-120 units of poly(lactic acid) per 100 units of DEX-OXn, as determined by ^{1}H-NMR). Attempts to modify poly(lactic acid) with maleic anhydride anchors *via* a radical reaction in order to ultimately increase the number of reactive groups for

further grafting with dextran afforded only a low degree of modification (0.8 - 2.2 %), and were not pursued further.

Nanoparticles formulated from CS-OXn materials *via* ionotropic gelation with sodium tripolyphosphate (TPP) had acceptable features for drug delivery (size 100-150 nm; zeta potential 40-50 mV). However, they were difficult to redisperse following purification by either ultracentrifugation or dialysis against deionised water, and gradual particle agglomeration was observed at physiological pH values (pH 7.0 to 7.4). Crosslinking of CS-OX4 with dextran sulphate (DEX-S) resulted in nanoparticles (200 – 400 nm; zeta potential - 30 mV; in acidic conditions, as prepared) with improved stability at neutral pH, however, redispersion following purification by centrifugation still showed stability problems.

Coating poly(lactic acid) nanoparticles with CS-OX4 in the presence of surfactants such as poly(vinyl alcohol), poloxamer 188 or poloxamer 407 provided stable nanoparticles at acidic pH (ca. 190 nm diameter; zeta potential 50 mV; pH 4). However, agglomeration was still observed when pH was changed to neutral (ca. 300-1200 nm; zeta potential ca. -10 mV; pH 7); best results were obtained when poloxamers in concentration 10 mg/mL were used.

Overall, nanoformulations containing CS-OXn derivatives showed redispersion difficulties and limited stability at neutral pH. While the formulations studied here would not be ideal for drug delivery to the brain, they could make good candidates for applications that can tolerate acidic conditions, such as topical skin delivery.

Complexation of butylglyceryl-dextran (DEX-OX4) with chitosan oligomers in the presence of poloxamer 407 as surfactant resulted in stable nanoparticles at neutral pH (ca. 200 nm diameter; zeta potential ca. - 1 mV; at pH 7.4) and which could be successfully loaded with Doxorubicin (degree of loading 4.1 % w/w). However, purification using centrifugation induced redispersion problems as seen with the nanoformulations based on alkylglyceryl-modified chitosans.

Nanoprecipitation of poly(lactic acid) into solutions of buylglyceryl-dextran (DEX-OX4) resulted into structures (100-200 nm diameter) that were stable at physiological conditions (pH 7.4; PBS buffer, 0.9 % saline), but further investigation using repeated centrifugation-redispersion cycles revealed that the layer of butylglyceryl-dextran coating the PLA core was unstable.

Graft copolymers (PLA-DEX-OXn, n= butyl-, octyl-) were obtained by covalently linking poly(lactic acid) to alkylglyceryl-dextran by means of zero-length crosslinkers (CDI, DCC). These materials were then formulated into nanoparticles using different methods: solvent displacement (*via* dialysis), nanoprecipitation and electrospraying. All three methods produced nanoparticles with similar characteristics (size range 100-200 nm; zeta potential -25 mV) that were loaded with hydrophilic model drugs/markers such as Fluorescein, Rhodamine B or Doxorubicin. Electrospraying showed superior loading compared to solvent displacement for Rhodamine B and Doxorubicin (4.93 % and 12.57 % vs. 0.32 % and 0.50 % respectively - all % w/w). The release profiles of all hydrophilic drugs/markers employed showed an initial burst phase followed by a release that could be monitored for several hours.

In vitro studies using brain endothelial cell cultures (mouse bEnd3 and human hCMEC/D3) revealed no toxicity for the nanoparticles prepared from dextran-based materials at doses below 2 mg/mL, although cell viability decreased to 80 % for 4 mg/mL. Nanoparticles prepared from PLA-DEX-OX4 exhibited different behaviour during electric cell substrate impedance sensing (ECIS) experiments compared to those obtained from PLA-DEX. The change in transendothelial electrical resistance (TEER) observed upon incubation of human or mouse endothelial cells with PLA-DEX-OX4 nanoparticles, which can be associated to changes in cell morphology that may indicate an effect at the tight junctions level, was more significant in the mouse model and was found to be concentration dependent.

Compared to PLA-DEX at the same concentration (4 mg/mL), PLA-DEX-OX4 nanoparticles were shown to enhance the FITC-labelled dextran flux through a Transwell-based

BBB model comprised of either mouse (bEnd3) or human (hCMEC/D3) brain endothelial cells. However, both mouse and human cell monoculture models were found to be leaky; they exhibited a significant flux of fluorescent tracer even for negative controls, with the mouse model being worse.

In ovo experiments assessed the effect of PLA-DEX-OX4 nanoparticles on simple organisms of chicken embryos. All embryos (n = 6) were alive after 24 h of incubation, which supports *in vitro* data indicating the lack of acute toxicity for PLA-DEX-OX4 nanoparticles. The chicken embryo biodistribution of Rhodamine B marker loaded into nanoparticles was similar to that exhibited by the free Rhodamine B solution employed as a control. This is likely to be due to the release of dye from nanoparticles combined with the leaky barriers present in the embryo at this stage. Confocal microscopy observations did not show any accumulation in a specific organ.

In comparison to nanoparticles prepared from alkylglyceryl-modified chitosan derivatives (CS-OX),which exhibited low stability at neutral pH and so make such formulations rather unsuitable for intravenous drug delivery, nanoparticles from poly(lactic acid)-*graft*-butylglyceryl dextran (PLA-DEX-OX4) were found to have promising characteristics that can encourage further research in the direction of brain drug delivery. They were stable at physiological pH and relatively non-toxic for mouse and human endothelial cells and chicken embryos. PLA-DEX-OX4 based nanoparticles were also observed to induce a dose-dependent change in TEER – indicative of a modification of the integrity of the endothelial cell epithelium – and to enhance the transport of FITC dextran through endothelial cell monocultures.

Employing a higher-level *in vitro* model of the blood brain barrier (*e.g.* one that simulates the support of endothelial cells by pericytes and astrocytes, the fluid flow, or the interaction of nanoparticles with plasma proteins) would be an important step in the further investigation of the potential of PLA-DEX-OX4 nanoparticles to act as permeating vectors that can transport a drug load through the BBB. As the preliminary *in ovo* study reported here could

not provide any information in terms of biodistribution, *in vivo* work employing a rodent model would be necessary in order to collect relevant data.

8

REFERENCES

1. Olesen J, Leonardi M. The burden of brain diseases in Europe. European Journal of Neurology. 2003 10(5):471-7.
2. Olesen J, Gustavsson A, Svensson M, Wittchen HU, Jönsson B, on behalf of the Csg, et al. The economic cost of brain disorders in Europe. European Journal of Neurology. 2012 19(1):155-62.
3. Pardridge W. Drug Targeting to the Brain. Pharmaceutical Research. 2007 24(9):1733-44.
4. Pardridge WM. Holy grails and in vitro blood-brain barrier models. Drug Discovery Today. 2004 9(6):258-.
5. Kreuter J. Nanoparticulate systems for brain delivery of drugs. Advanced Drug Delivery Reviews. 2001 47(1): 65-81.
6. Olivier J-C. Drug Transport to Brain with Targeted Nanoparticles. NeuroRX. 2005 2(1):108-19.
7. Soppimath KS, Aminabhavi TM, Kulkarni AR, Rudzinski WE. Biodegradable polymeric nanoparticles as drug delivery devices. Journal of Controlled Release. 2001 70(1-2):1-20.
8. Erdlenbruch B, Alipour M, Fricker G, Miller DS, Kugler W. Alkylglycerol opening of the blood-brain barrier to small and large fluorescence markers in normal and C6 glioma-bearing rats and isolated rat brain capillaries. British Journal of Pharmacology. 2003 140:1201-10.
9. Erdlenbruch B, Hulper P, Kugler W, Eibl H, Lakomek M, editors. Alkylglycerol-mediated increase in drug delivery to the normal brain and to brain tumors in rats: Regulation of drug transfer and comparison with hypertonic mannitol and bradykinin. 2nd Quadrennial Meeting of the World Federation of Neuro Oncology/6th Meeting of the European Association for Neuro-Oncology; 2005 May 05-08; Edinburgh, Scotland: Duke University Press.
10. Erdlenbruch B, Schinkhof C, Kugler W, Heinemann DEH, Herms J, Eibl H, et al. Intracarotid administration of short-chain alkylglycerols for increased delivery of methotrexate to the rat brain. British Journal of Pharmacology. 2003 139(4):685-94.
11. Population trends 136: Office for National Statistics, Great Britain2009.
12. Older people's day. Office for National Statistics, 2011 29 September 2011.
13. Andlin-Sobocki P, Jonsson B, Wittchen HU, Olesen J. Cost of disorders of the brain in Europe. European Journal of Neurology. 2005 12 Suppl 1:1-27.
14. Pathan SA, Iqbal Z, Zaidi SMA, Talegaonkar S, Vohra D, Jain GK, et al. CNS drug delivery systems: novel approaches. Recent patents on drug delivery & formulation. 2009 3(1):71-89.
15. Ndabahaliye A. Number of neurons in a human brain. In: Elert G, The Physics Factbook: World Book Inc; 2002. Available from http://hypertextbook.com/facts/2002/AniciaNdabahaliye2.shtml. Cited 22.11.2012
16. Choi J, Zheng Q, Katz HE, Guilarte TR. Silica-Based Nanoparticle Uptake and Cellular Response by Primary Microglia. Environmental Health Perspective. 2009 118(5).
17. Hurty A. The brain's silent majority. Stanford Medicine Magazine: Stanford University; Fall 2009. Available from http://stanmed.stanford.edu/2009fall/article6.html. Cited 22.11.2013

18. Pardridge W. Introduction to the Blood-Brain Barrier. Pardridge W, editor. Cambridge: Cambridge University Press; 2006.
19. Czosnyka M, Pickard JD. Monitoring and interpretation of intracranial pressure. Journal of Neurology, Neurosurgery & Psychiatry. 2004 75(6):813-21.
20. Gray H. Anatomy of the Human Body 20th edition. Lewis WH, editor. Phladelphia: Lea and Febinger, 1918; Bartleby, 2000.
21. Cecchelli R, Berezowski V, Lundquist S, Culot M, Renftel M, Dehouck M, et al. Modelling of the blood-brain barrier in drug discovery and development. Nature Reviews on Drug Discovery. 2007 6(8):650-61.
22. Abbott NJ, Ronnback L, Hansson E. Astrocyte-endothelial interactions at the blood-brain barrier. Nature Reviews on Neuroscience. 2006 7(1):41-53.
23. Zlokovic VB. Neurovascular mechanism of Alzheimers neurodegeneration. Trends in Neuroscience. 2005 28:202-8.
24. Pardridge WM. The Blood-Brain Barrier: Bottleneck in Brain Drug Development. NeuroRX. 2005 2(1):3-14.
25. Zlokovic VB. The blood-brain barrier in health and chronic neurodegenerative disorders. Neuron. 2008 57:178-201.
26. Bechmann I, Galea I, Perry VH. What is the blood-brain barrier (not)? Trends in Immunology. 2007 28(1):5-11.
27. Goldman E. Vitalfärbungen am Zentralnervensystem. Beitrag zur Physio-Pathologie des Plexus Choroideus und der Hirnhäute. [Intravital labelling of the central nervous system. A study on the pathophysiology of the choroid plexus and the meninges.]. Physikalisch-Mathematische Classe. 1913 1:1-64.
28. Reese TS, Karnovsky MJ. Fine structural localisation of a blood-brain barrier to exogenous peroxidase. Journal of Cell Biology. 1967(34):207-17.
29. Löscher W, Potschka H. Role of drug efflux transporters in the brain for drug disposition and treatment of brain diseases. Progress in Neurobiology. 2005 76(1):22-76.
30. Armulik A, Genove G, Mae M, Nisancioglu MH, Wallgard E, Niaudet C, et al. Pericytes regulate the blood-brain barrier. Nature. 2010 468(7323):557-61.
31. Hirschi KK, D'Amore PA. Pericytes in the microvasculature. Cardiovascular Research. 1996 32(4):687-98.
32. Lai CH, Kuo KH. The critical component to establish in vitro BBB model: Pericyte. Brain Research Reviews. 2005 50(2):258-65.
33. Sato Y, Rifkin DB. Inhibition of endothelial-cell movement by pericytes and smooth-muscle cells – activation of a latent transforming growth factor-beta-1-like molecule by plasmin during co-culture. Journal of Cell Biology. 1989 109(1):309-15.
34. Allt G, Lawrenson JG. Pericytes: Cell biology and pathology. Cells Tissues Organs. 2001 169(1):1-11.
35. Garcia CM, Darland DC, Massingham LJ, D'Amore PA. Endothelial cell-astrocyte i nteractions and TGF beta are required for induction of blood-neural barrier properties. Developmental Brain Research. 2004 152(1):25-38.
36. Chen Y, Liu L. Modern methods for delivery of drugs across the blood–brain barrier. Advanced Drug Delivery Reviews. 2012 64(7):640-65.
37. Goldstein GW. Endothelial cell-astrocyte interactions. A cellular model of the blood-brain barrier. Annals of the New York Academy of Sciences. 1988 529:31-9.
38. Anderson CM, Nedergaard M. Astrocyte-mediated control of cerebral microcirculation. Trends in Neurosciences. 2003 26(7):340-4.
39. Zozulya A, Weidenfeller C, Galla HJ. Pericyte-endothelial cell interaction increases MMP-9 secretion at the blood-brain barrier in vitro. Brain Research. 2008 1189:1-11.
40. Tilling T, Engelbertz C, Decker S, Korte D, Huwel S, Galla HJ. Expression and adhesive properties of basement membrane proteins in cerebral capillary endothelial cell cultures. Cell and Tissue Research. 2002 310(1):19-29.
41. Krol S. Challenges in drug delivery to the brain: Nature is against us. Journal of Controlled Release. 2012 164(2):145-55.

42. Ballabh P, Braun A, Nedergaard M. The blood-brain barrier: an overview: Structure, regulation, and clinical implications. Neurobiology of Disease. 2004 16(1):1-13.
43. Rutka JT, Myatt CA, Giblin JR, Davis RL, Rosenblum ML. Distribution of extracellular-matrix proteins in primary human-brain tumors - an immunohistochemical analysis. Canadian Journal of Neurological Sciences. 1987 14(1):25-30.
44. Rascher G, Fischmann A, Kroger S, Duffner F, Grote EH, Wolburg H. Extracellular matrix and the blood-brain barrier in glioblastoma multiforme: spatial segregation of tenascin and agrin. Acta Neuropathologica. 2002 104(1):85-91.
45. Pan W, Kastin AJ. Tumor necrosis factor and stroke: Role of the blood–brain barrier. Progress in Neurobiology. 2007 83(6):363-74.
46. Ábrahám CS, Deli MA, Joó F, Megyeri P, Torpier G. Intracarotid tumor necrosis factor-α administration increases the blood-brain barrier permeability in cerebral cortex of the new-born pig: quantitative aspects of double-labelling studies and confocal laser scanning analysis. Neuroscience Letters. 1996 208(2):85-8.
47. Wong D, Prameya R, Dorovini-Zis K. Adhesion and migration of polymorphonuclear leukocytes across human brain microvessel endothelial cells are differentially regulated by endothelial cell adhesion molecules and modulate monolayer permeability. Journal of Neuroimmunology. 2007 184(1–2):136-48.
48. Claudio L, Kress Y, Factor J, Brosnan CF. Mechanisms of edema formation in experimental autoimmune encephalomyelitis-the contribution of inflammatory cells. American Journal of Pathology. 1990 137(5):1033-45.
49. Fry KE. Development of a three-dimensional, all-human in vitro model of the blood-brain barrier for cancer metastasis studies [PhD. Thesis]. Portsmouth: University of Portsmouth; 2010.
50. Abbott NJ. Physiology of the blood-brain barrier and its consequences for drug transport to the brain. International Congress Series. 2005 1277:3-18.
51. Neuwelt E, Abbott NJ, Abrey L, Banks WA, Blakley B, Davis T, et al. Strategies to advance translational research into brain barriers. The Lancet Neurology. 2008 7(1):84-96.
52. Saitou M, Furuse M, Sasaki H, Schulzke JD, Fromm M, Takano H, et al. Complex phenotype of mice lacking occludin, a component of tight junction strands. Molecular Biology of the Cell. 2000 11(12):4131-42.
53. Wen HJ, Watry DD, Marcondes MCG, Fox HS. Selective decrease in paracellular conductance of tight junctions: role of the first extracellular domain of claudin-5. Molecular and Cellular Biology. 2004 24(19):8408-17.
54. Schmieder P. Tight Junctions. Available from http://www.fmp-berlin.de/schmieder/research/jpg/img_tight_junction.jpg. Cited 22.11.2012.
55. Davies DC. Blood-brain barrier breakdown in septic encephalopathy and brain tumours. Journal of Anatomy. 2002 200(6):639-46.
56. Nagy JI, Rash JE. Connexins and gap junctions of astrocytes and oligodendrocytes in the CNS. Brain Research Reviews. 2000 32(1):29-44.
57. Nagasawa K, Chiba H. Possible involvent of gap junctions in the barrier function of tight junctions of brain and endothelial cells. Journal of Cell physiology. 2006 208:123-32.
58. Weiss N, Miller F, Cazaubon S, Couraud P-O. The blood-brain barrier in brain homeostasis and neurological diseases. Biochimica et Biophysica Acta (BBA) - Biomembranes. 2009 1788(4):842-57.
59. Loscher W, Potoschka H. Drug resistance in brain diseases and the role of efflux transporter. Nature Reviews on Neuroscience. 2005 6:591-602.
60. Hillery AM, Lloyd AW, James S. Drug Delivery and Targeting for Pharmacists and Pharmaceutical Scientists. London: Taylor and Francis; 2001, page 45-62.
61. Pardridge WM. Blood-brain barrier delivery. Drug Discovery Today. 2007 12(1-2):54-61.

62. Wilz A, Pritchard EM, Li T, Lan J-Q, Kaplan DL, Boison D. Silk polymer-based adenosine release: Therapeutic potential for epilepsy. Biomaterials. 2008 29(26):3609-16.
63. Deli MA. Potential use of tight junction modulators to reversibly open membranous barriers and improve drug delivery. Biochimica et Biophysica Acta (BBA) - Biomembranes. 2009 1788(4):892-910.
64. Chopra D, Gulati M, Saluja V. Brain Permeable Nanoparticles. Recent Patents on CNS Drug Discovery. 2008 3:216-25.
65. Emerich DF, Snodgrass P, Pink M. Central anaesthetic action of loperamide following transient permeation of the blood-brain barrier with Cereport (RMP-7). Brain Research. 1998 801:259-66.
66. Emerich DF, Dean DL, Osborn C. The development of bradykinin agonist labradimil as a means to increase the permeability of the blood-brain barrier: From concept to clinical evaluation. Clinical Pharmacokinetic. 2001 40:105-23.
67. Erdlenbruch B, Alipour M, Fricker G, Miller DS, Kugler W, Eibl H, et al. Alkylglycerol opening of the blood-brain barrier to small and large fluorescence markers in normal and C6 glioma-bearing rats and isolated rat brain capillaries. British Journal of Pharmacology. 2003 140(7):1201-10.
68. Begley D. ABC transporters in the blood brain-barrier. Current Pharmaceutical Design. 2004 10:1295-312.
69. Kreuter J. Application of nanoparticles for the delivery of drugs to the brain. International Congress Series. 2005 1277(2):85-94.
70. Faraji AH, Wipf P. Nanoparticles in cellular drug delivery. Bioorganic & Medicinal Chemistry. 2009 17(8):2950-62.
71. Weber EL, Groebel EA. Cerebral edema associated with Giladel wafers: Two case studies. Neurooncology 2005 7:84-9.
72. Elkharraz K, Faisant N, Guse C, Siepmann F, Arica-Yegin B, Oger JM, et al. Paclitaxel-loaded microparticles and implants for the treatment of brain cancer: Preparation and physicochemical characterization. International Journal of Pharmaceutics. 2006 314(2):127-36.
73. Yang F-Y, Fu W-M, Yang R-S, Liou H-C, Kang K-H, Lin W-L. Quantitative Evaluation of Focused Ultrasound with a Contrast Agent on Blood-Brain Barrier Disruption. Ultrasound in Medicine and Biology. 2007 33(9):1421-7.
74. Moriyama E, Salcman M, Broadwell RD. Blood-brain barrier alteration after microwave-induced hyperthermia is purely a thermal effect: I. Temperature and power measurements. Surgical Neurology. 1991 35(3):177-82.
75. Lin JC, Yuan PMK, Jung DT. Enhancement of anticancer drug delivery to the brain by microwave induced hyperthermia. Bioelectrochemistry and Bioenergetics. 1998 47(2):259-64.
76. Preston E, Slinn J, Vinokourov I, Stanimirovic D. Graded reversible opening of the rat blood-brain barrier by intracarotid infusion of sodium caprate. Journal of Neuroscience Methods. 2008 168(2):443-9.
77. Tomasz A, Tuomanen E, inventors; Methods and compositions for reversibly permeabilizing the blood brain barrier, EP 0527810 A1, 1991.
78. Saijta A, Princi P, Costa G. Arecoline, but not haloperidol, induces changes in the permeability of the blood-brain barrier in the rat. Journal of Pharmacy and Pharmacology. 1990 42:135-8.
79. Nittby H, Brun A, Eberhardt J, Malmgren L, Persson BRR, Salford LG. Increased blood–brain barrier permeability in mammalian brain 7 days after exposure to the radiation from a GSM-900 mobile phone. Pathophysiology. 2009 16(2–3):103-12.
80. Chauhan NB. Trafficking of intracerebraly injected injected antisence oligonucleotides in the mouse brain. Nucleic Acid Drug Development. 2002 12:353-7.
81. Lam MF, Thomas MG, Lind CRP. Neurosurgical convection-enhanced delivery of treatments for Parkinson's disease. Journal of Clinical Neuroscience. 2011 18(9):1163-7.

82. Krauze MT, Saito R, Noble C, Bringas J, Forsayeth J, McKnight TR, et al. Effects of the perivascular space on convection-enhanced delivery of liposomes in primate putamen. Experimental Neurology. 2005 196(1):104-11.
83. Allard E, Passirani C, Benoit J-P. Convection-enhanced delivery of nanocarriers for the treatment of brain tumors. Biomaterials. 2009 30(12):2302-18.
84. Neuwelt EA. Modification of blood-brain barrier and the chemotherapy of malignant tumors. Federation Proceedings. 1984 43(2):214-9.
85. Siegal T. Blood brain barrier: Drug delivery and brain pathology. Springer. 2002:251-72.
86. Deli M, Ábrahám C, Kataoka Y, Niwa M. Permeability Studies on In Vitro Blood–Brain Barrier Models: Physiology, Pathology, and Pharmacology. Cellular and Molecular Neurobiology. 2005 25(1):59-127.
87. Inoue T, Nagara H, Kondo A, Fukui M, Tateishi J. Effects of intracarotid hyperosmolar mannitol in triethy tin (tet)-induced rat-brain oedema - preservation of blood-brain barrier. Brain Research. 1987 414(2):309-13.
88. Muldoon LL, Soussain C, Janhke K. Chemotherapy delivery issues in central nervous system malignancy: a reality check. Journal of Clinical Oncology. 2007 25:2295-305.
89. Borlongan CV, Emerich DF. Facilitation of drug entry into the CNS via transient permeation of blood brain barrier: laboratory and preliminary clinical evidence from bradykinin receptor agonist, Cereport. Brain Research Bulletin. 2003 60(3):297-306.
90. Erdlenbruch B, Jendrosek V, Eibl H, Kugler W, Lakomek M. Increased delivery of erucylphosphocholine to C6 gliomas by chemical opening of the blood-brain barrier using intracarotidal pentylglycerols in rats. Cancer Chemotherapy Pharmacology. 2002 50:299-304.
91. Hulper P, Dullin C, Kugler W, Lakomek M, Erdlenbruch B. Monitoring Proteins Using In Vivo Near-Infrared Time-Domain Optical Imaging after 2-O-Hexyldiglycerol-Mediated Transfer to the Brain. Molecular Imaging and Biology. 2011 13(2):275-83.
92. Erdlenbruch B, Jendrossek V, Eibl H, Lakomek M. Transient and controllable opening of the blood-brain barrier to cytostatic and antibiotic agents by alkylglycerols in rats. Experimental Brain Research. 2000 135(3):417-22.
93. Erdlenbruch B, Schinkhof C, Kugler W, Eibl H, Lakomek M. Enhanced drug delivery to the brain and brain tumors in rats by alkylglycerols and regulation of the effect by structural modifications. International Journal of Molecular Medicine. 2000 6(Supplement 1):S36.
94. Marigny K, Pedrono F, Martin-Chouly CAE, Yumine H, Saiag B, Legrand AB. Modulation of endothelial permeability by 1-O-alkylglycerols. Acta Physiologica Scandinavica. 2002 176(4):263-8.
95. Erdlenbruch B, Claudia S, Wilfried K, Dagmar EHH, Jochen H, Hansjörg E, et al. Intracarotid administration of short-chain alkylglycerols for increased delivery of methotrexate to the rat brain. British Journal of Pharmacology. 2003 139(4):685-94.
96. Brohult A, Brohult J, Brohult S. Biochemical effects of alkoxycerols and their use in cancer therapy. Acta Chemica Scandinavica. 1970 24(2):730-2.
97. Iagher F, Belo SRD, Naliwaiko K, Franzoi AM, de Brito GAP, Yamazaki RK, et al. Chronic Supplementation With Shark Liver Oil for Reducing Tumor Growth and Cachexia in Walker 256 Tumor-Bearing Rats. Nutrition and Cancer-an International Journal. 2011 63(8):1307-15.
98. Iannitti T, Palmieri B. An Update on the Therapeutic Role of Alkylglycerols. Marine Drugs. 2010 8(8):2267-300.
99. Davidson BC, ROTTANBURG D, Prinz W, Cliff G. The Influence of Shark Liver Oils on Normal and Transformed Mammalian Cells in Culture. In Vivo. 2007 21(2):333-7.
100. Pedrono F, Saiag B, Moulinoux JP, Legrand AB. 1-O-Alkylglycerols reduce the stimulating effects of bFGF on endothelial cell proliferation in vitro. Cancer Letters. 2007 251(2):317-22.

101. Cheminade C, Gautier W, Hichami A, Allaume P, Le Lannou D, Legrand AB. 1-O-alkylglycerols improve boar sperm motility and fertility. Biology of Reproduction. 2002 66(2):421-8.
102. Ved HS, Gustow E, Mahadevan V, Pieringer RA. Dodecylglycerol - a new type of antibacterial agent which stimulates autolysin activity in *Streptococus faecium* ATCC-9790. Journal of Biological Chemistry. 1984 259(13):8115-21.
103. Boeryd B, Nilsson T, Lindholm L, Lange S, Hallgren B, Stallberg G.. European Journal of Immunology. 1978 8(9):678-80.
104. Weber N. Biological effects of alkylglycerols. In Braquet P, Mangold HK, Vargaftig BB. Progress in Biochemical Pharmacology 1988 22: 48-57.
105. Gopinath D, Ravi D, Rao BR, Apte SS, Rambhau D. 1-O-Alkylglycerol vesicles (Algosomes): their formation and characterization. International Journal of Pharmaceutics. 2002 246(1-2):187-97.
106. Unger C, Eibl H, Vonheyden HW, Krisch B, Nagel GA. Blood-brain barrier and penetration of cytostatics. Klinische Wochenschrift. 1985 63(12):565-71.
107. Johansson BB, Nordborg C, Westerngern I. Physiology of the blood-brain barrier. Johansson BB, editor. Amsterdam: Elsevier; 1990.
108. Koo Y-EL, Reddy GR, Bhojani M, Schneider R, Philbert MA, Rehemtulla A, et al. Brain cancer diagnosis and therapy with nanoplatforms. Advanced Drug Delivery Reviews. 2006 58(14):1556-77.
109. Kreuter J. Nanoparticulate systems for brain delivery of drugs. Advanced Drug Delivery Reviews. 2001 47(1):65-81.
110. Kreuter J, Gelperina S. Use of nanoparticles for cerebral cancer. Tumori. 2008 94:271-7.
111. Molnár E. Modified-chitosan nanoparticles for drug delivery through the blood-brain barrier [Ph.D.] Portsmouth: University of Portsmouth; 2008.
112. Bodor N, Buchwald P. Brain targetted drug delivery-Experiences to date. American Journal of Drug Targeting. 2003(1):13-26.
113. Anderson BD. Prodrugs for improved CNS delivery. Advanced Drug Delivery Reviews. 1996 19:171-202.
114. Batrakova EV, Kabanov AV. Enhancement in drug delivery. Toitou E, Barry BW, editors. Boca Raton. CRC Press; 2006. Pp 272-309.
115. Kreuter J. Nanoparticles and microparticles for drug and vaccine delivery. Journal of Anantomy. 1996 189:503-5.
116. Prokop A, Davidson JM. Nanovehicular intracellular delivery systems. Journal of Pharmaceutical Sciences. 2008 97:3518-90.
117. El Andaloussi S, Lakhal S, Mäger I, Wood MJA. Exosomes for targeted siRNA delivery across biological barriers. Advanced Drug Delivery Reviews. 2013 65(3) 391-7.
118. Blasi P, Giovagnoli S, Schoubben A, Ricci M, Rossi C. Solid lipid nanoparticles for targeted brain drug delivery. Advanced Drug Delivery Reviews. 2007 59(6):454-77.
119. Batrakova EV, Kabanov AV. Pluronic block copolymers: Evolution of drug delivery concept from inert nanocarriers to biological response modifiers. Journal of Controlled Release. 2008 130(2):98-106.
120. Li Y, He H, Jia X, Lu W-L, Lou J, Wei Y. A dual-targeting nanocarrier based on poly(amidoamine) dendrimers conjugated with transferrin and tamoxifen for treating brain gliomas. Biomaterials. 2012 33(15):3899-908.
121. Jung T, Kamm W, Breitenbach A, Kaiserling E, Xiao JX, Kissel T. Biodegradable nanoparticles for oral delivery of peptides: is there a role for polymers to affect mucosal uptake? European Journal of Pharmaceutics and Biopharmaceutics. 2000 50(1):147-60.
122. Kreuter J. Nanoparticles as drug delivery for the brain. In: Benita S, editor. Microencapsulation, Methods and industrial applications. New York: Taylor and Francis; 2006.

123. Steiniger SCJ, Kreuter J, Khalansky AS, Skidan IN, Bobruskin AI, Smirnova ZS, et al. Chemotherapy of glioblastoma in rats using doxorubicin-loaded nanoparticles. International Journal of Cancer. 2004 109(5):759-67.
124. Lynch I, Dawson KA. Protein-nanoparticle interactions. Nanotoday. 2008 3:40-7.
125. Ramge P, Unger RE. Polysorbate 80 coating enhances uptake of PBCA nanoparticles by human and bovine primary brain capillary endothelical cells. European Journal of Neuroscience. 2000 12:1931-40.
126. Sun W, Xie C, Wang H, Hu Y. Specific role of polysorbate 80 coating on the targeting of nanoparticles to the brain. Biomaterials. 2004 25(15):3065-71.
127. Michaelis K, Hoffmann MM. Covalent linkage of apolipoprotein E to albumin nanoparticles strongly enhances the transport to the brain. Journal of Pharmacology and Experimental Therapy. 2006 317:1246-53.
128. Tahara K, Miyazaki Y, Kawashima Y, Kreuter J, Yamamoto H. Brain targeting with surface-modified poly(d,l-lactic-co-glycolic acid) nanoparticles delivered via carotid artery administration. European Journal of Pharmaceutics and Biopharmaceutics. 2011 77(1):84-8.
129. Lien C-F, Molnar E, Toman P, Tsibouklis J, Pilkington GJ, Gorecki DC, et al. In vitro assessment of alkylglyceryl-functionalized chitosan nanoparticles as permeating vectors for the blood-brain barrier. Biomacromolecules. 2012 13(4):1067-73.
130. Xin H, Chen L, Gu J, Ren X, wei Z, Luo J, et al. Enhanced anti-glioblastoma efficacy by PTX-loaded PEGylated poly(ε-caprolactone) nanoparticles: In vitro and in vivo evaluation. International Journal of Pharmaceutics. 2010 402(1–2):238-47.
131. Kopelman R, Lee Koo Y-E, Philbert M, Moffat BA, Ramachandra Reddy G, McConville P, et al. Multifunctional nanoparticle platforms for in vivo MRI enhancement and photodynamic therapy of a rat brain cancer. Journal of Magnetism and Magnetic Materials. 2005 293(1):404-10.
132. Doi A, Kawabata S, Iida K, Yokoyama K, Kajimoto Y, Kuroiwa T, et al. Tumor-specific targeting of sodium borocaptate (BSH) to malignant glioma by transferrin-PEG liposomes: a modality for boron neutron capture therapy. Journal of Neuro-Oncology. 2008 87(3):287-94.
133. Feng B, Tomizawa K, Michiue H, Miyatake S-i, Han X-J, Fujimura A, et al. Delivery of sodium borocaptate to glioma cells using immunoliposome conjugated with anti-EGFR antibodies by ZZ-His. Biomaterials. 2009 30(9):1746-55.
134. Tseng Y-L, Liu J-J, Hong R-L. Translocation of Liposomes into Cancer Cells by Cell-Penetrating Peptides Penetratin and Tat: A Kinetic and Efficacy Study. Molecular Pharmacology. 2002 62(4):864-72.
135. Bangham AD, Standish MM, Watkins JC. Diffusion of univalent ions across the lamellae of swollen phospholipids. Journal of Molecular Biology. 1965 13(1):238-52.
136. Allen TM, Cullis PR. Liposomal drug delivery systems: From concept to clinical applications. Advanced Drug Delivery Reviews. 2013 65(1):36-48.
137. Marjan JMJ, Allen TM. Long circulating liposomes: Past, present and future. Biotechnology Advances. 1996 14(2):151-75.
138. Li S-D, Huang L. Nanoparticles evading the reticuloendothelial system: Role of the supported bilayer. Biochimica et Biophysica Acta (BBA) - Biomembranes. 2009 1788(10):2259-66.
139. Blume G, Cevc G. Liposomes for the sustained drug release *in vivo*. Biochimica et Biophysica Acta (BBA) - Biomembranes. 1990 1029:91-7.
140. Afergan E, Epstein H, Dahan R, Koroukhov N, Rohekar K, Danenberg HD, et al. Delivery of serotonin to the brain by monocytes following phagocytosis of liposomes. Journal of Controlled Release. 2008 132(2):84-90.
141. Saito R, Krauze MT, Bringas JR, Noble C, McKnight TR, Jackson P, et al. Gadolinium-loaded liposomes allow for real-time magnetic resonance imaging of convection-enhanced delivery in the primate brain. Experimental Neurology. 2005 196(2):381-9.

142. Chen H, Tang L, Qin Y, Yin Y, Tang J, Tang W, et al. Lactoferrin-modified procationic liposomes as a novel drug carrier for brain delivery. European Journal of Pharmaceutical Sciences. 2010 40(2):94-102.
143. Qin Y, Chen H, Yuan W, Kuai R, Zhang Q, Xie F, et al. Liposome formulated with TAT-modified cholesterol for enhancing the brain delivery. International Journal of Pharmaceutics. 2011 419(1–2):85-95.
144. Martins S, Tho I, Reimold I, Fricker G, Souto E, Ferreira D, et al. Brain delivery of camptothecin by means of solid lipid nanoparticles: Formulation design, in vitro and in vivo studies. International Journal of Pharmaceutics. 2012 439(1–2):49-62.
145. Mehnert W, Mäder K. Solid lipid nanoparticles: Production, characterization and applications. Advanced Drug Delivery Reviews. 2001 47(2–3):165-96.
146. Martins S, Costa-Lima S, Carneiro T, Cordeiro-da-Silva A, Souto EB, Ferreira DC. Solid lipid nanoparticles as intracellular drug transporters: An investigation of the uptake mechanism and pathway. International Journal of Pharmaceutics. 2012 430(1–2):216-27.
147. Bertrand N, Leroux J-C. The journey of a drug-carrier in the body: An anatomo-physiological perspective. Journal of Controlled Release. 2012 161(2):152-63.
148. Liu D, Liu F, Song YK. Recognition and clearance of liposomes containing phosphatidylserine are mediated by serum opsonin. Biochimica et Biophysica Acta (BBA) - Biomembranes. 1995 1235(1):140-6.
149. Stolnik S, Illum L, Davis SS. Long circulating microparticulate drug carriers. Advanced Drug Delivery Reviews. 1995 16(2–3):195-214.
150. Moghimi SM, Hunter AC, Murray JC. Long-Circulating and Target-Specific Nanoparticles: Theory to Practice. Pharmacological Reviews. 2001 53(2):283-318.
151. Abra RM, Bosworth ME, Hunt CA. Liposome disposition in vivo: effects of pre-dosing with lipsomes. Research Communication in Chemical Pathology and Pharmacology. 1980 29(2):349-60.
152. Hardonk MJ, Dijkhuis FW, Hulstaert CE, Koudstaal J. Heterogeneity of rat liver and spleen macrophages in gadolinium chloride-induced elimination and repopulation. Journal of Leukocyte Biology. 1992 52(3):296-302.
153. Naito M, Nagai H, Kawano S, Umezu H, Zhu H, Moriyama H, et al. Liposome-encapsulated dichloromethylene diphosphonate induces macrophage apoptosis in vivo and in vitro. Journal of Leukocyte Biology. 1996 60(3):337-44.
154. Nguyen CA, Allémann E, Schwach G, Doelker E, Gurny R. Cell interaction studies of PLA-MePEG nanoparticles. International Journal of Pharmaceutics. 2003 254(1):69-72.
155. Torchilin VP, Trubetskoy VS. Which polymers can make nanoparticulate drug carriers long-circulating? Advanced Drug Delivery Reviews. 1995 16(2–3):141-55.
156. Rouzes C, Gref R, Leonard M, De Sousa Delgado A, Dellacherie E. Surface modification of poly(lactic acid) nanospheres using hydrophobically modified dextrans as stabilizers in an o/w emulsion/evaporation technique. Journal of Biomedical Materials Research. 2000 50(4):557-65.
157. Fournier C, Leonard M, Le Coq-Leonard I, Dellacherie E. Coating Polystyrene Particles by Adsorption of Hydrophobically Modified Dextran. Langmuir. 1995 11(7):2344-7.
158. He M, Zhao Z, Yin L, Tang C, Yin C. Hyaluronic acid coated poly(butyl cyanoacrylate) nanoparticles as anticancer drug carriers. International Journal of Pharmaceutics. 2009 373(1-2):165-73.
159. Olivier J-C, Huertas R, Lee HJ, Calon F, Pardridge WM. Synthesis of Pegylated Immunonanoparticles. Pharmaceutical Research. 2002 19(8):1137-43.
160. Ofokansi K, Winter G, Fricker G, Coester C. Matrix-loaded biodegradable gelatine nanoparticles as new approach to improve drug loading and delivery. European Journal of Pharmaceutics and Biopharmaceutics. 2010 76(1):1-9.
161. Liu Z, Jiao Y, Wang Y, Zhou C, Zhang Z. Polysaccharides-based nanoparticles as drug delivery systems. Advanced Drug Delivery Reviews. 2008 60(15):1650-62.

162. Zhang C, Wang W, Liu T, Wu Y, Guo H, Wang P, et al. Doxorubicin-loaded glycyrrhetinic acid-modified alginate nanoparticles for liver tumor chemotherapy. Biomaterials. 2012 33(7):2187-96.
163. Gavory C, Durand A, Six J-L, Nouvel C, Marie E, Leonard M. Polysaccharide-covered nanoparticles prepared by nanoprecipitation. Carbohydrate Polymers. 2011 84(1):133-40.
164. Zhang H, Gao F, Liu L, Li X, Zhou Z, et al. Pullulan acetate nanoparticles prepared by solvent diffusion method for epirubicin chemotherapy. Colloids and Surfaces B: Biointerfaces. 2009 71(1):19-26.
165. Agnihotri SA, Mallikarjuna NN, Aminabhavi TM. Recent advances on chitosan-based micro- and nanoparticles in drug delivery. Journal of Controlled Release. 2004 100(1):5-28.
166. Cho KY, Chung TW, Kim BC, Kim MK, Lee JH, Wee WR, et al. Release of ciprofloxacin from poloxamer-graft-hyaluronic acid hydrogels in vitro. International Journal of Pharmaceutics. 2003 260(1):83-91.
167. Sinha VR, Kumria R. Polysaccharides in colon-specific drug delivery. International Journal of Pharmaceutics. 2001 224(1–2):19-38.
168. Lai WF, Lin MC. Nucleic acid delivery with chitosan and its derivatives. Journal of Controlled Release. 2009 134(3):158-68.
169. Arnaz I, Harris R, Heras A. Chitosan Amphiphilic Derivatives. Chemistry and application. Current Organic Chemistry. 2010 14:308-30.
170. Zhi J, Wang Y, Luo G. Adsorption of diuretic furosemide onto chitosan nanoparticles prepared with a water-in-oil nanoemulsion system. Reactive and Functional Polymers. 2005 65(3):249-57.
171. Vandana M, Sahoo SK. Optimization of physicochemical parameters influencing the fabrication of protein-loaded chitosan nanoparticles Nanomedicine: Nanotechnology, Biology and Medicine. 2009 4(7):773-85.
172. Janes KA, Fresneau MP, Marazuela A, Fabra A, Alonso MJ. Chitosan nanoparticles as delivery systems for doxorubicin. Journal of Controlled Release. 2001 73(2-3):255-67.
173. Molnar E, Barbu E, Lien CF, Gorecki DC, Tsibouklis J. Toward Drug Delivery into the Brain: Synthesis, Characterization, and Preliminary In Vitro Assessment of Alkylglyceryl-Functionalized Chitosan Nanoparticles. Biomacromolecules. 2010 11(11):2880-9.
174. Fan W, Yan W, Xu Z, Ni H. Formation mechanism of monodisperse, low molecular weight chitosan nanoparticles by ionic gelation technique. Colloids and Surfaces B: Biointerfaces. 2012 90(0):21-7.
175. Loh JW, Schneider J, Carter M, Saunders M, Lim L-Y. Spinning disc processing technology: Potential for large-scale manufacture of chitosan nanoparticles. Journal of Pharmaceutical Sciences. 2010 99(10):4326-36.
176. Mitra S, Gaur U, Ghosh PC, Maitra AN. Tumour targeted delivery of encapsulated dextran-doxorubicin conjugate using chitosan nanoparticles as carrier. Journal of Controlled Release. 2001 74(1-3):317-23.
177. Chen Y, Mohanraj V, Wang F, Benson H. Designing chitosan-dextran sulfate nanoparticles using charge ratios. AAPS PharmSciTech. 2007 8(4):131-9.
178. Anitha A, Deepagan VG, Divya Rani VV, Menon D, Nair SV, Jayakumar R. Preparation, characterization, in vitro drug release and biological studies of curcumin loaded dextran sulphate–chitosan nanoparticles. Carbohydrate Polymers. 2011 84(3):1158-64.
179. Tiyaboonchai W, Limpeanchob N. Formulation and characterization of amphotericin B–chitosan–dextran sulphate nanoparticles. International Journal of Pharmaceutics. 2007 329(1–2):142-9.
180. Shu S, Zhang X, Wu Z, Wang Z, Li C. Delivery of protein drugs using nanoparticles self-assembled from dextran sulphate and quaternized chitosan. Journal of Controlled Release. 2011 152, Supplement 1(0):e170-e2.

181. Delair T. Colloidal polyelectrolyte complexes of chitosan and dextran sulphate towards versatile nanocarriers of bioactive molecules. European Journal of Pharmaceutics and Biopharmaceutics. 2011 78(1):10-8.
182. Qi J, Yao P, He F, Yu C, Huang C. Nanoparticles with dextran/chitosan shell and BSA/chitosan core--Doxorubicin loading and delivery. International Journal of Pharmaceutics. 2010 393(1-2):177-85.
183. Gaumet M, Gurny R, Delie F. Interaction of biodegradable nanoparticles with intestinal cells: The effect of surface hydrophilicity. International Journal of Pharmaceutics. 2010 390(1):45-52.
184. Li G, Zhuang Y, Mu Q, Wang M, Fang Ye. Preparation, characterization and aggregation behavior of amphiphilic chitosan derivative having poly (l-lactic acid) side chains. Carbohydrate Polymers. 2008 72(1):60-6.
185. Munier S, Messai I, Delair T, Verrier B, Ataman-Önal Y. Cationic PLA nanoparticles for DNA delivery: Comparison of three surface polycations for DNA binding, protection and transfection properties. Colloids and Surfaces B: Biointerfaces. 2005 43(3–4):163-73.
186. Liu L, Shi A, Guo S, Fang Ye, Chen S, Li J. Preparation of chitosan-polylactide graft copolymers *via* self-catalysis of phthaloylchitosan and their complexation with DNA. Reactive and Functional Polymers. 2010 70(5):301-5.
187. Dev A, Binulal NS, Anitha A, Nair SV, Furuike T, Tamura H, et al. Preparation of poly(lactic acid)/chitosan nanoparticles for anti-HIV drug delivery applications. Carbohydrate Polymers. 2010 80(3):833-8.
188. Yemisci M, Gursoy-Ozdemir Y, Caban S, Bodur E, Capan Y, Dalkara T. Transport of a caspase inhibitor across the blood brain barrier by chitosan nanoparticles. In: Duzgunes N, editor. Nanomedicine: Cancer, Diabetes, and Cardiovascular, Central Nervous System, Pulmonary and Inflammatory Diseases. San Diego: Elsevier Academic Press Inc; 2012. p. 253-69.
189. Tahara K, Sakai T, Yamamoto H, Takeuchi H, Hirashima N, Kawashima Y. Improved cellular uptake of chitosan-modified PLGA nanospheres by A549 cells. International Journal of Pharmaceutics. 2009 382(1-2):198-204.
190. Hombach J, Bernkop-Schnurch A. Chitosan solutions and particles: Evaluation of their permeation enhancing potential on MDCK cells used as blood brain barrier model. International Journal of Pharmaceutics. 2009 376(1-2):104-9.
191. Wang ZH, Wang ZY, Sun CS, Wang CY, Jiang TY, Wang SL. Trimethylated chitosan-conjugated PLGA nanoparticles for the delivery of drugs to the brain. Biomaterials. 2010 31(5):908-15.
192. Trapani A, De Giglio E, Cafagna D, Denora N, Agrimi G, Cassano T, et al. Characterization and evaluation of chitosan nanoparticles for dopamine brain delivery. International Journal of Pharmaceutics. 2011 419(1–2):296-307.
193. Haque S, Md S, Fazil M, Kumar M, Sahni JK, Ali J, et al. Venlafaxine loaded chitosan NPs for brain targeting: Pharmacokinetic and pharmacodynamic evaluation. Carbohydrate Polymers. 2012 89(1):72-9.
194. Fazil M, Md S, Haque S, Kumar M, Baboota S, Sahni Jk, et al. Development and evaluation of rivastigmine loaded chitosan nanoparticles for brain targeting. European Journal of Pharmaceutical Sciences. 2012 47(1):6-15.
195. Wang X, Chi N, Tang X. Preparation of estradiol chitosan nanoparticles for improving nasal absorption and brain targeting. European Journal of Pharmaceutics and Biopharmaceutics. 2008 70(3):735-40.
196. Nimesh S, Thibault M, Lavertu M, Buschmann M. Enhanced Gene Delivery Mediated by Low Molecular Weight Chitosan/DNA Complexes: Effect of pH and Serum. Molecular Biotechnology. 2010 46(2):182-96.
197. Gan Q, Wang T, Cochrane C, McCarron P. Modulation of surface charge, particle size and morphological properties of chitosan–TPP nanoparticles intended for gene delivery. Colloids and Surfaces B: Biointerfaces. 2005 44(2–3):65-73.

198. Kean T, Thanou M. Biodegradation, biodistribution and toxicity of chitosan. Advanced Drug Delivery Reviews. 2010 62(1):3-11.
199. Loretz B, Bernkop-Schnürch A. In vitro cytotoxicity testing of non-thiolated and thiolated chitosan nanoparticles for oral gene delivery. Nanotoxicology. 2007 1(2):139-48.
200. Katas H, Alpar HO. Development and characterisation of chitosan nanoparticles for siRNA delivery. Journal of Controlled Release. 2006 115(2):216-25.
201. Baldrick P. The safety of chitosan as a pharmaceutical excipient. Regulatory Toxicology and Pharmacology. 2010 56(3):290-9.
202. Khalikova E, Susi P, Korpela T. Microbial Dextran-Hydrolyzing Enzymes: Fundamentals and Applications. Microbiology and Molecular Biology Reviews. 2005 69(2):306-25.
203. De Belder AN. Dextran. Amershaw Bioscience. Report No.: 18-1166-12. 2003.
204. Caligur V. Dextran and Related Polysaccharides. BioFiles. 2008 3(10):17.
205. Wynter CVA, Chang M, De Jersey J, Patel B, Inkerman PA, Hamilton S. Isolation and characterization of a thermostable dextranase. Enzyme and Microbial Technology. 1997 20(4):242-7.
206. Moffitt E. Blood substitutes. Canadian Journal of Anaesthesia. 1975 22(1):12-9.
207. Grönwall A, Ingelman B. The Introduction of Dextran as a Plasma Substitute. Vox Sanguinis. 1984 47(1):96-9.
208. Quon CY. Clinical pharmacokinetics and pharmacodynamics of colloidal plasma volume expanders. Journal of Cardiothoracic Anaesthesia. 1988 2(6, Supplement 1):13-23.
209. McCahon R, Hardman J. Pharmacology of plasma expanders. Anaesthesia and Intensive Care Medicine. 2007 8(2):79-81.
210. Schafer-Korting M. Drug Delivery. Berlin; Springer; 2009. p192-207.
211. Arond LH, Frank HP. Molecular Weight Distribution and Molecular Size of a Native Dextran. The Journal of Physical Chemistry. 1954 58(11):953-7.
212. Paull JD. Dextrans. Development of Specifications in Biological Standardisation. 1987 67:133-8.
213. Martin J, editor. British National Formulary. 53 rd edition. London: BMJ Group and Pharmaceutical Press; 2010. p 181-3.
214. Neu B, Wenby R, Meiselman HJ. Effects of Dextran Molecular Weight on Red Blood Cell Aggregation. Biophysical Journal. 2008 95(6):3059-65.
215. de Belder AN. Dextran. Ullmann's Encyclopedia of Industrial Chemistry: Wiley-VCH Verlag GmbH & Co. KGaA; 2000.
216. Menu P, Longrois D, Faivre B, Donner M, Labrude P, Stoltz J-F, et al. Rheological behaviour of red blood cells suspended in haemoglobin solutions: *In vitro* study comparing dextran-benzene-tetra-carboxylate haemoglobin, stroma free haemoglobin and plasma expanders. Transfusion Science. 1999 20(1):5-16.
217. Kozak D, Chen A, Bax J, Trau M. Protein resistance of dextran and dextran-poly(ethylene glycol) copolymer films. Biofouling. 2011 27(5):497-503.
218. De Groot CJ, Van Luyn MJA, Van Dijk-Wolthuis WNE, Cadée JA, Plantinga JA, Otter WD, et al. In vitro biocompatibility of biodegradable dextran-based hydrogels tested with human fibroblasts. Biomaterials. 2001 22(11):1197-203.
219. Liebert T, Hornig S, Hesse S, Heinze T. Nanoparticles on the Basis of Highly Functionalized Dextrans. Journal of the American Chemical Society. 2005 127(30):10484-5.
220. Lemarchand C, Gref R, Couvreur P. Polysaccharide-decorated nanoparticles. European Journal of Pharmaceutics and Biopharmaceutics. 2004 58(2):327-41.
221. Bertholon I, Vauthier C, Labarre D. Complement Activation by Core–Shell Poly(isobutylcyanoacrylate)–Polysaccharide Nanoparticles: Influences of Surface Morphology, Length, and Type of Polysaccharide. Pharmaceutical Research. 2006 23(6):1313-23.

222. Osterberg E, Bergstrom K, Holmberg K, Schuman TP, Riggs JA, Burns NL, et al. Protein-rejecting ability of surface-bound dextran in end-on and side-on configurations: comparison to PEG. Journal of Biomedical Materials Research. 1995 29(6):741-7.
223. Passirani C, Barratt G, Devissaguet JP, Labarre D. Interactions of nanoparticles bearing heparin or dextran covalently bound to poly(methyl methacrylate) with the complement system. Life Sciences. 1998 62(8):775-85.
224. Farrell M, Beaudoin S. Surface forces and protein adsorption on dextran- and polyethylene glycol-modified polydimethylsiloxane. Colloids Surface B Biointerfaces. 2010 81(2):468-75.
225. Klint C, Truedsson L, Sturfelt G. Binding to Erythrocyte Complement Receptor Type 1 of BSA/ Anti-BSA Complexes Opsonized by C4A3 or C4B1 in the Presence of Serum. Scandinavian Journal of Immunology. 1995 42(4):425-32.
226. Romero-Cano MS, Vincent B. Controlled release of 4-nitroanisole from poly(lactic acid) nanoparticles. Journal of Controlled Release. 2002 82(1):127-35.
227. Vert M, Schwach G, Engel R, Coudane J. Something new in the field of PLA/PGA bioresorbable polymers? Journal of Controlled Release. 1998 53:85-92.
228. Lu D, Yang L, Zhou T, Lei Z. Synthesis, characterization and properties of biodegradable polylactic acid-[beta]-cyclodextrin cross-linked copolymer microgels. European Polymer Journal. 2008 44(7):2140-5.
229. Jun Pan YWSQBZYL. Grafting reaction of poly(lactic acid) with maleic anhydride and hexanediamine to introduce more reactive groups in its bulk. Journal of Biomedical Materials Research Part B: Applied Biomaterials. 2005 74B(1):476-80.
230. Luo Y, Wang Y, Niu X, Shang J. Evaluation of the cytocompatibility of butanediamine- and RGDS-grafted poly(dl-lactic acid). European Polymer Journal. 2008 44(5):1390-402.
231. Källrot M, Edlund U, Albertsson AC. Surface functionalization of degradable polymers by covalent grafting. Biomaterials. 2006 27(9):1788-96.
232. Gao X, Tao W, Lu W, Zhang Q, Zhang Y, Jiang X, et al. Lectin-conjugated PEG-PLA nanoparticles: Preparation and brain delivery after intranasal administration. Biomaterials. 2006 27(18):3482-90.
233. Rasal RM, Janorkar AV, Hirt DE. Poly(lactic acid) modifications. Progress in Polymer Science. 2010 35(3):338-56.
234. Gupta B, Revagade N, Hilborn J. Poly(lactic acid) fiber: An overview. Progress in Polymer Science. 2007 32(4):455-82.
235. Fambri L, Pegoretti A, Fenner R, Incardona SD, Migliaresi C. Biodegradable fibres of poly(l-lactic acid) produced by melt spinning. Polymer. 1997 38(1):79-85.
236. Proikakis CS, Mamouzelos NJ, Tarantili PA, Andreopoulos AG. Stability of poly(lactic acid) in aqueous solutions. Journal of Applied Polymer Science. 2003 87(5):795-804.
237. Anderson JM, Shive MS. Biodegradation and biocompatibility of PLA and PLGA microspheres. Advanced Drug Delivery Reviews. 1997 28(1):5-24.
238. Liu M, Dong J, Yang Y, Yang X, Xu H. Characterization and release of triptolide-loaded poly (D,L-lactic acid) nanoparticles. European Polymer Journal. 2005 41(2):375-82.
239. Gu M-q, Yuan X-b, Kang C-s, Zhao Y-h, Tian N-j, Pu P-y, et al. Surface biofunctionalization of PLA nanoparticles through amphiphilic polysaccharide coating and ligand coupling: Evaluation of biofunctionalization and drug releasing behavior. Carbohydrate Polymers. 2007 67(3):417-26.
240. Hu K, Li J, Shen Y, Lu W, Gao X, Zhang Q, et al. Lactoferrin-conjugated PEG-PLA nanoparticles with improved brain delivery: In vitro and in vivo evaluations. Journal of Controlled Release. 2009 134(1):55-61.
241. Lamalle-Bernard D, Munier S, Compagnon C, Charles M-H, Kalyanaraman VS, Delair T, et al. Coadsorption of HIV-1 p24 and gp120 proteins to surfactant-free anionic PLA nanoparticles preserves antigenicity and immunogenicity. Journal of Controlled Release. 2006 115(1):57-67.

242. Ma W-j, Yuan X-b, Kang C-s, Su T, Yuan X-y, Pu P-y, et al. Evaluation of blood circulation of polysaccharide surface-decorated PLA nanoparticles. Carbohydrate Polymers. 2008 72(1):75-81.
243. Messai I, Lamalle D, Munier S, Verrier B, Ataman-Önal Y, Delair T. Poly(d,l-lactic acid) and chitosan complexes: interactions with plasmid DNA. Colloids and Surfaces A: Physicochemical and Engineering Aspects. 2005 255(1–3):65-72.
244. Rouzes C, Leonard M, Durand A, Dellacherie E. Influence of polymeric surfactants on the properties of drug-loaded PLA nanospheres. Colloids and Surfaces B: Biointerfaces. 2003 32(2):125-35.
245. Fessi H, Puisieux F, Devissaguet JP, Ammoury N, Benita S. Nanocapsule formation by interfacial polymer deposition following solvent displacement. International Journal of Pharmaceutics. 1989 55(1):R1-R4.
246. Giovino C, Ayensu I, Tetteh J, Boateng JS. Development and characterisation of chitosan films impregnated with insulin loaded PEG-b-PLA nanoparticles (NPs): A potential approach for buccal delivery of macromolecules. International Journal of Pharmaceutics. 2012 428(1–2):143-51.
247. Kim I-S, Lee S-K, Park Y-M, Lee Y-B, Shin S-C, Lee KC, et al. Physicochemical characterization of poly(l-lactic acid) and poly(d,l-lactide-co-glycolide) nanoparticles with polyethylenimine as gene delivery carrier. International Journal of Pharmaceutics. 2005 298(1):255-62.
248. Verrecchia T, Spelnehauer G, Basile DV. Non-stealth (poly (lactic acid/albumin)) and stealth (poly (lactic acid-polyethylene glycol)) nanoparticles as injectable drug carriers. Journal of Controlled Release. 1995 36:49-61.
249. Gao X, Tao W, Lu W, Zhang Q, Zhang Y, Jiang X, et al. Lectin-conjugated PEG–PLA nanoparticles: Preparation and brain delivery after intranasal administration. Biomaterials. 2006 27(18):3482-90.
250. Essa S, Rabanel JM, Hildgen P. Characterization of rhodamine loaded PEG-g-PLA nanoparticles (NPs): Effect of poly(ethylene glycol) grafting density. International Journal of Pharmaceutics. 2011 411(1–2):178-87.
251. Nouvel C, Raynaud J, Marie E, Dellacherie E, Six JL, Durand A. Biodegradable nanoparticles made from polylactide-grafted dextran copolymers. Journal of Colloid and Interface Science. 2009 330(2):337-43.
252. Nagahama K, Mori Y, Ohya Y, Ouchi T. Biodegradable Nanogel Formation of Polylactide-Grafted Dextran Copolymer in Dilute Aqueous Solution and Enhancement of Its Stability by Stereocomplexation. Biomacromolecules. 2007 8(7):2135-41.
253. Choi KC, Bang JY, Kim C, Kim PI, Lee SR, Chung WT, et al. Antitumor effect of adriamycin-encapsulated nanoparticles of poly(DL-lactide-co-glycolide)-grafted dextran. Journal of Pharmaceutical Sciences. 2009 98(6):2104-12.
254. Choi K-C, Bang J-Y, Kim P-I, Kim C, Song C-E. Amphotericin B-incorporated polymeric micelles composed of poly(d,l-lactide-co-glycolide)/dextran graft copolymer. International Journal of Pharmaceutics. 2008 355(1–2):224-30.
255. De Jong WH, Eelco Bergsma J, Robinson JE, Bos RRM. Tissue response to partially in vitro predegraded poly-L-lactide implants. Biomaterials. 2005 26(14):1781-91.
256. Montjovent M-O, Mark S, Mathieu L, Scaletta C, Scherberich A, Delabarde C, et al. Human foetal bone cells associated with ceramic reinforced PLA scaffolds for tissue engineering. Bone. 2008 42(3):554-64.
257. Allémann E, Gurny R, Doelker E. Preparation of aqueous polymeric nanodispersions by a reversible salting-out process: influence of process parameters on particle size. International Journal of Pharmaceutics. 1992 87(1–3):247-53.
258. De Jaeghere F, Allémann E, Leroux J-C, Stevels W, Feijen J, Doelker E, et al. Formulation and Lyoprotection of Poly(Lactic Acid-Co-Ethylene Oxide) Nanoparticles: Influence on Physical Stability and In Vitro Cell Uptake. Pharmaceutical Research. 1999 16(6):859-66.
259. York P. Strategies for particle design using supercritical fluid technologies. Pharmaceutical Science & Technology Today. 1999 2(11):430-40.

260. Yeo S-D, Kiran E. Formation of polymer particles with supercritical fluids: A review. The Journal of Supercritical Fluids. 2005 34(3):287-308.
261. Weber C, Coester C, Kreuter J, Langer K. Desolvation process and surface characterisation of protein nanoparticles. International Journal of Pharmaceutics. 2000 194(1):91-102.
262. Jun JY, Nguyen HH, Paik S-Y-R, Chun HS, Kang B-C, Ko S. Preparation of size-controlled bovine serum albumin (BSA) nanoparticles by a modified desolvation method. Food Chemistry. 2011 127(4):1892-8.
263. Rao JP, Geckeler KE. Polymer nanoparticles: Preparation techniques and size-control parameters. Progress in Polymer Science. 2011 36(7):887-913.
264. Costa C, Santos AF, Fortuny M, Araújo PHH, Sayer C. Kinetic advantages of using microwaves in the emulsion polymerization of MMA. Materials Science and Engineering: C. 2009 29(2):415-9.
265. Thickett SC, Gilbert RG. Emulsion polymerization: State of the art in kinetics and mechanisms. Polymer. 2007 48(24):6965-91.
266. Shouldice GTD, Vandezande GA, Rudin A. Practical aspects of the emulsifier-free emulsion polymerization of styrene. European Polymer Journal. 1994 30(2):179-83.
267. Liu G, Liu P. Synthesis of monodispersed cross-linked nanoparticles decorated with surface carboxyl groups *via* soapless emulsion polymerization. Colloids and Surfaces A: Physicochemical and Engineering Aspects. 2010 354(1–3):377-81.
268. Wang S, Wang X, Zhang Z. Preparation of polystyrene particles with narrow particle size distribution by γ-ray initiated miniemulsion polymerization stabilized by polymeric surfactant. European Polymer Journal. 2007 43(1):178-84.
269. Lambert G, Fattal E, Pinto-Alphandary H, Gulik A, Couvreur P. Polyisobutylcyanoacrylate nanocapsules containing an aqueous core for the delivery of oligonucleotides. International Journal of Pharmaceutics. 2001 214(1–2):13-6.
270. Braunecker WA, Matyjaszewski K. Controlled/living radical polymerization: Features, developments, and perspectives. Progress in Polymer Science. 2007 32(1):93-146.
271. Lockman PR, Mumper MJ, Khan MA, Allen DD. Nanoparticle Technology for drug delivery across the blood-brain barrier. Drug Development and Industrial Pharmacy. 2002 28:1-12.
272. Cheng F-Y, al. e. Stabiliser-free poly(lactide-co-glycolide) nanoparticles for multimodal biomedical probes. Biomaterials. 2008 29:2104-12.
273. Mora-Huertas CE, Garrigues O, Fessi H, Elaissari A. Nanocapsules prepared via nanoprecipitation and emulsification–diffusion methods: Comparative study. European Journal of Pharmaceutics and Biopharmaceutics. 2012 80(1):235-9.
274. Kulterer MR, Reischl M, Reichel VE, Hribernik S, Wu M, Köstler S, et al. Nanoprecipitation of cellulose acetate using solvent/nonsolvent mixtures as dispersive media. Colloids and Surfaces A: Physicochemical and Engineering Aspects. 2011 375(1–3):23-9.
275. Yordanov G, Skrobanska R, Evangelatov A. Entrapment of epirubicin in poly(butyl cyanoacrylate) colloidal nanospheres by nanoprecipitation: Formulation development and in vitro studies on cancer cell lines. Colloids and Surfaces B: Biointerfaces. 2012 92(0):98-105.
276. Bilati U, Allémann E, Doelker E. Development of a nanoprecipitation method intended for the entrapment of hydrophilic drugs into nanoparticles. European Journal of Pharmaceutical Sciences. 2005 24(1):67-75.
277. Liu M, Zhou Z, Wang X, Xu J, Yang K, Cui Q, et al. Formation of poly(l,d-lactide) spheres with controlled size by direct dialysis. Polymer. 2007 48(19):5767-79.
278. Choi S-W, Kim J-H. Design of surface-modified poly(d,l-lactide-co-glycolide) nanoparticles for targeted drug delivery to bone. Journal of Controlled Release. 2007 122(1):24-30.
279. Kim SY, Shin ILG, Lee YM, Cho CS, Sung YK. Methoxy poly(ethylene glycol) and ϵ-caprolactone amphiphilic block copolymeric micelle containing indomethacin.: II.

Micelle formation and drug release behaviours. Journal of Controlled Release. 1998 51(1):13-22.
280. Michailova V, Berlinova I, Iliev P, Ivanov L, Titeva S, Momekov G, et al. Nanoparticles formed from PNIPAM-g-PEO copolymers in the presence of indomethacin. International Journal of Pharmaceutics. 2010 384(1–2):154-64.
281. Grigoriev DO, Miller R. Mono- and multilayer covered drops as carriers. Current Opinion in Colloid A; Interface Science. 2009 14(1):48-59.
282. Mora-Huertas CE, Fessi H, Elaissari A. Polymer-based nanocapsules for drug delivery. International Journal of Pharmaceutics. 2010 385(1–2):113-42.
283. Chognot D, Six JL, Leonard M, Bonneaux F, Vigneron C, Dellacherie E. Physicochemical evaluation of PLA nanoparticles stabilized by water-soluble MPEO–PLA block copolymers. Journal of Colloid and Interface Science. 2003 268(2):441-7.
284. Moinard-Chécot D, Chevalier Y, Briançon S, Beney L, Fessi H. Mechanism of nanocapsules formation by the emulsion–diffusion process. Journal of Colloid and Interface Science. 2008 317(2):458-68.
285. Quintanar-Guerrero D, Allemann E, Fessi H, Doelker E. Preparation techniques and mechanisms of formation of biodegradable nanoparticles from preformed polymers. Drug Development and Industrial Pharmacy. 1998 24(12):1113-28.
286. Bilati U, Allémann E, Doelker E. Strategic approaches for overcoming peptide and protein instability within biodegradable nano- and microparticles. European Journal of Pharmaceutics and Biopharmaceutics. 2005 59(3):375-88.
287. Jaworek A, Sobczyk AT. Electrospraying route to nanotechnology: An overview. Journal of Electrostatics. 2008 66(3–4):197-219.
288. Jaworek A. Micro- and nanoparticle production by electrospraying. Powder Technology. 2007 176(1):18-35.
289. Bock N, Dargaville TR, Woodruff MA. Electrospraying of Polymers with Therapeutic Molecules: State of the Art. Progress in Polymer Science. 2012 37(11):1510-1551.
290. Hartman RPA, Brunner DJ, Camelot DMA, Marijnissen JCM, Scarlett B. Electrohydrodynamic atomisation in the cone-jet mode physical modelling of the liquid cone and jet. Journal of Aerosol Science. 1999 30(7):823-49.
291. Chen D-R, Pui DYH, Kaufman SL. Electrospraying of conducting liquids for monodisperse aerosol generation in the 4 nm to 1.8 μm diameter range. Journal of Aerosol Science. 1995 26(6):963-77.
292. Ding L, Lee T, Wang C-H. Fabrication of monodispersed Taxol-loaded particles using electrohydrodynamic atomization. Journal of Controlled Release. 2005 102(2):395-413.
293. Xie J, Lim LK, Phua Y, Hua J, Wang C-H. Electrohydrodynamic atomization for biodegradable polymeric particle production. Journal of Colloid and Interface Science. 2006 302(1):103-12.
294. Ciach T. Microencapsulation of drugs by electro-hydro-dynamic atomization. International Journal of Pharmaceutics. 2006 324(1):51-5.
295. Sharma R, Ahuja M, Kaur H. Thiolated pectin nanoparticles: Preparation, characterization and ex vivo corneal permeation study. Carbohydrate Polymers. 2012 87(2):1606-10.
296. Sadeghi AMM, Dorkoosh FA, Avadi MR, Saadat P, Rafiee-Tehrani M, Junginger HE. Preparation, characterization and antibacterial activities of chitosan, N-trimethyl chitosan (TMC) and N-diethylmethyl chitosan (DEMC) nanoparticles loaded with insulin using both the ionotropic gelation and polyelectrolyte complexation methods. International Journal of Pharmaceutics. 2008 355(1–2):299-306.
297. Tsai ML, Bai SW, Chen RH. Cavitation effects versus stretch effects resulted in different size and polydispersity of ionotropic gelation chitosan–sodium tripolyphosphate nanoparticle. Carbohydrate Polymers. 2008 71(3):448-57.
298. Tan ML, Friedhuber AM, Dunstan DE, Choong PFM, Dass CR. The performance of doxorubicin encapsulated in chitosan-dextran sulphate microparticles in an osteosarcoma model. Biomaterials. 2010 31(3):541-51.

299. Zambito Y, Felice F, Fabiano A, Di Stefano R, Di Colo G. Mucoadhesive nanoparticles made of thiolated quaternary chitosan crosslinked with hyaluronan. Carbohydrate Polymers. 2013 92(1)33-40.
300. Hodges CS. Measuring forces with the AFM: polymeric surfaces in liquids. Advances in Colloid and Interface Science. 2002 99(1):13-75.
301. Boyd RD, Pichaimuthu SK, Cuenat A. New approach to inter-technique comparisons for nanoparticle size measurements; using atomic force microscopy, nanoparticle tracking analysis and dynamic light scattering. Colloids and Surfaces A: Physicochemical and Engineering Aspects. 2011 387(1-3):35-42.
302. Carr B. Nanoparticle tracking system analyses polydispersed samples. Laser Focus World. 2008 44(11):83-6.
303. Bootz A, Vogel V, Schubert D, Kreuter J. Comparison of scanning electron microscopy, dynamic light scattering and analytical ultracentrifugation for the sizing of poly(butyl cyanoacrylate) nanoparticles. European Journal of Pharmaceutics and Biopharmaceutics. 2004 57(2):369-75.
304. Spelter LE, Meyer K, Nirschl H. Screening of Colloids by Semicontinuous Centrifugation. Chemical Engineering & Technology. 2012 35(8):1486-94.
305. Vogel V, Langer K, Balthasar S, Schuck P, Mächtle W, Haase W, et al. Characterization of serum albumin nanoparticles by sedimentation velocity analysis and electron microscopyAnalytical Ultracentrifugation VI. In: Borchard W, Straatmann A, editors.: Springer Berlin / Heidelberg; 2002. p. 31-6.
306. Yang L, Broom MF, Tucker IG. Characterization of a Nanoparticulate Drug Delivery System Using Scanning Ion Occlusion Sensing. Pharmaceutical Research. 2012 29(9):2578-86.
307. Roberts GS, Kozak D, Anderson W, Broom MF, Vogel R, Trau M. Tunable Nano/Micropores for Particle Detection and Discrimination: Scanning Ion Occlusion Spectroscopy. 2010 6(23):2653-8.
308. Doane TL, Chuang CH, Hill RJ, Burda C. Nanoparticle zeta-Potentials. Accounts of Chemical Research. 2012 45(3):317-26.
309. Lourenco C, Teixeira M, Simoes S, Gaspar R. Steric stabilization of nanoparticles: Size and surface properties. International Journal of Pharmaceutics. 1996 138(1):1-12.
310. Schubert S, Delaney JT, Schubert US. Nanoprecipitation and nanoformulation of polymers: from history to powerful possibilities beyond the poly(lactic acid). Soft Matter. 2011, 7, 1581-8
311. Mattison K, Morfesis A, Kazsuba M. A Primer on Particle Sizing Using Dynamic Light Scattering. American Biotechnology Laboratory. 2003(12):20-2.
312. Gaumet M, Vargas A. Nanoparticles for drug delivery: The need for precision in reporting particle size parameters. European Journal of Pharmaceutics and Biopharmaceutics. 2008 69:1-9.
313. Dragovic RA, Gardiner C, Brooks AS, Tannetta DS, Ferguson DJP, Hole P, et al. Sizing and phenotyping of cellular vesicles using Nanoparticle Tracking Analysis. Nanomedicine-Nanotechnology Biology and Medicine. 2011 7(6):780-8.
314. NanoSight. NanoSight Ltd; 2012; Available from: http://www.nanosight.com/about/nanosight-directors. Accessed: 22.11.2013.
315. Malloy A. Exosome and Microvesicle Characterisation. Genetic Engineering and Biotechnology News. 2012 32(7):1-3
316. Bendre V, Gautam M, Carr R, Smith J, Malloy A. Characterisation of Nanoparticle Size and Concentration for Toxicological Studies. Journal of Biomedical Nanotechnology. 2011 7(1):195-6.
317. Gillespie C, Halling P, Edwards D. Monitoring of particle growth at a low concentration of a poorly water soluble drug using the NanoSight LM20. Colloids and Surfaces A: Physicochemical and Engineering Aspects. 2011 384(1–3):233-9.

318. Bogner A, Jouneau PH, Thollet G, Basset D, Gauthier C. A history of scanning electron microscopy developments: Towards "wet-STEM" imaging. Micron. 2007 38(4):390-401.
319. Stokroos I, Kalicharan D, Van der Want JJL, Jongebloed WL. A comparative study of thin coatings of Au/Pd, Pt and Cr produced by magnetron sputtering for FE-SEM. Journal of Microscopy-Oxford. 1998 189:79-89.
320. Donald AM. Environmental scanning electron microscopy for the study of 'wet' systems. Current Opinion in Colloid A; Interface Science. 1998 3(2):143-7.
321. Stabentheiner E, Zankel A, Polt P. Environmental scanning electron microscopy (ESEM)-a versatile tool in studying plants. Protoplasma. 2010 246(1-4):89-99.
322. Ruska E. The development of the electron microscope and of electron microscopy. Bioscience Reports. 1987 7(8):607-29.
323. Chang K-C, Chiang Y-W, Yang C-H, Liou J-W. Atomic force microscopy in biology and biomedicine. Tzu Chi Medical Journal. 2012 24(4):162-9.
324. Binnig G, Quate CF, Gerber C. Atomic Force Microscope. Physical Review Letters. 1986 56(9):930-3.
325. Santos NC, Castanho MARB. An overview of the biophysical applications of atomic force microscopy. Biophysical Chemistry. 2004 107(2):133-49.
326. Alonso JL, Goldmann WH. Feeling the forces: atomic force microscopy in cell biology. Life Sciences. 2003 72(23):2553-60.
327. San Paulo A, García R. High-Resolution Imaging of Antibodies by Tapping-Mode Atomic Force Microscopy: Attractive and Repulsive Tip-Sample Interaction Regimes. Biophysical Journal. 2000 78(3):1599-605.
328. Baalousha M, Lead JR. Rationalizing Nanomaterial Sizes Measured by Atomic Force Microscopy, Flow Field-Flow Fractionation, and Dynamic Light Scattering: Sample Preparation, Polydispersity, and Particle Structure. Environmental Science & Technology. 2012 46(11):6134-42.
329. Bell NC, Minelli C, Tompkins J, Stevens MM, Shard AG. Emerging Techniques for Submicrometer Particle Sizing Applied to Stober Silica. Langmuir. 2012 28(29):10860-72.
330. Vogel R, Willmott G, Kozak D, Roberts GS, Anderson W, Groenewegen L, et al. Quantitative sizing of nano/microparticles with a tunable elastomeric pore sensor. Analytical Chemistry. 2011 83(9):3499-506.
331. Roberts GS, Yu S, Zeng Q, Chan LCL, Anderson W, Colby AH, et al. Tunable pores for measuring concentrations of synthetic and biological nanoparticle dispersions. Biosensors and Bioelectronics. 2012 31(1):17-25.
332. Kozak D, Anderson W, Vogel R, Chen S, Antaw F, Trau M. Simultaneous Size and ζ-Potential Measurements of Individual Nanoparticles in Dispersion Using Size-Tunable Pore Sensors. ACS Nano. 2012 6(8):6990-7.
333. Kozak D, Anderson W, Vogel R, Trau M. Advances in resistive pulse sensors: Devices bridging the void between molecular and microscopic detection. Nano Today. 2011 6(5):531-45.
334. Malvern. Zeta Potential-An Introduction in 30 Minutes. Technical note.: Malvern Instruments 2005. Available from www.malvern.com. Accessed 22.11.2013.
335. Song Z, Feng R, Sun M, Guo C, Gao Y, Li L, et al. Curcumin-loaded PLGA-PEG-PLGA triblock copolymeric micelles: Preparation, pharmacokinetics and distribution in vivo. Journal of Colloid and Interface Science. 2011 354(1):116-23.
336. Riley T, Govender T, Stolnik S, Xiong CD, Garnett MC, Illum L, et al. Colloidal stability and drug incorporation aspects of micellar-like PLA–PEG nanoparticles. Colloids and Surfaces B: Biointerfaces. 1999 16(1–4):147-59.
337. Malvern. Electrophoretic Light Scattering, Frequently asked questions. 2012 [cited 2012 30.5.2012]; Available from: www.malvern.com.
338. Nakagawa S, Deli MA, Kawaguchi H, Shimizudani T, Shimono T, Kittel Á, et al. A new blood–brain barrier model using primary rat brain endothelial cells, pericytes and astrocytes. Neurochemistry International. 2009 54(3–4):253-63.

339. Malina KC-K, Cooper I, Teichberg VI. Closing the gap between the in-vivo and in-vitro blood–brain barrier tightness. Brain Research. 2009 1284(0):12-21.
340. Lauer R, Bauer R, Linz B, Pittner F, Peschek GA, Ecker G, et al. Development of an in vitro blood–brain barrier model based on immortalized porcine brain microvascular endothelial cells. Il Farmaco. 2004 59(2):133-7.
341. Markoutsa E, Pampalakis G, Niarakis A, Romero IA, Weksler B, Couraud P-O, et al. Uptake and permeability studies of BBB-targeting immunoliposomes using the hCMEC/D3 cell line. European Journal of Pharmaceutics and Biopharmaceutics. 2011 77(2):265-74.
342. Georgieva JV, Kalicharan D, Couraud PO, Romero IA, Weksler B, Hoekstra D, et al. Surface Characteristics of Nanoparticles Determine Their Intracellular Fate in and Processing by Human Blood-Brain Barrier Endothelial Cells In Vitro. Molecular Therapy. 2011 19(2):318-25.
343. Omidi Y, Campbell L, Barar J, Connell D, Akhtar S, Gumbleton M. Evaluation of the immortalised mouse brain capillary endothelial cell line, b.End3, as an in vitro blood-brain barrier model for drug uptake and transport studies. Brain Research. 2003 990(1-2):95-112.
344. Cecchelli R, Dehouck B, Descamps L, Fenart L, Buée-Scherrer V, Duhem C, et al. *In vitro* model for evaluating drug transport across the blood–brain barrier. Advanced Drug Delivery Reviews. 1999 36(2–3):165-78.
345. Hatherell K, Couraud P-O, Romero IA, Weksler B, Pilkington GJ. Development of a three-dimensional, all-human in vitro model of the blood–brain barrier using mono-, co-, and tri-cultivation Transwell models. Journal of Neuroscience Methods. 2011 199(2):223-9.
346. Neuhaus W, Lauer R, Oelzant S, Fringeli UP, Ecker GF, Noe CR. A novel flow based hollow-fiber blood–brain barrier in vitro model with immortalised cell line PBMEC/C1–2. Journal of Biotechnology. 2006 125(1):127-41.
347. Siddharthan V, Kim YV, Liu S, Kim KS. Human astrocytes/astrocyte-conditioned medium and shear stress enhance the barrier properties of human brain microvascular endothelial cells. Brain Research. 2007 1147(0):39-50.
348. Edwards-Smallbone J, Pleass RJ, Khan NA, Flynn RJ. *Acanthamoeba* interactions with the blood–brain barrier under dynamic fluid flow. Experimental Parasitology. 2012 132(3):367-72.
349. McCoy MH, Wang E. Use of electric cell-substrate impedance sensing as a tool for quantifying cytopathic effect in influenza A virus infected MDCK cells in real-time. Journal of Virological Methods. 2005 130(1–2):157-61.
350. Rempe R, Cramer S, Hüwel S, Galla H-J. Transport of Poly(n-butylcyano-acrylate) nanoparticles across the blood–brain barrier in vitro and their influence on barrier integrity. Biochemical and Biophysical Research Communications. 2011 406(1):64-9.
351. Stins MF, Badger J, Sik Kim K. Bacterial invasion and transcytosis in transfected human brain microvascular endothelial cells. Microbial Pathogenesis. 2001 30(1):19-28.
352. Giaever I, Keese CR. Monitoring fibroblast behavior in tissue culture with an applied electric field. Proceedings of the National Academy of Sciences. 1984 81(12):3761-4.
353. Iannone M, Cosco D, Cilurzo F, Celia C, Paolino D, Mollace V, et al. A novel animal model to evaluate the ability of a drug delivery system to promote the passage through the BBB. Neuroscience Letters. 2010 469(1):93-6.
354. Mattheolabakis G, Taoufik E, Haralambous S, Roberts ML, Avgoustakis K. In vivo investigation of tolerance and antitumor activity of cisplatin-loaded PLGA-mPEG nanoparticles. European Journal of Pharmaceutics and Biopharmaceutics. 2009 71(2):190-5.
355. Harivardhan Reddy L, Sharma RK, Chuttani K, Mishra AK, Murthy RSR. Influence of administration route on tumor uptake and biodistribution of etoposide loaded solid lipid nanoparticles in Dalton's lymphoma tumor bearing mice. Journal of Controlled Release. 2005 105(3):185-98.

356. Kaul G, Amiji M. Biodistribution and targeting potential of poly(ethylene glycol)-modified gelatin nanoparticles in subcutaneous murine tumor model. Journal of Drug Targeting. 2004 12(9-10):585-91.
357. Ataman-Önal Y, Munier S, Ganée A, Terrat C, Durand P-Y, Battail N, et al. Surfactant-free anionic PLA nanoparticles coated with HIV-1 p24 protein induced enhanced cellular and humoral immune responses in various animal models. Journal of Controlled Release. 2006 112(2):175-85.
358. Guillon C, Mayol K, Terrat C, Compagnon C, Primard C, Charles M-H, et al. Formulation of HIV-1 Tat and p24 antigens by PLA nanoparticles or MF59 impacts the breadth, but not the magnitude, of serum and faecal antibody responses in rabbits. Vaccine. 2007 25(43):7491-501.
359. Himeno A, Akagi T, Uto T, Wang X, Baba M, Ibuki K, et al. Evaluation of the immune response and protective effects of rhesus macaques vaccinated with biodegradable nanoparticles carrying gp120 of human immunodeficiency virus. Vaccine. 2010 28(32):5377-85.
360. Sincai M, Ganga D, Ganga M, Argherie D, Bica D. Antitumor effect of magnetite nanoparticles in cat mammary adenocarcinoma. Journal of Magnetism and Magnetic Materials. 2005 293(1):438-41.
361. Song C, Labhasetwar V, Cui X, Underwood T, Levy RJ. Arterial uptake of biodegradable nanoparticles for intravascular local drug delivery: Results with an acute dog model. Journal of Controlled Release. 1998 54(2):201-11.
362. Choi EW, Koo HC, Shin IS, Chae YJ, Lee JH, Han SM, et al. Preventive and therapeutic effects of gene therapy using silica nanoparticles–binding of GM-CSF gene on white blood cell production in dogs with leukopenia. Experimental Hematology. 2008 36(9):1091-7.
363. Riffault S, Meyer G, Deplanche M, Dubuquoy C, Durand G, Soulestin M, et al. A new subunit vaccine based on nucleoprotein nanoparticles confers partial clinical and virological protection in calves against bovine respiratory syncytial virus. Vaccine. 2010 28(21):3722-34.
364. Zambaux M-F, Faivre-Fiorina B, Bonneaux F, Marchal S, Merlin J-L, Dellacherie E, et al. Involvement of neutrophilic granulocytes in the uptake of biodegradable non-stealth and stealth nanoparticles in guinea pig. Biomaterials. 2000 21(10):975-80.
365. Fondevila M, Herrer R, Casallas MC, Abecia L, Ducha JJ. Silver nanoparticles as a potential antimicrobial additive for weaned pigs. Animal Feed Science and Technology. 2009 150(3–4):259-69.
366. Fent K, Weisbrod CJ, Wirth-Heller A, Pieles U. Assessment of uptake and toxicity of fluorescent silica nanoparticles in zebrafish (*Danio rerio*) early life stages. Aquatic Toxicology. 2010 100(2):218-28.
367. Chio C-P, Chen W-Y, Chou W-C, Hsieh N-H, Ling M-P, Liao C-M. Assessing the potential risks to zebrafish posed by environmentally relevant copper and silver nanoparticles. Science of The Total Environment. 2012 420(0):111-8.
368. Pandey A, Chandra S, Chauhan LKS, Narayan G, Chowdhuri DK. Cellular internalization and stress response of ingested amorphous silica nanoparticles in the midgut of *Drosophila melanogaster*. Biochimica et Biophysica Acta (BBA) - General Subjects. 2013 1830(1)2256-2266.
369. Pineda L, Sawosz E, Hotowy A, Elnif J, Sawosz F, Ali A, et al. Effect of nanoparticles of silver and gold on metabolic rate and development of broiler and layer embryos. Comparative Biochemistry and Physiology Part A: Molecular and Integrative Physiology. 2012 161(3):315-9.
370. Vargas A, Pegaz B, Debefve E, Konan-Kouakou Y, Lange N, Ballini J-P, et al. Improved photodynamic activity of porphyrin loaded into nanoparticles: an in vivo evaluation using chick embryos. International Journal of Pharmaceutics. 2004 286(1–2):131-45.

371. Vargas A, Zeisser-Labouèbe M, Lange N, Gurny R, Delie F. The chick embryo and its chorioallantoic membrane (CAM) for the *in vivo* evaluation of drug delivery systems. Advanced Drug Delivery Reviews. 2007 59(11):1162-76.
372. Lange N, Ballini JP, Wagnieres G, van den Bergh H. A new drug-screening procedure for photosensitizing agents used in photodynamic therapy for CNV. Investigative Ophthalmological Visual Science. 2001 42(1):38-46.
373. Hlywka JJ, Beck MM, Bullerman LB. The use of the chicken embryo screening test and brine shrimp (*Artemia salina*) bioassays to assess the toxicity of fumonisin B1 mycotoxin. Food and Chemical Toxicology. 1997 35(10–11):991-9.
374. Vargas GE, Mesones RV, Bretcanu O, López JMP, Boccaccini AR, Gorustovich A. Biocompatibility and bone mineralization potential of 45S5 Bioglass-derived glass–ceramic scaffolds in chick embryos. Acta Biomaterialia. 2009 5(1):374-80.
375. Ribatti D, Vacca A, Ranieri G, Sorino S, Roncali L. The Chick Embryo Chorioallantoic Membrane as an in vivo Wound Healing Model. Pathology - Research and Practice. 1996 192(10):1068-76.
376. Clancy AA, Gregoriou Y, Yaehne K, Cramb DT. Measuring properties of nanoparticles in embryonic blood vessels: Towards a physicochemical basis for nanotoxicity. Chemical Physics Letters. 2010 488(4–6):99-111.
377. Ordahl CP, Williams BA, Denetclaw W. 9 Determination and Morphogenesis in Myogenic Progenitor Cells: An Experimental Embryological Approach. In: Charles PO, editor. Current Topics in Developmental Biology: Academic Press; 1999. p.319-67.
378. Xie W, Xu P, Wang W, Liu Q. Preparation and antibacterial activity of a water-soluble chitosan derivative. Carbohydrate Polymers. 2002 50(1):35-40.
379. Choi K-C, Bang J-Y, Kim C, Kim P-I, Lee S-R, Chung W-T, et al. Antitumor effect of adriamycin-encapsulated nanoparticles of poly(DL-lactide-co-glycolide)-grafted dextran. Journal of Pharmaceutical Sciences. 2009 98(6):2104-12.
380. Hornig S, Liebert T, Heinze T. Structure Design of Multifunctional Furoate and Pyroglutamate Esters of Dextran by Polymer-Analogous Reactions. Macromolecular Bioscience. 2007 7(3):297-306.
381. Mauleón D, Pujol MD, Rosell G. B-Adrenergic antagonists: N-alkyl and N-amidoethyl (arylalkoxy)propanolamines related to propranolol. European Journal of Medicinal Chemistry. 1988 23(5):421-6.
382. Bonini C, Federici C, Rossi L, Righi G. C-1 reactivity of 2,3 epoxy alcohols via oxirane opening with metal-halides - applications and synthesis of naturally occuring 2,3-octanediol, muricatan, 3-octanol, and 4-dodecanolide. Journal of Organic Chemistry. 1995 60(15):4803-12.
383. Nishimura S, Kohgo O, Kurita K, Kuzuhara H. Chemospecific manipulations of a rigid polysaccharide: syntheses of novel chitosan derivatives with excellent solubility in common organic solvents by regioselective chemical modifications. Macromolecules. 1991 24(17):4745-8.
384. Leonard M, Fournier C, Dellacherie E. Comparative Pore Structure Analysis of Dextran-Coated Polystyrene Particles. Journal of Colloid and Interface Science. 1999 220(2):380-6.
385. Masten S. n-Butyl Glycidyl Ether (BGE) [CAS No. 2426-08-6] Review of Toxological Literature. North Carolina: Integrated Laboratory Systems, Inc. 2004.
386. Pahimanolis N, Vesterinen A-H, Rich J, Seppala J. Modification of dextran using click-chemistry approach in aqueous media. Carbohydrate Polymers. 2010 82(1):78-82.
387. Gil EC, Colarte AI, El Ghzaoui A, Durand D, Delarbre JL, Bataille B. A sugar cane native dextran as an innovative functional excipient for the development of pharmaceutical tablets. European Journal of Pharmaceutics and Biopharmaceutics. 2008 68(2):319-29.
388. Houga C, Le Meins JF, Borsali R, Taton D, Gnanou Y. Synthesis of ATRP-induced dextran-b-polystyrene diblock copolymers and preliminary investigation of their self-assembly in water. Chemical Communications. 2007(29):3063-5.

389. Stenekes RJH, Talsma H, Hennink WE. Formation of dextran hydrogels by crystallization. Biomaterials. 2001 22(13):1891-8.
390. Ramirez JC, Sanchez-Chaves M, Arranz F. Functionalization of dextran with chloroacetate groups: immobilization of bioactive carboxylic acids. Polymer. 1994 35(12):2651-5.
391. Sánchez-Chaves M, Arranz F. Synthesis of amidoxime-containing modified dextran. Polymer. 1996 37(19):4403-7.
392. Vollmer A, Voiges K, Bork C, Fiege K, Cuber K, Mischnick P. Comprehensive analysis of the substitution pattern in dextran ethers with respect to the reaction conditions. Analytical and Bioanalytical Chemistry. 2009 395(6):1749-68.
393. Karmarkar S, Garber R, Kluza J, Koberda M. Gel permeation chromatography of dextrans in parenteral solutions: Calibration procedure development and method validation. Journal of Pharmaceutical and Biomedical Analysis. 2006 41(4):1260-7.
394. Dubin PL, Principi JM. Failure of universal calibration for size-exclusion chromatography of rodlike macromolecules vs. random coils and globular proteins. Macromolecules. 1989 22(4):1891-6.
395. Rankin JC, Jeanes A. Evaluation of the Periodate Oxidation Method for Structural Analysis of Dextrans. Journal of the American Chemical Society. 1954 76(17):4435-41.
396. Chmelík J, Chmelíková J, Novotny MV. Characterization of dextrans by size-exclusion chromatography on unmodified silica gel columns, with light-scattering detection, and capillary electrophoresis with laser-induced fluorescence detection. Journal of Chromatography A. 1997 790(1–2):93-100.
397. Nordmeier E. Stattic and dynamic light scattering;solution behavior of pullulan and dextran in comparison. Journal of Physical Chemistry. 1993 97(21):5770-85.
398. Shenoy NR, Bailey JM, Shively JE. Carboxylic acid-modified polyethylene: a novel support for the covalent immobilization of polypeptides for C-terminal sequencing. Protein Science. 1992 1(1):58-67.
399. Bhat VT, James NR, Jayakrishnan A. A photochemical method for immobilization of azidated dextran onto aminated poly(ethylene terephthalate) surfaces. Polymer International. 2008 57(1):124-32.
400. Heinze T, Liebert T, Koschella A. Esterification of Polysaccharides. Heinze T: editor, Springer Laboratory; New York. 2006. p.169-180.
401. de Jong SJ, De Smedt SC, Wahls MWC, Demeester J, Kettenes-van den Bosch JJ, Hennink WE. Novel Self-assembled Hydrogels by Stereocomplex Formation in Aqueous Solution of Enantiomeric Lactic Acid Oligomers Grafted To Dextran. Macromolecules. 2000 33(10):3680-6.
402. Xufeng N, Yanfeng L, Yonggang L, Chunhua F, Jia C, Yuanliang W. Design of bioinspired polymeric materials based on poly(lactic acid) modifications towards improving its cytocompatibility. Journal of Biomedical Materials Research Part A. 2008 84A(4):908-16.
403. Luo Y, Wang Y, Niu X, Fu C, Wang S. Synthesis, characterization and biodegradation of butanediamine-grafted poly(dl-lactic acid). European Polymer Journal. 2007 43(9):3856-64.
404. Hwang SW, Lee SB, Lee CK, Lee JY, Shim JK, Selke SEM, et al. Grafting of maleic anhydride on poly(L-lactic acid). Effects on physical and mechanical properties. Polymer Testing. 2012 31(2):333-44.
405. De Beer EL, Bottone AE, Voest EE. Doxorubicin and mechanical performance of cardiac trabeculae after acute and chronic treatment: a review. European Journal of Pharmacology. 2001 415(1):1-11.
406. Wang QZ, Chen XG, Liu N, Wang SX, Liu CS, Meng XH, et al. Protonation constants of chitosan with different molecular weight and degree of deacetylation. Carbohydrate Polymers. 2006 65(2):194-201.
407. Lin W-C, Yu D-G, Yang M-C. pH-sensitive polyelectrolyte complex gel microspheres composed of chitosan/sodium tripolyphosphate/dextran sulfate: swelling kinetics and drug delivery properties. Colloids and Surfaces B: Biointerfaces. 2005 44(2–3):143-51.

408. Mora-Huertas CE, Fessi H, Elaissari A. Influence of process and formulation parameters on the formation of submicron particles by solvent displacement and emulsification–diffusion methods: Critical comparison. Advances in Colloid and Interface Science. 2011 163(2):90-122.
409. Schatz C, Lucas J-M, Viton C, Domard A, Pichot C, Delair T. Formation and Properties of Positively Charged Colloids Based on Polyelectrolyte Complexes of Biopolymers. Langmuir. 2004 20(18):7766-78.
410. Ur-Rehman T, Tavelin S, Gröbner G. Chitosan in situ gelation for improved drug loading and retention in poloxamer 407 gels. International Journal of Pharmaceutics. 2011 409(1–2):19-29.
411. Rouzes C, Gref R, Leonard M, Delgado ADS, Dellacherie E. Surface modification of poly(lactic acid) nanospheres using hydrophobically modified dextrans as stabilizers in an o/w emulsion/evaporation technique. Journal of Biomedical Materials Research. 2000 50(4):557-65.
412. Hans ML, Lowman AM. Biodegradable nanoparticles for drug delivery and targeting. Current Opinion in Solid State and Materials Science. 2002 6(4):319-27.
413. Siparsky GL, Voorhees KJ, Miao F. Hydrolysis of Polylactic Acid (PLA) and Polycaprolactone (PCL) in Aqueous Acetonitrile Solutions: Autocatalysis. Journal of Polymers and the Environment. 1998 6(1):31-41.
414. Krauland AH, Alonso MJ. Chitosan/cyclodextrin nanoparticles as macromolecular drug delivery system. International Journal of Pharmaceutics. 2007 340(1–2):134-42.
415. Katas H, Chen S, Osamuyimen AA, Cevher E, Alpar HO. Effect of preparative variables on small interfering RNA loaded Poly(D,L-lactide-co-glycolide)-chitosan submicron particles prepared by emulsification diffusion method. Journal of Microencapsulation. 2008 25(8):541-8.
416. Garay-Jimenez JC, Young A, Gergeres D, Greenhalgh K, Turos E. Methods for purifying and detoxifying sodium dodecyl sulfate–stabilized polyacrylate nanoparticles. Nanomedicine: Nanotechnology, Biology and Medicine. 2008 4(2):98-105.
417. Ottenbrite RM, Kim SW, editors. Polymeric Drugs & Drug Delivery Systems. Lancaster, Pennsylvania: Technomic Publishing Company, Inc.; 2001.
418. Diep V, Joan B. PBMC Thawing protocol 2009. Available online from http://hipc.stanford.edu/sops/pbmc-thawing-protocol. Access date 22.11.2012
419. Mosmann T. Rapid colorimetric assay for cellular growth and survival: Application to proliferation and cytotoxicity assays. Journal of Immunological Methods. 1983 65(1–2):55-63.
420. Invitrogen. PrestoBlue™ Cell Viability Reagent Protocol, Product Information Sheet. In: Technologies L, MAN00032322010. Available from www.Invitrogen.com. Access date 22.11.2013.
421. Artursson P. Epithelial transport of drugs in cell culture. I: A model for studying the passive diffusion of drugs over intestinal absorptive (Caco-2) cells. Journal of Pharmaceutical Sciences. 1990 79(6):476-82.
422. Omidi Y, Campbell L, Barar J, Connell D, Akhtar S, Gumbleton M. Evaluation of the immortalised mouse brain capillary endothelial cell line, b.End3, as an in vitro blood–brain barrier model for drug uptake and transport studies. Brain Research. 2003 990(1–2):95-112.
423. Brown RC, Morris AP, O'Neil RG. Tight junction protein expression and barrier properties of immortalized mouse brain microvessel endothelial cells. Brain Research. 2007 1130(1):17-30.
424. Li GL, Simon MJ, Cancel LM, Shi ZD, Ji XY, Tarbell JM, et al. Permeability of Endothelial and Astrocyte Cocultures: In Vitro Blood-Brain Barrier Models for Drug Delivery Studies. Annals of Biomedical Engineering. 2010 38(8):2499-511.
425. Weksler BB, Subileau EA, Perrière N, Charneau P, Holloway K, Leveque M, et al. Blood-brain barrier-specific properties of a human adult brain endothelial cell line. The FASEB Journal. 2005 19(13):1872-4.

426. Fasler-Kan E, Suenderhauf C, Barteneva N, Poller B, Gygax D, Huwyler J. Cytokine signaling in the human brain capillary endothelial cell line hCMEC/D3. Brain Research. 2010 1354(0):15-22.
427. Poller B, Gutmann H, Krahenbuhl S, Weksler B, Romero I, Couraud PO, et al. The human brain endothelial cell line hCMEC/D3 as a human blood-brain barrier model for drug transport studies. Journal of Neurochemistry. 2008 107(5):1358-68.
428. Cucullo L, Couraud PO, Weksler B, Romero IA, Hossain M, Rapp E, et al. Immortalized human brain endothelial cells and flow-based vascular modeling: a marriage of convenience for rational neurovascular studies. Journal of Cerebral Blood Flow and Metabolism. 2008 28(2):312-28.
429. O'Brien J, Wilson I, Orton T, Pognan F. Investigation of the Alamar Blue (resazurin) fluorescent dye for the assessment of mammalian cell cytotoxicity. European Journal of Biochemistry. 2000 267(17):5421-6.
430. Rice J. Introduction and training in tissue culture techniques. University of Portsmouth. Portsmouth. 2009. p. 21-2.
431. Gaillard PJ, de Boer AG. Relationship between permeability status of the blood–brain barrier and in vitro permeability coefficient of a drug. European Journal of Pharmaceutical Sciences. 2000 12(2):95-102.
432. Ragnaill MN, Brown M, Ye D, Bramini M, Callanan S, Lynch I, et al. Internal benchmarking of a human blood–brain barrier cell model for screening of nanoparticle uptake and transcytosis. European Journal of Pharmaceutics and Biopharmaceutics. 2011 77(3):360-7.
433. Avdeef A. How well can in vitro brain microcapillary endothelial cell models predict rodent in vivo blood–brain barrier permeability? European Journal of Pharmaceutical Sciences. 2011 43(3):109-24.
434. Barar J, Omidi Y. Bioelectrical and Permeability Properties of Brain Microvasculature Endothelial Cells: Effects of Tight Junction Modulators. Journal of Biological Sciences. 2008 8(3):556-62.
435. Hamburger V, Hamilton HL. A series of normal stages in the development of the chick embryo. Journal of Morphology. 1951 88(1):49-92.
436. Fan W, Yan W, Xu Z, Ni H. Formation mechanism of monodisperse. Low molecular weight chitosan nanoparticles by ionic gelation technique. Colloids and Surfaces B: Biointerfaces 2012 90(0): 21-27.

9

APPENDICES

APPENDIX I **^{1}H-and ^{13}C-NMR spectra of DEX-OX4**

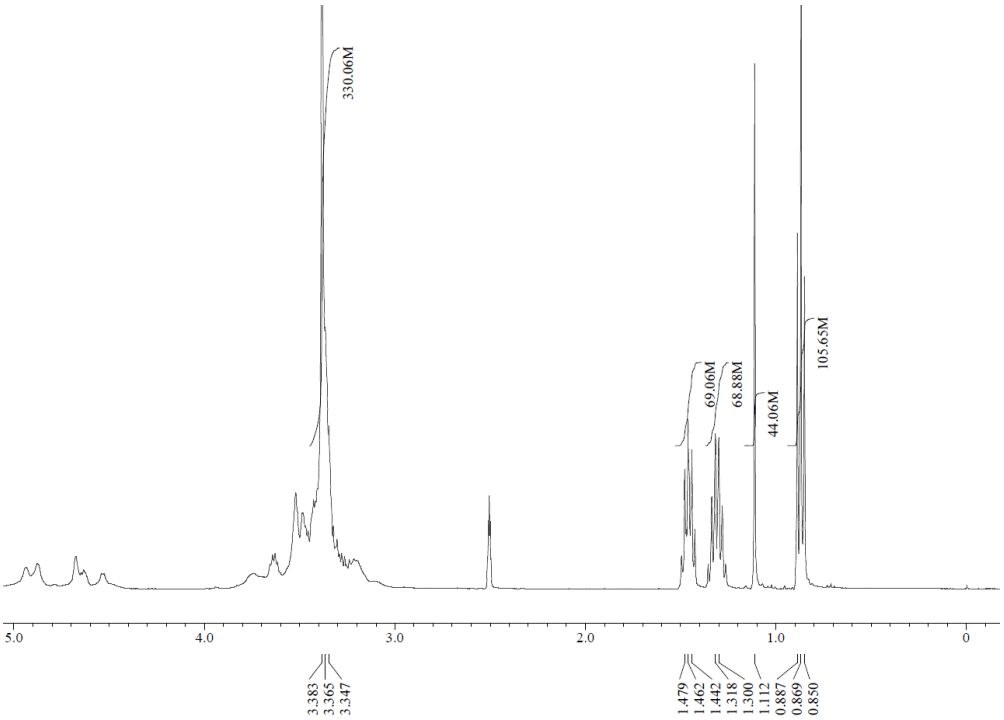

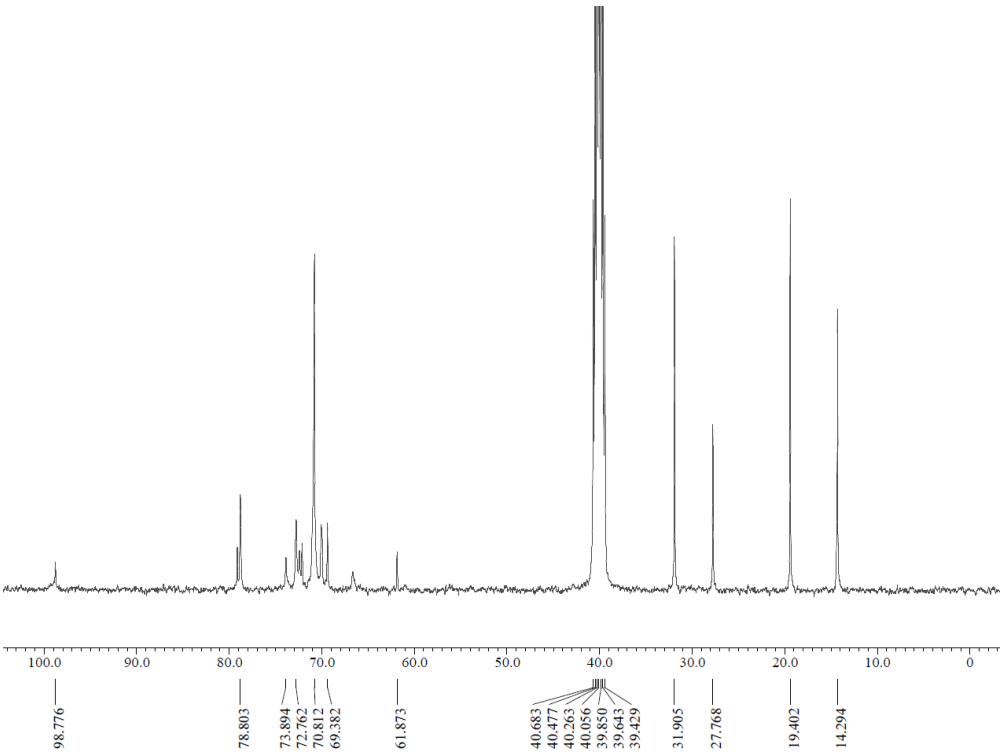

DEX-OX4
Off white solid

DMSO soluble, water soluble

FT-IR (ATR; ν_{max}; cm-^{1}): 3227 (O-H str, OH pyranose ring); 2872 (C-H, str pyranose ring, CH_2 of butyl group); 1336 (C-O-H def, pyranose ring, alkylglycerol); 1111 (C-O-C, str, glycoside linkage); 1006 (C-O def, pyrnose ring, alkylglycerol); 913, 866 (C-C def, pyranose ring); 526 (C-C-O def, alkylglycerol)

^{1}H-NMR (400MHz; DMSO-d; δ; ppm): 0.9 (m, 3H, alkylglyceryl terminal-CH_3); 1.3 (m, 2H, alkylglyceryl-3-CH_2); 1.5 (m, 2H, alkylglyceryl-2CH_2); 3.2 (m, 2H, dextran 2CH, 4CH); 3.4 (m, 1H, dextran 3CH); 3.6 (m, 2H, dextran 5CH, 6CH'); 3.7 (s, 1H, dextran 6CH) 4.7 (s, 1H, dextran 1CH)

^{13}C-NMR (100MHz; DMSO-d; δ; ppm): 14.29 (butylglycerol terminal CH_3,); 19.40 (butylglycerol-3CH_2); 27.00 (butylglycerol-2CH_2);31.36 (butylglycerol-1CH_2);61.80 (dextran-6CH_2); 69.38 (dextran-2CH); 70.81 (dextran-4CH); 72.76 (dextran-5CH); 73.64 (dextran-3CH); 98.77 (dextran anomeric-1CH)

APPENDIX II **^{1}H-and ^{13}C-NMR spectra of DEX-OX8**

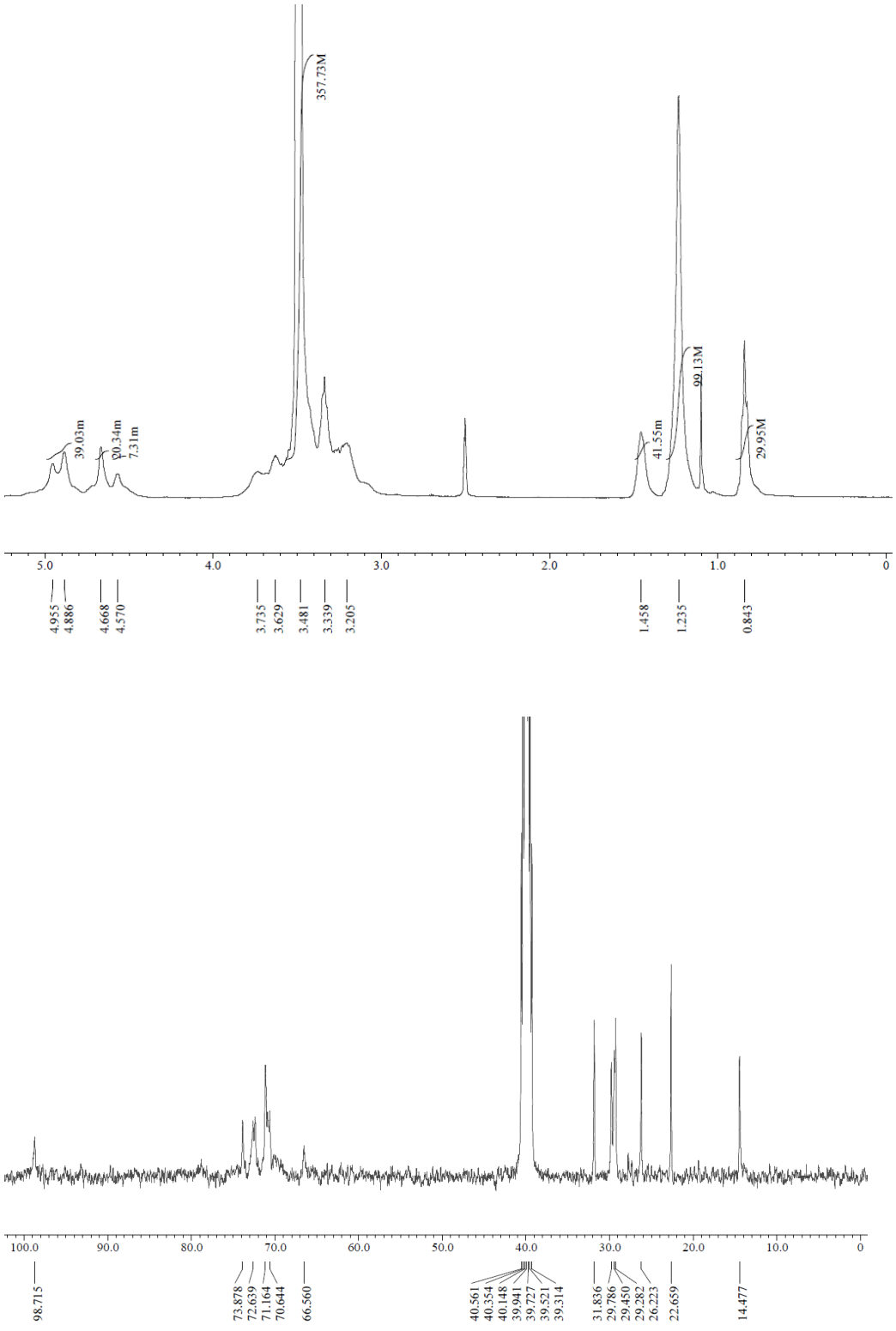

DEX-OX8
Beige solid

DMSO soluble, water soluble

FT-IR (ATR; ν_{max}; cm-^{1}): 3322 (O-H str, OH pyranose ring); 2922 (C-H, str pyranose ring, CH_2 of butyl group); 1346 (C-O-H def, pyranose ring, alkylglycerol); 1149 (C-O-C, str, glycoside linkage), 1000 (C-O def, pyrnose ring, alkylglycerol);915, 852 (C-C def, pyranose ring); 506 (C-C-O def, alkylglycerol)

^{1}H-NMR (400MHz; DMSO-d; δ; ppm): 0.8 (m, 3H, alkylglyceryl terminal-CH_3); 1.2 (m, 12H, alkylglyceryl-2-7CH_2); 1.4 (m, 2H, alkylglyceryl-1CH_2); 3.2 (m, 2H, dextran 2CH, 4CH); 3.3 (m, 1H, dextran 3CH); 3.6 (m, 2H, dextran 5CH, 6CH'); 3.7 (s, 1H, dextran 6CH) 4.7 (s, 1H, dextran 1CH)

^{13}C-NMR (100MHz; DMSO-d; δ; ppm): 14.48 (octylglycerol terminal-CH_3,); 22.66 (octylglycerol-7CH_2); 26.22 (octylglycerol-6CH_2); 29.22 (octylglycerol-5CH_2); 29.28 (octylglycerol-4CH_2); 29.45 (octylglycerol-3CH_2); 29.78 (octylglycerol-2CH_2); 31.86 (octylglycerol-1CH_2); 66.56 (dextran-6CH_2); 70.74 (dextran-2CH); 71.164 (dextran-4CH); 72.63 (dextran-5CH); 73.87 (dextran-3CH); 99.71 (dextran anomeric-1CH)

APPENDIX III **^{1}H-and ^{13}C-NMR spectrum of PLA- DEX-OX4**

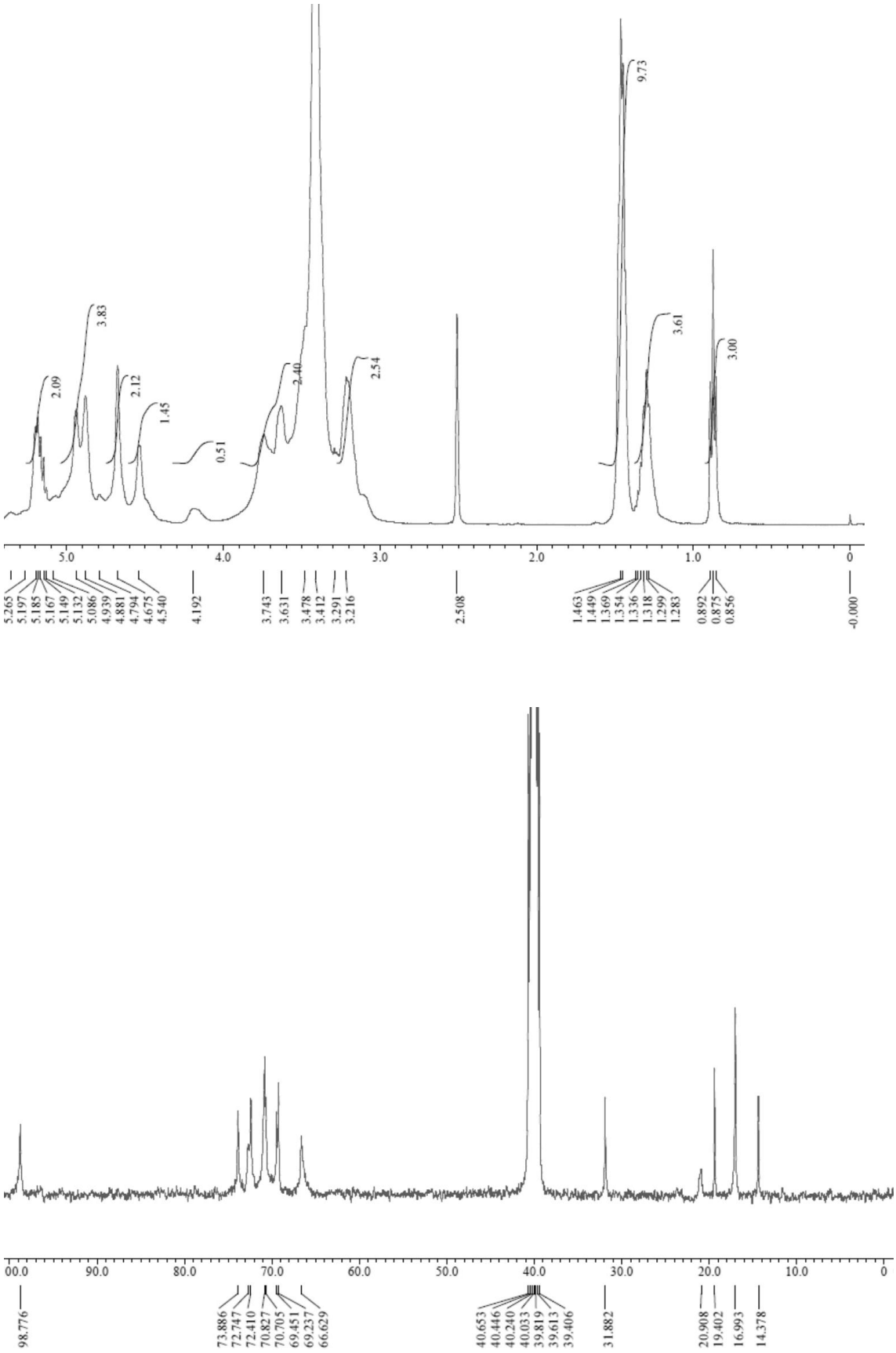

PLA-DEX-OX4
Off white solid

DMSO soluble, water soluble

FT-IR (ATR; ν_{max}; cm-^{1}): 3387 (O-H str, OH pyranose ring); 2941 (C-H, str pyranose ring, CH_2 of butyl group); 1755 (C=O str, poly(lactc acid)); 1451 (C-O-H def, pyranose ring, alkylglycerol); 1148 (C-O-C, str, glycoside linkage), 1001 (C-O def, pyrnose ring, alkylglycerol); 915, 852 (C-C def, pyranose ring); 506 (C-C-O def, alkylglycerol)

^{1}H-NMR (400MHz; DMSO-d; δ; ppm): 0.9 (m, 3H, alkylglyceryl terminal-CH_3); 1.3 (m, 2H, alkylglyceryl-3-CH_2); 1.4 (s, 3H, poly(lactic acid)CH_3); 3.2 (m, 2H, dextran 2CH, 4CH); 3.4 (m, 1H, dextran 3CH); 3.6 (m, 2H, dextran 5CH, 6CH'); 3.7 (s, 1H, dextran 6CH); 4.7 (s, 1H, dextran 1CH); 5.2 (m, 1H, poly(lactic acid) CH)

^{13}C-NMR (100MHz; DMSO-d; δ; ppm): 14.38 (butylglycerol terminal CH_3,);16.99 (poly(lactic acid)CH_3); 19.40 (butylglycerol-3-CH_2); 20.09 (butylglycerol-2CH_2);31.88 (butylglycerol-1CH_2); 66.62 (poly(lactic acid)CH); 69.24 (dextran -6CH_2); 70.71 (dextran -2CH); 70.82 (dextran -4CH); 72.74 (dextran -5CH); 73.88 (dextran -3CH); 98.76 (dextran anomeric -1CH)

APPENDIX IV **^{1}H-and ^{13}C-NMR spectrum of PLA- DEX-OX8**

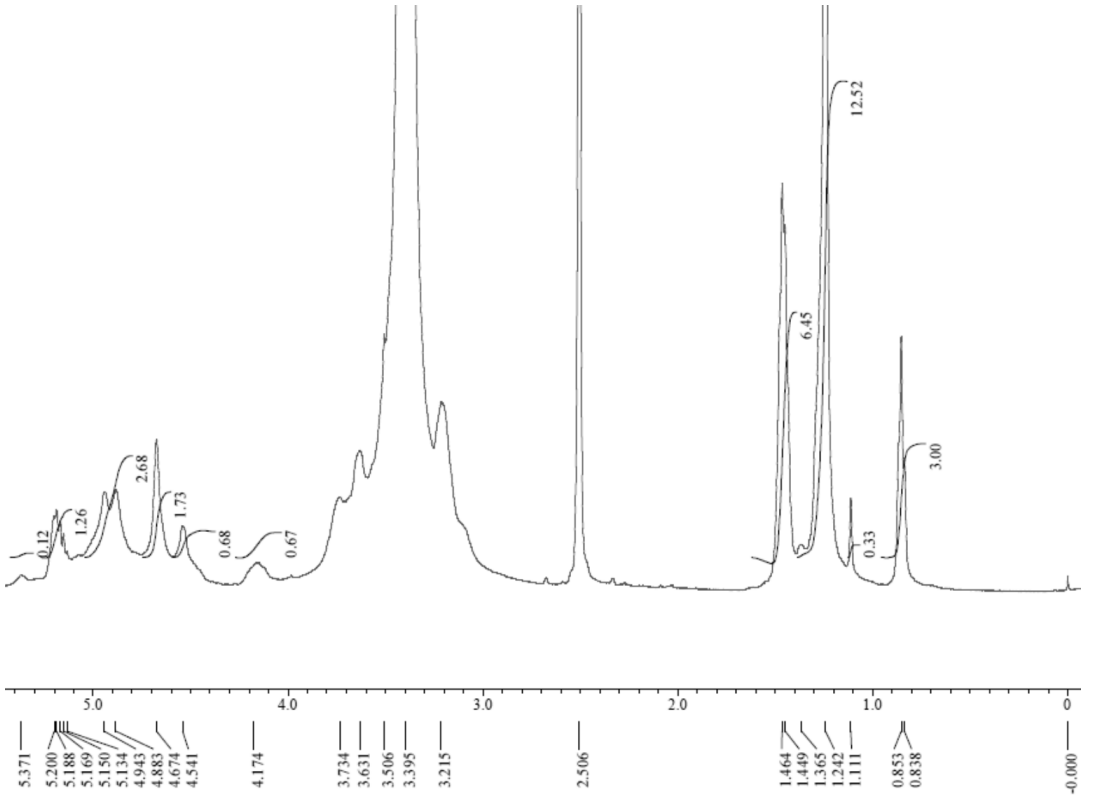

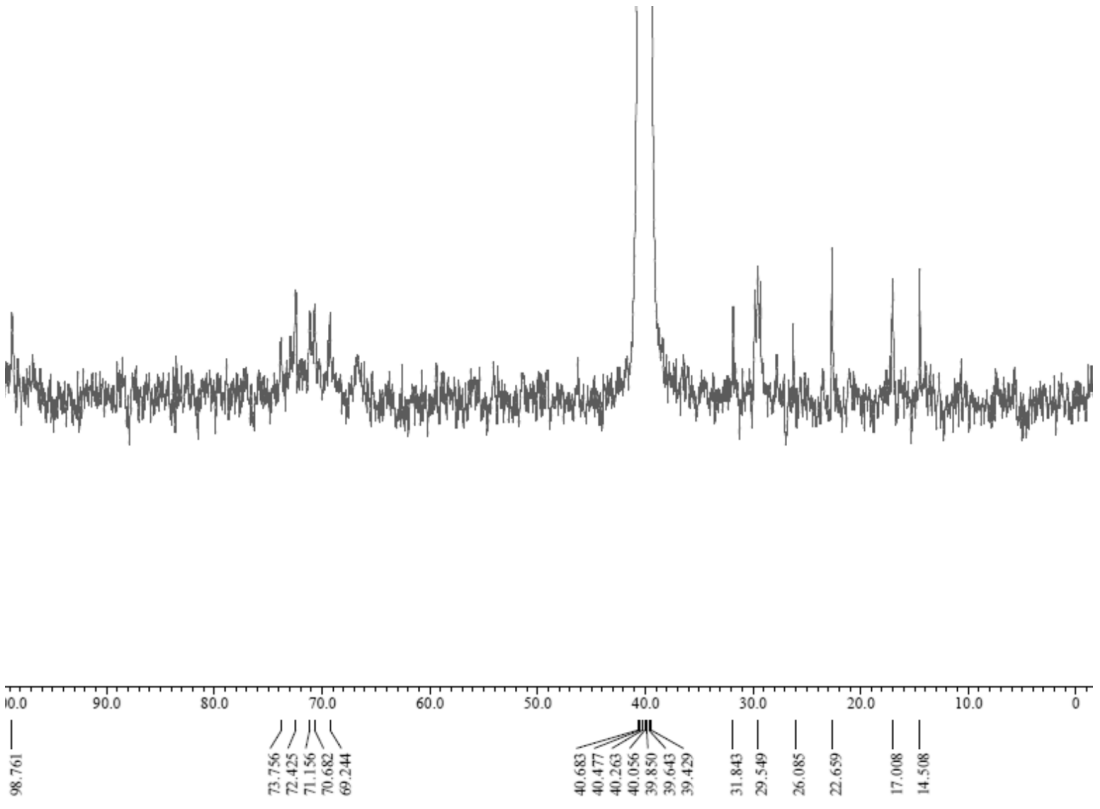

PLA-DEX-OX8
Off white solid

DMSO soluble, water soluble

FT-IR (ATR; ν_{max}; cm-^{1}): 3360 (O-H str, OH pyranose ring); 2933 (C-H, str pyranose ring, CH_2 of butyl group); 1754(C=O str, poly(lactc acid)); 1452(C-O-H def, pyranose ring, alkylglycerol); 1184 (C-O-C, str, glycoside linkage), 1008 (C-O def, pyrnose ring, alkylglycerol); 905, 852 (C-C def, pyranose ring); 539 (C-C-O def, alkylglycerol)

^{1}H-NMR (400MHz; DMSO-d; δ; ppm): 0.8 (m, 3H, alkylglyceryl terminal-CH_3); 1.2 (s, 12H, alkylglyceryl-2-7CH_2); 1.5 (s, 3H, poly(lactic acid)CH_3); 3.2 (m, 2H, dextran 2CH, 4CH); 3.3 (m, 1H, dextran 3CH); 3.6 (m, 2H, dextran 5CH, 6CH'); 3.7 (s, 1H, dextran 6CH) 4.8 (s, 1H, dextran 1CH); 5.2 (m, 1H, poly(lactic acid) CH)

^{13}C-NMR (100MHz; DMSO-d; δ; ppm): 14.51 (octylglycerol terminal-CH_3,); 17.01 (poly(lactic acid)CH_3); 22.69 (octylglycerol-7CH_2); 26.08 (octylglycerol-6CH_2); 29.22 (octylglycerol-5CH_2); 29.28 (octylglycerol-4CH_2); 29.45 (octylglycerol-3CH_2); 29.78 (octylglycerol-2CH_2); 31.86 (octylglycerol-1CH_2); 66.62 (poly(lactic acid)CH); 69.24 (dextran-6CH_2); 70.68 (dextran-2CH); 71.15 (dextran-4CH); 72.45 (dextran-5CH); 73.75 (dextran-3CH); 98.76 (dextran anomeric-1CH)

APPENDIX V **GPC spectra of DEX-OX4 and DEX-OX8**

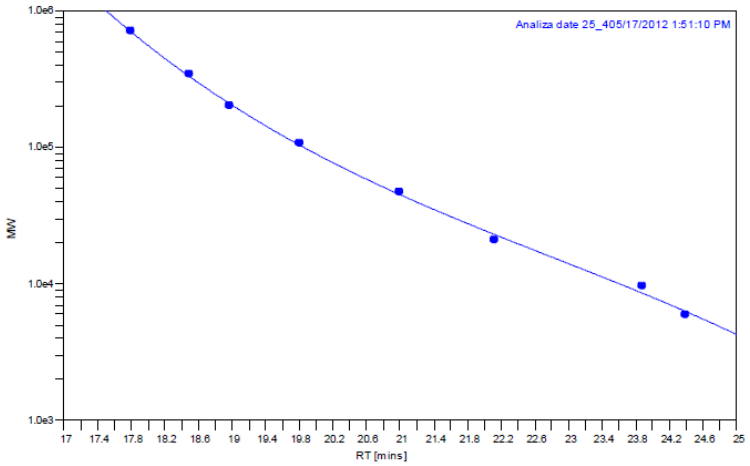

GPC: Calibration of pullulan standards of range of MW: 0.6 × 10^4, 1 × 10^4, 2.17 × 10^4, 4.88 × 10^4 and 11.3 × 10^4, 21 × 10^4, 36.6 × 10^4, 80.5 × 10^4 g/mol.

Narrow standard curve: $y= 51.17 - 5.693x + 0.2389x^2 - 0.00349x^3$

DEX-OX4

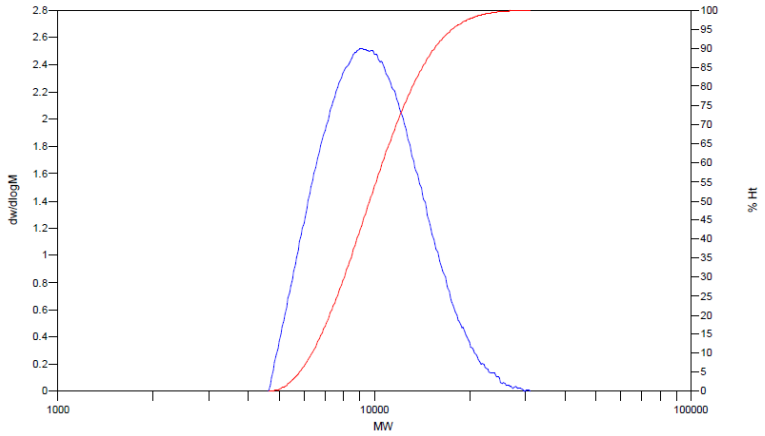

DEX-OX8

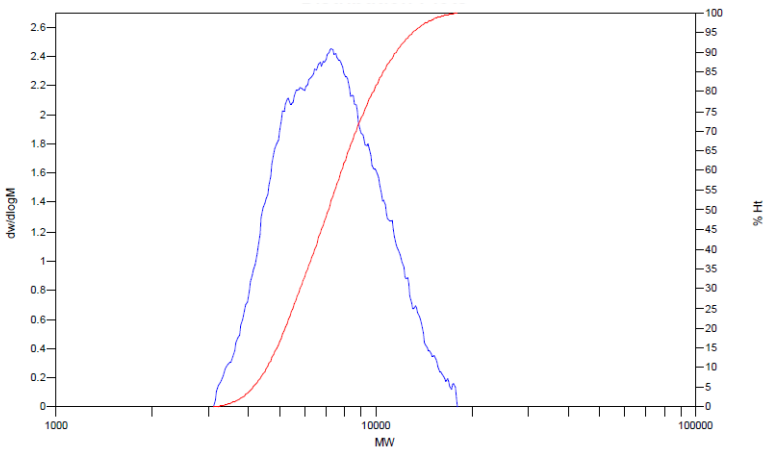

APPENDIX VI **Calibration curve of Evans Blue in acetic acid**

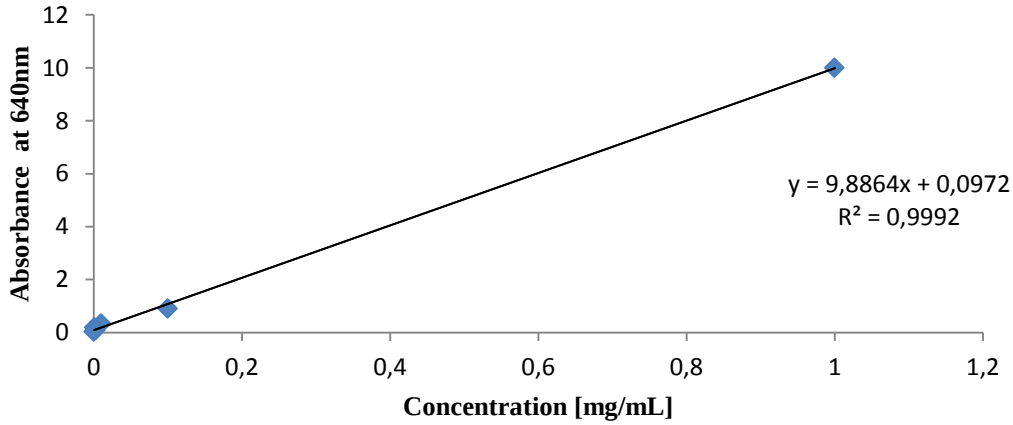

UV-Vis calibration curve of Evans Blue in acetic acid (55 %)

APPENDIX VII **Calibration curve of Doxorubicin in water**

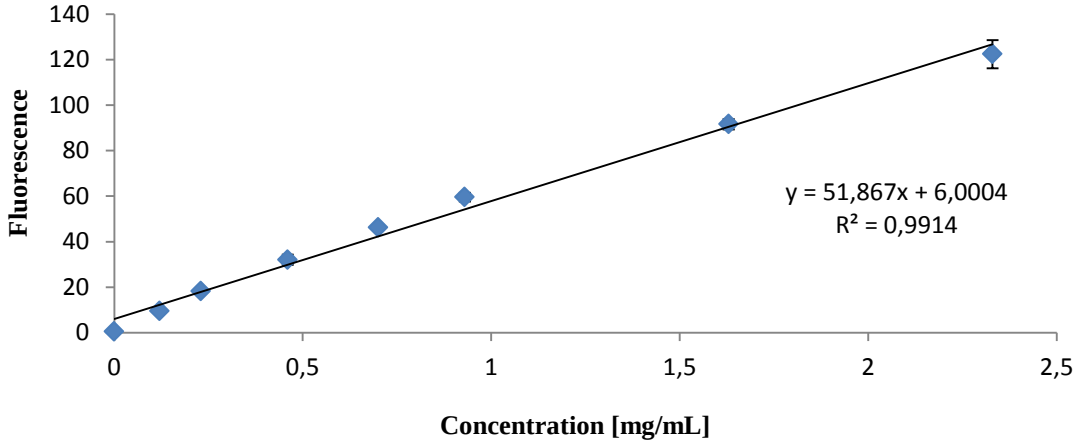

Fluorescence calibration curve of Doxorubicin in water, excitation 480 nm, emission 590 nm

APPENDIX VIII **Calibration curve of FITC, Rhodamine B and Doxorubicin in DMSO**

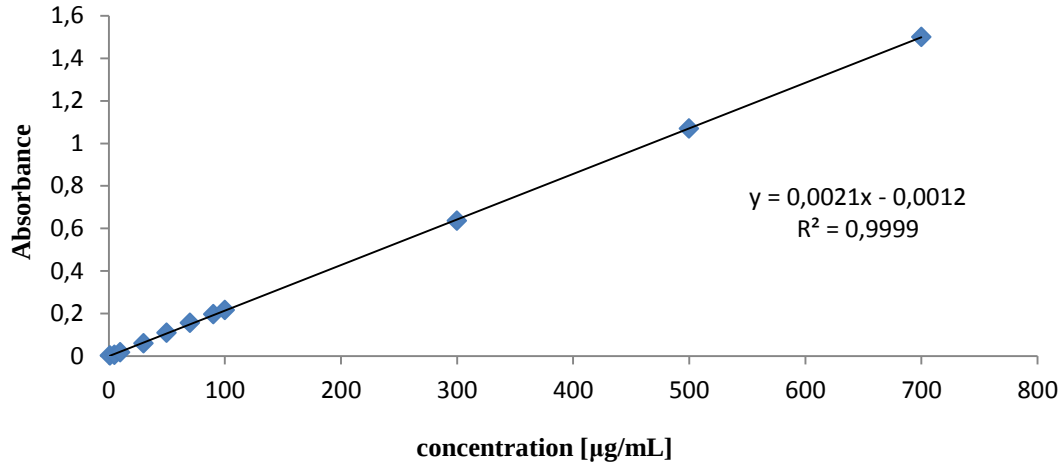

UV-Vis calibration curve of absorbance at 493 nm Fluorescein Isothiocyanate in DMSO.

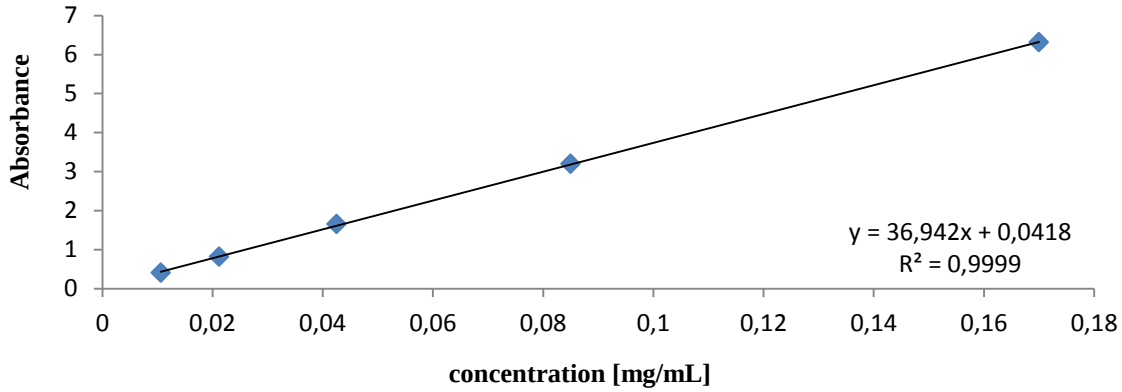

UV-Vis calibration curve of absorbance at 318 nm, Rhodamine B in DMSO.

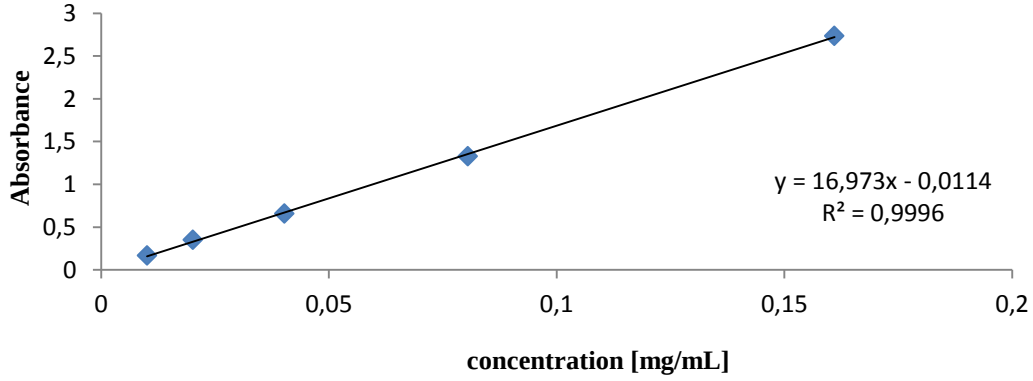

UV-Vis calibration curve of absorbance at 478 nm, Doxorubicin in DMSO.

APPENDIX IX **Calibration curve of FITC, Rhodamine B and Doxorubicin in PBS**

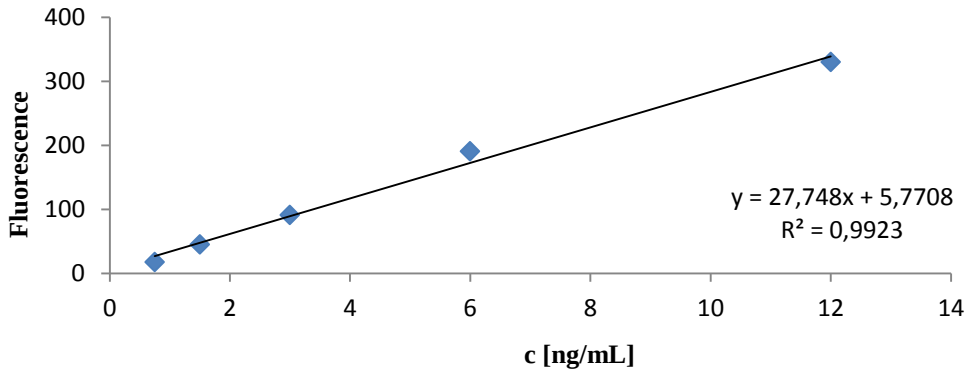

Fluorescence calibration curve - Doxorubicin in PBS (excitation/emission 475 nm/ 570 nm, respectively)

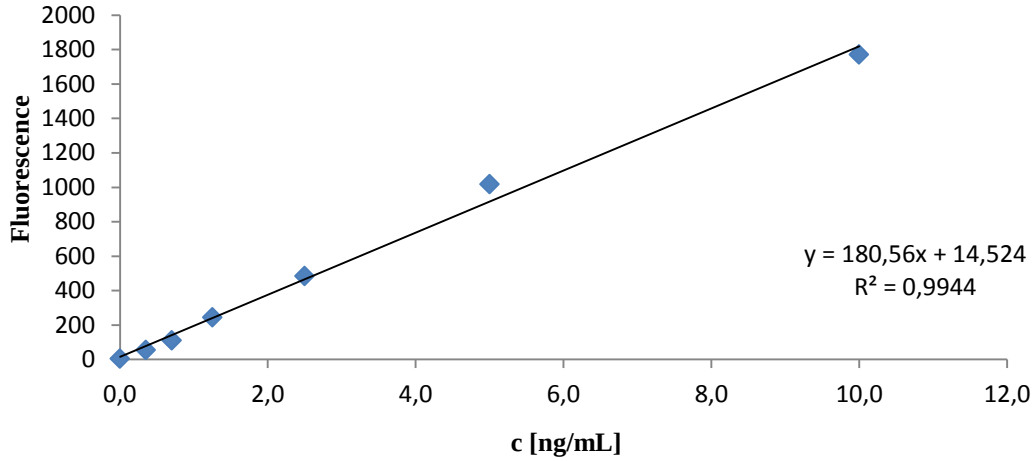

Fluorescence calibration curve - Rhodamine B in PBS (excitation/emission 540/625 nm, respectively)

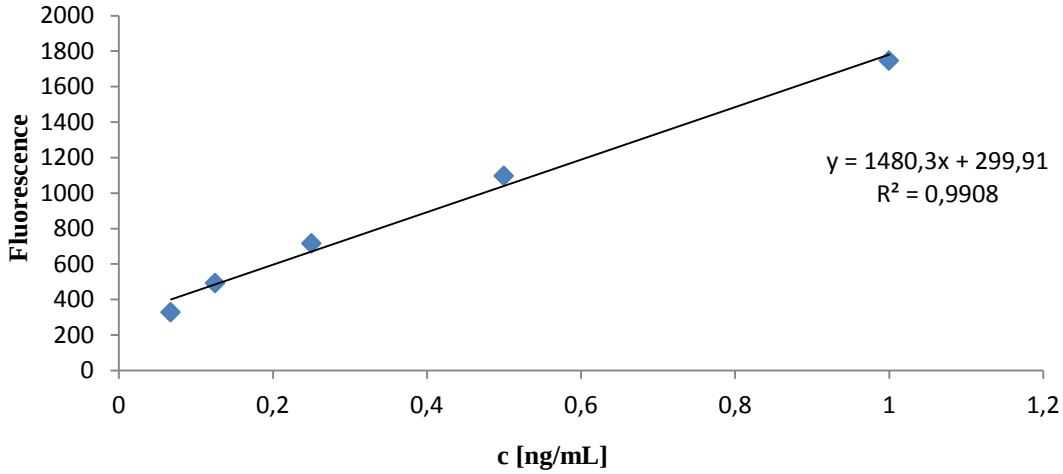

Fluorescence calibration curve - fluorescein isothiocyanate in PBS (excitation/emission 485/525 nm, respectively)

APPENDIX X Calibration of cell seeding density

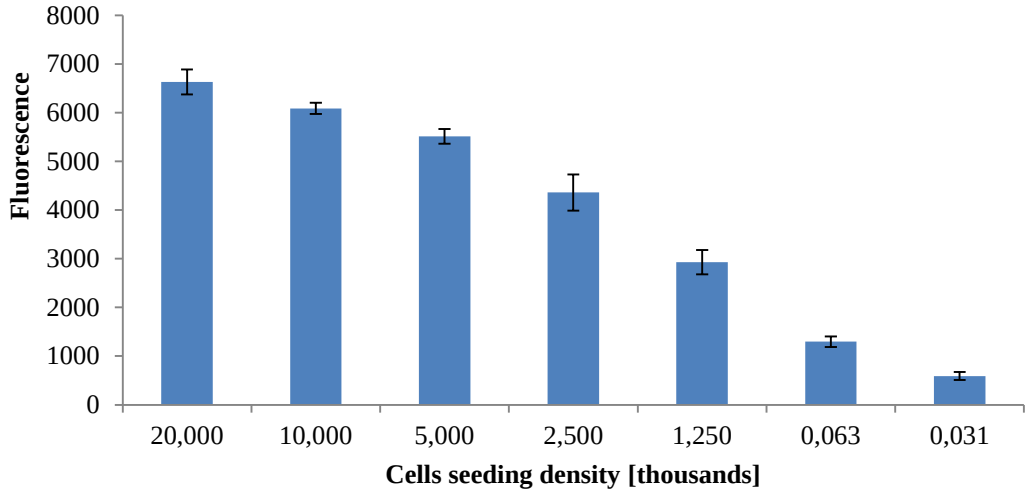

Calibration hCMEC/D3, PrestoBlue assay, intensity vs. seeding numbers of cells, PrestoBlue Assay.

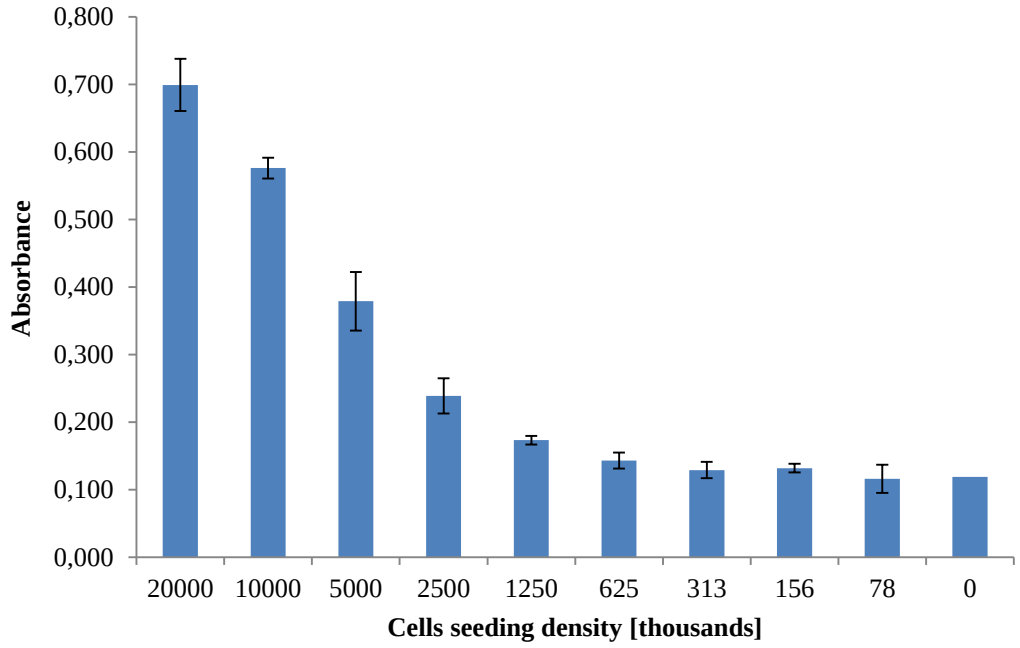

Calibration bEnd3, MTT assay, intensity vs. seeding numbers of cells, MTT assay.

APPENDIX XI Cytotoxicity protocols

MTT assay

A solution of3-(4,5-Dimethylthiazol-2-yl)-2,5-diphenyltetrazolium bromide (MTT) in serum-free DMEM (5 mg/mL; kept in dark at 2 - 8 °C until use) was equilibrated at 37 °C and then diluted (1:4) with serum-free DMEM to create the working solution. bEnd3 mouse endothelial cells were seeded onto 96 well-plates (at a density of 10^4 cells per well) which were incubated in 200 µL media (DMEM with 10 % FBS added) for 24 h. The wells on the edge of the plate were filled with PBS to prevent uneven evaporation of the media under the plate cover. In each well, 50 µL of media was then removed and replaced with 50 µL of PBS-based nanoformulation containing a specific concentration of nanoparticles (obtained by redispersing by sonication for 5 min, a known mass of ultracentrifugation pellet or lyophilisate). After incubation, medium was removed from the wells and replaced with 100 µL of the MTT working solution (prepared as described above). The plate was incubated at 37 °C in dark for 1 hour, then the media was removed and replaced with 100 µL of DMSO, to dissolve the formazan crystals. After an additional 1 hour of dissolution process in dark at on the bench room temperature (25 °C), the plate was inserted into the plate reader PolarStar Optima (BMG Labtech), shaken horizontally for 30 seconds and the absorbance of the plates was read at 570 nm. The viability of the cells was displayed as per cent relative to PBS treatment. PBS was used as a negative control for toxicity, Digitonin (10 mg/mL) was used as a positive control, and average value for empty wells with media was subtracted as a background signal.

Presto Blue assay

hCMEC/D3 human endothelial cells were seeded onto 96 well-plates (10^4 cells per well), which were incubated in 200 µL of EGM-2 medium (containing FBS 2 % v/v) for 24 hours. The wells on the edge of the plate were filled with PBS to prevent uneven evaporation of the media under the plate cover during. After 24 h, 50 µL of media was removed and replaced with 50 µL of PBS-based nanoformulation containing a specific concentration of nanoparticles (obtained by redispersing by sonication for 5 min, a known mass of ultracentrifugation pellet or lyophilisate). After incubation for 30 minutes, the medium (110.0 µL) was removed from each well and replaced with 10.0 µl of the Presto Blue solution (to allow dilution factor 10 between cell media and Presto Blue), followed by incubation for 30.0 min at 37.0 °C in darkness. The fluorescence (excitation 540 nm / emission 590 nm) was then read using a PolarStar Optima (BMG Labtech) plate reader.

APPENDIX XII Transwell: FITC-DEX calibration

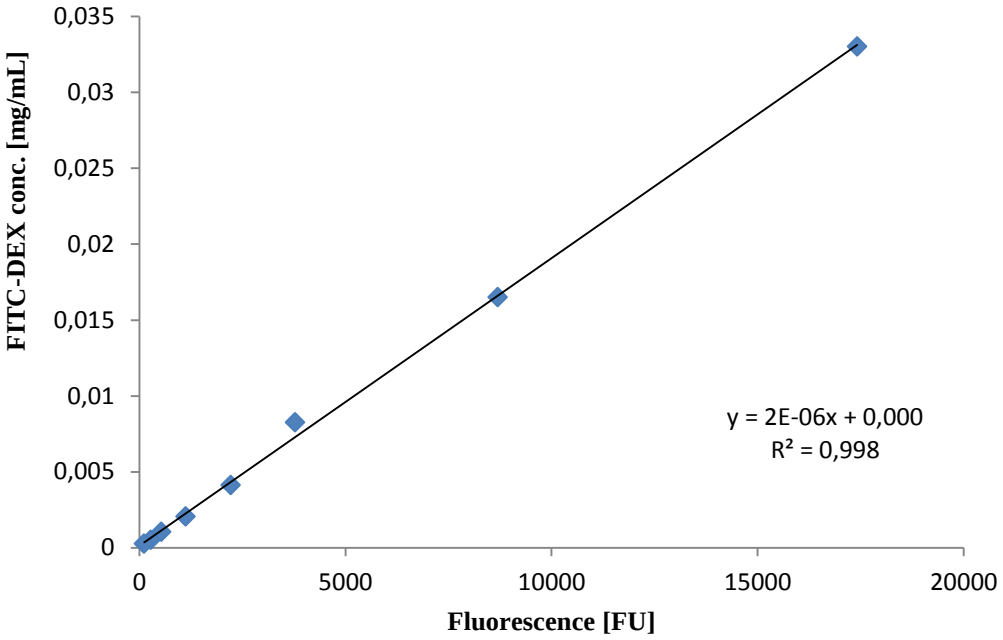

Calibration line representing fluorescence vs. concentration of FITC-labelled dextran (FITC-DEX) in EGM-2 media

APPENDIX XIII **Microscopic images of sections of chicken embryos**

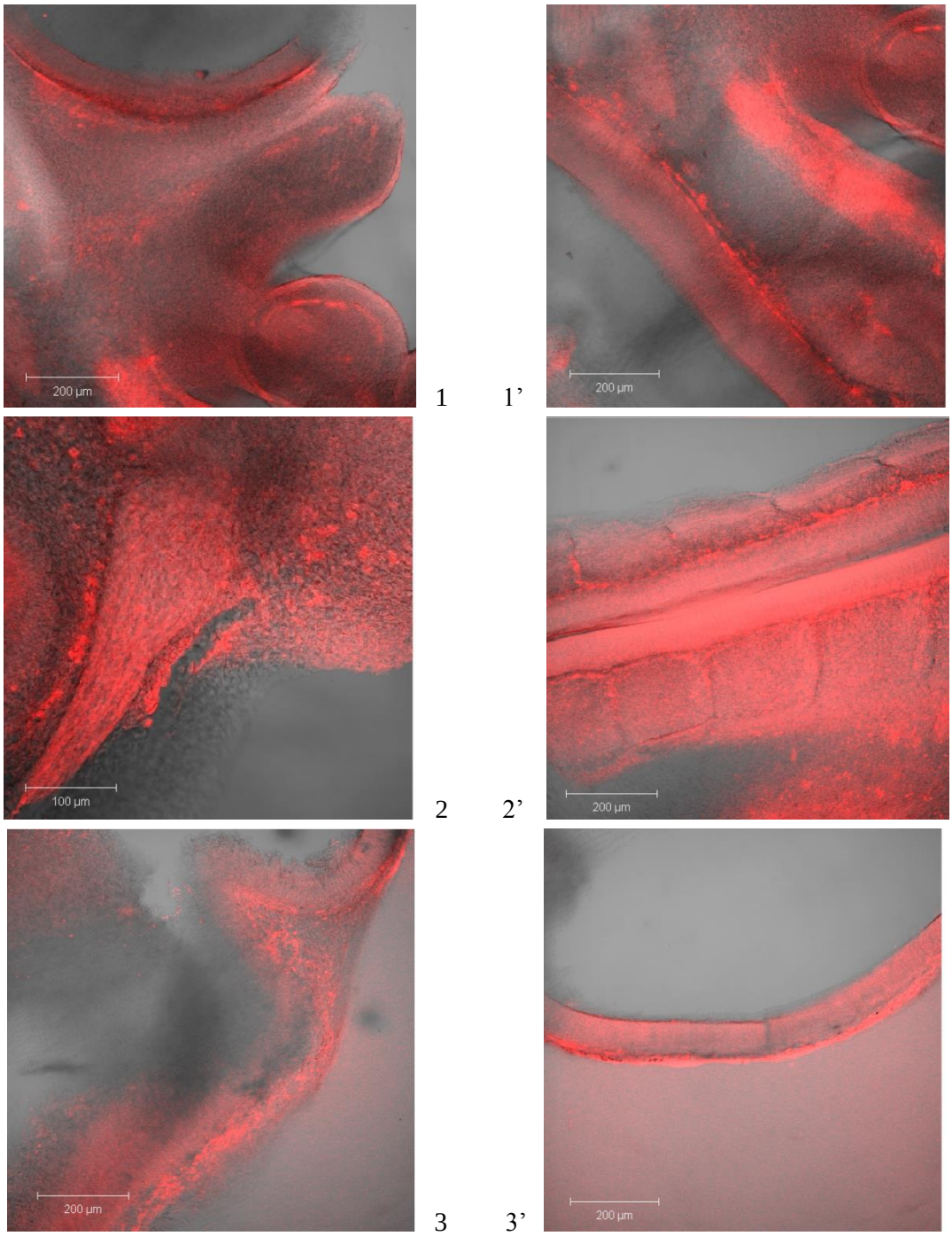

Chicken embryos, following 24 hours incubated with Rhodamine B labelled nanoparticles or free dye as a control. DIC (Nomarski) normalised and fluorescent image merge, vibratome sections 50 µm thick.

Nanoparticles from PLA-DEX-OX4

1 Olfactory region

2 Trunk section

3 Neuroepithelium

Rhodamine B solution - control

1' Trunk section

2' Somnites (trunk)

3' Neuroepithelium